Understanding the determinants and improving detection of bone fragility in female chickens

Isabela Vitienes

Department of Biological and Biomedical Engineering, Faculty of Medicine

Supervisor: Dr. Bettina M. Willie

McGill University, Montreal, QC, Canada

August 15, 2024

A thesis submitted to McGill University in partial fulfillment of the requirements of the degree of Doctor of Philosophy

Content

List of Figures

Chapter 2 (pg.3-36)

behaviour. Bone stiffness is defined as the slope in the elastic region. Mechanical properties annotated on the curve are a function of both the bone's material and structural properties. B) Stress-strain curve describing tissue-level mechanical properties (bone material properties), which are independent of bone volume and structure.

- **Figure 8: Housing and genotype groups.** A) Caged housing systems, B) Low complexity aviary, C) High complexity aviary, D) Lohamnn LSL-Lite (white-feathered) and Lohmann Brown (brown-feathered) genetic strains. White-feathered chickens had heavier pectoral muscles and lighter leg muscles (Vitienes et al., 2021).
- **Figure 9: Fracture detection methods.** A) In vivo palpation. Image reproduced with permission from Kittelsen et al., 2023. B) Radiograph image where a fracture is visible (white arrow).
- **Figure 10:** Schematic illustrating possible explanations for keel bone damage. Diagram reproduced with permission from M. J. Toscano et al., 2020.
- **Figure 11: In vivo strain gauging.** A) Quarter bridge Wheatstone bridge circuit used to detect and amplify strain-derived voltage drops originating from the strain gauge (SG). Illustration reproduced with permission from Biewener, 1992. B) Image of a rosette (circular) and axial (rectangular) strain gauges prepared for in vivo implantation. C) Image of a surgically exposed medial aspect of a tibiotarsus with a visible gauge attached to the medial surface.
- **Figure 12: Computed tomography sources of error.** A) Illustration of the effects of partial volume effect. Depending on the position of the object relative to the pixel coordinates, the shape and attenuation is altered. Reproduced with permission from Sperrin & Winder, 2014. B) Exemplary images of a cross-section of a beam. The image on the left has beam hardening effects, evidenced by the bright halo on the outer edge of the beam. The image on the right has undergone beam hardening correction to more accurately depict the density distribution of the beam. Reproduced with permission from Roche et al., 2010.
- **Figure 13: Image segmentation and binarization.** The raw greyscale image is separated into regions – cortical and medullary canal regions in this case – using morphological operations. Then, the image is binarized to between what is bone and not by thresholding, which produces binary masks.

Benjamini-Hochberg post-hoc (non-italicized) and t-test (italicized). Note: plots within each row share the same y-axis scaling.

- **Figure 6:** Effect of breed and rearing housing on anterior shear strains and peak axial and bending strains during steady locomotor activities (mean ± sd). ANOVA main effects: a) breed, b) rearing housing, c) interaction. Data has been normalized to the median step frequency per group, to control for within-chicken variations in step frequency. Groups with significant unadjusted or adjusted p-values indicated by bars with p-values above: Benjamini-Hochberg post-hoc (non-italicized) and t-test (italicized). Note: plots within each row share the same y-axis scaling.
- **Figure 7:** Effect of breed and rearing housing on longitudinal strains during non-steady activities (mean ± sd). Each column includes a different activity type measured and each row includes the anatomical site of the tibiotarsal midshaft sampled. ANOVA main effects: a) breed, b) rearing housing, c) interaction. Groups with significant unadjusted or adjusted p-values indicated by bars with p-values above: Benjamini-Hochberg post-hoc (non-italicized) and t-test (italicized). Note: Plot A has a different y-axis scaling than the rest of the row of anterior strains. All other plots within a given row share the same y-axis scaling.
- **Figure 8:** Effect of breed and rearing housing on principal tensile and compressive strains, and tensile strain orientation during non-steady activities (mean ± sd). ANOVA main effects: a) breed, b) rearing housing, c) interaction. Groups with significant unadjusted or adjusted p-values indicated by bars with p-values above: Benjamini-Hochberg post-hoc (non-italicized) and t-test (italicized). Note: Plot D has a different y-axis scaling than the rest of the row. All other plots within a given row share the same y-axis scaling.
- **Figure 9:** Effect of breed and rearing housing on anterior shear strains and peak axial and bending strains during non-steady activities (mean ± sd). ANOVA main effects: a) breed, b) rearing housing, c) interaction. Groups with significant unadjusted or adjusted p-values indicated by bars with p-values above: Benjamini-Hochberg post-hoc (non-italicized) and t-test (italicized). Note: plots within each row share the same y-axis scaling.
- **Supplemental Fig. 1:** Effect of breed and rearing housing on step frequency during A) ground locomotion, B) uphill locomotion, and C) downhill locomotion, (mean ± sd). ANOVA main effects: a) breed, b) rearing housing, c) interaction. Significant Tukey-Kramer post-hoc

comparisons indicated by bars, with p-values above. Note: each step frequency data point corresponds to the step frequency from a segment of locomotion recorded.

- **Supplemental Fig. 2:** Effect of breed and rearing housing on raw (not normalized) locomotor longitudinal strains (mean ± sd). Each column includes a different activity type measured and each row includes the anatomical of the tibiotarsal midshaft sampled. Data for locomotor activities has been normalized to the median step frequency per group, to control for within chicken variations in step frequency. ANOVA main effects: a) breed, b) rearing housing, c) interaction. Groups with significant unadjusted or adjusted p-values indicated by bars with p-values above: Benjamini-Hochberg post-hoc (non-italicized) and t-test (italicized). Note: plots within each row share the same y-axis scaling.
- **Supplemental Fig. 3:** Effect of breed and rearing housing on raw (not normalized) locomotor principal strains, and tensile strain orientation during ground, uphill, and downhill locomotion (mean ± sd). ANOVA main effects: a) breed, b) rearing housing, c) interaction. Groups with significant unadjusted or adjusted p-values indicated by bars with p-values above: Benjamini-Hochberg post-hoc (non-italicized) and t-test (italicized). Note: plots within each row share the same y-axis scaling.
- **Supplemental Fig. 4:** Effect of breed and rearing housing on raw (not normalized) peak shear, axial, and bending strains during ground, uphill, and downhill locomotion (mean ± sd). ANOVA main effects: a) breed, b) rearing housing, c) interaction. Groups with significant unadjusted or adjusted p-values indicated by bars with p-values above: Benjamini-Hochberg post-hoc (non-italicized) and t-test (italicized).
- **Supplemental Figure 5:** Loading patterns at the anterior surface during steady and non-steady activities. A. Illustration depicting the loading pattern of the tibiotarsus associated to three regions of the plot. At the y-axis, fractional tensile strain ratio (FTSR) indicates the relative contribution of principal tensile strain to the overall amount of principal strain. Tensile strain orientation is the angle of the axis of principal tensile strain relative to the bone's longitudinal axis. Adapted from Moreno et al. 2008 (Moreno et al., 2008). B-D. Steady activities. E-G. Non-steady activities. The line intersecting the y-axis delineates an FTSR = 0.5, when principal tensile and principal compressive contribute equally. The lines intersecting the x-axis delineate a tensile strain orientation of 22.5° and 67.5°. When the tensile strain orientation

is within this range, the axis of tensile strain is closer to 45° than to being either aligned with the bone's longitudinal or transverse axis.

- **Supplemental Figure 6:** Strains measured from the three independent elements of the rosette gauge during an exemplary segment of ground locomotion. ε_b corresponds to the element aligned with the bone's longitudinal axis, whereas ε_a and ε_c are rotated 45 degrees clockwise and counterclockwise, respectively.

Chapter 4 (pg. 91-120)

- **Figure 1: Finite element methods.** A) In vivo experimental loading setup simulated by the finite element modelling. Load is applied to the ankle in the direction of the load axis (dashed blue line) while the knee is held fixed in a flexed position. The load axis was rotated by approximately 10° in the posterior direction relative to the bone's axis. B) FEM knee (proximal) and ankle (distal) contact surfaces mimicking the in vivo experimental conditions.
- **Figure 2: Tissue mineral density variation throughout the tibiotarsi** (n=1/genetic strain [2]/housing [3])**.** A) Mean ± standard deviation of the average volumetric tissue mineral density (vTMD, gHA/cm^3) across the tibiotarsus length. For each bone, vTMD was averaged at 1% bone length intervals (denoted $\overline{\text{vTMD}}$), and the plotted mean ± sd is taken across the 6 bones. B) Mean ± standard deviation of the coefficient of variation (CV, %) of $\overline{\text{vTMD}}$ across the tibiotarsus length. For each bone, the CV was calculated at each 1% bone length interval, and then averaged across the 6 bones. C) Midshaft cross section of each bone showing variations in vTMD, and the respective slice histogram beside. Each histogram is annotated with the peak vTMD and the proportion (%) of pixels included in the box, which encompasses pixels below the average mean vTMD assigned to the homogeneous model (0.52 gHA/cm^3).
- **Figure 3: Average mechanical behaviour along the bone length** (n=1 tibiotarsus/genetic strain [2]/housing [3])**.** Striped regions on the plot background indicate the 5% bone length sections across which data is averaged. A) Lateral and anterior aspect views of a tibiotarsus, scaled and aligned to the x axes of plots below. B-C) Mean (line) ± standard deviation (shaded) of the average principal strain (green: tensile, $\bar{\varepsilon}_{max}$; red: compressive, $\bar{\varepsilon}_{min}$) at 5% bone length sections for heterogeneous and homogeneous models, respectively. D-E) Mean of the percent of tensile and compressive elements within each 5% bone-length section for heterogeneous

and homogeneous models, respectively. F-G) Mean ± sd of the average von Mises stress ($\overline{\sigma}_v$) at 5% bone length sections for heterogeneous and homogeneous models, respectively.

- **Figure 4: Principal strain distribution** (n=1 tibiotarsus /genetic strain [2]/housing [3])**.** For each element, the principal strain with the highest magnitude (max (abs)) is shown. Positive strains are tensile, negative strains are compressive. A) Each bone seen from the anterior and posterior aspects. Bones are scaled to a common length. B) Cross sectional strain distributions of an exemplary bone at the 52-64% bone length region, where the transition from convex (proximal) to concave (distal) bending occurs (as visualized from the anterior aspect).
- **Figure 5: Regional variation in stress** (n=1 tibiotarsus/genetic strain [2]/housing [3])**.** Mean ± standard deviation of the average von Mises stress $\overline{\sigma}_v$ in cortical (green), trabecular (blue), and total (cortical ∪ trabecular, black) elements at the proximal metaphysis, midshaft, and distal metaphysis.
- **Figure 6: Homogeneous model strains and stresses in individual bones** (n=1/genetic strain [2]/housing [3])**.** Shaded regions on the plot background indicate the 5% bone length sections across which data is averaged. A) Average principal strain (tensile: $\overline{\varepsilon}_{max}$, compressive: $\overline{\varepsilon}_{min}$) and B) von Mises stress ($\overline{\sigma}_v$) along the length of each bone. For each bone, strains or stress is averaged across elements within 5% bone length sections.
- **Figure 7: Bone morphology along the bone length** (n=6-8 tibiotarsi/genetic strain [2]/housing [3]). For each bone, morphological outcomes were measured at each slice and averaged across 5% bone length sections (plot background stripes). Mean values per group (genetic strain x housing) are plotted. ANOVA p-values for the effects of bone length section (L), genetic strain (GS), housing (H), and all two-way interactions (L*GS, L*H, GS*H) are indicated within each plot. There were no section-dependent effects of housing (L*H); in the cases where there was a significant interaction between bone length section and genetic strain, significant (yellow) and trending (orange) pairwise comparisons between genetic strains are indicated below for each section.
- **Figure 8: Correlation between bone morphology and mechanical properties** (6 bones, n=1 tibiotarsus/genetic strain [2]/housing [3])**.** Mean ± standard deviation (across bones) of the Pearson correlation coefficients for the linear correlation between each morphological parameter and the von Mises stress along the bone length. Correlations were calculated for

whole bone data, as well as separately for each third of the bone length (proximal, middle, and distal 33%). Listed on the left of each plot are the median correlation p-values.

Chapter 5 (pg. 123-149)

- **Figure 1: In vivo loading methodology.** A) Image of a chicken undergoing axial compressive loading to the right hindlimb. The knee (right) is held fixed while load-controlled displacement is applied to the ankle (left). B) Illustration of the loading set up. Load is applied at an angle distal the bone's axis. C) Triangular waveform implemented in the controlled loading protocol. Oscillations between 10 (preload) and 180 (peak load) N are applied, with a 0.1s rest period between each bout, and a 5s rest period every four bouts. Rest insertions have been shown to potentiate the response to loading (Srinivasan et al., 2002, 2003).
- **Figure 2: Effect of controlled loading on diaphyseal cortical, trabecular, and medullary bone.** A) cortical volumetric tissue mineral density, B) cortical thickness, C) cortical area, D) total area, E) cortical area fraction, F) trabecular volumetric tissue mineral density, G) trabecular bone volume fraction, H) trabecular number, I) medullary volumetric tissue mineral density, J) medullary bone volume fraction. Outcomes were measured in a volume of interest centered at the tibiotarsal midshaft, comprising of 5% of the tibiotarsal length. The statistical model used included genetic strain (GS; white or brown), rearing housing (H; Conv, Low, or High), limb (L; non-loaded or loaded), anatomical region (R; A, M, P, L), and all 2-way interactions as predictors, and we present here only significant effects of limb (loading, L) and/or its interaction with the other 3 predictors. Significant pairwise comparison (paired t-test) between non-loaded and loaded limbs are indicated by *, while trending pairwise comparisons are indicated by #. Significance for all tests was set at $p < 0.05$, and trending as $1 < p \leq 0.05$.
- **Figure 3: Histomorphometric measures of bone formation.** A) Exemplary confocal images of a non-loaded and loaded midshaft surface. B) Single labelled surfaces normalized to bone surface were quantified for periosteal and endosteal surfaces of the tibiotarsus midshaft of non-loaded (white) and loaded (blue) limbs. The statistical model used included genetic strain (GS; white or brown), rearing housing (H; Conv, Low, or High), limb (L; non-loaded or loaded), surface (S; periosteal or endosteal) and all 2-way interactions as predictors, and we present here only significant ANOVA effects of limb (loading, L) and/or its interaction with

the other 3 predictors. Significant (normal) and trending (italic) pairwise comparison p-values comparing non-loaded and loaded limbs are indicated. Significance for all tests was set at $p < 0.05$.

- **Figure 4: Serum markers for bone resorption** measured in chickens that underwent loading (blue) and a separate non-loaded control group (white). The statistical model used included genetic strain (GS; white or brown), rearing housing (H; Conv, Low, or High), loading group (L; non-loaded or loaded), and all 2-way interactions as predictors, and we present here only significant ANOVA effects of loading group (L) and/or its interaction with the other 2 predictors. Significant Tukey's post hoc t-test between non-loaded and loaded chickens are indicated by *. Significance for all tests was set at $p < 0.05$.

Chapter 6 (pg. 152-165)

- **Figure 14: Keel bone radiography.** A) Chickens are suspended by their feet for radiograph imaging. They are positioned with the lateral side of their body parallel to the detector. B) Tagged visual analogue scale used for radiograph image scoring of keel fracture severity. Reproduced from Rufener et al., 2018.
- **Figure 15: Ex vivo fracture and deviation scoring.** A) Fractures were classified based on their location within illustrated regions A-E. B) Top image depicts a washboard deviation (pink arrow) and a boot deviation (red arrow). Below, axes about which tip (medial-lateral), ventral (cranial-caudal), and dorsal (ventral-dorsal) deviations occur.
- **Figure 3: Fracture scoring.** A) Histogram of fracture scores with annotated percentage of chickens assigned each score. B) Percentage of total fractures identified that were mild (pink) and moderate (red). C) Histogram of fractures by location, stratified by mild (pink) and moderate (red).
- **Figure 4: Deviation scoring.** A) Histogram of deviation scores with annotated percentage of chickens assigned each score. B) Percentage of total deviations classified as either mild (light blue) and moderate (dark blue). C) Histogram of deviations according to type. *Washboard* (*WB*) and *Boot* are only of mild type, while *Tip*, *Ventral*, and *Dorsal* types are stratified into mild (light blue) and moderate (dark blue).
- **Figure 5: Correlation** between fracture and deviation scores. 2D histogram of fracture and deviation scores, and the Spearman's rho correlation between them.

- **Figure 6: Correlations** between palpation (A and C) or radiograph (B and D) scores and deviation (A and B) or fracture score (C and D). Spearman's correlation coefficient (ρ) and p value noted below each colour bar.

List of Tables

length. Note: Curvature, bone length, and structural parameters are pooled from loaded and non-loaded limbs of the same group of chickens, whereas P1NP is pooled from a group of loaded and another groups of non-loaded chickens.

Abstract

Each year, in Canada, about 25 million commercial laying hens produce more than nine billion eggs, providing affordable, nutrient-dense food for consumers. However, studies have reported up to 97% fracture prevalence in these commercial flocks by the end of their lives, which poses a major welfare concern and has a detrimental impact on the sustainability of the egg-farming industry. Providing increased opportunities for physical activity by housing design is currently the main strategy used to improve welfare and bone health in commercial hens. My research investigates how genetics and experience of physical activity during youth influence bone structure, bone mechanical behaviour, and bone mechanoadaptation, and validates common methods of fracture detection and severity assessment. All studies examine chickens of two commercially relevant genetic strains, who were raised in several different styles of housing that allow for varying types and amounts of physical activity.

First, I characterized the in vivo mechanical behaviour of the tibiotarsi of young chickens during habitual activities, using strain gauge sensors to measure strains engendered in vivo. I found that the tibiotarsus undergoes a complex strain environment and that torsion is the predominant source of mechanical strain. Genetic strain and loading history both influenced the in vivo mechanical behaviour of the bone, with sedentary chickens exhibiting higher in vivo mechanical strain levels compared to those with a more active loading history. These findings provide important context to interpreting bone structural and material properties as determinants of these in vivo strains, and directly informed my third study investigating the bone's mechanoresponse to controlled loading.

Next, I sought to characterize whole bone mechanical behaviour due to axial compressive loading and assess its correlation to bone material and structural properties. I created finite element models mimicking our axial compressive loading model, with either heterogeneous or homogeneous tissue mineral density-derived elastic moduli, and correlated the simulated engendered stresses to measures of bone structure along the length of the bone. I found that mineral density heterogeneity did not influence stress magnitudes or patterns along the bone length, and I identified a set of structural parameters with a strong negative correlation to engendered stress levels. These findings inform future interpretations of the effect of interventions that aim to

improve tissue mineral density as a means to improve bone stiffness and provide a set of candidate stiffening structural parameters that can be targeted by genetic selection.

In a third study, I performed in vivo controlled loading over a 2-week period to study the bone mechanoresponse, using a load waveform protocol that has been shown to successfully elicit bone formation in murine models. Applied load levels were set to engender mechanical strains above the measured habitual levels from my first study. I found that loaded limbs had impaired bone structure and decreased bone surface undergoing formation, compared to non-loaded limbs. These results indicate that the mechanoresponse is different in chickens compared to murine models; future studies are warranted to investigate the osteogenic components of load stimuli in chickens.

My last study focuses on adult chickens during the laying phase and sought to cross-validate commonly used methods of keel bone damage detection and severity assessment. Chickens underwent in vivo palpation to categorize them as either having or lacking fracture(s). Then, bones were radiographed, given a fracture severity score based on this image, and scored again based on visual inspection of the keel. Then, palpation and radiograph scores were correlated against the dissected keel scores. I found that although palpation lacks precision and accuracy, it was still more highly correlated to dissected fracture scores than the radiograph scores.

Overall, the findings from this thesis inform about the determinants of bone health in young female chickens, and what detection and outcome measures of bone health are meaningful and informative in this group. This research also contributes to the general pool of knowledge on bone biomechanics and mechanobiology in birds, and towards understanding bone's form-function relationship.

Resume

Chaque année, au Canada, environ 25 millions de poules pondeuses commerciales produisent plus de neuf milliards d'œufs, ce qui contribue de manière substantielle à l'alimentation quotidienne de la population. Des études ont fait état d'une prévalence de 97 % de fractures dans les troupeaux commerciaux à la fin de leur vie, ce qui pose un problème majeur de bien-être et a un impact négatif sur la durabilité de l'industrie de l'élevage d'œufs, qui doit fournir aux consommateurs des aliments abordables et riches en nutriments. La principale stratégie actuellement utilisée pour améliorer le bien-être et la santé des os des poules commerciales consiste à leur offrir davantage de possibilités d'activité physique grâce à la conception de leur logement. Mes recherches portent sur la manière dont la génétique et l'expérience de l'activité physique au début de la vie influencent la structure osseuse, le comportement mécanique des os et la mécano-adaptation des os, et valident les méthodes courantes de détection des fractures et d'évaluation de leur gravité. Toutes les études portent sur des poulets de deux souches génétiques commercialement pertinentes, qui ont été élevés dans plusieurs styles de logement différents permettant de varier les types et les quantités d'activité physique.

Tout d'abord, j'ai caractérisé le comportement mécanique in vivo du tibiotarse de jeunes poulets au cours d'activités habituelles, en utilisant des capteurs à jauge de contrainte pour mesurer les déformations engendrées in vivo. J'ai constaté que le tibiotarse subit un environnement de déformation complexe et que la torsion est la source prédominante de déformation mécanique. La contrainte génétique et l'historique de la charge ont tous deux influencé le comportement mécanique in vivo de l'os, les poulets sédentaires présentant des niveaux de contrainte mécanique in vivo plus élevés que ceux dont l'historique de la charge est plus actif. Ces résultats fournissent un contexte important pour l'interprétation des propriétés structurelles et matérielles de l'os en tant que déterminants de ces déformations in vivo, et ont directement inspiré ma troisième étude portant sur la réponse mécanique de l'os à une mise en charge contrôlée.

Ensuite, j'ai cherché à caractériser le comportement mécanique de l'os entier sous l'effet d'une charge de compression axiale et à évaluer sa corrélation avec le matériau osseux et les propriétés structurelles. J'ai créé des modèles d'éléments finis imitant notre modèle de charge de compression axiale, avec des modules élastiques hétérogènes ou homogènes dérivés de la densité minérale des tissus, et j'ai établi une corrélation entre les contraintes engendrées simulées et les mesures de la structure osseuse sur la longueur de l'os. J'ai constaté que l'hétérogénéité de la densité

minérale n'influençait pas les amplitudes ou les modèles de contrainte sur la longueur de l'os, et j'ai identifié un ensemble de paramètres structurels présentant une forte corrélation négative avec les niveaux de contrainte engendrés. Ces résultats éclairent les interprétations futures de l'effet des interventions visant à améliorer la densité minérale des tissus en tant que moyen d'améliorer la rigidité osseuse et fournissent un ensemble de paramètres structurels candidats à la rigidité qui peuvent être ciblés par la sélection génétique.

Dans une troisième étude, j'ai effectué une mise en charge contrôlée in vivo sur une période de deux semaines pour étudier la réponse mécanique de l'os, en utilisant un protocole de forme d'onde de charge qui s'est avéré efficace pour provoquer la formation d'os dans des modèles murins. Les niveaux de charge appliqués ont été fixés de manière à engendrer des contraintes mécaniques supérieures aux niveaux habituels mesurés lors de ma première étude. J'ai constaté que les membres soumis à une charge présentaient une structure osseuse altérée et une diminution de la formation de surface osseuse par rapport aux membres non soumis à une charge. Ces résultats indiquent que la mécanoréponse est différente chez les poulets par rapport aux modèles murins ; des études futures sont justifiées pour étudier les composants ostéogéniques des stimuli de charge chez les poulets.

Ma dernière étude porte sur des poules adultes pendant la phase de ponte et vise à valider de manière croisée les méthodes couramment utilisées pour détecter les lésions de l'os de la carène et en évaluer la gravité. Les poulets ont subi une palpation in vivo qui a permis de les classer en fonction de la présence ou de l'absence de fracture(s). Ensuite, les os ont été radiographiés, un score de gravité de la fracture leur a été attribué sur la base de cette image, et un autre score a été attribué sur la base d'une inspection visuelle de la quille. Les résultats de la palpation et de la radiographie ont ensuite été mis en corrélation avec les résultats de la quille disséquée. J'ai constaté que même si la palpation manque de précision et d'exactitude, la corrélation entre les scores de fracture disséquée et les scores de radiographie est plus forte.

Dans l'ensemble, les résultats de cette thèse nous renseignent sur les déterminants de la santé osseuse chez les jeunes poulets femelles et sur les mesures de détection et de résultats de la santé osseuse qui sont significatives et informatives pour ce groupe. Cette recherche contribue également à l'ensemble des connaissances sur la biomécanique osseuse et la mécanobiologie chez les oiseaux, et à la compréhension de la relation forme-fonction de l'os.

Acknowledgements

First and foremost, I would like to thank my supervisor, Dr. Bettina Willie. Since joining her lab as a young inexperienced undergraduate student, she has kindly and dedicatedly mentored me, taught me most of what I know about bone and how to conduct research, and so often inspired me. I am extremely lucky to have had the opportunity of working with her.

Next, I'd like to acknowledge my PhD committee members: Dr. Russell P. Main, Dr. Tina Widowski, and Dr. Pierre Moffatt. Thank you to Dr. Main, who with rigor and attention to detail taught me about conducting animal experiments and about bone biomechanics. Thank you to Dr. Widowski, who guided me as I dove into the world of poultry science and animal welfare, gave me invaluable feedback, and warmly welcomed me during my visits to the University of Guelph and trips to poultry conferences. And thank you to Dr. Moffatt for his encouragement and for challenging me to think outside the box.

Thank you to all the co-authors that I have had the pleasure of working with and learning from, especially Dr. Ana Rentsch. Catherine Julien, a pillar of the Willie lab, merci de m'avoir aidée à planifier et à réaliser des expériences, et de soutenir tous mes besoins en matière d'administration et de fournitures. To the rest of my lab mates past and present: all the time spent with you over these years in the lab (or over zoom…) discussing about bones and problem solving has been without a doubt the highlight of this whole experience. Special shoutout to Jack, David, and Taylor – your friendship has been such a meaningful outcome from this.

Thank you to Prof. Robert Funnell, Prof. Allen Ehrlicher, Pina Sorrini and Sabrina Teoli form the Biomedical Engineering department, the McGill animal care committee, Alain Diotte from McGill's poultry facility, the staff at the RI-MUHC molecular imaging lab and the Shriners histology lab, Patricia D'Iorio, and to the maintenance staff at the Shriners hospital (dissecting feathered animals can get messy!).

Last but certainly not least, thank you to my parents and family – given and chosen – for your care, love, and unwavering support. Any accomplishment of mine is also yours.

Contributions to Original Knowledge

The overarching theme of the research presented in this thesis is the investigation into determinants of skeletal health in the commercial egg-laying hen population: I characterized structural, mechanical, adaptive features of the bones of commercial egg laying (female) chickens and elucidated how these features are influenced by genetic strain and loading history. This knowledge serves to inform farmers about practices that can improve the bone health of their flocks and subsequent research as to what detection and outcome measures of bone health are meaningful and influential in chickens.

In the first study (Chapter 4) I characterized the in vivo mechanical behaviour of the hindlimb's tibiotarsi of young chickens. I measured the mechanical strains engendered at the tibiotarsus during a range of habitual activity types. I found that, in vivo, the tibiotarsus undergoes a complex loading environment comprised of axial compression, bending, and torsion, with torsion being the predominant source of mechanical strain. Genetic strain and loading history both influenced the in vivo mechanical behaviour of the bone, and sedentary chickens generally exhibited higher in vivo mechanical strain levels compared to those with a more active loading history. These findings provide important context to interpreting bone structural and material properties as determinants of these in vivo strains, and directly informed our subsequent study investigating the bone's mechanoresponse to controlled loading.

Next (Chapter 5), I characterized whole bone mechanical behaviour due to axial compressive loading and assessed its correlation to bone material and structural properties. I found that variations in tissue mineral density of up to 200mgHA/cm^3 did not influence stress levels or patterns along the bone length. Furthermore, I found a strong negative correlation between engendered stress levels and a variety of cross-sectional structural parameters. Stress magnitude, but not patterns along the bone length differed between genetic strain and loading history groups. These findings inform future interventions aimed at increasing tissue mineral density as a means to improve bone strength and provide a set of candidate stiffening structural parameters that can serve as targets to prevent fracture.

In a third study (Chapter 6), I characterized the bone mechanoresponse to controlled in vivo loading in these chickens. I surprisingly found that loading had a minimal effect on the bones' microstructure, and where present, the effect was detrimental – loaded limbs had impaired bone

microstructure compared to non-loaded limb. This reveals that the bone mechanoresponse is different in chickens compared to murine models, highlighting the need for further research into these differences.

Lastly (Chapter 7), I sought to cross-validate three commonly used methods of detecting and quantifying levels of damage in keel bones – in vivo palpation, radiography, and visual inspection and scoring of dissected bones. I found that although palpation (the most cost- and time-effective method) lacks precision, accuracy, and underestimates the number of fractures, it has a significant and strong positive correlation to fracture severity, more so than radiograph image-based scores, which require more time and equipment to perform.

Aside from these specific, primary applications, this research also contributes to the general pool of knowledge on bone biomechanics and mechanobiology, which is sparse in chickens and avian species, particularly in comparison to data from mammalian species.

Author Contributions

Chapter 3: In vivo mechanical behaviour of the tibiotarsus of young egg-laying hens during physical activity

Published in *Bone*, 2024, under the title "Breed and loading history influence in vivo skeletal strain patterns in pre-pubertal female chickens"

- *Isabela Vitienes*: conceptualization, investigation, formal analysis, writing (original draft),
- *Nicholas Mikolajewicz*: formal analysis, writing (review and editing)
- *Seyedmahdi Hosseinitabatabaei:* investigation, writing (review and editing)
- *Alice Bouchard:* investigation, writing (review and editing)
- *Catherine Julien:* investigation, writing (review and editing)
- *Gabrielle Graceffa*: investigation, writing (review and editing)
- *Ana Rentsch*: investigation, writing (review and editing)
- *Tina Widowski*: funding acquisition, supervision, writing (review and editing)
- *Russell P. Main*: funding acquisition, supervision, writing (review and editing)
- *Bettina M. Willie*: conceptualization, funding acquisition, supervision, investigation, formal analysis, writing (review and editing)

Chapter 4: In vivo mechanical behaviour of the tibiotarsus of young egg-laying hens during controlled loading

In submission at *Bone reports*, under the title "Tissue mineral density heterogeneity did not influence the in vivo mechanical behaviour of chicken tibiotarsi"

- *Isabela Vitienes:* conceptualization, investigation, formal analysis, writing (original draft)
- *Catherine Julien:* investigation, writing (review and editing)
- *Russell P. Main*: funding acquisition, supervision
- *Ana Rentsch:* investigation, writing (review and editing)
- *Tina Widowski:* funding acquisition, supervision, writing (review and editing)
- *Sara Checa:* conceptualization, supervision, writing (review and editing)
- *Bettina M. Willie:* conceptualization, funding acquisition, supervision, investigation, formal analysis, writing (review and editing)

Chapter 5: Tibiotarsal mechanoresponse to in vivo controlled loading

In preparation for submission, under the title "In vivo controlled loading impaired bone mineral density and microstructure of young female chicken tibiotarsi"

- *Isabela Vitienes*: conceptualization, investigation, formal analysis, writing (original draft)
- *Mayumi Umebayashi:* investigation, writing (review and editing)
- *Annie Mao:* investigation, writing (review and editing)
- *Catherine Julien:* investigation, writing (review and editing)
- *Nabhaan Farooqi:* investigation, writing (review and editing)
- *Ana Rentsch:* investigation, writing (review and editing)
- *Russell P. Main:* funding acquisition, supervision
- *Tina Widowski:* funding acquisition, supervision, writing (review and editing)
- *Bettina M. Willie:* conceptualization, funding acquisition, supervision, investigation, formal analysis, writing (review and editing)

Chapter 6: Validation of keel bone damage scoring

In preparation for submission, under the title "In vivo palpation based fracture detection correlates to ex vivo fracture severity score"

- *Isabela Vitienes*: conceptualization, investigation, formal analysis, writing (original draft)
- *Ana Rentsch:* investigation, writing (review and editing)
- *Hanna Gonzalez:* investigation, writing (review and editing)
- *Matthew Angoh:* investigation, writing (review and editing)
- *Tina Widowski:* conceptualization, funding acquisition, supervision, writing (review and editing)
- *Bettina M. Willie:* conceptualization, funding acquisition, supervision, investigation, formal analysis, writing (review and editing)

Non-thesis publications and studies in progress

- Willie BM, Zimmermann E, **Vitienes I,** Main RP, Komarova SV, Bone adaptation: safety factors and load predictability in shaping skeletal form, *Bone*, 21;131:115114, 2020.
- van Tol A, Schemenz V, Wagermaier W, Roschger A, Razi H, **Vitienes I**, Fratzl P, Willie BM, Weinkamer R, The mechanoresponse of bone is closely related to the osteocyte lacunocanalicular network architecture, *Proceedings of the National Academy of Sciences,* 22;117(51):32251-32259, 2020.
- Rentsch AK, Harlander A, Siegford JM, **Vitienes I**, Willie BM, Widowski TM, Rearing laying hens: the effect of aviary design and genetic strain on pullet exercise and perching behavior, *Frontiers in Animal Science*, 4: 1176702, 2023.
- Hosseinitabatabaei S, **Vitienes I**, Rummler M, Birkhold A, Rauch F, Willie BM, Non-invasive quantification of bone remodeling dynamics in adults with osteogenesis imperfecta using timelapse HR-pQCT, *Journal of Bone and Mineral Research*, In revision.
- Schemenz V, Rummler M, van Tol A, **Vitienes I**, Thiele T, Hartman MA, Burghammer M, Fratzl P, Weinkamer R, Willie BM, Wagermaier W, Correlations between osteocyte lacuna-canalicular network and material characteristics in healthy and mechanically stimulated murine cortices, *Journal of Structural Biology,* In preparation.
- **Vitienes I***, Ross E*, Widowski T, Willie BM, The effect of early rearing environment on skeletal traits in laying hen pullets, *Bone*, In preparation (* shared first authorship)
- **Vitienes I**, Beatrice Steyn, Michal Kulasek, Taylor DeVet, TBD, Svetlana Komaraova, Willie BM, Meta analysis and systematic review investigating the effect of non-invasive in vivo controlled loading on bone structure and (re)modeling dynamics, *TBD*, Study ongoing.
- **Vitienes I**, Tina Widowski, Paul Zaslansky, Willie BM, Preventing bone fractures in chickens: high contrast high resolution imaging of osteocyte lacunae within the calcium reservoir, medullary bone, Study ongoing.
- **Vitienes I**, Setareh Khorshidparast, Tina Widowski, Willie BM, Investigating the etiology of keel bone fragility: effect of age on keel bone structure and (re)modeling dynamics, Study ongoing.
- Hadil Jallad, **Vitienes I**, Pierre Moffat, Craniofacial and tibial morphology alterations in a mouse model for osteogenesis imperfecta, Study ongoing.

Chapter 1 – Introduction

Osteoporosis is a condition characterized by bone weakness, attributed to below-optimal levels of bone mineral density, bone volume, and/or functionally impaired bone structure. This condition is not exclusive to humans and has been a major concern in the commercial egg farming industry. Osteoporosis and its associated high fracture incidence was first observed in caged laying hens in the 1950's, and is thought to be influenced by the lack of dynamic load bearing activity associated with caged-housing. In addition, high calcium demands associated with genetic selection to increase the rate of egg-laying in commercial genetic strains (calcium is sourced from bones for the mineralization of the eggshell) is also a contributor to osteoporosis in hens.

Many other factors both genetic and environmental may contribute to the development of osteoporosis, and often do, making it a challenging condition to treat and prevent. Detection is also challenging (osteoporosis is commonly referred to as the "silent" disease), requiring an understanding of bone mechanical behaviour, how it is influenced by bone structure and material properties, and the ability to assess this in vivo. Understanding the etiology of this condition and being able to detect it are necessary means to the ultimate end goal, which is developing treatment and prevention interventions to improve the welfare of these animals.

Osteoporosis continues to be a prevalent disease affecting millions of humans despite being the focus population of considerable research efforts into this condition; much less is known about bone biology, bone adaptation, and determinants of bone health in avian species, such as chickens. The work presented in this doctoral thesis contributes to filling this gap in knowledge, providing information about 1) the etiology of bone fragility in chickens, 2) meaningful outcome measures for detection of bone fragility, and 3) the effects of mechanical stimuli as an intervention to treat and prevent bone fragility.

The next chapter (chapter 2) gives a detailed background on the biological, contextual, and methodological concepts, which are the pillars for the subsequent chapters (3-6) that present four experimental studies. All studies focused on female (egg-laying) chickens of two commercially relevant genetic strains, that were raised in various environments (housing systems) that favor different amounts/types of physical activity. Across all studies, genetic strain and loading history (housing environment) are considered as independent variables, to assess their influence on the

measured outcomes in addition to characterizing these outcomes themselves. The first three studies are concerned with the tibiotarsus (functionally similar to the mammalian tibia), whereas the last study shift focus towards the keel bone (functionally similar to the mammalian sternum).

The first study (chapter 3) aimed at measuring and characterizing the mechanical stimuli that the tibiotarsus is subject to habitually, to understand the mechanical environment to which the bone structure and material properties are tailored. The next study (chapter 4) investigates how sensitive the bone's mechanical behaviour is to variations in bone mineral density, and how a variety of outcomes, which describe the shape and structure of bone relate to its mechanical behaviour. The third study (chapter 5) investigates bone adaptation, using information learnt in study 1 (habitual levels of mechanical stimuli) to study the bone's mechanoresponse to above-habitual mechanical strain levels. The last study assesses the validity of various commonly used measures of keel bone fracture severity. The final chapters (6-7) present an overarching discussion of the findings of these four studies and overall conclusions.

Chapter 2 – Background

2.1 Subject: Bone

2.1.1 General bone biology background

Bones evolved over 500 million years ago in aquatic animals (Eames et al., 2012). Before this point, mineralized tissues existed in the form of exoskeletons, which limited animal body size, restricted body surface sensation, and limited movement and locomotion (Wagner & Aspenberg, 2011). The transition towards inner body skeletal elements was a major adaptive advantage in terms of locomotion. It permitted the development of a strong muscular system, improving locomotor efficiency and speed, and therefore expanding the radius of habitation of these early vertebrates (Wagner & Aspenberg, 2011). At this point, the bone's ability to serve as a mineral reservoir was less important, because minerals were readily accessible, dissolved in their surrounding water; in fact, it is thought that mineralized tissues evolved as an adaptation to deal with unwanted excessive mineral aggregation which was occurring due to high marine calcium concentrations present at the time (Wagner & Aspenberg, 2011). With the evolution of tetrapods and the transition from water to land, vertebrates were no longer readily exposed to large amounts of dissolved calcium in their surroundings – instead, calcium became available only at the time of feeding, resulting in large, frequent fluctuations in amounts of circulating calcium. Because calcium is a key signaling molecule in all cellular life (Krebs et al., 2015), mechanisms in the gut, kidneys, and bones began to evolve to control the movement of calcium and ensure its continuous availability for cellular signaling, and bone began to assume its secondary role as a calcium reservoir.

At its base, bone tissue is made up of a composite material: elastic collagen fibers which form a scaffold upon which crystals of carbonated hydroxyapatite aggregate. These mineralized fibers are then arranged into a complex architecture with motifs that vary across hierachnical length scales and differ spatially within and and across anatomical sites depending on the specific local in vivo mechanical environment (G. C. Reilly & Currey, 1999; Reznikov et al., 2018). This composition and hierarchical design produces a tissue that is stiff yet flexible and tough, capable of withstanding high forces. However, this composite tissue is only a part of what makes up bone

altogether – approximately 10% of bone volume consists of cells: osteoblasts, osteoclasts, and osteocytes. The osteocytes comprise 90% of this cell population (L. F. Bonewald, 2011), and reside within small cavities in the bone termed lacunae, forming a dense network (Fig. 1). Osteocyte lacunae are connected by even smaller channels, canaliculi, through which osteocytes extend their dendritic processes and come into contact with other neighbouring osteocytes, allowing them to communicate with each other (L. Bonewald, 2018) (Fig. 1).

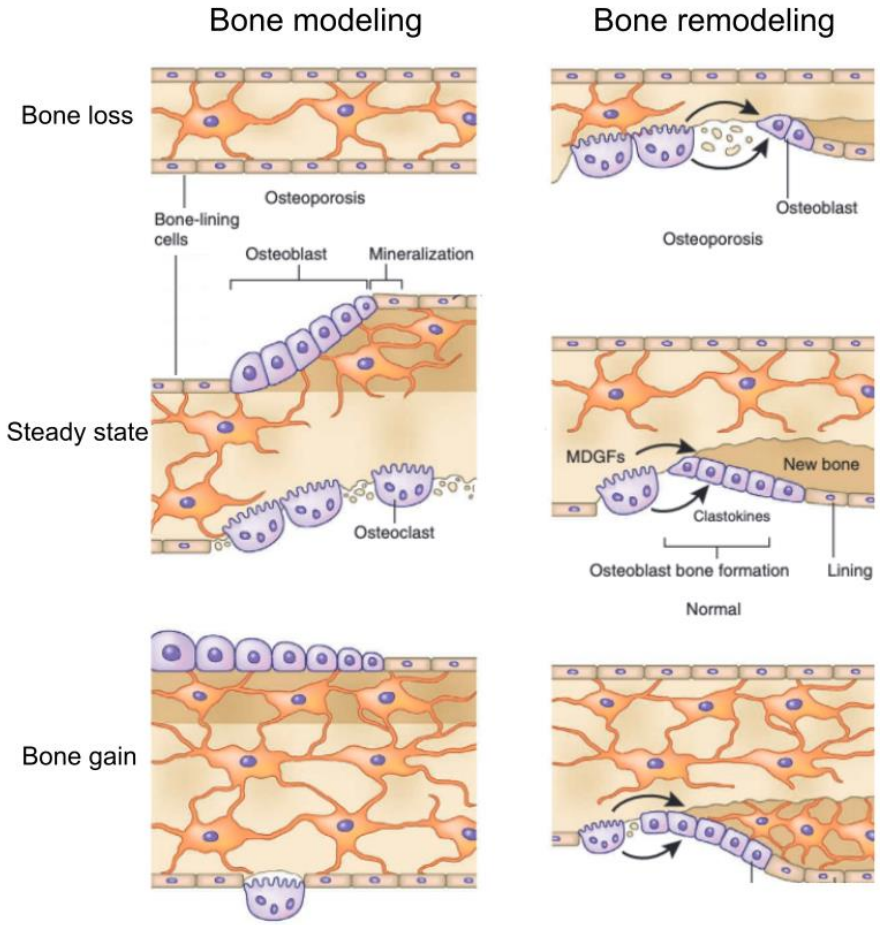

Figure 1: Bone modeling and remodeling. Both processes can result in bone loss, quiescence (steady state), or bone gain. When bone formation and resorption are balanced (whether they are coupled as in remodelling or spatially separate as in modeling), bone volume is at steady state. When these two processes become unbalanced, bone loss (resorption > formation) or gain (formation > resorption) results. Adapted with permission from Baron & Kneissel, 2013.

By means of this connectivity osteocytes are able to carry out their arguably main function: orchestrating bone adaptation (Schaffler & Kennedy, 2012). A hallmark feature of bone, of

significant interest in this thesis, is its ability to adapt to mechanical stimuli. This was first officially recognized by Julius Wolff in the 1800's (Wolff, 1892), who stated that bones were able to alter their internal structures according to mathematical rules to decrease internal stresses. Forces derived from muscle contractions or ground reaction forces act on the bone and cause it to deform. These deformations (and/or downstream signals produced by the deformation) are sensed by the osteocytes, which then convert this mechanical stimulus into a biochemical one, interpret the signal, and subsequently communicate with effector cells to coordinate the tailored mechanoadaptive response (Willie, Zimmerman, et al., 2020).

The effector cells are osteoblasts, bone-forming cells, and osteoclasts, bone-resorbing cells. Upon receiving signals from osteocytes, osteoblasts and/or osteoclasts will act to increase or decrease bone volume or alter the bone shape with a net zero change in bone volume, via a process called bone modelling. Modeling is characterized by the locally independent activity of osteoblasts and osteoclast (Fig. 1), although they may be active simultaneously at different locations (e.g. bone formation at the periosteal surface and bone resorption at the endosteal surface to widen the bone and increase its polar moment of inertia). During adulthood, bone modelling predominantly occurs as a means of bone adaptation to mechanical stimuli, whereas during youth, it is the main process by which bones grow longitudinally and radially (Burr, 2019).

Osteoblasts and osteoclasts do not always act to adapt to mechanical stimuli; they also work to renew bone tissue in a process called bone remodelling (Fig. 1). Here, their activity is spatially coupled; a team of osteoclasts and osteoblasts, called the bone multicellular unit (BMU) (Frost, 1969), tread along the bone surface or through canals found within the bone and sequentially resorb (osteoclasts) and then form (osteoblasts) bone. Bone remodelling serves to renew bone tissue and is common throughout all stages of life, occurring most frequently at the endosteal, periosteal, and trabecular surfaces, and, in certain species, intracortically. During youth and at the beginning of adulthood, bone remodelling does not alter overall bone mass, but with aging there is a shift in the balance between formation and resorption favouring resorption and thus leading to a net decrease in bone volume (Dempster & Lindsay, 1993). Bone remodelling can be spatially targeted or stochastic (Burr, 2019). One trigger of targeted bone remodelling is microdamage (Burr et al., 1985), where small cracks accumulate due to repeated cycles of loading or loading at high levels. Microdamage is to a certain extent beneficial because the microcracks

dissipate energy as the loading occurs and therefore prevent overt fracture (Pezzotti & Sakakura, 2003), so long as they are repaired before they coalesce into larger cracks which do impair bone structural integrity.

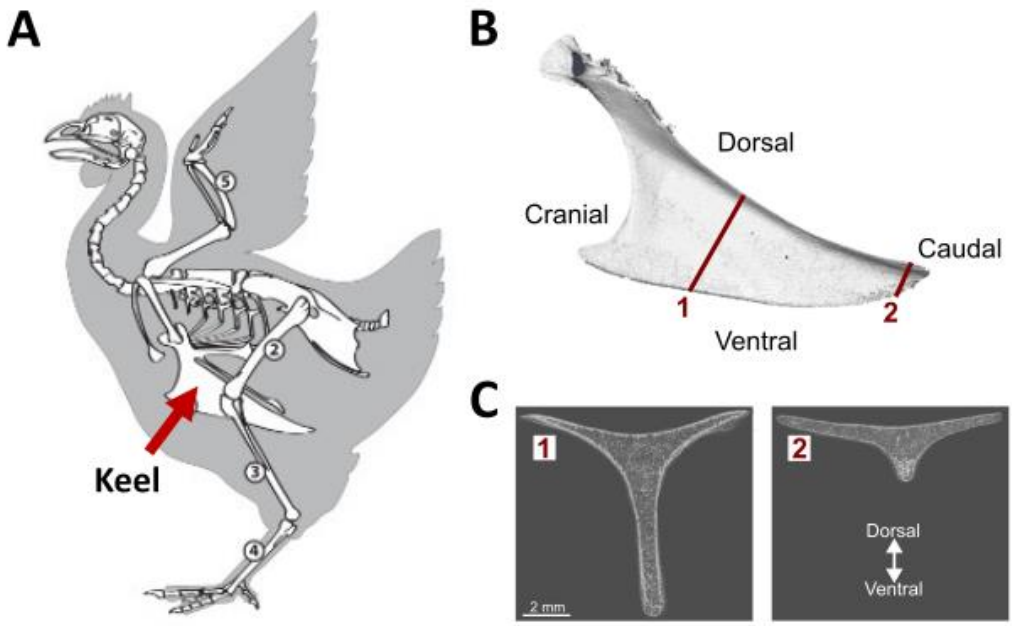

Figure 2: Chicken keel bone. A) Whole chicken skeleton, **B)** Lateral aspect of a keel bone. Anatomical aspects referred to throughout this thesis are annotated, **C)** Cross sections taken at positions 1 and 2 from panel B, showing the characteristic cross-sectional "T" shape of the keel bone.

In mammals and birds, bone grows via two processes: endochondral and intramembranous ossification (Berendsen & Olsen, 2015; Romanoff, 1960). During endochondral growth, an initial scaffold made of cartilage (type X collagen) is deposited by chondrocytes, beginning at a discrete ossification center. The cartilage then becomes mineralized and subsequently remodelled into bone (type I collagen scaffold). Endochondral ossification is the method by which bones elongate. Intramembranous ossification instead does not involve a cartilaginous intermediate stage – bone is directly deposited by osteoblasts on the surface of existing bone or mineralized cartilage. The number and location of ossification centers where endochondral ossification occurs differs across species. Mammalian tibiae begin growing at a primary ossification center at the mid-diaphysis, and later on, secondary ossification centers appear at the proximal and/or distal epiphyses (Burr, 2019). In the avian tibiotarsus, secondary ossification centers do not appear, and bone elongation occurs via bone formation at the proximal and distal ends of the primary ossification center

(Whitehead, 2004a). This distinction may have important implications in terms of growth rates and cessation of growth. In mammals, eventually the epiphyseal ossification centers fuse to the primary ossification center, impeding further growth and therefore providing a reliable way to ascertain that growth has ceased, whereas in birds, whether growth completely ceases or continues throughout adulthood but at a decreased rate compared to youth remains unclear, and likely varies between avian species. Growth and ossification patterns of the keel bone (Fig. 2) have yet to be described for chickens (*Gallus gallus*). In other avian species, a cartilage scaffold grows, and mineralization initiates at multiple ossification centers (Hogg, 1980). The number, location, and timeline of appearance of these ossification centers in the chicken keel remains unknown, but complete ossification of the keel bone of females has been shown to be achieved during adulthood at 30-40 weeks (Buckner et al., 1948, 1949), and is influenced by genetic (Fawcett et al., 2020) and environmental (T. M. Casey-Trott, Korver, et al., 2017a; Fawcett et al., 2020) conditions.

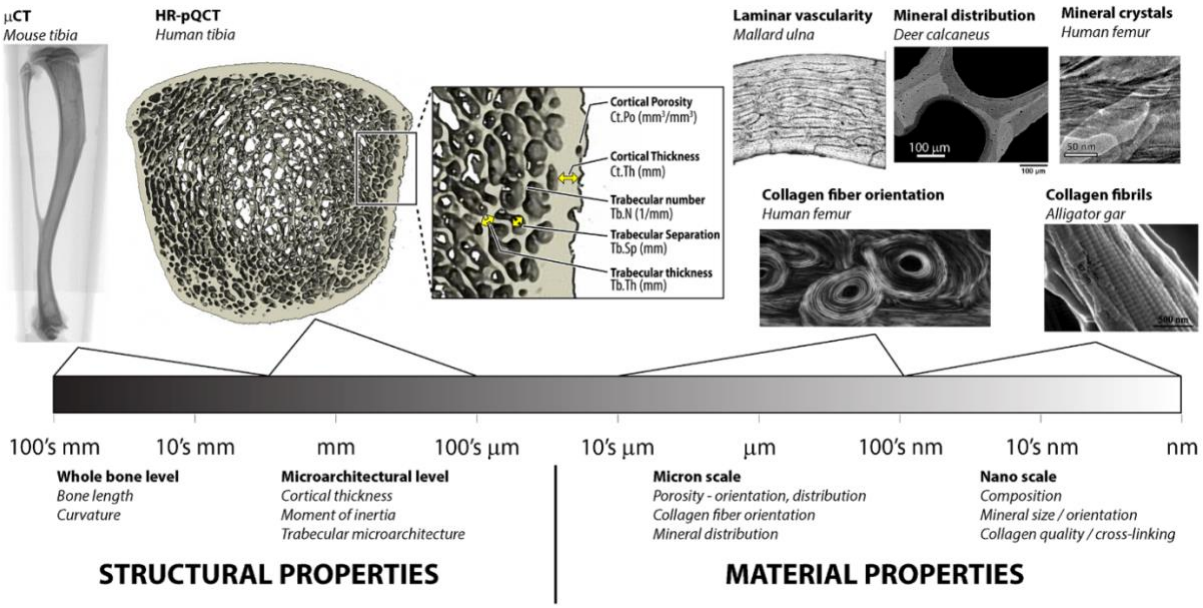

Figure 3: Bone's hierarchical structure. Characteristics across different length scales can be grouped into structural and material properties Willie et al., 2020.

Bone is hierarchically structured (Fig. 3), with specific organizational features at different length scales that compound to produce a complex, tough structure made up of an anisotropic material that deforms viscoelastically. At the micron-level, mineralized collagen fibres can exist organized into discrete sheets or lamellae that are arranged along surfaces of the bone or concentrically surrounding vascular channels. The orientation of lamellae with respect to the

bone's long axis varies regionally seemingly tailored to local in vivo mechanical behaviour; for example, bone regions that habitually undergo tensile strain have been shown to have lamellae parallel to the principal tensile axis, whereas regions under compression have lamellae oriented at an angle from the principal compressive axis (Riggs, Lanyon, et al., 1993; Riggs, Vaughan, et al., 1993; Skedros et al., 2004, 2006, 2007). Space between lamellae and within small spaces between arranged lamellar collagen fibers are filled with disordered collagen fibers (Reznikov et al., 2014) to makeup a compact volume. When time for precise arrangement of collagen fibres is not available, such as during rapid growth or bone healing, bone tissue completely composed of disordered fibers is produced instead, called woven bone (Shapiro & Wu, 2019). Woven bone therefore is mechanically inferior to lamellar bone (J. D. Currey, 2003) and under physiological conditions is usually eventually remodelled into lamellar bone.

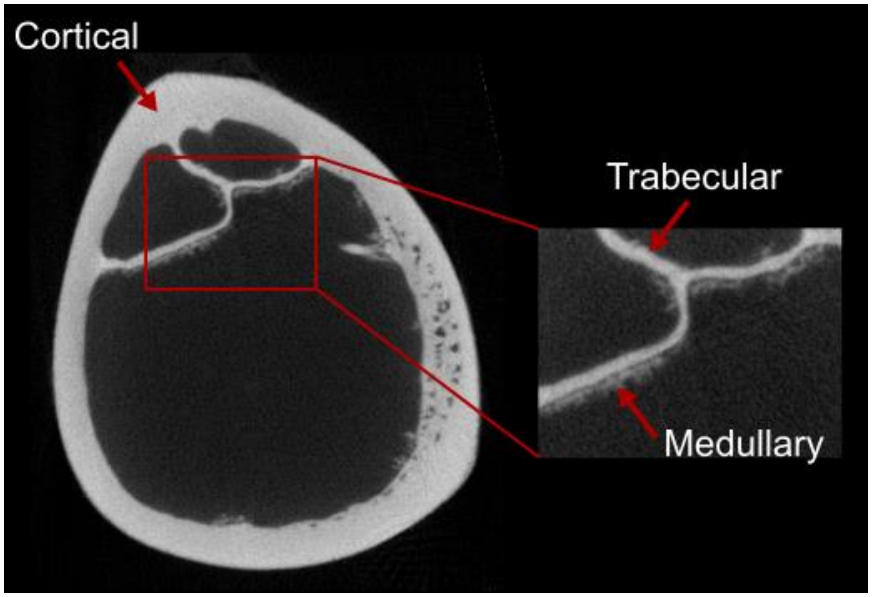

Figure 4: Cortical, trabecular, and medullary bone at the tibiotarsus midshaft of a 16 week old (onset of puberty) chicken. MicroCT image taken at 9 µm isotropic voxel size. Medullary bone can be seen as a less mineralized (darker grey colour), with a more disordered/less compact appearance, lining regions of the endosteal surfaces.

Macroscopically, lamellar bone generally makes up cortical and trabecular bone (Fig. 4). In female birds, an additional type of bone termed medullary bone develops at the onset of sexual maturity (C. Dacke, 1979), characterized by its dynamic fluctuations which temporally correlate with the oviposition cycle (C. G. Dacke et al., 1993; Kerschnitzki et al., 2014). It is therefore thought to function as a labile source of calcium for the mineralization of the eggshell. Medullary

bone appears to consist of small "trabecular-like" structures which are found at endosteal surfaces and within intracortical pores, composed of woven-like bone (Bonucci & Gherardi, 1975). Compared to cortical and trabecular, medullary bone is more calcified, with a higher apatite-to-collagen ratio and contains more non-collagenous proteins, proteoglycans, and carbohydrates (Prondvai & Stein, 2014). However, medullary bone often appears less mineralized (lower greylevel) in tomographic images (Fig. 4), due to its small size and partial volume effects. Further characterization of the cellular and molecular mechanisms responsible for the spatial and temporal dynamics of medullary bone formation are warranted.

Skeletal phenotype is shaped in part by adaptive plasticity but also by genetics. It has been shown that 45-92% of the population-wide variability in skeletal phenotype is attributed to genetics, the rest being determined by environmental factors. Some genetic effects can be in the form of single-gene mutations that cause large effects on bone traits, but genetic variation can also come in the form of inherited heterogeneity in the expression of a large set of genes that results in smaller scale variability in complex traits (Burr, 2019).

Hormones play an important role in bone metabolism. Particularly notable is estrogen, which has been shown to be a major regulator of bone metabolism through its pleiotropic effects on bone cells (Khosla et al., 2012) – estrogen inhibits osteoclast bone resorption (Kameda et al., 1997), regulates bone formation by osteoblasts (Bain et al., 1993; Chow et al., 1992; Samuels et al., 1999), and maintains osteocyte viability (Florencio-Silva et al., 2018). In female chickens specifically, there is a marked increase in estrogen from 16-20 weeks of age (Johnson & van Tienhoven, 1980; Whitehead & Fleming, 2000) which correlates with the onset of the formation of medullary bone at approximately 16 weeks of age. Concrete evidence as to the mechanism by which estrogen is involved in medullary bone formation is lacking, but it is known that the formation of medullary bone is estrogen-dependent (Beck & Hansen, 2004; C. G. Dacke et al., 1993). Studies have shown that administration of estrogen can elicit medullary bone formation in male birds (Landauer et al., 1941; Miller & Bowman, 1981). Moreover, oscillations in serum levels of estrogen coincide temporally with the oviposition cycle (Etches & Cheng, 1981; Johnson & van Tienhoven, 1980).

A widely cited study from the 90's used fluorochrome labels to track bone formation in femurs of pre-pubescent and sexually mature female chickens (see section 2.3.4 for details about this methodology). They observed that, in contrast to the immature chickens which exhibited bone

formation at periosteal and intracortical surfaces, mature femurs were devoid of any periosteal and intracortical bone formation and instead had substantial medullary bone formation (Hudson et al., 1993). Other authors have since interpreted these findings as proof that, in response to the marked increase in estrogen following the onset of lay in chickens, osteoblasts undergo a switch in the type of bone they deposit and thereafter only produce medullary bone, while osteoclasts continue to resorb bone indiscriminately. If this were the case it would lead to a decrease in cortical and trabecular bone, rendering the bone weaker and explaining the observed osteoporotic phenotype seen in commercial laying hens, which is progressive throughout the lay phase. However, there have been no studies that have proven this – that osteoblasts undergo a switch and only form medullary bone during lay, and that said change in osteoblast behaviour is directly triggered by estrogen. Further investigations into medullary bone-forming osteoblast behaviour by histomorphometry, histology, and single-cell RNA sequencing are warranted. Moreover, efforts to stimulate cortical and trabecular bone formation as interventions to address osteoporosis in this population should not be discarded on the basis that this type of bone cannot be formed during lay.

2.1.2 Changes to bone with age

Most of what is known about the aging of bone has been gleaned from research on mammalian models, but it is reasonable to suspect that certain themes are so inherent to the structural function of bone that they are widely conserved across other vertebrate species, including birds. During growth, long bones grow longitudinally (endochondral ossification at growth plate(s)) and cross-sectionally by progressive periosteal expansion and endosteal bone resorption/quiescence. This expansion increases the bone's polar moment of inertia, drastically increasing the bone's ability to resist bending and torsional shear. During adulthood, this expansion continues, but the rate of endosteal resorption slowly overcomes that of periosteal formation, resulting in a progressive decrease in cortical bone thickness which weakens the bone (Birkhold et al., 2014). Mechanical loading has been shown to attenuate this endosteal resorption, therefore mitigating this age-related impairment in bone strength (Birkhold et al., 2016). Aging also affects bone material quality which compounds the structural deterioration of bone (Boskey & Coleman, 2010). Studies have shown changes in bone mineral properties, mineral density heterogeneity, collagen cross-linking, water composition, among others, with age (Boskey & Coleman, 2010). The direct link, however,

between the nature of these changes and their effects on bone mechanical properties remains poorly understood.

Effects of aging on bone structure are in part attributed to changes in bone mechanoresponsiveness. In mice, whereas young and adults animals adapt to loading by increased bone formation and decreased bone resorption, loading does not lead to a decrease in bone resorption in elderly mice, therefore decreasing the net positive effect on bone volume (Birkhold et al., 2014; Razi, Birkhold, Weinkamer, et al., 2015). Subsequent studies showed that with age, in vivo loading engenders lower strain stimuli (Willie et al., 2013), suggesting that it is not (only) the mechanoadaptive machinery that is affected by age, but rather that changes in bone material properties influence the way in which the bone deforms, ultimately affecting the stimulus that the mechanoadaptive machinery itself is sensing and responding to. In chickens, aging has been shown to be associated to decreased tibiotarsal trabecular thickness and cortical bone volume, bone volume fraction, and bone mineral density (Yamada et al., 2021). Studies investigating the effects on bone material properties and mechanoadaptation are lacking, as well as studies focusing on aging of the keel bone in particular.

2.1.3 Effects of exercise and loading on bone

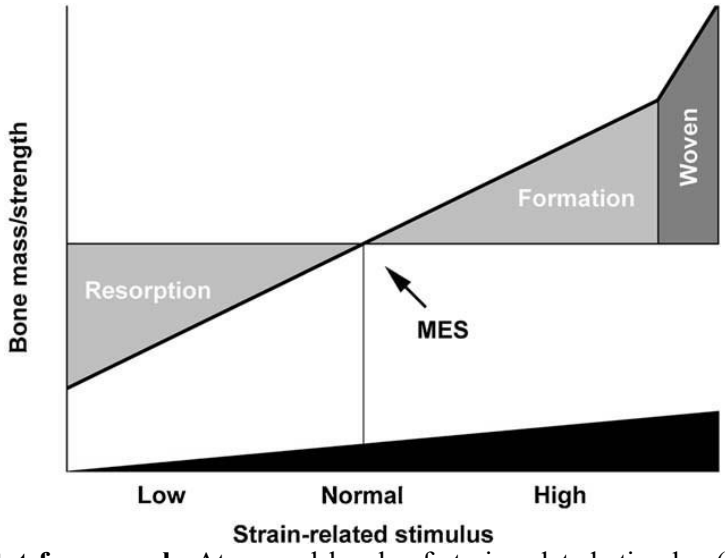

Figure 5: Mechanostat framework. At normal levels of strain-related stimulus (or minimum effective strain, *MES*) no net formation or resorption occurs. Low and high levels of strain related stimulus result in bone resorption or formation, which alters bone mass and thus bone strength. When strain-related stimulus is very high, woven instead of lamellar bone is formed. This figure has been adapted from Sugiyama et al., 2012 with permission.

The so-called mechanostat framework, inspired by the household thermostat, describes the relationship between a mechanical stimulus and the mechanoresponse it elicits. It states that bone adaptation is a self-regulating system; there is a level of strain-related stimulus to which the bone is habituated, and when the strain stimulus increases or decreases from this set point, net bone formation or bone resorption will occur, respectively, to adjust the bone's volume and re-establish the set strain (Fig. 5) (Frost, 1987). This is an oversimplification of a very complex process, and many experiments have since shed light onto features of the mechanical stimulus other than its magnitude that influence the bone's response (see paragraph below, osteogenic components of strain) (Lanyon & Rubin, 1984; Sun et al., 2018; Yang et al., 2017). But what this framework does capture is that the purpose of bone adaptation is optimization – to produce a bone that is just strong enough to resist fracture in loading conditions that it will likely encounter, minimizing the metabolic cost of producing and maintaining this tissue. The main way in which bone mechanoadaptation is studied is by in vivo loading experiments that stimulate a mechanoadaptive response which is then analyzed, either at the level of the outcome of the tissue response (mechanoresponse) or the activity of the cellular mediators (mechanoresponsiveness).

Experimental models that allow the investigator to tightly control the load regime that the animal is subjected to (see section 2.3.5 on extrinsic loading models) have revealed that the bone does not respond to all stimuli equally. First of all, load must be applied dynamically; static loading, even if at otherwise osteogenic magnitudes, does not elicit a mechanoresponse (Lanyon & Rubin, 1984). Given a cyclic stimulus, other parameters that describe the stimulus waveform (Fig. 6) and influence the mechanoresponse are:

1. Number of cycles: Early experiments using a turkey ulna model performed cyclical axial compressive loading and varied the number of load cycles applied during each session, ranging from none to 1800 cycles/day and found that the mechanoresponse was detectable with as few as 4 cycles/day, and plateaued at 36 cycles/day (Rubin & Lanyon, 1984b; Sun et al., 2018; Yang et al., 2017).
2. Cycle frequency and rest insertions: There is a linear increase in the mechanoresponse with increasing cycle frequency (number of cycles per second) up until a certain point, after which there is a plateau (Warden & Turner, 2004). To increase the cycle frequency, the rate of loading and unloading must increase; therefore, it is impossible to untangle

these two variables – cycle frequency and load rate. Interestingly, if the cycle frequency is reduced by inserting rest pauses in between each bout and keeping the load rate fixed, the mechanoresponse is enhanced (short-term rest insertions, Srinivasan et al., 2002). Moreover, if the total number of load cycles per day is held fixed but they are administered in multiple sessions throughout the day as opposed to all at once, the mechanoresponse is also enhanced (Robling et al., 2000; Yang et al., 2017). It is thought that these rest periods, both across short and long time scales, are beneficial because mechanisms responsible for mechanosensation at the cellular level may become saturated, and these rest periods allow for a return to optimal sensitivity.

3. Engendered strain magnitude: The difference between the magnitude of strain engendered and habitual strain levels is positively associated to the magnitude of the mechanoresponse (Rubin & Lanyon, 1985; Sugiyama et al., 2012) as long as the engendered strain is within the lamellar bone formation window and does not cause damage to the bone (Frost, 2004). This is the mechanostat. Recent advances in live osteocyte imaging have showed that there is an exponential relationship between the engendered strain magnitude and the amount of osteocytes responding (Lewis et al., 2017), suggesting that changes in the response magnitude are mediated by changes in the number of responding cells as opposed to changes in the magnitude of each cell's response.
4. Engendered strain rate: The rate at which the bone is strained (με/s) is inextricably related on the magnitude of strain achieved in each cycle (με/cycle) and the cycle frequency (cycles/s) by the equation

$$\text{rate } (\mu\varepsilon/s) = \text{frequency (bouts/s)} \times \text{magnitude } (\mu\varepsilon/\text{bout})$$

such that it is not possible to assess the influence of strain rate independent of frequency and magnitude. When strain rate was increased by increasing the cycle frequency (Mosley & Lanyon, 1998) or the strain magnitude (Turner et al., 1995) the mechanoresponse was enhanced.

5. Engendered strain mode: Bone is locally adapted to strains of a specific mode. If loading produces strain levels that are below habitual magnitudes, but the direction of strain is different, for example the bone is subjected to tensile strain as opposed to habitual

compression, a mechanoresponse will occur (Rubin & Lanyon, 1984b; van der Meulen et al., 2006).

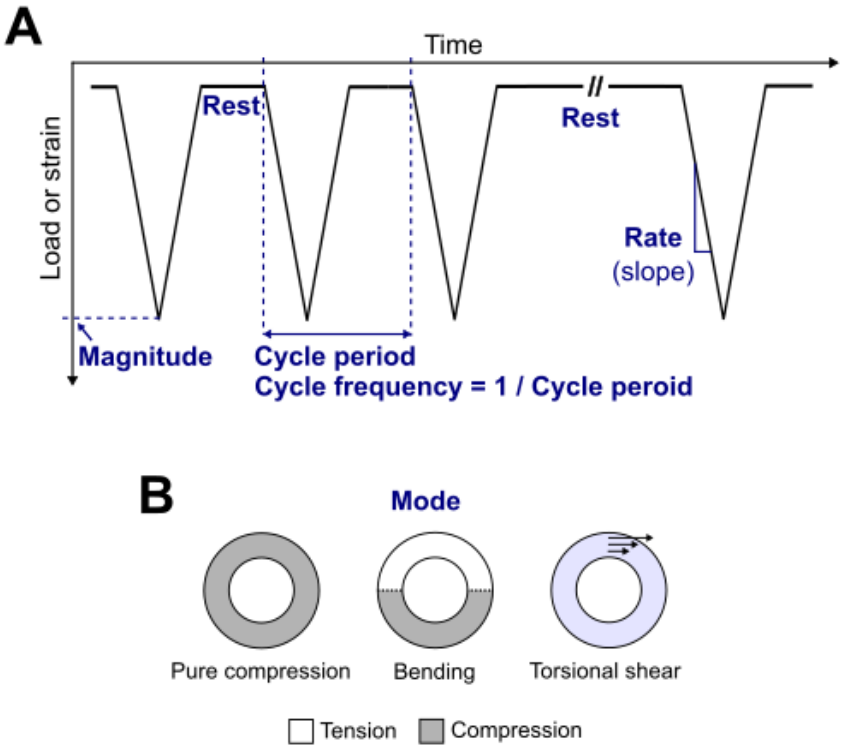

Figure 6: Osteogenic components of mechanical stimuli. A) Idealized load or strain stimulus waveform, depicted as a triangular waveform, with parameters of interest – magnitude, frequency, rate, and rest periods – annotated in blue. B) Independent of the stimulus waveform, the stimulus can be further characterized based on the mode(s) of strain induced, which can be pure compression, bending, shear, or a combination of these.

2.1.4 Bone biomechanics

Whole-bone mechanical behaviour is determined by its stiffness and strength which can be measured from bone load-deformation tests (Fig. 7 A) (Jepsen et al., 2015; van der Meulen et al., 2001). This test consists of applying a continuously increasing force to the bone (ideally such that the mode of engendered strain is similar to what occurs in vivo), while measuring the distance that the force-applying actuator moves, until the bone breaks. These curves reveal that, at the whole-bone level, bone undergoes elastic deformation at low load levels (linear portion of the curve), and that after the so-called yield point, plastic deformations begin to occur (non-linear portion of the curve) until the bone fails at the ultimate load. When deformations occur within the elastic regime, the bone will return to its resting state once the applied load is removed. Conversely, once plastic

deformation is reached permanent damage will occur and remain even after the load is removed. The energy required to break the bone is termed work-to-fracture, and is equal to the area under (integral of) the force-displacement curve.

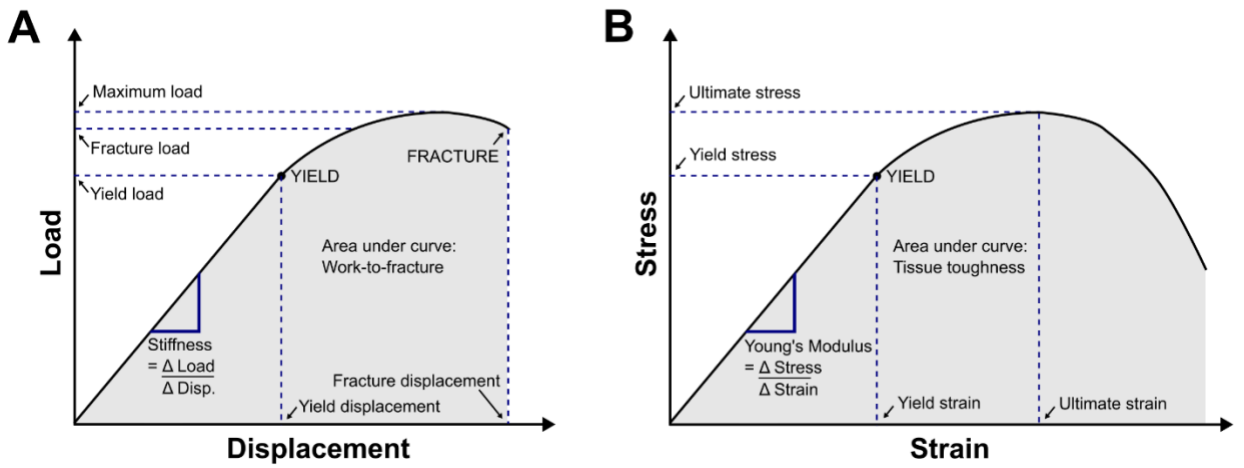

Figure 7: Whole bone and tissue mechanical properties. Both plots have a linear (elastic) and nonlinear (plastic) region. A) Load-displacement curve describing whole bone mechanical behaviour. Bone stiffness id quantified as the slope in the elastic region. Mechanical properties annotated on the curve are a function of both the bone's material and structural properties. B) Stress-strain curve describing tissue-level mechanical properties (bone material properties). Properties annotated on the curve are independent of bone volume and structure.

Force displacement curves provide an overall concise description of the mechanical behaviour of the bone, but often it is of interest to further understand how the bone deforms (strain modes, Fig. 6 B) and the local strains that arise due to loading, as this is the stimulus triggering bone adaptation. In vivo mechanical strains engendered during habitual activities (background strains) are what bones have adapted to withstand across the lifetime of an organism and provides context to understand why certain bones may be shaped/composed a certain way. Background strains can be experimentally measured by surgically attaching strain gauges to bones (see section 2.3.1) and measuring strains while the animal performs whatever activities are of interest to measure (Biewener, 1992). An important design feature of bone that is elucidated from the measurements of background strains is a bone's safety factor (the ratio of yield or failure strain to background strain) which quantifies how overbuilt they are and thus their ability to withstand unexpectedly high loads (Alexander, 1981). As illustrated by the mechanostat theory, bones adapt to be just strong enough to resist fracture in likely loading conditions. So, in a sense, the safety

factor accounts for this notion of what is “likely”. Experiments on bone from a range of species have measured safety factors ranging from 1.4 to 10 (Alexander, 1981; Biewener, 1993).

Interestingly, research shows that not all bones within a skeleton have the same safety factor, and that sacrifices to safety factor may be necessary when there are competing needs for calcium. For example, calcium deprivation-driven bone resorption has been shown to occur disproportionately at certain skeletal sites (Lanyon et al., 1986). It is thought that this process has evolved to minimize the overall impact on the skeletal integrity of the organism. This may explain why in commercial egg-laying hens, who have been genetically selected to produce eggs more frequently thus producing a greater calcium demand on their bones, their keel bone is particularly weakened and susceptible to fracture – as natural selection is concerned, the chickens are able to survive (albeit likely with substantial pain and discomfort) and reproduce while having keel bone fractures, whereas perhaps the fracture of long bones or vertebrae would have more of an impact on survival and reproduction. This theory is supported by the fact that commercial hens that are active (such that the keel is dynamically loaded by pectoral muscle contractions) still exhibit high incidence of keel bone fracture (Rufener & Makagon, 2020), whereas studies selecting for improved keel bone traits associated to increased strength have shown decreased prevalence of keel bone damage in these birds (Stratmann et al., 2016).

Background strains have been measured for a broad set of species (spanning amphibian, reptilian, avian, mammalian, and osteicthyan geni), bones (mainly long bones and cranial bones), and during different types of activities (habitual and non-habitual) (Main, 2021a; Vitienes et al., 2023). At the tibia or tibiotarsus, peak background strains have been measured in the range of 600-5,180 με, whereas generally cortical bone has been shown to begin yielding at 9800 ue in compression and 8700 με in shear, and fail at approximately 20,000 με in compression (Mirzaali et al., 2016; Morgan et al., 2018).

Background strain gauging studies usually report peak measured strains, and less often include strain rate, which is an important parameter that influences bone adaptation (see section 2.1.3 on the osteogenic components of strain). Some studies measure in vivo strains while the animal is locomoting on a treadmill, which allows for control of step (i.e. cycle) frequency and the measurements of strains during different gait regimes (e.g. walking versus running). In other scenarios it may be more of interest to measure completely unrestricted behaviour. The choice of

what type of behaviour to measure – restricted or unrestricted – ultimately depends on the questions being asked.

Whole bone mechanics are a function of bone mass (volume and density), bone structure, and bone material properties. Standard structural measures of bone mass that can be calculated for cortical, trabecular, woven, and medullary bone are bone volume (BV) and volumetric tissue mineral density which is calculated as the average density of voxels labelled as bone (vTMD). It is important to note that, at this length scale, this measure of tissue mineral density is not a material property, because it is still a function of smaller unresolved porosities which will contribute to the average mineral density measured from the microCT image. These volume and density measures describe how much bone there is and how mineralized it is, but do not inform as to how this bone is organized in space. One whole-bone structural parameter commonly reported is bone curvature, as this creates a moment arm which enables bone bending. Microarchitectural measures of bone structure (Bouxsein et al., 2010) (Fig. 3) differ between bone types given that differences in structure is what differentiates the bone types in the first place. For cortical bone, cross-sectional measures of bone area (Ct.Ar = Ct.BV / heigh of VOI), total area (T.Ar = TV/height of VOI), periosteal perimeter (Ps.Pm), cortical area fraction (Ct.Ar/T.Ar), second and polar moments of inertia (Imax, Imin, pMOI), eccentricity (Imax/Imin), cortical thickness (Ct.Th) are all important determinants of mechanical behaviour. Trabecular bone is described by trabecular thickness (Tb.Th), trabecular number (Tb.N), trabecular spacing (Tb.Sp), and trabecular bone volume fraction (Tb.BV/TV). There are no standard outcomes for medullary bone structure characterization, but measures used to analyze trabecular bone would be appropriate given its small trabecular-like structure. Higher resolution imaging is required, however, to measure these features in medullary bone compared to what is required for trabecular bone.

Tissue material properties encompass features that range different length scales (Fig. 3). Starting at the larger end of the spectrum, there is bone porosity (vascular, lacunar, canalicular). Sometimes, imaging resolution is high enough such that bone vascular porosity can be considered a microstructural and not material property. Smaller scale features are independent of bone volume and distribution and instead are a function of physical and chemical bone properties; these are considered measures of bone quality. The strength, stiffness, and toughness of the bone tissue itself are described by a stress-strain curve, which is similar to a force-displacement curve which

describes whole bone mechanics, but instead is independent of volume (stress = force per unit area, strain = displacement per unit length) (Fig. 7 B). These factors can be related to properties of the constituents of bone, namely collagen and mineral, or related to the organization of these constituents (Willie, Zimmerman, et al., 2020). In terms of constituent properties, there is collagen maturity and cross-link quantity, and the size and orientation of mineral particles. In terms of their organization, there is collagen fiber orientation, and the distribution of mineral. These factors are known to influence the bone's mechanical behaviour, but a clear understanding of how they are capable of this is still lacking. For example, aging is associated with an increase in collagen cross-linking, and thus it is thought that the impairments to bone strength with aging are in part mediated by this increase in collagen cross-linking (Nyman et al., 2006). Yet, when cross-linking is inhibited, such as in the pathological condition of Lathyrism, bone strength is also impaired (Paschalis et al., 2011). These findings suggest that cross-linking quality, in addition to amount, is important.

2.2 Context: Commercial egg-laying hens

2.2.1 The egg-farming industry

Each year, in Canada, about 25 million laying hens produce more than nine billion eggs, generating $1.6 billion dollars in revenue. With approximately 6g of protein per egg and vitamins A, D, E, folate, iron, and zinc, they are an affordable, environmentally friendly, high quality food source. Ensuring the continued sustainability of this industry is therefore important, and includes further understanding of the determinants of chicken skeletal health and wellbeing.

Commercial egg-laying hens, *Gallus gallus domesticus*, are descendants from wild red junglefowl (*Gallus gallus*) which interbred with other junglefowl (grey, Sri Lankan, green). Domestication is thought to have occurred from a single domestication event approximately 8,000 years ago in Southeast Asia (M.-S. Wang et al., 2020). Young (chicks) and pre-pubescent (pullets) female chickens do not lay eggs; it is only after sexual maturity, which occurs at around 18 weeks of age, that they begin to lay eggs. Junglefowl and other avian species lay eggs in clutches – a group of eggs are laid consequently, after which a pause in egg-laying occurs. Domesticated chickens instead have been genetically selected to always stay in lay; commercial layers produce on average an egg a day until around 70 weeks of age when they are considered spent and euthanized.

D

	Muscle Weights, g/kg [1] (±SE)			
	Pectoralis Major		Leg Muscle Group [2]	
	Mean	*p*-Value	Mean	*p*-Value
White	47.9 (0.48) [a]	<0.0001	77.0 (0.73) [a]	<0.0001
Brown	42.9 (0.51) [b]		81.3 (0.79) [b]	

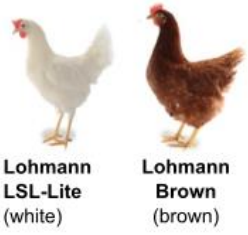

Lohmann LSL-Lite (white)

Lohmann Brown (brown)

Figure 8: Housing and genotype groups. A) Caged housing systems, B) Low complexity aviary, C) High complexity aviary, D) Lohamnn LSL-Lite (white-feathered) and Lohmann Brown (brown-feathered) genetic strains. White-feathered chickens had heavier pectoral muscles and lighter leg muscles (Vitienes et al., 2021).

A variety of genetic strains are used in commercial egg-farming in Canada, among which are the Lohmann LSL Lite (white-feathered, white eggs) and Lohmann Brown (brown-feathered,

brown eggs) genetic strains (Fig. 8 D). The Lohmann LSL Lite commercial genetic strains originates from the White Leghorn, while the Lohmann Brown commercial genetic strain are derived from Rhode Island Red, Plymouth Rock, Australorp, and New Hampshire (Malomane et al., 2019). These genetic strains are substantially different from each other, both physiologically and behaviourally. Lohmann Brown chickens are larger and generally produce less eggs. Their body composition is different compared to Lohmann LSL Lite in that they have larger, wider lower limbs, likely related to the fact that they are also less aerial than the Lohmann LSL Lite (Pufall et al., 2021; Rentsch et al., 2023a). Lohmann LSL Lite chickens are smaller, more active and agile, and use their wings to flap and perform aerial transitions more often than Lohmann Brown chickens. In terms of the keel bone, which is the main bone of interest when it comes to fractures in this population (see section 2.2.2) (Fig. 2), Lohmann LSL-Lite keels are larger, mineralize more rapidly, and fracture less often than Lohmann Brown keels (Rufener & Makagon, 2020).

Fertilized eggs spend 18 days in an incubator after which time they hatch, receive vaccines, and are sent to pullet farms where they remain until they begin to lay. Laying housing are equipped with infrastructure to facilitate the collection of eggs. Housing systems can be in the form of cages (normal or enriched with nesting boxes and a perch) (Fig. 8 A), or more open-concept variations called aviaries (Fig. 8 B-C). Within each general type of system, there are variations depending on the company producing the infrastructure.

2.2.2 Osteoporosis in commercial egg-laying hen flocks

Bone brittleness and high fracture incidence in commercial egg-laying hens was first reported in the 1950's (Couch, 1955), which we now know to be attributed, at least in part, to osteoporosis (Whitehead & Fleming, 2000). Studies have reported 30-97% fracture prevalence in flocks by the end of lay (T. M. Casey-Trott & Widowski, 2016; Hardin et al., 2019; Lay et al., 2011; M. A. Nasr et al., 2015; Richards et al., 2011; Rodenburg et al., 2008; M. Toscano et al., 2018; Whitehead & Fleming, 2000; Wilkins et al., 2011). It remains unclear whether age-related changes to bone structural and material properties play a role in fracture.

The keel bone is by far the most fractured bone. In addition to keel bone fractures (KBF), keel bones also often exhibit pronounced deviations, and keel bone damage (KBD) is a term used to describe both fracture and deviation; whether these are associated and deviations render bones more susceptible to fractures remains unknown. Keel bone fractures are thought to be painful (M.

A. F. Nasr et al., 2012) and therefore considered a serious welfare concern. In addition to disuse osteoporosis and structural impairment due to high calcium demand-related resorption, another factor contributing to fracture prevalence under investigation is the influence of keel bone mineralization delays – studies tracking KBD prevalence longitudinally have shown that prevalence sharply increases at the onset of lay, up until approximately 40 weeks of age after which it begins to plateau, coinciding with the finalization of keel bone mineralization (Rufener & Makagon, 2020).

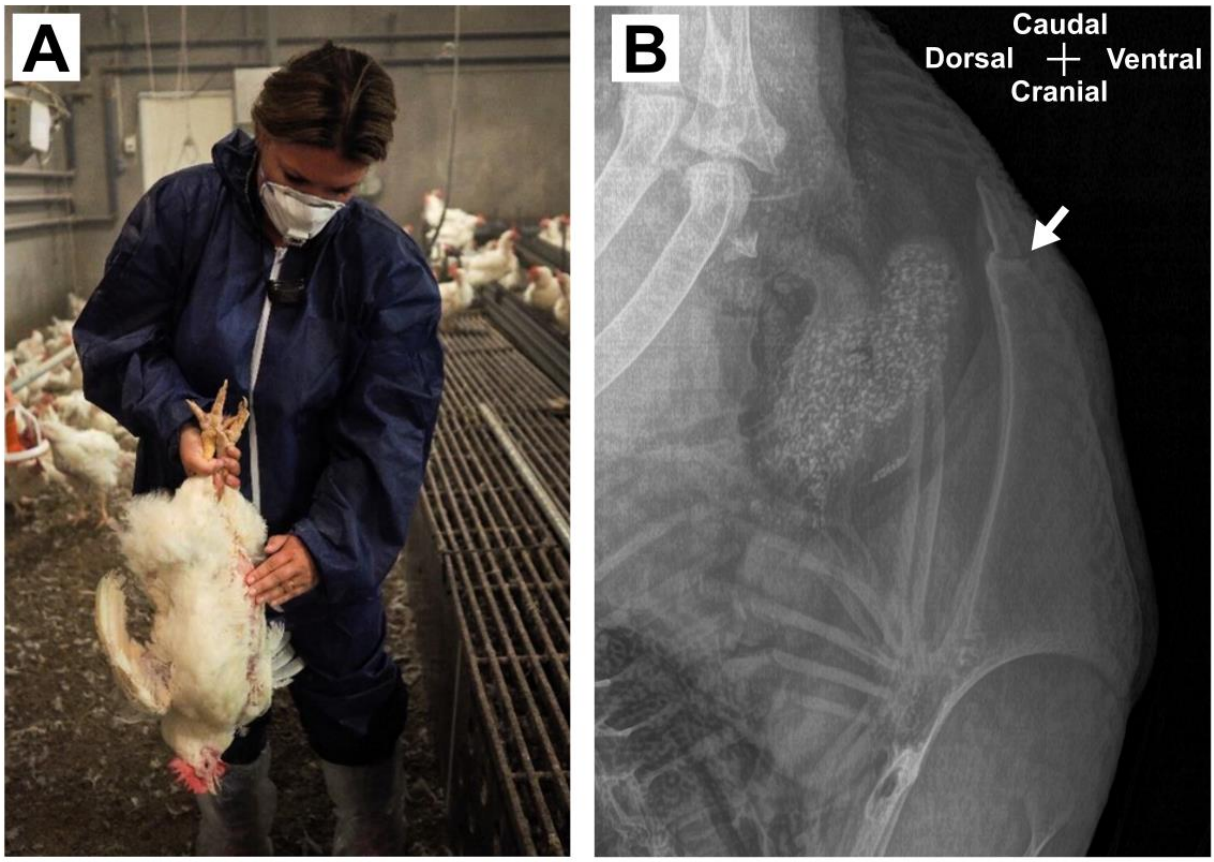

Figure 9: Fracture detection methods. A) In vivo palpation. Image reproduced with permission from Kittelsen et al., 2023. B) Radiograph image where a fracture is visible (white arrow).

One of the reasons why there is such a broad range in reported fracture and KBD incidence is that different methods of detections are used across studies, some of which are not reliable and underestimate the prevalence (Rufener & Makagon, 2020). The most common detection method is palpation (Petrik et al., 2013), which can be done relatively quickly on live chickens. It is a cost effective method, but relies on the presence of a fracture callus to identify a fracture and it is

difficult with this method to detect fractures at the tip of the keel bone. Palpation therefore lacks precision and accuracy, and likely underestimates KBD prevalence (T. Casey-Trott et al., 2015). Radiography is also used to assess KBD in vivo (Fig. 9 B). This method takes more time and is stressful for the birds but provides much more information on the status of the keel bone. Scoring rubrics have been published to quantify the severity of KBD from radiograph images (Rufener et al., 2018), which must be performed by trained highly qualified personnel; consistency and agreement between scorers is a concern, which affects comparability across studies (T. Casey-Trott et al., 2015; Rufener & Makagon, 2020). Keel bone fracture and deviation severity can also be scored by observing dissected keel bones. The downside of this method is that it is done post-mortem, and old healed fractures are difficult to identify. Furthermore, the relationship between number of fractures and severity of damage – as quantified by existing rubrics – and the actual pain and discomfort experienced by the chickens is not well understood. Regardless of the mode of detection, a big hindrance towards understanding the causes of keel bone damage is that it is not practically possible to know when the damage occurs. Unlike other animals which will exhibit behavioural signs of discomfort and pain, chickens are exceptionally good at masking pain, to avoid predation in the wild. Other logistical problems also play a role, such as the ability to follow individual chickens longitudinally in large flocks.

2.2.3 Increased opportunities for physical activity to address osteoporosis

Efforts to address the widespread osteoporosis have looked to genetics to select for chickens with superior bone strength and improving nutrition to maximize calcium intake and absorption. However, the intervention with the biggest effects on bone health-related measures have been to provide increased opportunities for physical activity and load bearing.

Housing hens in a variety of non-cage housing systems such as aviaries (Abrahamsson & Tauson, 1995; Fleming et al., 2006; Knowles & Broom, 1990; Leyendecker et al., 2005; Newman & Leeson, 1998), modified furnished cages (Jendral et al., 2008), or free-range systems (Shipov et al., 2010) have been shown to improve bone health and strength and reduce osteoporosis. In these studies, the benefits to bone are assessed by postmortem 3-point bending of long bones. However, non-cage housing has still been associated with high levels of keel bone fractures, higher than what occurs in caged birds (Rufener & Makagon, 2020). It is hypothesized that this is attributed to falls and collisions occurring more frequently in non-caged systems. However, there

is data showing that fractures are not always associated with inflammatory markers of trauma (Thøfner et al., 2020). It is clear that the problem is complex and multifactorial (Fig. 10), which opens many avenues for interventions and treatments.

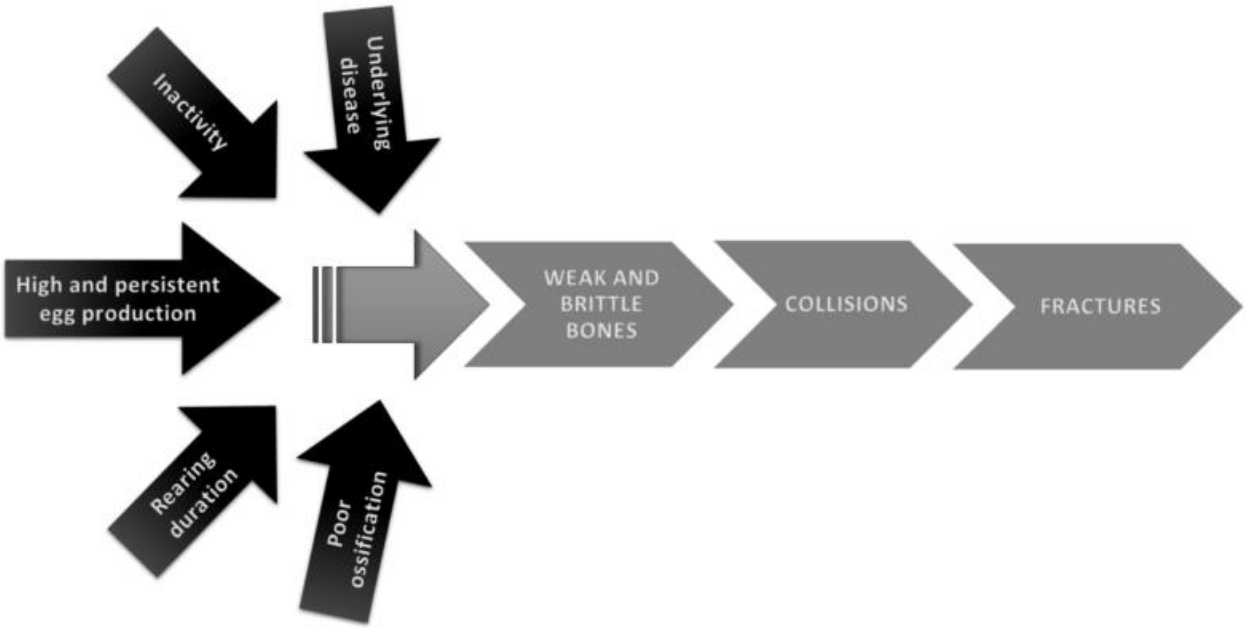

Figure 10: Schematic illustrating possible explanations for keel bone damage. Diagram reproduced from M. J. Toscano et al., 2020.

More research aiming to address osteoporosis by focusing on the contribution of disuse has recently shown that increased load bearing activity particularly during youth has long-lasting effects on bone (T. M. Casey-Trott). This approach has been effective in human studies showing that exercise during youth had life-long lasting effects (Warden et al., 2014), and studies in mammals showing that bone is most mechanoresponsive during youth (Birkhold et al., 2014). In Lohmann LSL-Lite chickens, hens housed life-long in cages compared to hens raised in aviary housing and then moved to cages at onset of sexual maturity through lay (up to 73 weeks) had higher tibiotarsal total cross-sectional area, cortical cross-sectional area, and cortical bone mineral density, all assessed by quantitative computed tomography (200-1000 μm resolution) (T. M. Casey-Trott, Korver, et al., 2017b). Interestingly, these authors also showed that among the hens raised in aviaries, there was also a lower overall prevalence of keel bone fractures (detected by palpation) (T. M. Casey-Trott, Guerin, et al., 2017). In contrast, multiple other studies showed

increased keel bone fracture prevalence when housing (not necessarily during youth) in non-cage systems (Riber & Hinrichsen, 2016; Rodenburg et al., 2008).

The success of housing-based interventions to elicit bone formation is dependent on the willingness of the chickens to be active and utilize the space which they are given access to. Studies quantifying behaviour of Lohmann Brown and Lohmann LSL-Lite pullets (prior to onset of lay) housed in different types of commercially available rearing aviaries (either in commercial farms or research facilities, which replicated commercial conditions), showed that the aviary style affects the amount and types of activity that the chickens perform, and this effect is dependent on genetic strain (Pufall et al., 2021; Rentsch et al., 2023a). The general findings from these studies were that the white-feathered pullets were more active than the brown-feathered pullets, and that the style of aviary influenced the activity levels of white- but not brown-feathered pullets.

2.3. Methods: Assessment of bone mechanical, structural, and adaptive properties

2.3.1 Experimental measurements of bone mechanical behaviour

Strain gauges are simple devices that can sense the deformation of the surface upon which they are attached. In essence, they are a circuit with a single component: a resistor which attenuates the current of the circuit, reflected by a voltage drop across the resistor (Ohm's law, voltage (V) = current (I) × resistance (R)) (Fig. 11 A). When the object being measured is strained, so is the strain gauge resistor that is attached to it, causing its resistance to change. If the strain (ε) is tensile, the resistance will increase, and if it is compressive, the resistance will decrease, by virtue of the design of the gauge. Therefore, the voltage drop across the resistor when it is at rest $V_{nominal} = I \times R_{nominal}$ will differ from the voltage drop across the strained resistor $V_{strained} = I \times R_{strained}$. By measuring the voltage drops at the strained state and knowing the current being sent across the resistor (which remains constant), you can deduce the strained resistance $R_{strained} = V_{strained} R_{nominal} / V_{nominal}$. The relationship between strain and change in resistance is called the gauge factor:

$$GF = \frac{(R_{strained} - R_{nominal})/R_{nominal}}{\varepsilon}$$

and is related to the material properties of the resistor (resistivity) and cross-sectional area of the resistor's foil grid; this number along with the nominal resistance of the gauge are provided by the

manufacturers of commercially available strain gauges. To obtain precise measurements of small strains, a Wheatstone bridge circuit is used which serves to amplify the signal, thereby decreasing the signal-to-noise ratio (Fig. 11 A). A variety of configurations of Wheatstone bridges exist; for amplifying signals from individual strain gauges, the quarter-bridge configuration is used.

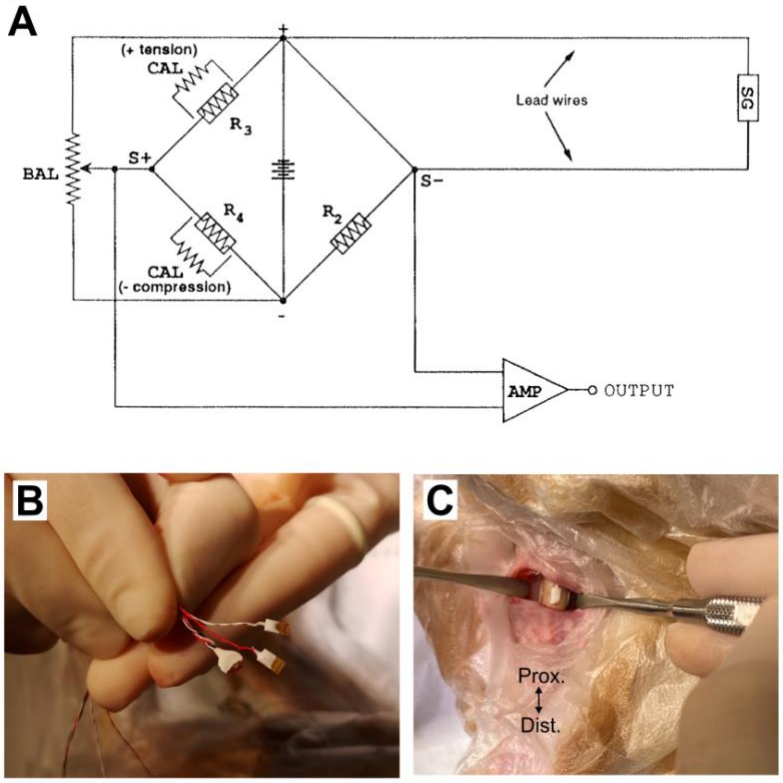

Figure 11: In vivo strain gauging. A) Quarter bridge Wheatstone bridge circuit used to detect and amplify strain-derived voltage drops originating from the strain gauge (SG). Illustration reproduced with permission from Biewener, 1992. B) Image of rosette (circular) and axial (rectangular) strain gauges prepared for in vivo implantation. C) Image of a surgically exposed medial aspect of a tibiotarsus with a visible gauge attached to the medial surface.

Strain gauges can come in axial or rosette configurations (Fig. 11 B). Axial gauges can only measure strain in one direction, and therefore the orientation in which they are attached to the surface will dictate which direction of strain they measure. Whereas rosette strain gauges are composed of three superimposed axial gauges, measure strains along three axes which span 360°. The strains measured from the three rosette elements form a basis that spans the plane parallel to the gauge attachment surface, and can therefore be used to calculate axial strain in any direction parallel to that plane, as well as principal (peak tensile and compressive strains in the plane) and

shear strains (Biewener, 1992). Usually, rosette gauges are preferrable since they provide more information, but they are larger than axial gauges, thus if the object measured is small, as occurs with certain bones, it may not be able to accommodate a rosette.

Strain gauges were originally created for applications in the field of mechanical and civil engineering, but methods have been developed to implant them on the bone surfaces of living animals and people, and measure in vivo bone strains (Biewener, 1992). This requires applying various coating layers onto the gauge circuit and lead-wire attachment sites to protect the circuit from bodily fluids. Background strain gauging is the methodology by which strain gauges are surgically attached to the surface of a bone, and once the animal recovers from surgery, strains are measured during certain activities. Baseline strains are measured while the animal is still under anesthesia to account for differences in the nominal and relaxed resistances, effectively taring the circuit. This is important because the strain acquisition system will measure strain in relation to the gauge's nominal resistance, thereby over- or under-estimated the true strain if the relaxed resistance differs from the nominal (this commonly occurs, since the bone surface is not usually flat, and attaching it causes it to deform slightly).

These experiments are challenging and require modifications to the signal acquisition hardware classically used for strain gauging to address logistical difficulties that arise. One main issue that arises is substantial lead wire desensitization. To allow the animal to freely perform background activities, a long wire is needed to connect the implanted strain gauge to the Wheatstone bridge circuit. In a perfect world, the only energy lost in the system would be the voltage drop across the strain gauge resistor, but in reality, the wires themselves act as resistors. The Wheatstone bridge is designed with a variable resistor that essentially tares the system and balances out resistance from lead wire desensitization as well as the resistance introduced upon attaching the gauge ($R_{relaxed} - R_{nominal}$). But if the hardware is limited in the amount of resistance it can compensate for, therefore this needs to be taken into account when making the wires to connect the gauges to the bridge.

In vivo strain gauging is also used to measure whole bone stiffness. Assuming the applied loads are within the elastic region of the bone force-displacement curve, you can deduce the approximate stiffness by applying loads of varying magnitudes to the limb, measuring the engendered strains, and fitting a line to these points. This application is essential for performing

strain-matched loading experiments to study the bone's mechanoresponse. Here, long wires are not needed and lead wire desensitization is not a problem. It is important however to have a hardware setup that allows you to measure strain and force simultaneously. Many loading machines have ports where the signal from the load cell is outputted, which then can be added as an input to the strain acquisition hardware.

2.3.2 Simulation of bone mechanical environment by finite element modeling

Strain gauging is valuable but limited in that it only tells us strains occurring at the discrete site of gauge attachment. It is not possible to cover the bone in strain gauges for in vivo measurements, and often it is not even possible to attach a single gauge in a particular location of interest, but rather we are limited to a spot which is surgically accessible and sufficiently large to fit the strain gauge. Moreover, with strain gauging we are limited to measuring strains on the bone's surface. Therefore, finite element modelling is a useful approach to model strains across the entire bone and can be validated using experimentally measured strains from strain gauging.

Finite element analysis requires the geometry of the object being modelled in the form of a mesh, information about the object's material properties, and the definition of boundary conditions that replicate the loading condition modelled.

1. A mesh of the bone can be created from a thresholded whole bone microCT image, taken at a high enough resolution to resolve trabecular bone structures. For a given study, if multiple models are being made, it is important to use the same threshold to binarize the CT images and create meshes with approximately the same number of elements.
2. The material property of the bone is described by the elastic modulus (E) and the Poisson ratio (υ) which are functions of a range of microstructural and compositional properties.
    a. The elastic modulus (E) can be approximated as a function of the bone ash density (ρ_{ash}) by the equation $E = k \times {\rho_{ash}}^{\alpha}$, where k and α are constants (J. D. Currey, 1988a, 2004a). Given the anisotropy of bone, the value of the α exponent (and therefore E) should theoretically be specific to the direction of deformation, but it has been shown that modelling the bone with isotropic (as opposed to orthotropic) material properties has negligible effects on the finite element outcomes (Peng et al., 2006). The value of α has been reported to range between 1.5-3.0 for bone

(Helgason et al., 2008). The mineral density values obtained from microCT images is related to the ash mineral density of the bone, and we assume this relationship to be linear: $\mu = m \times \rho_{ash}$, where μ is mineral density and m is a constant. Therefore, we can rewrite the elastic modulus equation as $E = k' \times \mu^{1.5}$, where $k' = {}^{k}/_{m^{\alpha}}$. Using a data point of measured elastic modulus (E*, by nanoindentation) and the associated tissue mineral density of this region (μ*, measured by microCT or synchrotron radiation microCT), we can solve for k' to obtain an equation relating tissue mineral density to elastic modulus. This data point can be obtained from the literature or measured experimentally but should be from bones that are as similar as possible (in anatomical location, age, sex, genotype) to those being modelled.

b. The Poisson ratio describes how much a material deforms in the direction perpendicular to the direction of loading, relative to the deformation in the direction of loading. Poisson ratios have only been measured in human and equine bones and are reported to range between 0.09 and 0.63 (Ashman et al., 1984; Pithioux et al., 2002; D. T. Reilly & Burstein, 1975; Shahar et al., 2007). Studies conducting finite element modelling of bone often use a homogeneous Poisson ratio of 0.35, as an approximate midpoint in this range.

3. Boundary conditions consist of constraints to the movement of the object being modelled, the magnitude and direction of the force being applied, and the surface upon which it is applied.

The deformation of each mesh element is fully described by a strain tensor, composed of normal and shear components. Normal components describe the isotropic tension and compression of the element, whereas shear components describe the distortion. Principal tensile and compressive strains are therefore normal components of the overall strain of an element. Principal strains are common outputs of finite element analyses and provide additional information compared to stress outcomes as strain has a magnitude and a direction. Since bone structural and material properties are differentially adapted to modes of strain, assessing strain as opposed to stress outcomes are particularly of interest. Stress outcomes however are valuable in that they provide a concise measure of the forces present at a discrete location. The stress at a particular

location can also be decomposed into normal and shear components, as with strain. Normal stresses act perpendicular to the surface of the particle in question (in the case of finite element modelling, a mesh element), whereas shear stresses act parallel to the surface. The so-called von Mises stress is a scalar value calculated as a function of the shear stress orthogonal components (x, y, z). This parameter was originally formulated as a means to predict failure of ductile materials under complex loading, because the yielding of these materials is dependent on the shear and not normal components of stress. It is generally used as a summary parameter to compile information about the shear stress state of a loaded object and is valuable when analyzing the mechanical competence of bone because bone is weakest in shear.

2.3.3 Characterization of bone structure and mineral density by computed tomography

Computed tomography is an x-ray imaging technique where a series of x-ray images are taken and reconstructed into a 3-dimensional (Kak & Slaney, 2001). This technique is well suited to the study of bones given that bone's distinguishing feature (especially from neighbouring tissues) is its mineral content, which is exactly what this imaging modality "sees". Moreover, compared to histological methods, CT-imaging is both non-destructive and volumetric, thus enabling the extraction of a greater amount of information from a given sample.

X-ray imaging, which is the basis of CT-imaging, takes advantage of the fact that an object will attenuate incoming x-ray beams by an extent which is proportional to the atomic number of the mass it is composed of, in other words its density. To image an object, an x-ray beam is directed at it, and a detector behind the object captures the photons that were not absorbed or deflected by the object. The x-ray image is therefore essentially a shadow, where areas on the detector of less photon density correspond to areas of higher density in the object imaged, along the axis of the electron beam; this x-ray image is a 2-dimensional projection. Computed tomography involves rotating the sample (or, equivalently, the x-ray beam and detector) by 180°, while taking an image every certain number of degrees (rotational image frequency). These raw projection images are then mathematically "combined" by filtered back projection to produce a 3-dimensional image composed of a set of 2-dimensional cross-sectional slices.

Computed tomography is inherently limited by two primary sources of error – partial volume effects and beam hardening (Fig. 12). Their effects can be minimized, sometimes until rendered negligible, but nevertheless should be considered. Partial volume effects arise because

images are made up of a set of discrete pixels. Within the volume being imaged, there may be interfaces between regions of different densities, as occurs for example at the surface of a bone (bone to air interface). In the discretized image of the bone, the pixels along the bone surface will have a grey value that is influenced by both the bone tissue as well as the surrounding air or soft tissue (of lower density). Thus, this error manifests itself as an apparent layer of lower-density tissue at all bone-to-not bone interfaces which is not actually there. If the pixel size is small enough relative to the structures of the bone that are intended to be captured, then the effect can become negligible as the inclusion or exclusion of these partial volume pixels will not significantly influence the morphometric and densitometric outcomes.

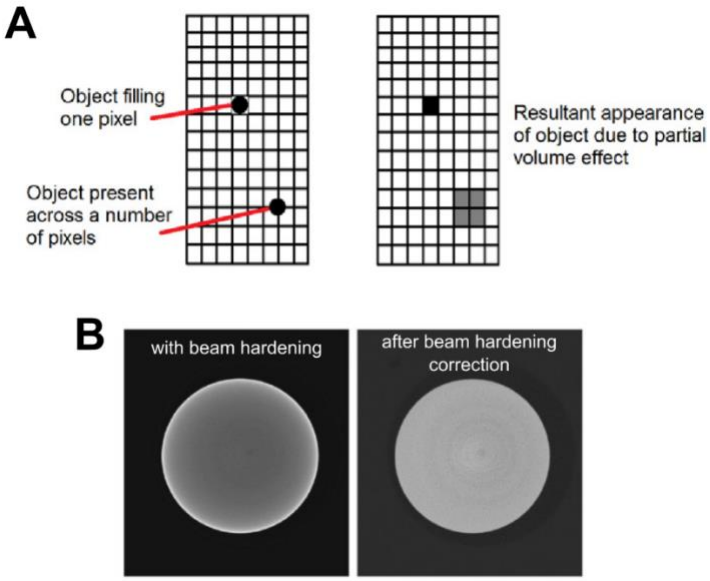

Figure 12: Computed tomography sources of error. A) Illustration of the effects of partial volume effect. Depending on the position of the object relative to the pixel coordinates, the shape and attenuation is altered. Reproduced with permission from Sperrin & Winder, 2014. B) Exemplary images of a cross-section of a beam. The image on the left has beam hardening effects, evidenced by the bright halo on the outer edge of the beam. The image on the right has undergone beam hardening correction to more accurately depict the density distribution of the beam. Reproduced with permission from Roche et al., 2010.

The beam used for lab-based microCT is polychromatic, meaning that it contains electrons that have a range of energies. As the beam passes through the object being imaged, electrons in the low-energy portion of the spectrum will be preferentially attenuated, effectively filtering the beam such that the energy spectrum of the incident beam is lower than that of the beam that exits the sample. This source of error therefore influences the accuracy of the image grey values as a

reflection of the object's density. Beam hardening will have a greater effect in regions of the object that are thicker, and is the reason why it is best to orient the object being imaged such that the rotation occurs about the axis of the object's longest width (in the case of a long bone, ideally the bone rotates about it's long axis). Filters are used to narrow the spectrum of the incident beam, but more sophisticated imaging modalities are required for imaging with a monochromatic beam (synchrotron radiation micro computed tomography).

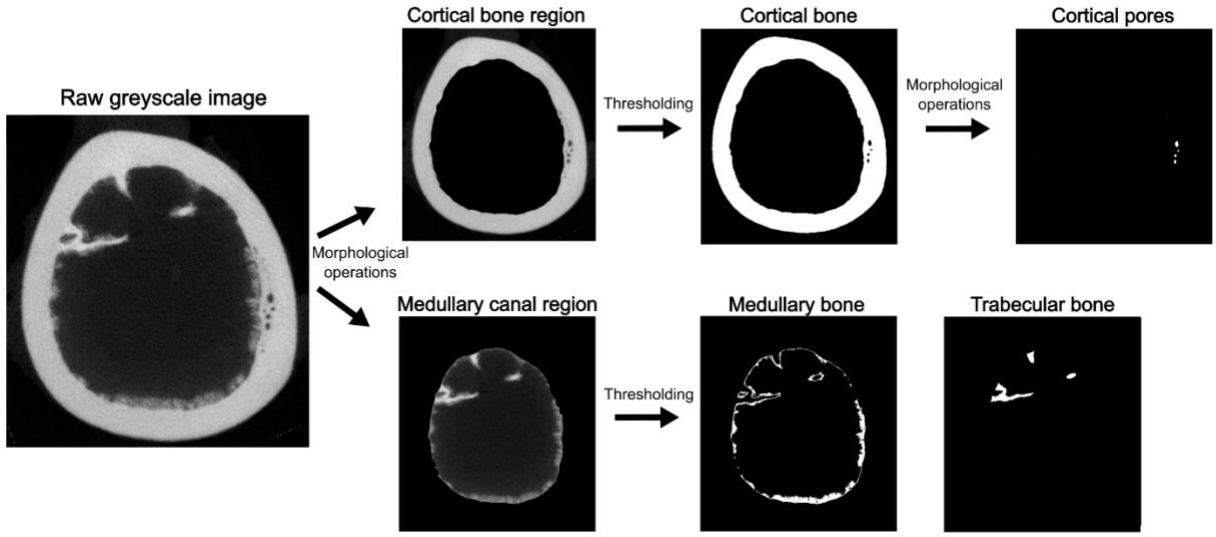

Figure 13: Image segmentation and binarization. The raw greyscale is separated into regions – cortical and medullary canal regions in this case – using morphological operations. Then, bone is separated from background by thresholding, which produces binary masks.

Image segmentation is necessary to separate bone regions (cortical, trabecular, woven, medullary, Fig. 13) such that they can be analyzed separately. Segmentation can be automated by using a sequence of morphological operations on binary masks, which then are used to select specific regions. This step is essential, given that each bone type has distinct biological functions, morphological features, and may also have different mineralization levels – for example, trabecular bone is often less mineralized than cortical. Once the image has been "divided" into regions and calibrated, a global threshold must be determined for each bone type that will be used to distinguish bone from background in all images used in a given study. The pixel values of microCT images originally are in greyscale units, and this grey value will be largely dependent on the x-ray source status and other environmental conditions. Therefore, to compare images that have been taken at different times, or between different scanners, the images must be calibrated. Images are usually

calibrated to units of mineral density, mass of hydroxyapatite per unit volume. Calibration phantoms are objects of known density that are imaged at the same time as the bones. By imaging two calibration phantoms of different, known densities, and measuring the average grey value in the image of each phantom, a linear equation can be derived that relates grey value to mineral density (under the assumption that the relationship between density and x-ray attenuation is indeed linear). The global thresholds used to distinguish bone from background then must be in units of mineral density (e.g. gHA/cm^3). The Otsu method is an option for determining candidate thresholds; it is an algorithm that takes as input the image histogram and iteratively tests out each possible threshold value to find the one which minimizes the variance within separated groups. Other approaches used to determine thresholds are the mirror point method and 30% bone peak (Bouxsein et al., 2010). Regardless of the method used, it is imperative to visually inspect the thresholding result and adjust the value such that the threshold works well for all images in the study, selecting for what visually is clearly bone.

The pixel values of microCT images originally are in greyscale units, and this grey value will be largely dependent on the x-ray source status and other environmental conditions. Therefore, to compare images that have been taken at different times, or between different scanners, the images must be calibrated. Images are usually calibrated to units of mineral density, mass of hydroxyapatite per unit volume. Calibration phantoms are objects of known density that are imaged at the same time as the bones. By imaging two calibration phantoms of different, known densities, and measuring the average greyvalue in the image of each phantom, a linear equation can be derived that relates greyvalue to mineral density (under the assumption that the relationship between density and x-ray attenuation). Tissue mineral density can then be calculated as the average pixel value within the thresholded bone region. Structural and cross-sectional morphological parameters can be measured from the thresholded images (binary images).

2.3.4 Characterizing bone (re)modelling dynamics by histomorphometry

Bone histomorphometry is the gold standard approach to investigating bone formation dynamics (Dempster et al., 2013). This method relies on the usage of fluorochromes which are administered in vivo and bind to surfaces of newly formed bone. Unless this newly formed bone is subsequently resorbed, the fluorochromes will remain attached to the bone tissue, and can be subsequently visualized post-mortem. This is a destructive, 2-dimensional ex vivo methodology.

Bones are embedded in plastic and sectioned to expose the surface of interest, after which the surface is imaged using a confocal microscope to visualize the fluorochrome labels. New non-invasive microCT-based time-lapse morphometry approaches that employ in vivo sequential CT imaging and image registration to compare voxels over time in 3-dimensions have shown that the surface chosen for histomorphometric analysis has a significant effect on the outcome measures and this dependency introduces a substantial amount of variability in this outcome (Birkhold et al., 2014). Fluorochrome-based histomorphometry remains, however the gold standard approach, likely due to the decreased accessibility of in vivo microCT imaging. When a single administration of fluorochromes is given, it is possible to quantify the minimum percent of bone surface undergoing bone formation at the time of administration. It is the minimum, because it is possible that certain surfaces, which appear unlabeled did undergo formation followed by resorption, or never underwent formation. Multiple administrations of fluorochromes can be given such that rates of bone formation can be derived as a function of the distance between subsequent labels and the amount of time between administrations. Moreover, with a double administration experimental model, some information about bone resorption can be deduced, for example if the first label is lacking but the second is there, this indicates that resorption followed by formation occurred (Birkhold et al., 2015).

2.3.5 In vivo controlled loading to elicit a mechanoresponse

A main way that bone mechanoadaptation is studied is by performing in vivo loading experiments that stimulate a mechanoadaptive response which is then analyzed, either at the level of the outcome of the response (mechanoresponse) or the activity of the cellular mediators (mechanoresponsiveness) (Main et al., 2020). The mechanoresponse is stimulated by loading the bone to produce deformations that are osteogenic. Loading experiments are roughly categorized into intrinsic and extrinsic models, based on the nature of the load stimulus that is applied. In intrinsic models, the animal it motivated to enhance its physical activity which leads to anabolic loading of the bone. Extrinsic models alternatively employ a machine with an actuator to apply tightly controlled forces to a limb. Both models have their pros and cons. With intrinsic models, an internal control is lacking, and the effect of loading can be confounded with effects of a general physiological response to exercise. Furthermore, the stimulus that the bone is sensing is not controlled – exercise protocols can produce different mechanical strain stimuli across age- and

weight-matched subjects likely due to variations in a wide array of factors such as muscle engagement, bone geometry, gait, etc. Extrinsic loading models conversely allow for more tightly controlled experiments and the ability to account for confounding variables. Limb loading allows for within subject comparisons between loaded and non-loaded limbs, and the ability to define the load stimulus has allowed for parametric studies investigating osteogenic components of strain. The downside of extrinsic loading models is that loads might be administered in a nonphysiological mode, however commonly used models today have implemented loading contact surfaces, load directions, and waveform protocols that mimic ground reaction force-derived in vivo loading. One limitation of this method however is its inability to recapitulate mechanical stimuli derived from muscle contractions.

A commonly used version of the in vivo non-invasive extrinsic loading model is the tibial axial compression model (Main et al., 2020).The lower limb is placed horizontally in the loading machine, and the knee and ankles are constrained by custom-made fixtures. While the knee is fixed, load is applied to the ankle by an actuator controlled by feedback from a load cell. Studies using this model in mice have shown that subjecting mice to daily loading sessions for 1 week is sufficient to elicit a measurable tissue level mechanoresponse (Yang et al., 2017).

When conducting these experiments, all parameters that define the load waveform must be determined: load magnitude, number of cycles per session, cycle frequency, load rate, rest insertions (duration and location within the waveform) (Fig. 6 A). It is also important to use fixtures that secure the joints properly, to avoid any bruising and soft tissue damage that may influence the animal's activity during the rest of the day. Comparing results from different studies requires consideration of differences in the load waveform, given the substantial evidence about how the mechanoresponse is affected by the different osteogenic components.

When aiming to compare the mechanoresponse of two groups, it is possible that differences in bone size, structure, and material properties result in differences in whole bone stiffness such that, when subjected to the same level of load, different levels of strains are engendered in the two groups at comparable bone sites. Since bone cells adapt to mechanical strain (derived) stimuli, the gold-standard is to implement a strain-matched protocol (Main et al., 2020), meaning that load levels are chosen such that all experimental groups receive the same amount of mechanical strain. A preliminary experiment is required where strain gauges are attached to the bones of a set of

animals from each group, and the bones are loaded at a range of load magnitudes while engendered strains are measured. Assuming a linear relationship between applied load and engendered strain, it is possible to fit a line to these data points and deduce a load-strain calibration equation, which is simply a linear equation of the form $y = mx$ where m is the whole bone stiffness. Using group-specific calibration equations, it is then possible to deduce group-specific load levels that will engender a fixed strain level. Bone stiffness is a function of bone geometry and material properties, and therefore changes with age, between genotypes, sex, and between healthy and mutant mice.

The main methods to quantify the mechanoresponse are micro-computed tomography-based measures of bone mass (volume and mineral density) and structure (whole bone length and geometry, cross-sectional microstructure), and histomorphometric measures of (re)modelling dynamics (see sections 2.3.3 and 2.3.4). In cases where these methods are not amenable, for example in humans, byproducts of bone formation and resorption in serum can also be measured by enzyme-linked immunosorbent assays (ELISA). This outcome is not site specific as the byproducts measured are systemic (Christenson, 1997).

Chapter 3 – In vivo mechanical behaviour of the tibiotarsus of young chickens during physical activity

Manuscript status: Published in *Bone* in 2022

Breed and loading history influence in vivo skeletal strain patterns in pre-pubertal female chickens

Isabela Vitienes[a,b,c], Nicholas Mikolajewicz[a], Seyedmahdi Hosseinitabatabaei[a,b,c], Alice Bouchard[a,c], Catherine Julien[a,c], Gabrielle Graceffa[a,c], Ana Rentsch[d], Tina Widowski[d], Russell P. Main[e,f], Bettina M. Willie[a,b,c,†]

[a]Research Centre, Shriners Hospital for Children-Canada, Montreal, Canada
[b]Department of Biological and Biomedical Engineering, McGill University, Montreal, Canada
[c]Faculty of Dental Medicine and Oral Health Sciences, McGill University, Montreal, Canada
[d]Department of Animal Bioscience, University of Guelph, Guelph, Canada
[e]Weldon School of Biomedical Engineering, Purdue University, Indiana, U.S.A
[f]Department of Basic Medical Sciences, Purdue University, Indiana, U.S.A

Abstract

The influence of loading history on in vivo strains within a given specie remains poorly understood, and although in vivo strains have been measured at the hindlimb bones of various species, strains engendered during modes of activity other than locomotion are lacking, particularly in non-human species. For commercial egg-laying chickens specifically, there is an interest in understanding their bones' mechanical behaviour, particularly during youth, to develop early interventions to prevent the high incidence of osteoporosis in this population. We measured in vivo mechanical strains at the tibiotarsus midshaft during steady activities (ground, uphill, downhill locomotion) and non-steady activities (perching, jumping, aerial transition landing) in 48 pre-pubescent female (egg-laying) chickens from two breeds that were reared in three different housing systems, allowing varying amounts and types of physical activity. Mechanical strain patterns differed between breeds, and were dependent on the activity performed. Mechanical strains were also affected by rearing environment: chickens that were restricted from performing dynamic load bearing activity due to caged-housing generally exhibited higher mechanical strain levels during steady, but not non-steady activities, compared to chickens with prior dynamic load-bearing activity experience. Among chickens with prior experience of dynamic load bearing activity, those reared in housing systems that allowed more frequent physical activity did not exhibit lower mechanical strains. In all groups, the tibiotarsus was subjected to a loading environment consisting of a combination of axial compression, bending, and torsion, with torsion being the predominant source of strain. Aerial transition landing produced the highest strain levels with unusual strain patterns compared to other activities, suggesting it may produce the strongest anabolic response. These results exemplify how different breeds within a given specie adapt to maintain different patterns of mechanical strains, and how benefits of physical activity in terms of resistance to strain are activity-type dependent and do not necessarily increase with increased physical activity. These findings directly inform controlled loading experiments aimed at studying the bone mechanoresponse in young female chickens and can also be associated to measures of bone morphology and material properties to understand how these features influence bone mechanical properties in vivo.

Introduction

The material properties and spatial organization of bone tissue are tailored to the bone's in vivo mechanical functions (J. D. Currey, 2003). Existing evidence suggests that this is achieved through adaptive processes wherein the bone senses mechanical strain stimuli and modulates regional bone mass to maintain genetically encoded local target strain levels (Biewener & Bertram, 1993; Frost, 2004; Hsieh & Turner, 2001; Roux, 1881). These local target strain levels can be known by measuring mechanical strains engendered during activities performed habitually (Meakin et al., 2013, 2014), and provides context to whole bone morphology (Bertram & Biewener, 1988; de Margerie et al., 2005; Javaheri et al., 2020; Lanyon, 1987; Pauwels, 1980) and material properties (Keenan et al., 2017; Riggs, Lanyon, et al., 1993; Skedros et al., 1996, 2009). *In* vivo strains inform the calculation of bone safety factors, the ratio of in vivo strains to failure strains, which indirectly describe how capable a bone is of withstanding unexpected loading events (J. Currey, 2014; Willie, Zimmermann, et al., 2020). It has been theorized that bones which are subjected to highly predictable loads will sacrifice safety factor for load predictability (Bertram & Biewener, 1988). For example, bone curvature decreases bone strength but ensures that the bone will bend in a predictable way, such that adaptations can be regionally tailored to resist specifically tensile or compressive strains (G. C. Reilly & Currey, 1999; Skedros et al., 1996). Data on how bones deform in vivo is therefore critical towards understanding the functionality of a bone`s structure and bone mechanoadaptation.

There is specifically an interest in the egg-farming industry in understanding the mechanical and adaptive behaviour of the bones of commercial egg-laying hens (female chickens that produce eggs for human consumption) to address disuse osteoporosis and high fracture incidence in this population (Whitehead, 2004b). Like mammals, the bones of chickens (and avian species in general) develop through elongation by endochondral ossification and cross-sectional expansion by intramembranous ossification (Whitehead, 2004b). Chicken bones are osteocytic and undergo intracortical remodelling (Hudson et al., 1993), and the appearance of secondary osteons begins to occur in females at the onset of sexual maturity at 16-18 weeks of age (Whitehead, 2004b). Although data on female chickens are lacking, sexual maturity has been shown to coincide with closure of the growth plates in long bones of male turkeys (Klingensmith et al., 1986). Modern commercial hens have been genetically selected for early onset of sexual maturity and to remain

continuously in lay from 18-72 weeks of age, instead of fluctuating between periods of lay and rest throughout adulthood. At 72 weeks they are considered spent hens and euthanized.

Commercial hens and pullets (young, pre-pubertal hens) have traditionally been housed in extremely limiting conventional cages where there is only enough space to remain standing or sitting; there is insufficient room for them to walk, run, perch, or flap their wings. The lack of opportunity for physical activity provided to the pullets raised in conventional cages likely contributes to their bone fragility (Fleming et al., 2006; Whitehead, n.d.) since bone adapts to habitual loading conditions. Research in rodents, humans, and turkeys showed that bones are most mechanoresponsive during youth (Bassey et al., 1998; Birkhold et al., 2014; Main et al., 2014; Rubin et al., 1992), and these effects of mechanical stimuli during youth are long-lasting (Javaheri et al., 2020; Warden et al., 2014; Welten et al., 1994). Therefore, stimulating increased accumulation of lamellar bone in pullets via increased mechanical stimuli is a promising approach to address adult hen bone fragility, but there lacks knowledge on bone adaptation in these groups. To prevent bone fragility and address welfare concerns, the use of alternative housing systems that provide the pullets and hens with more spacious environments is being pursued. Alternative housing includes non-cage systems, such as aviaries, which allow for dynamic load-bearing activity (T. M. Casey-Trott, Korver, et al., 2017a, 2017b; Hester et al., 2013; Regmi et al., 2015, 2016; Rufener & Makagon, 2020; Tanka Khanal, 2020; Widowski et al., 2017). Commercially available aviaries vary widely in their size, infrastructure, and complexity, which has been shown to significantly affect the amount of physical activity performed by pullets (Pufall et al., 2021; Rentsch et al., 2023b), and it is unknown whether similar improvements in bone health would be observed when rearing pullets in different styles of commercial aviaries. It also remains unclear if various breeds would reap similar benefits.

Long bone in vivo habitual strains have been characterized across multiple skeletal sites in over 25 species (Aamodt et al., 1997; Biewener et al., 1996; Biewener & Bertram, 1993; Biewener & Dial, 1995; Biewener & Taylor, 1986; Blob et al., 2014; Blob & Biewener, 1999; Butcher et al., 2008, 2011; Carter et al., 1980; Copploe et al., 2015; Demes et al., 1998, 2001; Fritton et al., 2000; Goodship et al., 1979; Gross et al., 1992; Keller & Spengler, 1982, 1989; Lanyon, 1972, 1973; Lanyon et al., 1981; Lanyon & Bourn, 1979, 1979; Lee et al., 2002; Lieberman et al., 2004; Main & Biewener, 2007; Manley et al., 1982; Milgrom et al., 2000; Moreno et al., 2008; Mosley et al.,

1997; Nunamaker et al., 1990; Rabkin et al., 2001; Rubin & Lanyon, 1982, 1982, 1984a, 1984b; Sheffield et al., 2011; Sugiyama et al., 2012; Swartz et al., 1989, 1992; Young et al., 2017; Young & Blob, 2015), including chickens (Biewener et al., 1986; Carrano & Biewener, 1999; Loitz & Zernicke, 1992; Rubin & Lanyon, 1982), to better understand how physiological, anatomical, and behavioural differences shape bone structure and influence its mechanical properties. Most studies have measured strains of the hind limb bones during locomotion, either on a treadmill where speed is controlled or free locomotion. Strain measurements from common breeds of chickens during unrestricted, varied activities have yet to be reported. Additionally, it remains unknown how loading history, determined by the housing system in which pullets are reared, would affect in vivo strain magnitudes and patterns in long bones during habitual activities.

Thus, our study aims to investigate the in vivo mechanical strains at the tibiotarsus during a variety of activities performed by two common commercial breeds of pullets. The pullets were raised (reared) in three different styles of commercial housing: two of the rearing housings were aviaries while the third rearing housing was conventional cages. Given that brown-feathered pullets have higher body weight, we hypothesize that 1) brown-feathered pullets will experience higher strains compared to white-feathered pullets. We also hypothesize that 2) across all sampled activities, mechanical strains will be higher in pullets reared in conventional cages compared to aviary-reared pullets.

Methods

Pullet Housing and Management

All animal use and procedures were approved by the University of Guelph animal care committee (AUP #4127) and the McGill University animal care committee (AUP #8083). Over a two-year period, three consecutive flocks of Lohmann Selected Leghorn Lite (*W*, white-feathered) and Lohmann Brown Lite (*B*, brown-feathered) female chickens (*Gallus gallus domesticus*) were obtained from a commercial hatchery at the age of one day old. The pullets were reared from 1 day of age to 14 weeks at the University of Guelph in either conventional rearing cages (*Conv*: Ford Dickinson, Mitchell, Ontario, Canada) (Fig. 1A), or one of two styles of commercial aviaries. The aviaries had either low or high spatial complexity (*Low*: Natura Primus, Big Dutchman, Holland, MI, U.S.A; *High*: NivoVaria, Jansen Poultry Equipment, Netherlands, and Farmer

Automatic Portal Pullet, Clark Ag Systems, Caledonia, ON, Canada) (Fig. 1B-C) and have been shown to motivate different amounts of physical activity (Pufall et al., 2021). Pullets of each breed were housed separately. For each flock, the *Low* complexity aviaries were duplicated and installed back-to-back within a room, therefore housing both breeds separately in the same room. *B* and *W* pullets in *High* complexity aviaries were housed in separate rooms for each flock, as the aviaries were too large to duplicate within a single room.

Figure 1: Rearing housing system photos and illustrations during the brooding (0-6 weeks) and post-brooding (7-14 weeks) phases. A) Conventional cage, B) Low complexity rearing aviary, C) High complexity rearing aviary.

Pullets were reared in *Conv* cages with 30 pullets/cage (h: 40 cm, w: 76 cm, d: 66 cm) during weeks 0-6 (167 cm^2/pullet), and 15 pullets/cage during weeks 6-14 (334 cm^2/pullet space allowance) (Fig. 1A). For each flock, a total of 300 pullets per breed were reared in *Low* aviaries (Fig. 1B). Chicks were confined to a brooding compartment (height: 50 cm, width: 122 cm, depth: 94 cm) from 0-6 weeks of age (space allowance of 76 cm^2/pullet from week 0-3 and 198 cm^2/pullet from weeks 3-6). Brooding compartments were equipped with two perches, an internal feeding trough, and a line of nipple drinkers. After 6 weeks of age, the brooding compartments were opened, allowing access to the litter floor, three tiers, additional perches, and ramps, increasing the space allowance to 118 cm^2/pullet within the system and 74 cm^2/pullet of litter space, for a total of 192 cm^2/pullet. The *High* housing group had 600 pullets per breed per flock. During weeks 0-6 they had access to six perches and platforms and a space allowance of 128-138 cm^2/pullet. Pullets had a space allowance of 307-340 cm^2/pullet thereafter, once they were granted access to outer platforms, an additional perch, and litter space (Fig. 1C). During weeks 0-6, *High* aviaries were also equipped with two feed troughs, and two lines of nipple drinkers. Maximum perch or platform height did not differ between *Low* and *High* (170 cm), but *High* had a greater number of perches and platforms, and therefore more variety in perch and platform height. In addition to differences in 2-dimensional space allowance, the aviary housing systems (*Low*, *High*) offer more vertical space (via access to tiers, platforms, and perches) and are more spatially complex, compared to *Conv*. Feed, vaccination, lighting, and temperature programmes were constant across groups; further details are reported elsewhere (Rentsch et al., 2023b; Ross, 2021).

A total of 48 fourteen-week-old *W* and *B* pullets were randomly sampled [n=8/breed (2)/rearing housing system (3)] and transported from the University of Guelph to McGill University (Donald McQueen Shaver Poultry Complex) across three separate occasions over the course of 2 years. The experiment was therefore broken down into three rounds, where a subset of animals was analyzed per round. During each round, upon arrival at McGill, the *W* and *B* pullets were housed in separate identical rooms consisting only of litter floor (total area of 13.2 m^2). Pullets were fed *ad lib* standard age-appropriate crumble diet. A lighting schedule of 10h of light per day, at 10 lux, was maintained, and rooms were kept at 20°C. Pullets were allowed to acclimate for at least 72 h prior to the onset of the experiment. Time constraints allowed for experimentation

on two pullets per day, and thus each round of the experiment occurred over at most a 14-day period. Pullets were weighed the morning prior to undergoing surgery.

Surgical Procedure to Attach Strain Gauges to the Chicken Tibiotarsus

Pullets were sedated with 0.5-1% of isoflurane at 1 L/min O_2 flow rate using a mask, and then intubated and maintained under anesthesia at 2-4% isoflurane. Feathers were minimally plucked from the medial side of the right hindlimb and a 2 cm^2 region above the right side of the pelvis (Fig. 2A). The length of the tibiotarsus was then measured (distal tibiotarsal medial condyle to proximal medial tibiotarsal plateau, located via palpation) and the midpoint of the bone marked on the skin. We considered the bone midpoint a functionally equivalent site across breeds, as the relative position of structures attached to long bones has been shown to be invariant during growth in chickens(Grant et al., 1980). Incision areas on the limb and pelvic regions were cleaned using chlorohexidine, and pullets were wrapped in sterile cling wrap and laid on their right side on a sterile surgical drape. A 1 cm long incision was made above the medial side of the right tibiotarsus midshaft. To access the medial aspect of the tibiotarsus, blunt dissection was performed between the *gastrocnemius pars medialis* and the *tibialis cranialis*. Further blunt dissection of the *extensor digitorum longus* and *flexor digitorum longus* exposed the anterior and posterior sites of the tibiotarsus midshaft, respectively.

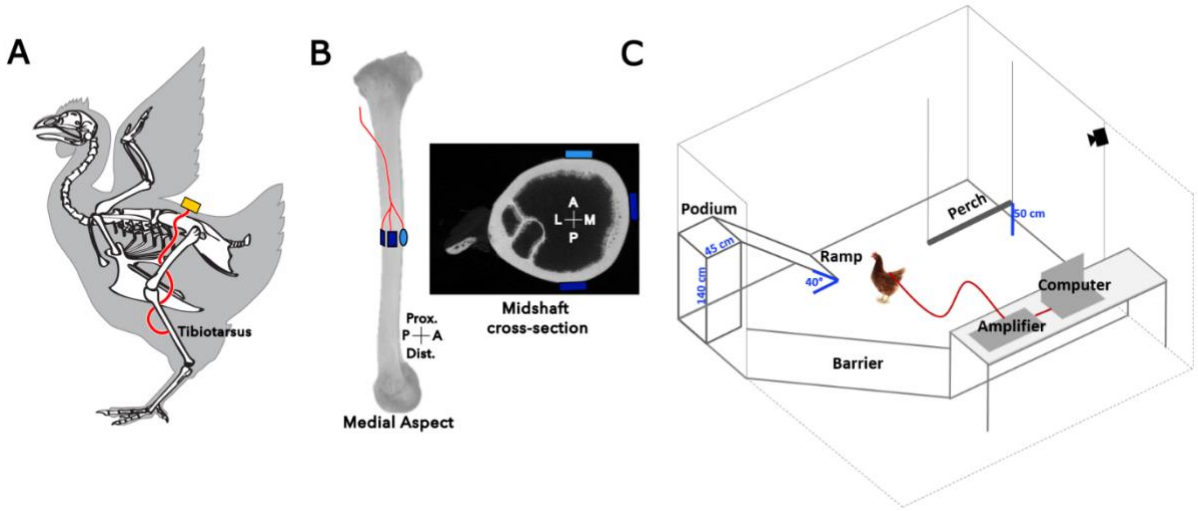

Figure 2: Experimental methods. A. Chicken skeleton, with strain gauge lead wires (*red*) and breakout plug (*yellow*) at pelvic region. **B.** Medial and cross-sectional aspects of the tibiotarsus, with attached strain gauges at the midshaft: one rosette on anterior surface (*light blue*), and two single element gauges on medial

and posterior surfaces (*dark blue*). **C.** Illustration of experiment arena and data acquisition equipment. Dimensions of podium, ramp inclination, and perch height are indicated in blue.

Strain gauge preparation was performed prior to surgery according to methods described previously (Biewener, 1992). Briefly, gauges were instrumented with 36" insulated wire, (36TDQ; Pheonix Wire Inc., Vermont, U.S.A), coated, and connected to a 10-position female breakout plug (5-534206-5; TE Connectivity, Canada). A first coating of epoxy resin (M-Bond AE-10, Micro-Measurements, U.S.A) was applied to the lead wire solder pads, followed by a coat of xylene-based latex (M-Coat D; MicroMeasurements, U.S.A) and thereafter polyurethane (M-Coat A; MicroMeasurements, U.S.A). During surgery, a long pair of forceps was used to make a subcutaneous tunnel from the limb incision site to the plucked region above the pelvis, along the medial side of the thigh (inguinal region) and moving laterally at the hip around the trunk towards the pelvic region, where an incision was made to expose the forceps and the wired gauges were tunnelled back to the limb incision site. Care was taken to avoid damaging the lead wire insulation when bringing the gauges through the subcutaneous tunnel. Sites of approximately 4 mm^2 on the anterior, medial, and posterior surface of the tibiotarsus midshaft (Fig. 2B) were prepared for gauge attachment by light scraping with a periosteal elevator to remove any periosteal tissue, dried with 100% ethanol, and defatted with methyl ethyl ketone. One rosette (FRA-1-11; Tokyo Sokki Kenkyujo Co., Ltd, Tokyo, Japan) and two single-element (EA-06-015LA-120; Micro-Measurements, U.S.A) gauges were attached to the anterior (rosette), medial, and posterior aspects (Fig. 2B) using cyanoacrylate adhesive (Ultra Liquid Control Super Glue; LePage, Canada). Anterior, medial, and posterior gauges were attached at the same cross-sectional level of the bone, with the central element of the rosette or the single-element gauges positioned in alignment with the bone's longitudinal axis.

Following gauge attachment to the bone, muscle fascia overlying the *gastrocnemius pars medialis* and the *tibialis cranialis* were sutured discontinuously (coated Vicryl 4-0 27"; ETHICON, U.S.A), and 1.5 cm of wire was tucked in subcutaneously at the midshaft incision site to avoid tugging on attached gauges during in vivo data collection. Similarly, 1.5-2 cm of wire was tucked away subcutaneously at the pelvic region incision site. Both limb and pelvic skin incisions were closed by continuous suturing. We locally administered 2-3 drops of a buprenorphine-lidocaine cocktail to each sutured incision site as an analgesic. Two elastic strings

were glued to either side of the breakout plug and sutured to nearby skin of the pelvic region to further avoid tension in lead wires and gauge detachment. Isoflurane was then slowly decreased while post-operative injections of saline (subcutaneous, 7 mL/kg) and meloxicam (NSAID, intramuscular, 0.09 mL/kg) were administered. Pullets recovered for 2-3h before experimental recordings were made.

Strain Data Collection

Following surgery recovery, pullets were alert and did not show signs of pain or lameness. Strain signals were measured by connecting the breakout plug at the flank region of the pullet to a 3 m long shielded cable (326-BSV; Micro-Measurements, U.S.A) connected to a bridge amplifier (System 8000 Scanner; Micro-Measurements, U.S.A) (Fig. 2A, C). Quarter-bridge channels were balanced and calibrated (±1000 με shunt calibration) prior to recordings while holding the pullet in the air such that the limbs bore no weight. Strains were recorded (StrainSmart, Micro-Measurements, U.S.A) using an excitation voltage of 3V and sampled at 1 kHz. A custom trigger circuit with input to the amplifier was used to digitally label strain data collected with the type of behaviour being performed at that moment. Therefore, a total of 6 channels were recorded corresponding to the three elements of the anterior rosette gauge (Fig. S6), the two single element gauges on the medial and posterior surfaces, and the trigger. Every time the trigger was pressed, the experimenter logged the timestamp of the trigger and the associated behaviour being performed by the pullet. This allowed the association between strain data and behaviour type. Video footage was collected with a smartphone of the entire arena to be used in conjunction with the trigger data and activity log to further inform the association between strain data and activity being performed.

An area of approximately 8 m^2 within a 13.6 m^2 room was enclosed by a clear plastic sheet and 0.5 m high barriers (Fig. 2C). The arena contained a custom-built wooden podium (140 × 45 × 45 cm), a detachable ramp (218 cm, 40° inclination), and a round perch (2.5 cm diameter, 0.5 m high, wood) suspended by rope. The perch was held in place while perching data was collected. The ramp surface was covered with a 1 cm thick rubber slab and 1 cm^2 wire mesh sheet. Ramp angle and surface was selected based on reported recommendations (LeBlanc et al., 2018). All wood surfaces were treated with water sealant and were regularly cleaned. Strains were collected across 6 trials according to the different behaviours measured: ground locomotion, uphill ramp locomotion, downhill ramp locomotion, perching, jumping, and aerial transition landing. We

considered the pullet to be perching when the abdomen was in contact with the perch, and the knee and ankle were in complete flexion. Jumping did not involve wing flapping and the landing trajectory was mainly vertical, whereas aerial transition landing involved the use of wing flapping and a generally horizontal approach to the ground. The ramp and perch were introduced into the arena only for ramp locomotion (uphill and downhill) and perching trials, respectively. One experimenter remained with the chicken, motivating different activities by light taps to the back of the feet, and holding the attached cable. A second experimenter would trigger, log activity type and timestamp, and monitor recordings on the computer. Collection trials for ground, uphill, and downhill locomotion consisted of at least one segment of three or more consecutive steady steps. Perching events were each recorded for 1 min. For jumping and aerial transition landing events, two repeats of each activity type were collected. Carcasses were frozen for later dissection. Following dissection, bones were fixed in 70% ethanol.

In vivo strain analysis

Raw strain data was plotted in sets of 30 s intervals for visual inspection. Using plots, video footage, and trigger/activity log information, segments of interest containing sets of at least three steady steps (ground, uphill, and downhill locomotion), 30s of recording (perching), or an event of interest and subsequent steps (jumping and aerial transition landing) were extracted. Each segment of interest was analyzed using custom Python scripts (https://github.com/BWillieLab/InVivo_StrainGauging) which prompts the user to select graphic user input points to temporally flank swing phases and peak strain phases. Data was filtered using a fourth order Butterworth filter with a cut-off frequency of 40 Hz. Data from each segment was then zeroed by subtracting strain values by the average strain measured during the nearest swing phase. For ground, uphill, and downhill locomotion, one swing phase within each segment of consecutive steps was selected to zero the segment by subtracting the mean strain value of the swing phase from the whole segment. Peak strains during each step within the segment were averaged, resulting in one average peak strain value per segment of steps. Locomotion step frequency (step s^{-1} [Hz]) was also derived for each segment of ground, uphill, and downhill locomotion from the number of steps and segment duration. For perching, strains were zeroed using the closest (temporally) locomotor segment swing phase measured, and peak strains were measured as the average strain across a 1-minute period. Zero values for jumping and aerial

transition landing events were selected from a swing phase during locomotion immediately following the jump when possible, or from the closest (temporally) locomotor segment swing phase (either ground, uphill, or downhill), and peak strain was determined at the time of landing. Data points where peak zeroed-strain magnitude was zero were excluded, as well as data points further than 5 median absolute deviations away from the mean.

We collected longitudinal strain measurements at the anterior, medial, and posterior site, from the central element of the rosette strain gauge (anterior) or the single-element gauges aligned with the bone's longitudinal axis within a margin of error of ±10°. In sparse cases where the angle offset of the rosette was undeterminable (e.g., detachment of rosette before being able to measure), the offset was set to zero, i.e., the axial element of the rosette gauge was assumed to be in line with the bone's longitudinal axis. From zeroed rosette strain data measured at the midshaft's anterior surface, principal tensile (ε_t) and compressive (ε_c) strains as well as the angle of principal tensile strain relative to the bone's longitudinal axis (adjusted in cases where the rosette gauge was misaligned relative to the bone's long axis), referred to as tensile strain orientation (θ_t), were determined, under the assumption of a planar strain state (38). Graphic user inputs created during the analysis of longitudinal strains that flank regions of swing phase and peak strains were reutilized to calculate peak ε_t, ε_c, and θ_t. Positive θ_t denotes a lateral (counterclockwise) rotation from the bone's longitudinal axis, whereas negative angles denote a medial (clockwise) rotation, as viewed from the proximal end of the tibiotarsus.

Measures of shear strain (γ) and fractional tensile strain ratio (FTSR) at the time of peak principal strain on the anterior surface were then derived (Carter, 1978; Moreno et al., 2008):

$$\gamma = 2 \times \sin\theta_t \times \cos\theta_t \times (\varepsilon_t - \varepsilon_c)$$

$$FTSR = \frac{\varepsilon_t}{\varepsilon_t + |\varepsilon_c|}$$

where ε_t and ε_c are principal tensile and compressive strains, respectively. The FTSR indicates how dominant principal tensile strain is relative to principal compressive strain. Equal amounts of tensile and compressive principal strain (i.e., FTSR = 0.5) is indicative of a strain environment consisting solely of torsion, therefore FTSR can also be interpreted as an indicator of the dominance of torsion (as opposed to bending or axial compression). We also used longitudinal

strain recordings from the anterior and posterior axial gauges to derive peak axial (ε_{ax}) and bending strains (ε_b), using the following equations (Main, 2007):

$$\varepsilon_{ax} = \frac{\varepsilon_{anterior} + \varepsilon_{posterior}}{2}$$

$$\varepsilon_b = \left|\frac{\varepsilon_{anterior} - \varepsilon_{posterior}}{2}\right|$$

Ground, uphill, and downhill locomotion strain data points consist of the mean peak strain across a segment of 3 or more consecutive steps. Data from as many segments as available were analyzed; based on differences in willingness to locomote, some chickens had more segments than others, and each segment of steps was performed at varying locomotor step frequencies given this was not controlled for. Perching data points are averages across the measured duration (1 min), and data points from jumping and aerial transition landing consist of the average peak strains across the two replicates performed. Due to strain gauge failure and data exclusion, the sample size of our reported data was lower than n=8 for some parameters; exact sample sizes for each strain gauge site and activity are shown in Table S1 and Fig. 3 legend.

Mixed effects model and outcome correction

To evaluate how mechanical strain outcomes are influenced by housing and breed, a linear mixed-effects model was implemented using *lmer* (*lme4* R package, v 1.1-27.1). For each mechanical strain outcome per activity type, the fixed effects were rearing housing, breed, body weight, and step frequency (only available for ground, uphill, and downhill locomotion), and we adjusted for the random effect of each chicken to account for repeated measures (i.e., multiple segments recorded per chicken). The model was formulated as:

$$y_{ijk} \sim (F_i \times M_i) + \left(H_j \times G_k\right) + (1|C_i) + e_{ijk}$$

where y is the mechanical strain outcome of interest (continuous), F is step frequency (continuous), M is weight (continuous), H is housing condition (categorical; $H = \{Conv, Low, High\}$), G is breed (categorical; $G = \{B, W\}$), $1|C$ is the random effect for each chicken, and e is the residual error for the i^{th} chicken, the j^{th} housing condition, and k^{th} breed. An intercept term was also included, but not shown. The interaction terms $F \times M$ and $H \times G$ were justified following the observation that there were crude associations between step frequency and weight (Fig. 3A), and housing and breed (Fig. 3B), respectively. For activities where step

frequency was not available (perching, jumping, and aerial transition landing), the step frequency term F was omitted from the model. Ground, uphill, and downhill locomotion strain data points consisted of the average peak strain across consecutive steps within a segment. For these data points, the inverse standard deviation of peak strains within a segment $[sd(y)^{-1}]$ were used to weight each observation, thereby penalizing segments of steps with high intra-segment variability in strain [*lmer(…, weights=1/sd)*]. Model fits were verified by ensuring that residuals were centered around zero and normally distributed, and by visual inspection.

To account for variability in step frequency within ground, uphill, and downhill locomotion segments sampled from a given chicken and enable visual comparisons of plotted data between groups, we adjusted strain outcomes as if they were obtained from chickens with constant step frequencies per group. This was necessary given that in vivo strains have been widely shown to be influenced by locomotor speed (Biewener et al., 1983; Gatesy & Biewener, 1991; Loitz & Zernicke, 1992), which we did not control for and was not resemblant of habitual locomotor speed in their rearing housing environments. This was accomplished by using the fitted models above to predict new strain outcomes using original housing conditions, breeds, and chicken labels, and substituting chicken-specific step frequencies for group-median step frequencies. All strain values reported hereafter are normalized for step frequency unless otherwise specified.

Statistical Analysis

Two-way ANOVA was performed on strain data (prior to normalization for step frequency) to determine effects of rearing housing and breed (and interaction term) on strain outcomes, followed by pairwise Student's t-tests. Multiple comparison p-values are reported as adjusted (Benjamini-Hochberg procedure) p-values denoted with the letter *q*. Unadjusted pairwise comparison and ANOVA p-values are denoted with the letter *p*. Differences between breed groups are reported as the percentage difference of strain magnitude in B relative to W ($\%\Delta_{B-W} = \left({}^{(|B| - |W|)}/_{W}\right) \times 100$). Differences in strain magnitudes between the *Low* or *High* housing group relative to *Conv* are also reported as percentage differences ($\%\Delta_{A} = \left({}^{(|A| - |Conv|)}/_{Conv}\right) \times 100$, where A is specified in each case to be either *Low* or *High*). The effect of breed and rearing housing on body weight and step frequency was assessed by two-way ANOVA, and post-hoc comparisons using Tukey-Kramer correction with p-values denoted

by the letter *q*. We adjusted for the random effect of each chicken to account for repeated measures of step frequency (i.e., multiple step frequencies from multiple segments recorded per chicken). Significance was set at 0.05 (for both unadjusted and adjusted).

Results

Locomotor step frequency and body weight are dependent on breed and rearing housing

We investigated the effect of breed (*B* or *W*) and rearing housing (*Conv, Low, High)* on pullet body weight and locomotor step frequency to determine whether these variables needed to be included as predictors in our statistical model. We found that breed influenced body weight ($p < 0.001$), where *B* pullets had higher weights compared to *W* (19%, $p < 0.001$, Fig. 3A). Breed and rearing housing had an interactive effect on body weight ($p = 0.001$): although rearing housing did not influence *B* weight, in *W* pullets *High* had 13% greater weight compared to *Low* ($q = 0.038$, Fig. 3A).

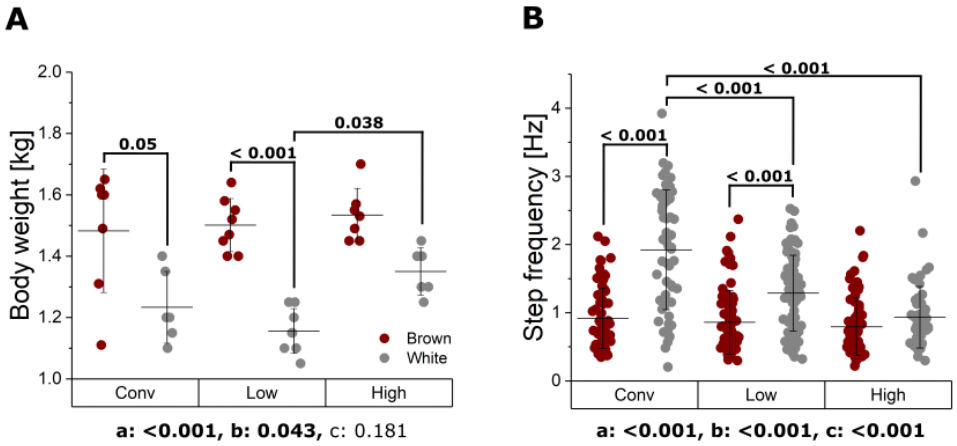

Figure 3: Effect of breed and rearing housing on A) body weight, and B) step frequency pooled for the three locomotor activities (ground, uphill, downhill) (mean ± sd) (n=6 for *W Conv* and *W High*, n=7 for *B Conv* and *B High*, n=8 for *B Low* and *W Low*). ANOVA main effects: a) breed, b) rearing housing, c) interaction. Significant Tukey-Kramer post-hoc comparisons indicated by bars specifying groups being compared, with p-values above. Note: each step frequency data point corresponds to the step frequency from a segment of locomotion recorded. Each individual chicken contributed multiple segments, and the number of segments varied across chickens.

Breed and rearing housing had individual and interactive effects on step frequency pooled from the three locomotor activities measured ($p < 0.001$ for breed and rearing housing effects)

(Fig. 3B). *B* pullets had lower step frequency compared to *W*, when reared in *Conv* (-51%, q < 0.001) and *Low* (-37%, q < 0.001) (Fig. 3B). Rearing housing did not affect step frequency in *B*, while in *W* step frequency progressively decreased with increased rearing housing complexity (*High* relative to *Conv*: -48%, q < 0.001; *Low* relative to *Conv*: -29%, q < 0.001; *High* relative to *Low*: -27%, q = 0.003); meaning that *W Conv* pullets had greater experimental step frequency than *W High* pullets. The effect of breed and rearing housing on pooled step frequency was the same for ground locomotion and downhill locomotion individually, while rearing housing did not influence uphill locomotion step frequency (Fig. S2), coinciding with lower step frequencies and consequent smaller effect size during uphill compared to ground (*B*: -42%, *W*: -52%) and downhill locomotion (*B*: -34%, *W*: -46%) (Fig. S1).

Strain patterns differ between brown and white pullets

We analyzed longitudinal strains from the axial elements at the anterior, medial, and posterior surfaces of the tibiotarsal midshaft, derived principal and shear strains from the rosette at the anterior surface, and cross-sectional measures of axial and bending strain derived from anterior and posterior longitudinal strain measurements. Strain patterns were generally less variable during ground, uphill, and downhill locomotion, compared to perching, jumping, and landing. We highlight this by presenting results separated into steady locomotor activities (ground, uphill, and downhill locomotion) and non-steady (perching, jumping, and aerial transition landing) activities. To account for a given pullet's variability in step frequency across locomotor segments sampled, given the positive relationship between step frequency and strain magnitude, strain outcomes were recalculated with our mixed-effects model using constant step frequencies for each group. We selected a median step frequency per housing/breed group and per locomotor activity, given the effect of breed and rearing housing on step frequency (Fig. 3B). Unadjusted locomotor strain data are reported in the supplementary section (Fig. S2-4).

Breed influenced longitudinal strains only during steady locomotor activities (Fig. 4). During ground locomotion, breed affected longitudinal strains at all 3 anatomical sites: *B* anterior strains were less tensile (-16%, p = 0.002, Fig. 4A), medial strains less compressive (-87%, p < 0.001, Fig. 4D), and posterior strains more compressive (18%, p = 0.048, Fig. 4G) compared to *W*. During uphill locomotion, breed only affected medial longitudinal strains, with *B* strains being less compressive (-66%, p = 0.004, Fig. 4B). During downhill locomotion, medial strains were

tensile in *B* whereas compressive in *W*, with lower in magnitude in *B* (-68%, $p < 0.001$, Fig. 4F), and posterior strains were more compressive in *B* compared to *W* (88%, $p = 0.007$, Fig. 4I). Breed also affected principal tensile (ε_t), principal compressive (ε_c), and tensile strain orientation (θ_t) during ground and downhill, but not uphill, locomotion (Fig. 5). During ground locomotion, *B* generally had higher ε_c (98%, $p < 0.001$, Fig. 5D), and lower θ_t (-19%, $p < 0.001$). During downhill locomotion, *B* had lower ε_t (-38%, $p < 0.001$, Fig. 5C), and specifically in pullets reared in High, ε_t was 38% lower in *B* ($q = 0.026$, Fig. 5C) compared to *W*.

Shear (γ), peak axial (ε_{ax}), and peak bending (ε_b) strains were affected by breed during all steady activities (Fig. 6). During ground locomotion, γ was generally positive and higher in *B* (26%, $p = 0.025$, Fig. 6A), while ε_{ax} was more compressive (137%, $p = 0.001$, Fig. 6B) compared to *W*. During uphill locomotion, γ was lower (-46%, $p < 0.001$, Fig. 6D) in *B* compared to *W*. During downhill locomotion, γ was also lower in *B* compared to *W* (-54%, $p < 0.001$, Fig. 6G), and specifically within pullets reared in *Low* (-77%, $q = 0.006$, Fig. 6G). Downhill ε_{ax} (101%, $p = 0.011$, Fig. 6H) and ε_b (49%, $p = 0.032$, Fig. 6I) were higher in *B* compared to *W*.

Anterior, medial, and posterior longitudinal strains, ε_c, θ_t, ε_{ax}, and ε_b during non-steady activities were unaffected by breed (Fig. 7-9). ε_t and γ strain were affected during jumping and aerial transition landing, but not perching. During jumping, ε_t was less tensile in *B* compared to *W* (-75%, $p < 0.001$, Fig. 8B), and specifically *High* reared *B* pullets had less tensile ε_t compared to *W* (-73%, $q = 0.004$, Fig. 8B). During jumping, γ was lower in *B* compared to *W* (-25%, $p = 0.046$, Fig. 9D). During aerial transition landing, γ was higher in *B* compared to *W* (169%, $p = 0.036$, Fig. 9G).

Conventional cage reared pullets had higher strains during steady activities and lower strains during non-steady activities, compared to aviary-reared pullets

Rearing housing affected longitudinal and derived strains during steady activities (Fig. 4-6). Rearing housing influenced anterior, but not medial or posterior, longitudinal strains during ground locomotion ($p < 0.001$, $\Delta_{High} = -43\%$, $\Delta_{Low} = -68\%$, Fig. 4A), uphill locomotion ($p = 0.002$, $\Delta_{High} = -35\%$, $\Delta_{Low} = -50\%$, Fig. 4B), and downhill locomotion ($p = 0.003$, $\Delta_{High} = -27\%$, $\Delta_{Low} = -56\%$, Fig. 4C). During ground locomotion, rearing housing affected ε_t ($p < 0.001$, $\Delta_{High} = -28\%$, $\Delta_{Low} = -28\%$, Fig. 5A). Axial and bending strains, but not shear, were influenced by rearing

housing during ground and uphill locomotion: Rearing housing influenced ε_{ax} ($p = 0.008$, Δ_{High} = 88%, Δ_{Low} = 134%, Fig. 6B) and ε_b ($p < 0.001$, Δ_{High} = -37%, Δ_{Low} = -43%, Fig. 6C) during ground locomotion, and ε_b during uphill locomotion ($p = 0.032$, Δ_{High} = -22%, Δ_{Low} = -36%, Fig. 6F). However, housing and breed interacted to affect γ during ground locomotion ($p = 0.042$, Δ_{High} = -8%, Δ_{Low} = -17%, Fig. 6A). Pairwise comparisons were nonsignificant, but when we compared average strain levels between housing groups whenever housing had a significant effect, we consistently observed the pattern of *Conv* ≥ *High* ≥ *Low* in strain magnitude, with the percentage (%) difference between *Low* or *High* compared to *Conv* being higher than the % difference between *Low* and *High*. The direction of principal strain as quantified by θ_t was affected by rearing housing during ground locomotion ($p = 0.023$, Fig. 5G) and downhill locomotion ($p = 0.044$, Fig. 5I), and there was an interactive effect of breed and housing on θ_t during ground ($p = 0.001$, Fig. 5G) and uphill ($p = 0.017$, Fig 5H) locomotion.

Longitudinal strains, derived strains, and strain patterns were also affected by rearing environment during non-steady activities (Fig. 7-9). During jumping, rearing housing affected ε_t ($p = 0.006$, Δ_{High} = 166%, Δ_{Low} = 82%, Fig. 8B), and there was an interactive effect of rearing housing and breed on γ during jumping ($p = 0.002$, Brown: Δ_{High} = 113%, Δ_{Low} = 133%, White: Δ_{High} = -29%, Δ_{Low} = -73%, Fig. 9D). During aerial transition landing, rearing housing affected longitudinal posterior strains ($p = 0.042$, Δ_{High} = 123%, Δ_{Low} = 93%, Fig. 7I) and ε_{ax} ($p = 0.041$, Δ_{High} = 396%, Δ_{Low} = 294%, Fig. 9H). There were also no significant pairwise comparisons in strains during non-steady activities, but we see a consistent pattern, where the effect of housing is significant, of *High* ≥ *Low* ≥ *Conv*. As in steady activities, the % difference between aviary groups relative to *Conv* is greater than the % difference between aviary groups. θt was affected by rearing housing during jumping ($p = 0.044$, Fig. 8H), where *High B* pullets had higher θt compared to *Conv B* (68%, $q = 0.007$, Fig. 8H) and *Low B* (110%, $q = 0.003$).

The tibiotarsal midshaft experiences a combined loading environment dominated by torsion, with the highest strains produced during jumping and aerial transition landing

Across all activities sampled (and considering step frequency normalized locomotor data), longitudinal strains averaged 166 με, -139 με, and -522 με in *B*, and 251 με, -466 με, and -446 με in *W*, at the anterior, medial, and posterior sites, respectively (Table S2). The highest longitudinal

strains were achieved during jumping (-656 με) and aerial transition landing (-698 με) at the posterior surface (Table S3). The anterior surface was always in tension except during aerial transition landing, with mildly compressive strains averaging -64 με (Table S3). Anterior principal tensile and compressive strains averaged 529 με and -617 με in *B*, and 953 με and -602 με in *W* respectively, across all activities (Table S4), with peak levels achieved during jumping (ε_t = 1151 με) and aerial transition landing (ε_c = -1423 με) (Table S2). Tensile strain orientation was always positive, meaning that the axis of anterior principal tensile strain was always rotated counter-clockwise (laterally, if viewed in proximal-distal direction) relative to the bone's longitudinal axis. Anterior shear strains were on average 733 με in *B* and 784 με in *W* (Table S4). Peak average shear strains occurred during jumping (1071 με) but were nearly as high during aerial transition landing (931 με) and uphill locomotion (922 με) (Table S2). Peak axial strains averaged -167 με in *B* and -104 in *W*, and peak bending strains averaged 418 με in *B* and 461 με in *W* (Table S4), with bending strains being generally higher than axial strains across all activities sampled (Table S4).

Tibiotarsal strain patterns were more variable during non-steady activities compared to steady activities: during steady activities, 55% of measured tensile strain orientation data points lied within the range of 22.5°-67.5°, meaning closer to the diagonal (45°) than to the longitudinal or transverse axis of the bone whereas during non-steady behaviour only 27% lied within this range. During steady activities, principal tensile and compressive strains generally contributed equally to the overall principal strain (fractional tensile strain ratio (FTSR) near 0.5), with an average FTSR of 0.47 and a coefficient of variance (CV) of 29% (Fig. S5). During non-steady activities, FTSR averaged at 0.42 and was more variable, with a CV of 73% (Fig. S5). Group averages stratified by activity type (steady, non-steady) are included in the supplementary section (Tables S2, 4-7).

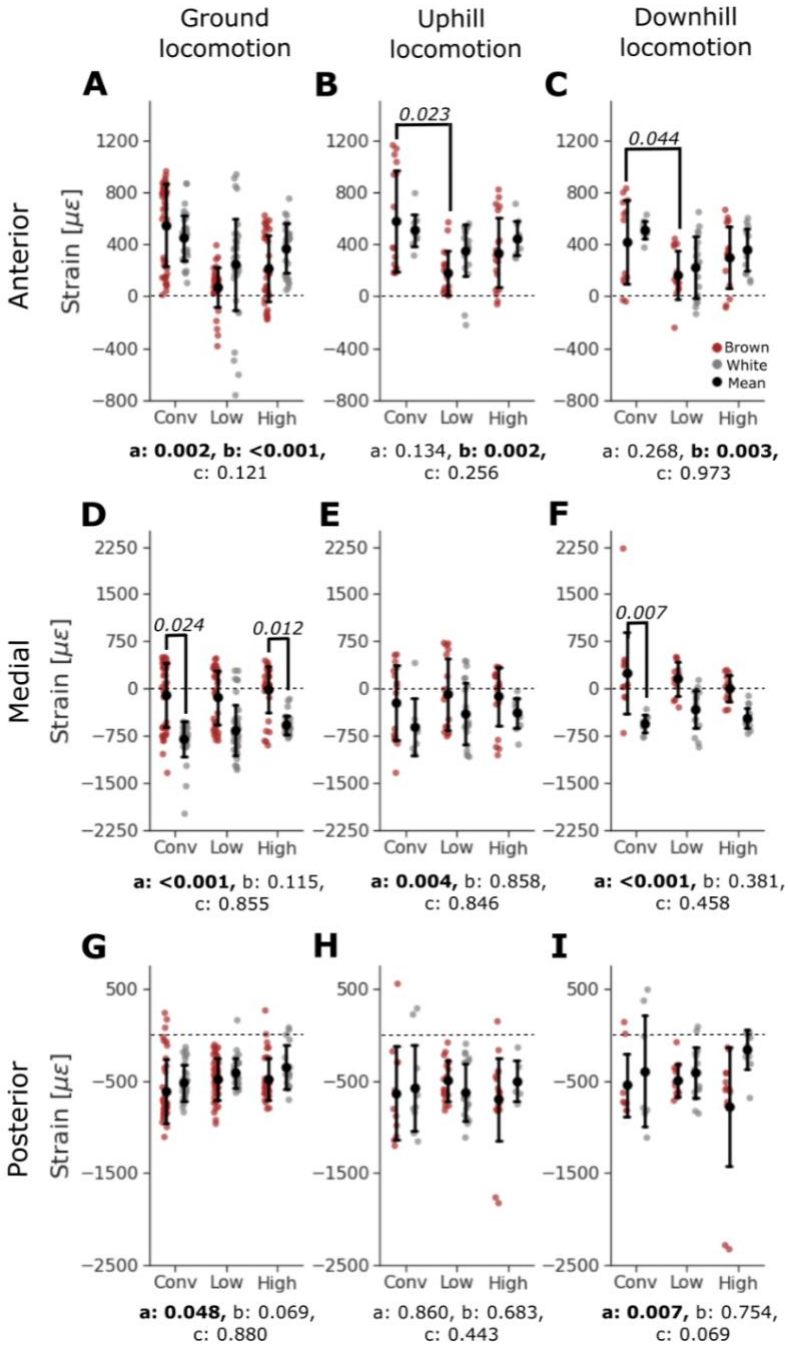

Figure 4: Effect of breed (*Brown*, *White*) and rearing housing (*Conv*, *Low*, *High*) on longitudinal strains during steady locomotor activities (mean ± sd). Data is normalized to the median step frequency per group, to control for within-chicken variations in step frequency. ANOVA main effects: a) breed, b) rearing housing, c) interaction. Groups with significant unadjusted (t-test) p-values indicated by bars with italicized p-values above. Note: plots within each row share the same y-axis scaling.

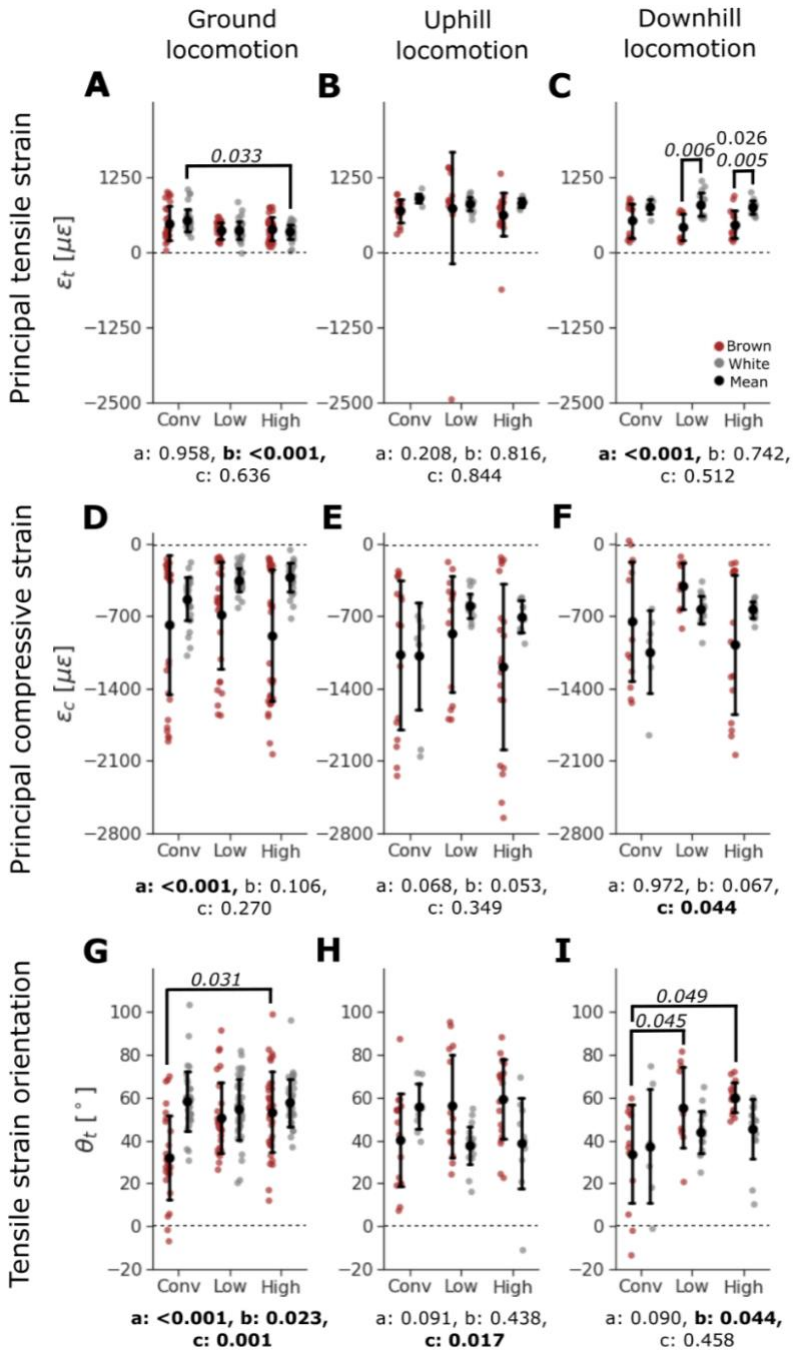

Figure 5: Effect of breed and rearing housing on principal tensile and compressive strains, and tensile strain orientation during steady locomotor activities (mean ± sd). Data has been normalized to the median step frequency per group, to control for within-chicken variations in step frequency. ANOVA main effects: a) breed, b) rearing housing, c) interaction. Groups with significant unadjusted or adjusted p-values indicated by bars with p-values above: Benjamini-Hochberg post-hoc (non-italicized) and t-test (italicized). Note: plots within each row share the same y-axis scaling.

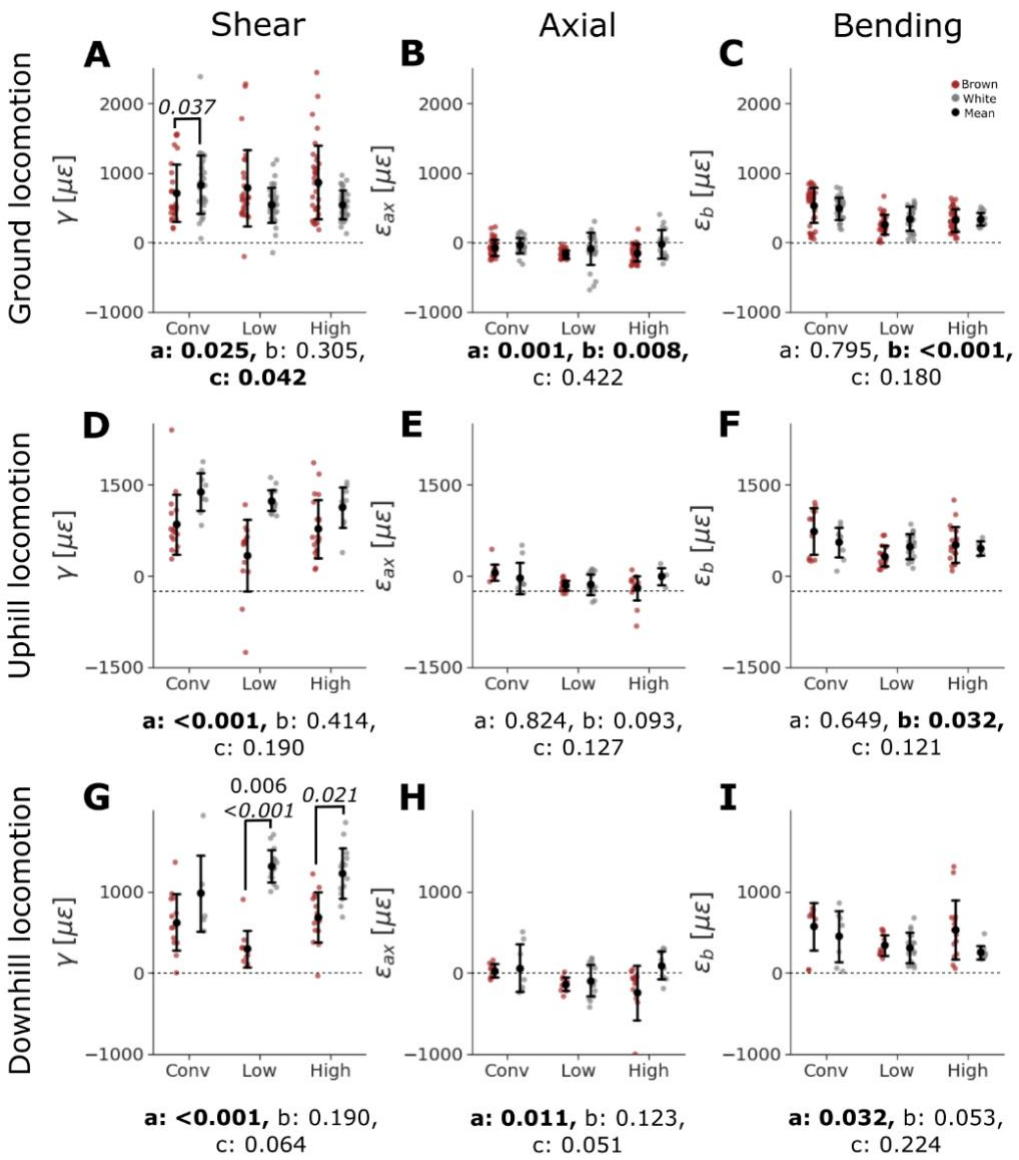

Figure 6: Effect of breed and rearing housing on anterior shear strains and peak axial and bending strains during steady locomotor activities (mean ± sd). ANOVA main effects: a) breed, b) rearing housing, c) interaction. Data has been normalized to the median step frequency per group, to control for within-chicken variations in step frequency. Groups with significant unadjusted or adjusted p-values indicated by bars with p-values above: Benjamini-Hochberg post-hoc (non-italicized) and t-test (italicized). Note: plots within each row share the same y-axis scaling.

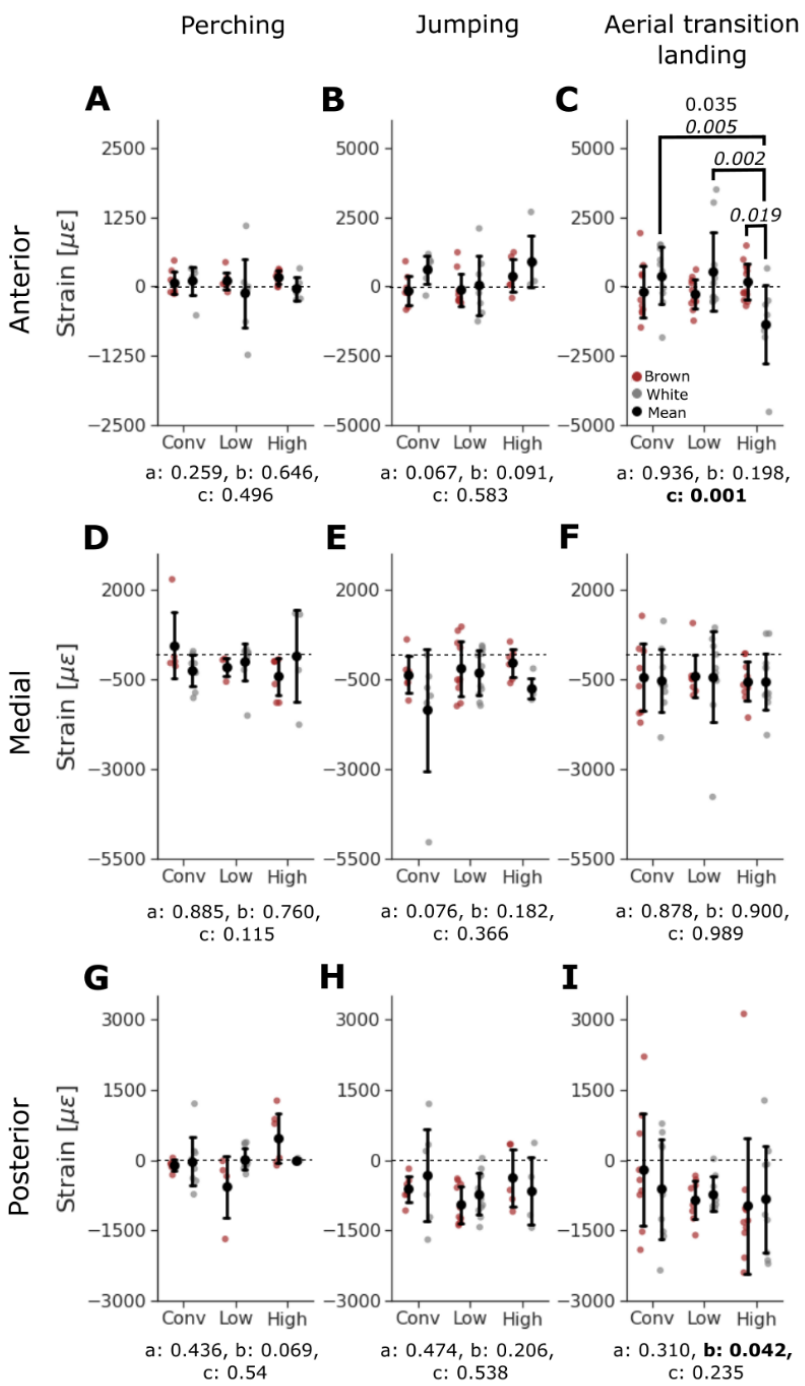

Figure 7: Effect of breed and rearing housing on longitudinal strains during non-steady activities (mean ± sd). Each column includes a different activity type measured and each row includes the anatomical site of the tibiotarsal midshaft sampled. ANOVA main effects: a) breed, b) rearing housing, c) interaction. Groups with significant unadjusted or adjusted p-values indicated by bars with p-values above: Benjamini-Hochberg post-hoc (non-italicized) and t-test (italicized). Note: Plot A has a different y-axis scaling than the rest of the row of anterior strains. All other plots within a given row share the same y-axis scaling.

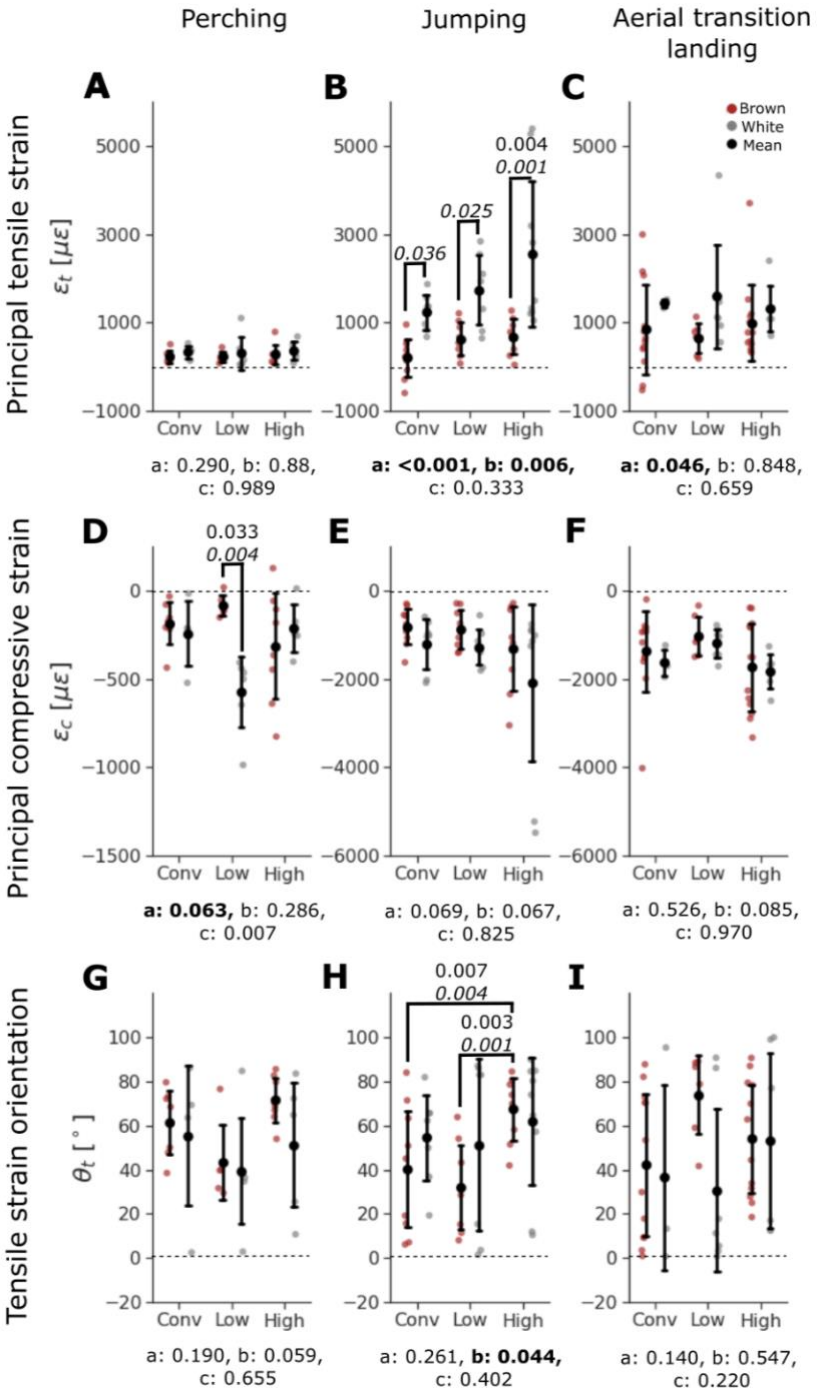

Figure 8: Effect of breed and rearing housing on principal tensile and compressive strains, and tensile strain orientation during non-steady activities (mean ± sd). ANOVA main effects: a) breed, b) rearing housing, c) interaction. Groups with significant unadjusted or adjusted p-values indicated by bars with p-values above: Benjamini-Hochberg post-hoc (non-italicized) and t-test (italicized). Note: Plot D has a different y-axis scaling than the rest of the row. All other plots within a given row share the same y-axis scaling.

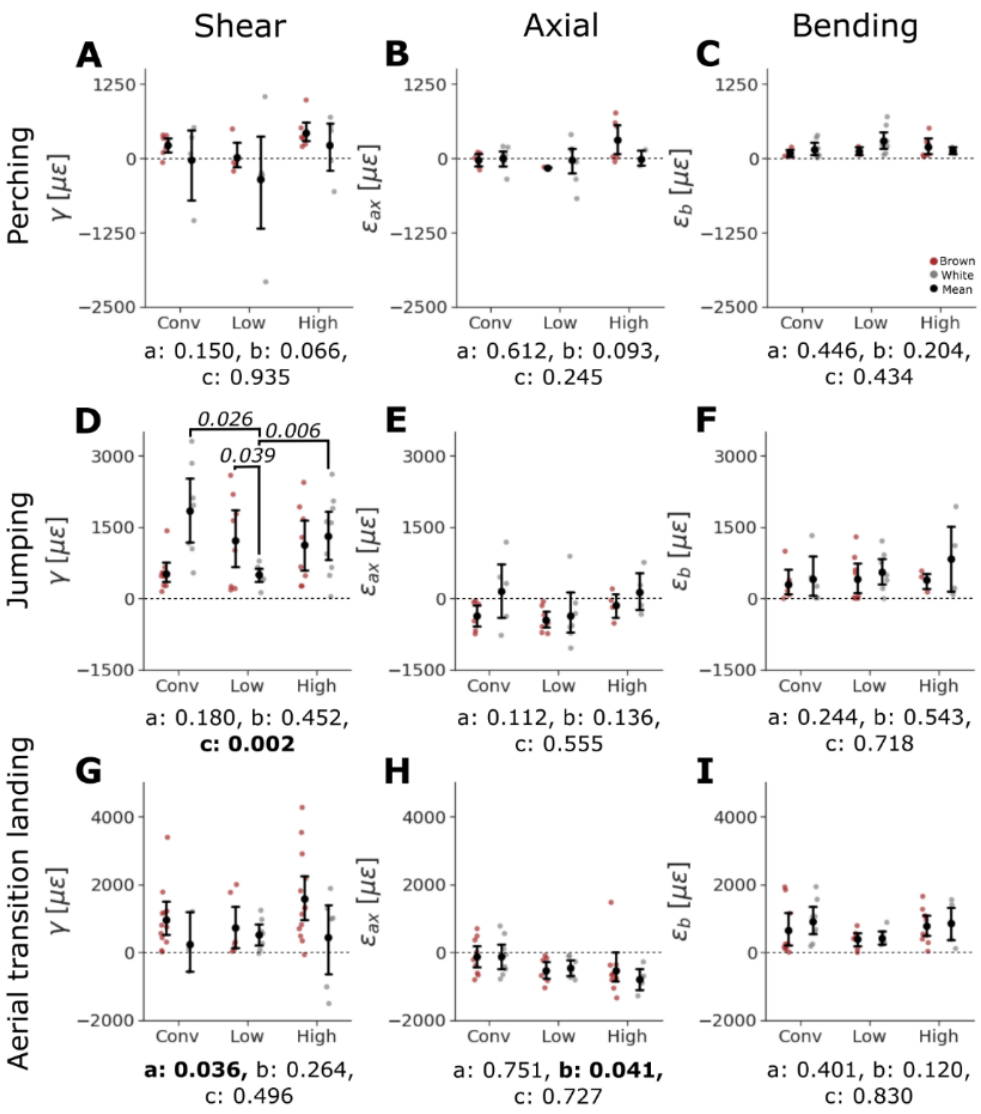

Figure 9: Effect of breed and rearing housing on anterior shear strains and peak axial and bending strains during non-steady activities (mean ± sd). ANOVA main effects: a) breed, b) rearing housing, c) interaction. Groups with significant unadjusted or adjusted p-values indicated by bars with p-values above: Benjamini-Hochberg post-hoc (non-italicized) and t-test (italicized). Note: plots within each row share the same y-axis scaling.

Discussion

In the current study, we assessed whether rearing housing and/or breed influenced mechanical strain magnitudes and patterns at the tibiotarsal midshaft during various activities performed by pullets. We grouped behaviours measured into steady (ground, uphill, and downhill locomotion) and non-steady (perching, jumping, and aerial transition landing) to facilitate interpretation, given

that we observed lower variability in steady compared to non-steady strains and similar patterns in terms of the effects of breed and rearing housing within each of these activity categories. We evaluated the effect of breed with Lohmann Brown Lite (brown feathered) and Lohmann LSL-Lite (white feathered) pullets since they are widely used in commercial egg farming, and differences in physiology and behaviour have been reported between them (32,43–47). In addition to a group reared in conventional cages, we selected two aviary styles representing different ends of the spectrum in terms of design complexity. Aviary complexity categorization was largely influenced by the spatial complexity during the brooding phase (up to 6 weeks of age): pullets in the *Low* but not *High* complexity aviary were restricted from using ramps and platforms. The *Low* and *High* complexity aviaries also differ in that the *High* complexity style has more perches and platforms and is therefore able to accommodate a higher number of birds using these structures.

Previous studies have examined in vivo tibiotarsal strains in avian species such as chickens (Biewener et al., 1986), turkeys (Rubin & Lanyon, 1984a), and emu (Main & Biewener, 2007). These studies measured strains during locomotion performed either on a treadmill or freely on the ground. In the current study, we measured strains during not only locomotor, but a range of activity types known to be naturally performed by chickens. In doing so we aimed to learn how genetic background and loading history influences bone mechanical properties. These data are critical to address the high incidence of osteoporosis and bone fractures that is endemic in this population and to determine what levels and types of physical activity enhance bone health. We hypothesized that both breed and rearing environment would affect mechanical strains measured. Specifically, we hypothesized that 1) Lohmann Brown (*B*) pullets would have higher strains compared to Lohmann LSL Lite (*W*) given their higher body weight, lower 3-point bending strength, and lower midshaft cortical thickness (Ross, 2021) and that 2) across all sampled activities, longitudinal and derived mechanical strains would be higher in pullets reared in conventional cages compared to aviary-reared pullets, as they are not adapted to activities of such intensity.

Our data did not support our first hypothesis in all strain outcomes for all activities. Instead, we observed a much more nuanced result with *B* pullets experiencing higher strain magnitudes compared to *W* for certain outcome parameters and during certain activities. We saw that breed affected longitudinal strains only during a subset of the activities sampled, namely during steady activities, while derived principal strains and shear were affected during both steady

and non-steady activities. These results indicate that *B* and *W* tibiotarsi undergo different loading conditions with different relative contributions of axial compression, bending, and torsion. In vivo strains are determined by the magnitude and direction of load, along with the structural and material properties of the bone withstanding the load. *B* and *W* pullets differ significantly in body weight, which is differentially distributed in the two breeds analyzed in this study. Normalized to body weight, *B* pullets have significantly lower pectoralis major, pectoralis minor, and bicep weights, and higher leg muscle weights (Pufall et al., 2021; Ross, n.d.). *B* pullets also have significantly lower keel bone area, humerus, radius, tibiotarsus, and femur length, and higher keel percent cartilage, also normalized to body weight (Pufall et al., 2021; Ross, n.d.). Although it has not been explicitly shown in these two breeds, these differences in muscle weights and bone lengths likely produce differences in the position of the center of mass and orientation of the ground reaction force vector relative to the tibiotarsus (Carrano & Biewener, 1999). Changes in center of mass position and limb orientation have been shown to affect levels of torsion in the femur of chicken (Carrano & Biewener, 1999); this is a possible explanation for the observed effect of breed on anterior shear strains that we see at the tibiotarsus midshaft. There are also possible effects of genetics independent of differences in anatomy or activity: in humans, multiple identical stress fractures were observed in monozygotic twins (Singer et al., 1990), and in chickens specifically, multiple studies have shown inheritance of bone characteristics affecting osteoporosis (Bishop et al., 2000; Dunn et al., 2007; Raymond et al., 2018).

Our second hypothesis regarding the effect of rearing housing was partially supported. Although pairwise comparisons were not significant, we saw a consistent pattern in parameters that were affected by rearing housing style. During steady activities, *Conv* pullets generally had higher strains compared to aviary-reared pullets. In contrast and unexpectedly, *Conv* pullets generally had lower strains compared to aviary-reared pullets during the non-steady activities jumping and aerial transition landing. We show that jumping and aerial transition landings produce the highest strains in both breeds, but these activities are only performed in aviary systems and have been shown to occur much less frequently than steady activities (Pufall et al., 2021; Rentsch et al., 2023b). Therefore, steady activities were likely the predominant driver of bone adaptation, and the bone adaptations induced by the steady activities to decrease the strain during steady activities may not have the same effect during non-steady activities.

Across activities measured, when housing is a significant predictor of strain we consistently see the pattern of *Low* pullets having lower strain magnitudes compared to *High* pullets, meaning that *Low* pullets tended to have limbs that are better able to resist bone deformation during these measured activities than *High* pullets. In a study that measured pullet behaviour in similar commercial aviaries, pullets housed in *High* aviaries performed more locomotion (walking and running), aerial transitions, and vertical transitions compared to those in *Low*, quantified as the number of occurrences per 30 min (Pufall et al., 2021). Whether these differences in number of locomotor and transition events translate to differences in bone adaptation is unclear and warrants further investigation. Studies examining how the number of loading cycles applied during in vivo controlled loading affect the mechanoresponse report that only a few daily loading cycles (reported ranging 5-60) are sufficient to produce an anabolic response, and that increasing the number of cycles beyond this level does not significantly increase the anabolic response (Rubin & Lanyon, 1984b; Sun et al., 2018; Umemura et al., 1997; Yang et al., 2017). Conversely, there is a clear dose-dependent relationship between the magnitude of applied load and the anabolic response in controlled loading studies, so long as the induced strain is within the window of lamellar bone formation (Hsieh & Turner, 2001; Sugiyama et al., 2012; Turner et al., 1994). Therefore, although *High* pullets may perform locomotion and aerial/vertical transitions more frequently (Pufall et al., 2021), if the *Low* pullets habitually encounter higher ground reaction forces for example by jumping from higher heights, this could lead to a stronger adaptive response, higher in vivo axial stiffness, and lower in vivo strains in *Low* compared to *High* groups. This explanation is supported by results showing that, compared to treadmill walking, high-impact drops were shown to produce higher strains and more bone formation in the mid-diaphysis of the tarsometatarsal of growing roosters (Judex & Zernicke, 2000), but further investigation into the mechanoresponse in pullets is required.

Measured peak in vivo tibiotarsal/tibial strain magnitudes across vertebrates broadly range from 600 με to 5180 με (peak longitudinal or principal strains, tensile or compressive depending on site measured) (Lanyon et al., 1975; Main, 2021a; Milgrom et al., 2000, 2015, 2022). Specifically in birds, previous studies have examined in vivo strains at the tibiotarsus of the chicken, emu, and turkey, during ground locomotion and report average peak principal tensile strain ranging from -1863 με to -2350 με measured at the midshaft (Biewener et al., 1986, p. 19;

Main & Biewener, 2007; Rubin & Lanyon, 1984a). We report peak longitudinal strain magnitudes of up to 698 με at the posterior midshaft and peak principal strain magnitudes at the anterior surface of up to 1473 με, both measured during aerial transition landing. We show that the tibiotarsus undergoes a combined loading environment in which torsion predominates. This agrees with other studies evaluating strains of the tibiotarsus and femur in birds (Biewener et al., 1986; Carrano & Biewener, 1999; Main & Biewener, 2007; Rubin & Lanyon, 1984a), and other previous reports showing that tibiotarsal bone cross-sectional geometry approximates an eccentric ellipsoid (Levenston et al., 1998; Ross, n.d.). We also show that aerial transition landing leads to unusual cross-sectional strain patterns evidenced by the fact that the anterior surface is in compression unlike during all other activities sampled where it is in tension. Aerial transition landing therefore may be an activity type that most strongly elicits bone formation. Further investigation comparing bone microstructure between *Conv* and aviary-reared groups can give insight as to whether there is higher bone mass and improved microstructure among birds with loading histories that include aerial transition landing. In humans, strains have been recorded as high as -3647 in compression, 1473 in tension, and 4967 in shear (Milgrom et al., 2015), and have been shown to be variable across individuals (Milgrom et al., 2022). These strain magnitudes are notably higher than what we report here for the pullet tibiotarsus, likely a reflection of the activity performed by the humans being more vigorous than that performed by the pullets. Nevertheless, we similarly see variability in strains across individuals, and high shear strains.

As early as at 11 weeks of age, Lohmann Brown Lite pullets were significantly heavier than Lohmann LSL Lite pullets, regardless of their rearing housing (Ross, 2021). This difference arises sometime after 6 weeks of age; at 6 weeks there is no difference in body weight between *B* and *W* pullets, regardless of what rearing environment they reside in (Ross, 2021). Although we did not see a significant interaction between breed and rearing housing on body weight, from pairwise comparisons we saw that rearing housing tended to affect body weight in *W*, but not *B* pullets. In addition, *B* birds were heavier than *W* birds when reared in *Conv* and *Low*, but not *High*. This finding warranted the inclusion of body weight as a predictor in our statistical model, allowing us to assess effects of breed and rearing housing on mechanical strains independent of body weight. *W* pullets reared in *High* complexity aviaries had significantly greater body weight compared to white birds reared in *Low*; but there was no difference in fat or lean content normalized to body

weight between *High* and *Low* pullets. We similarly investigated whether there was an effect of breed and rearing housing on measured step frequency to determine whether it should be included as another predictor in our model. Locomotor behaviours sampled in this study (ground, uphill, and downhill locomotion) were performed without controlling for speed (i.e. no treadmill), with the benefit of allowing for more natural behaviour. The effect of locomotor speed (Biewener et al., 1983; Gatesy & Biewener, 1991; Loitz & Zernicke, 1992), as well as body weight (Biewener, 1982; Biewener & Bertram, 1994; Carrano & Biewener, 1999; Main & Biewener, 2007), on mechanical strains has been widely reported in vertebrates, including avian species. These studies report that mechanical strain magnitudes increase with increasing body weight and locomotor speed. Although locomotor speed and step frequency are not equivalent, step frequency increases with increasing locomotor speed especially in smaller bipeds (Loitz & Zernicke, 1992). We saw that the qualitative relationship between step frequency and mechanical strain magnitudes is the same as what is described between speed and mechanical strain, namely that mechanical strains increased with increasing step frequency. Pooling all locomotor segments, we found that breed and rearing housing had individual and interactive effects on step frequency. *W* pullets exhibited higher step frequency than *B* pullets, and similar to what we saw with body weight, housing did not affect step frequency in *B* but it did in *W*. The biggest difference between *B* and *W* was seen when reared in *Conv*. *W* pullets had progressively decreasing step frequency with increasing housing spatial complexity, up until the point where there was no longer a difference between *B* and *W* in the high complexity reared group. This interactive effect of housing and breed on step frequency pooled from all three locomotor activities was present during ground and downhill locomotion but not uphill locomotion, where only breed had a significant effect on step frequency. The pullets moved much more slowly during uphill locomotion, so it is likely that the effect of rearing housing, being less prominent than that of breed, was not perceivable at these low speeds. It is important to note that the locomotor step frequency at which we collected strain data is not necessarily reflective of habitual locomotor step frequency and speed but rather of fear responses. A clear example of this is that we measured higher locomotor speed in white pullets reared in *Conv* compared to those reared in *Low* and *High* complexity aviaries, although habitually the *Conv* pullets are barely able to locomote at all by virtue of being in a cage.

A limitation in our study was that pullets underwent a wait period of 3-14 days before experimentation where they were all housed in an open-concept floor-based system. This was necessary since pullets were raised in commercial housing systems at the University of Guelph, but the experiments were performed at McGill University's poultry complex (~6.5h drive away). Pullets were sampled randomly for experimentation, so if there was an effect of this wait time, it would be randomly distributed and therefore consistent across breed and housing groups. Moreover, alterations in bone mechanical properties due to changes in housing systems have been observed 20 days after relocating, but were not seen 10 days after relocating (Newman & Leeson, 1998), suggesting that this maximum 14 day wait period was likely not long enough to have a significant effect on the study results.

We chose to examine young, prepubertal chickens to specifically investigate how early loading history influences bone mechanics, and to avoid confounding variables that arise during the egg-laying phase, which is when the main differences in bone remodelling dynamics arise between birds and mammals. Nevertheless, future studies examining in vivo strains in adult and elderly chickens are warranted. Future studies investigating the effects of other non-caged housing systems are also warranted. Given our finding that jumping produces the highest in vivo strains, we would further hypothesize that aviary systems like the ones we tested which contain perches and platforms that motivate jumping would have a stronger influence on bone adaptation compared to floor-based or free-range systems. Although we report differences in strains between groups, whether these differences are meaningful in terms of their stimulatory effect on bones remains unclear and requires further investigation. Measurements of bone geometry, microstructure, whole bone curvature, ultrastructure, and material properties are important determinants of in vivo strains that would address this question; however, this is beyond the scope of this study.

Differences in muscle mass and muscle contractile forces also may be contributing to the observed differences in the in vivo strains between breeds and housing groups. In humans, muscle contraction has been shown to be the predominant source of strain compared to the influence of ground reaction forces (Nigg & Wakeling, 2001). The effect of muscle contractile forces on bone deformation depends on the attachment sites and attachment surface sizes, and in humans, it was shown that muscle contraction led to decreased in vivo strains (Milgrom et al., 2015). Further investigation into the effect of breed and loading history on muscle attachment sites, muscle

contractile forces, and their influence on in vivo strains could be valuable towards the prevention of osteoporosis in these breeds of female chickens.

Our key findings were: 1) different breeds of chickens adapted to maintain different in vivo strain patterns, 2) among birds with experience of dynamic load bearing activity (aviary reared birds), increased frequency of activity did not lead to decreased in vivo strains, and 3) the effect of loading history on in vivo strains was activity-type dependent. From these data we conclude that Lohmann Brown and Lohmann LSL Lite pullet tibiotarsi are optimized to withstand different relative amounts of bending, compression, and torsion. In comparing in vivo strains between conventional caged and aviary-reared birds, we conclude that the effects of adaptation to physical activity on in vivo strains are dependent on the activity type being performed. Future studies aiming to characterize in vivo background strains and how they may be affected by any given intervention should therefore sample strains during a range of activity types. Differences in spatial features of aviary rearing environments coincide with differences in in vivo tibiotarsal strains, with *Low* complexity aviaries with less variability in heights of platforms/perches/tiers from which the pullets can jump off from generally leading to lower habitual strains and therefore lower fracture risk, likely due to increased opportunities for high impact load bearing activities. These findings inform future studies aiming to study the bone mechanoresponse in these groups (breed, rearing housing), as controlled loading experiments require knowledge of habitual strain levels to be able to experimentally engender anabolic strains above this habitual level according to the mechanostat theory (3). They also may be generalizable to chickens of different ages, given that in vivo strains measured at functionally equivalent sites during treadmill locomotion were shown to be unchanged across ontogeny (4, 8, 12, and 17 weeks of age) in white leghorn chickens (Biewener et al., 1986). Our results provide valuable information regarding the mechanical environment that the pullet tibiotarsus is subjected to, with which we and others can associate measures of bone geometry, morphology, microstructure, ultrastructure, and material properties to understand how bones are designed to carry out their mechanical function. These data will likely inform which rearing housing environments and levels of physical activities are best for improving bone health and animal welfare in egg-laying hens of different strains.

Author Contributions

Study conception and design: TW, BW; Data acquisition: IV, BW, AB, SH, CJ, GG, AR; Analysis and interpretation of data: IV, NM, BW, RM, TW; Drafting of Manuscript: IV. All authors contributed to the critical revision and approval of the final manuscript.

Acknowledgements

We thank Alain Diotte and Paul Meldrum from McGill's Donald McQueen Shaver Poultry Complex for assisting with care of the pullets during the experimental period, Dr. Jim Gourdon for assistance and training on surgical procedures, and Taylor deVet and Roland Kuchling for help transporting chickens. We also thank Mark Lepik for contributions to illustrations, and Phoenix Wire Inc. for donating strain gauging wires. The study was funded by the Canadian Poultry Research Council, Fédération des producteurs d'oeufs du Québec, NSERC Discovery grant (RGPIN-2019-05374), Shriners Hospitals for Children, and FRQS Programme de bourses de chercheur.

Supplemental Figures

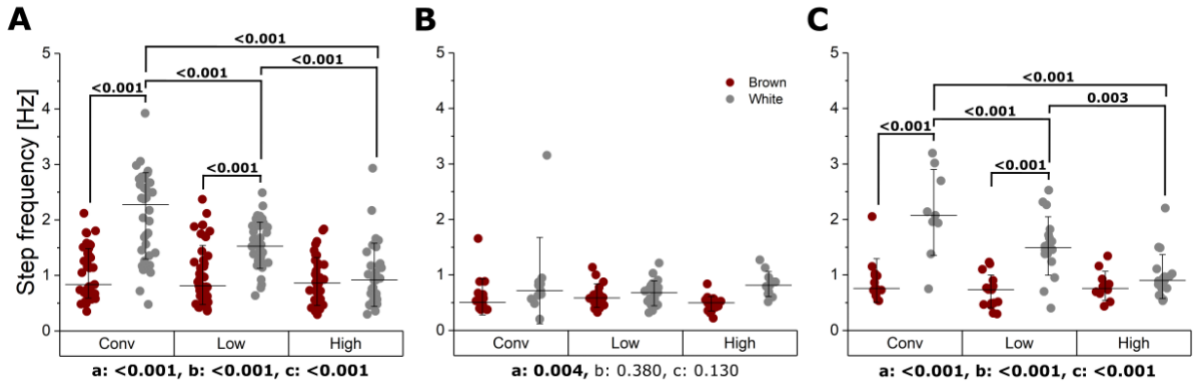

Supplemental Fig. 1: Effect of breed and rearing housing on step frequency during A) ground locomotion, B) uphill locomotion, and C) downhill locomotion, (mean ± sd). ANOVA main effects: a) breed, b) rearing housing, c) interaction. Significant Tukey-Kramer post-hoc comparisons indicated by bars, with p-values above. Note: each step frequency data point corresponds to the step frequency from a segment of locomotion recorded.

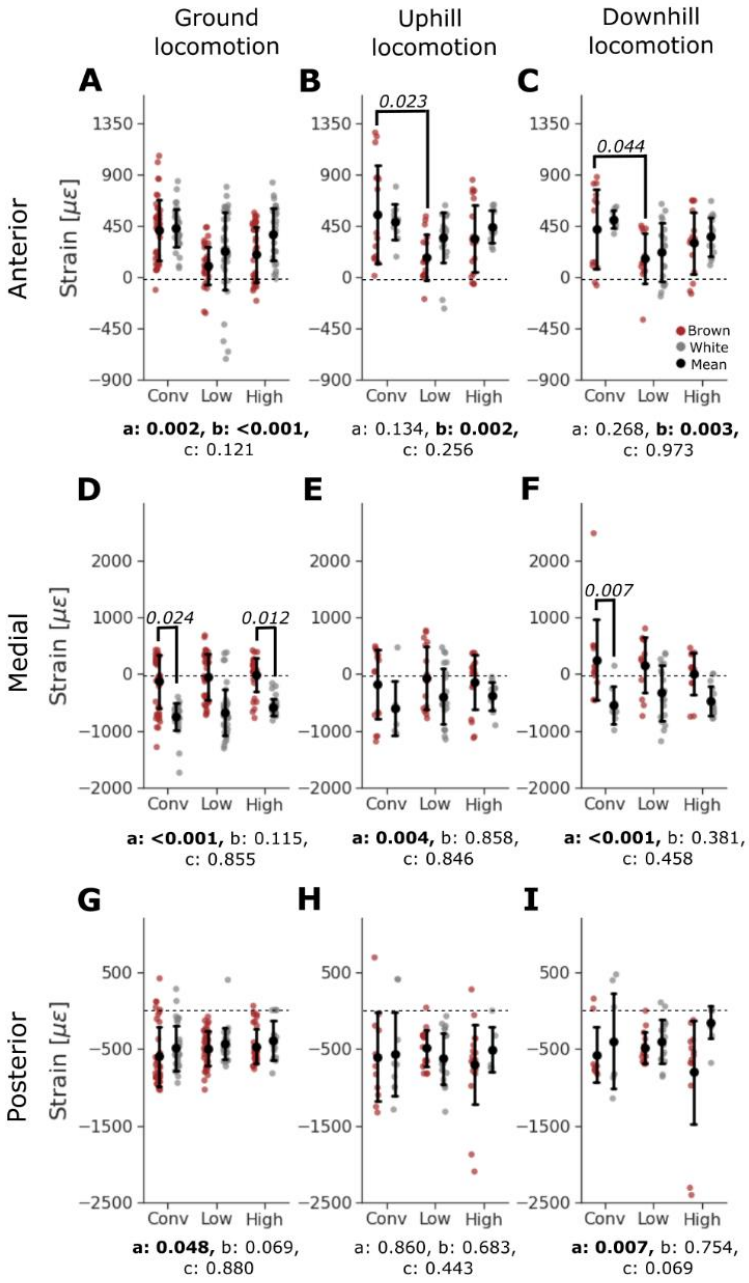

Supplemental Fig. 2: Effect of breed and rearing housing on raw (not normalized) locomotor longitudinal strains (mean ± sd). Each column includes a different activity type measured and each row includes the anatomical of the tibiotarsal midshaft sampled. Data for locomotor activities has been normalized to the median step frequency per group, to control for within chicken variations in step frequency. ANOVA main effects: a) breed, b) rearing housing, c) interaction. Groups with significant unadjusted or adjusted p-values indicated by bars with p-values above: Benjamini-Hochberg post-hoc (non-italicized) and t-test (italicized). Note: plots within each row share the same y-axis scaling.

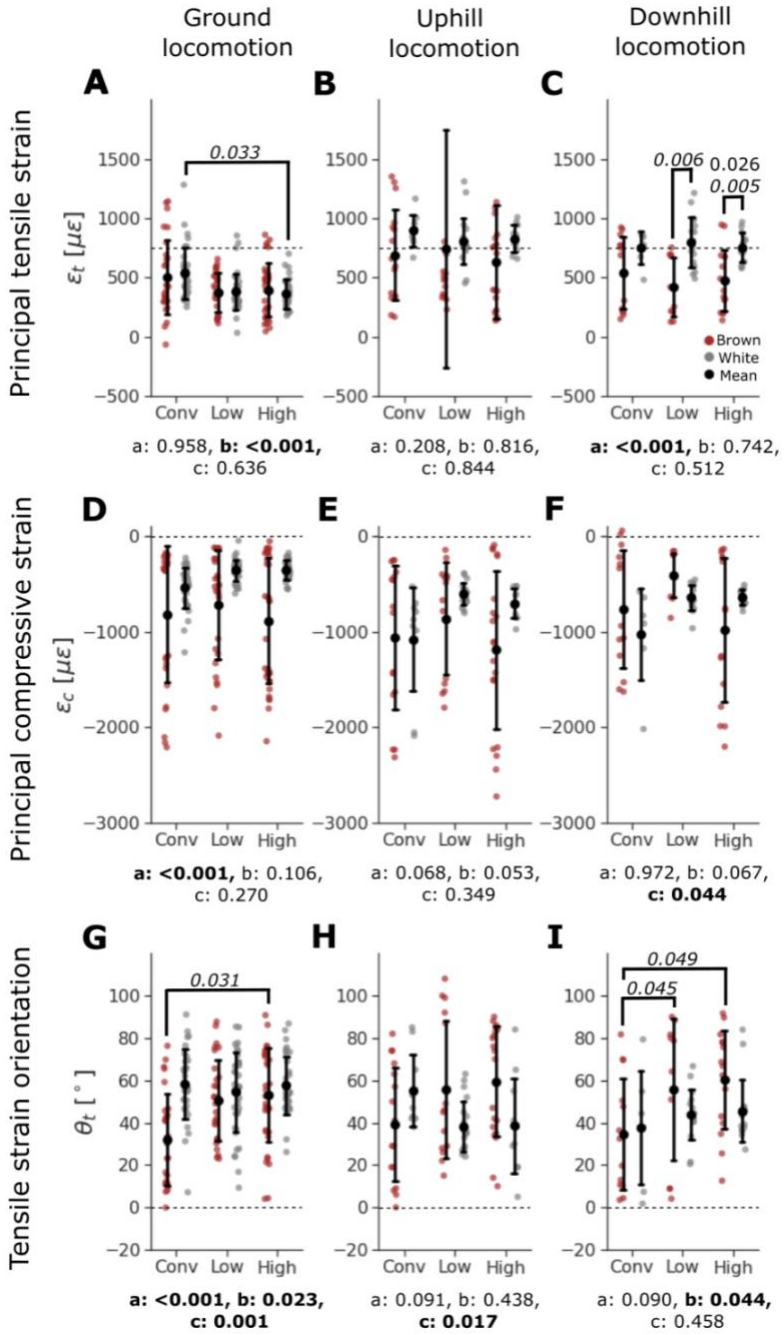

Supplemental Fig. 3: Effect of breed and rearing housing on raw (not normalized) locomotor principal strains, and tensile strain orientation during ground, uphill, and downhill locomotion (mean ± sd). ANOVA main effects: a) breed, b) rearing housing, c) interaction. Groups with significant unadjusted or adjusted p-values indicated by bars with p-values above: Benjamini-Hochberg post-hoc (non-italicized) and t-test (italicized). Note: plots within each row share the same y-axis scaling.

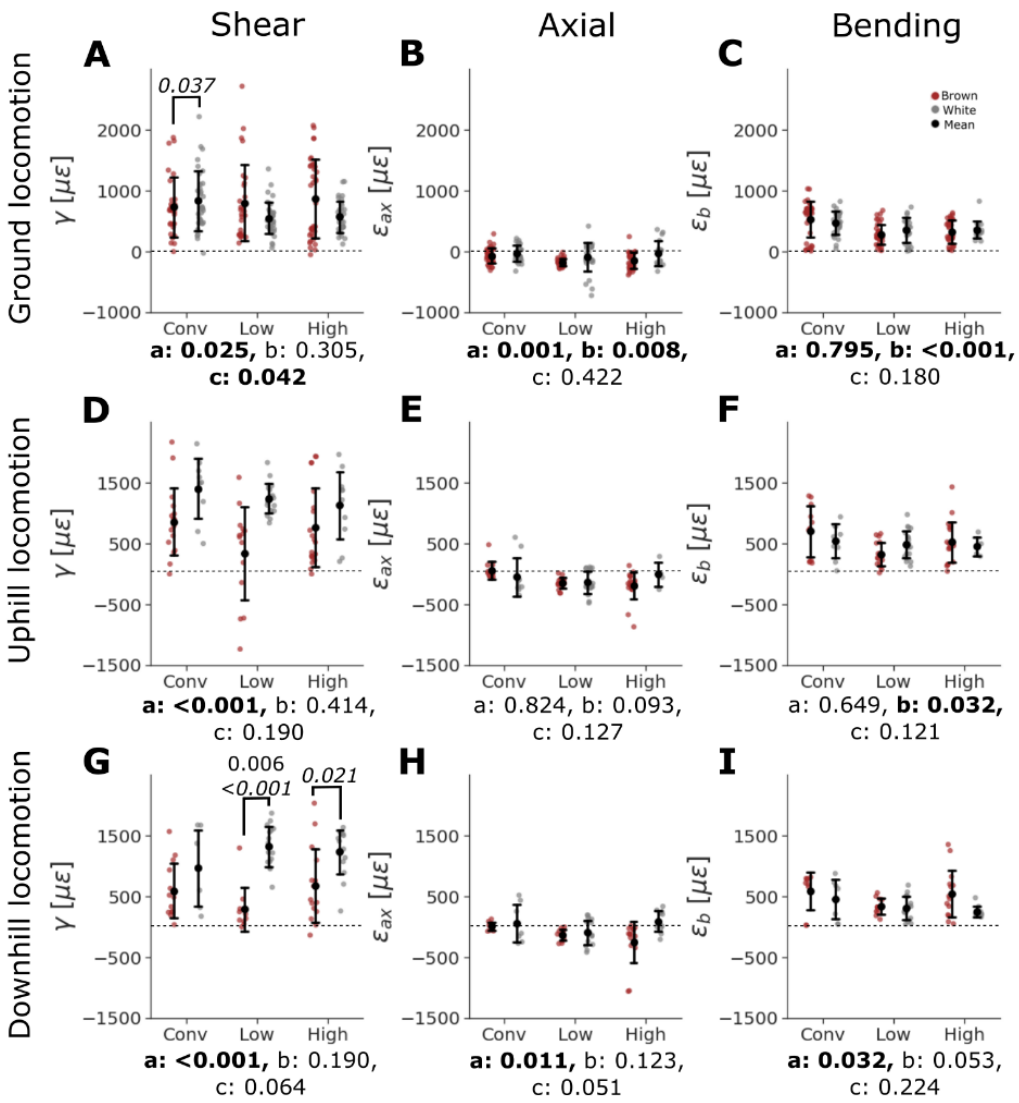

Supplemental Fig. 4: Effect of breed and rearing housing on raw (not normalized) peak shear, axial, and bending strains during ground, uphill, and downhill locomotion (mean ± sd). ANOVA main effects: a) breed, b) rearing housing, c) interaction. Groups with significant unadjusted or adjusted p-values indicated by bars with p-values above: Benjamini-Hochberg post-hoc (non-italicized) and t-test (italicized).

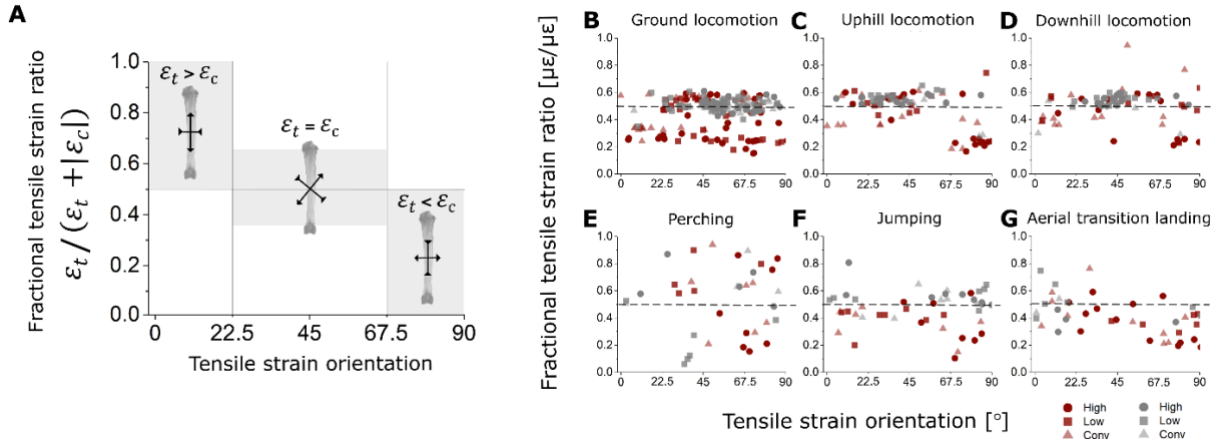

Supplemental Figure 5: Loading patterns at the anterior surface during steady and non-steady activities. A) Illustration depicting the loading pattern of the tibiotarsus associated to three regions of the plot. At the y-axis, fractional tensile strain ratio (FTSR) indicates the relative contribution of principal tensile strain to the overall amount of principal strain. Tensile strain orientation is the angle of the axis of principal tensile strain relative to the bone's longitudinal axis. Adapted from Moreno et al. 2008 (Moreno et al., 2008). B-D) Steady activities. E-G) Non-steady activities. The line intersecting the y-axis delineates an FTSR = 0.5, when principal tensile and principal compressive contribute equally. The lines intersecting the x-axis delineate a tensile strain orientation of 22.5° and 67.5°. When the tensile strain orientation is within this range, the axis of tensile strain is closer to 45° than to being either aligned with the bone's longitudinal or transverse axis.

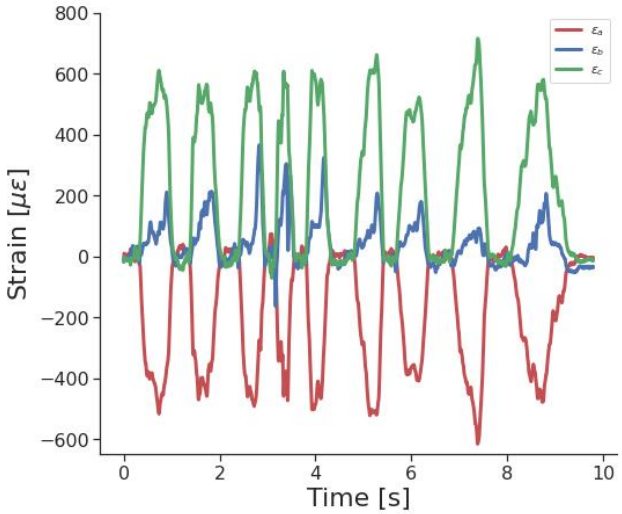

Supplemental Figure 6: Strains measured from the three independent elements of the rosette gauge during an exemplary segment of ground locomotion. ε_b corresponds to the element aligned with the bone's longitudinal axis, whereas ε_a and ε_c are rotated 45 degrees clockwise and counterclockwise, respectively.

Supplemental Table 1: Sample sizes for each group, parameter, and activity combination.

			Ground locomotion	**Uphill locomotion**	**Downhill locomotion**	**Perching**	**Jumping**	**Aerial transition landing**
Anterior longitudinal	***Conv***	***B***	7	5	4	6	4	6
		W	6	5	5	6	4	6
	Low	***B***	8	6	7	5	5	7
		W	8	7	8	6	4	6
	High	***B***	7	7	7	7	4	8
		W	6	6	5	5	3	5
Medial longitudinal	***Conv***	***B***	7	5	4	4	3	5
		W	5	4	5	5	4	5
	Low	***B***	7	5	5	2	4	5
		W	8	7	8	6	4	6
	High	***B***	6	7	6	6	4	6
		W	6	6	5	4	3	5
Posterior longitudinal	***Conv***	***B***	7	4	3	4	4	5
		W	5	4	4	6	4	5
	Low	***B***	6	6	5	3	4	5
		W	8	6	7	6	4	4
	High	***B***	7	7	7	6	3	6
		W	4	4	3	3	2	4
ε_{ax}, ε_b	***Conv***	***B***	7	4	3	4	4	5
		W	5	4	4	6	4	5
	Low	***B***	6	6	5	3	4	5
		W	7	6	7	6	4	4
	High	***B***	7	7	7	6	3	6
		W	4	4	3	3	2	4
ε_t, ε_c, θ_t, γ	***Conv***	***B***	5	5	4	5	5	7
		W	5	4	3	4	4	2
	Low	***B***	7	5	7	3	4	4
		W	7	6	7	3	4	4
	High	***B***	7	7	7	7	5	8
		W	6	6	5	5	5	3

Supplemental Table 2: Averages of normalized strain (με) and tensile strain orientation (°) outcome measures per group during steady activities.

		Longitudinal			Derived					
		Anterior	**Medial**	**Posterior**	ε_t	ε_c	θ_t	γ	ε_{ax}	ε_b
	Total	339	-266	-522	596	-745	49	840	-91	431
	B	317	-32	-580	525	-869	49	678	-126	454
	W	364	-513	-452	674	-616	47	1035	-49	409
	Conv	503	-268	-549	630	-858	42	852	2	563
	Low	214	-270	-486	599	-585	49	808	-127	346
	High	330	-250	-538	560	-817	53	855	-122	419
B	***Conv***	515	-27	-593	573	-870	35	729	7	615
	Low	141	-24	-488	507	-656	54	473	-150	311
	High	284	-42	-652	499	-1016	58	777	-193	460
W	***Conv***	491	-652	-494	733	-890	51	1066	-4	499
	Low	274	-464	-479	658	-531	45	1033	-104	381
	High	392	-479	-334	641	-556	47	968	24	350

Supplemental Table 3: Mean longitudinal and derived strains (με) measured during sampled activities, averaged across the 6 experimental groups (2 breeds x 3 housing environments).

	Longitudinal strains			Derived strains				
	Anterior	**Medial**	**Posterior**	**εt**	**εc**	**γ**	**εax**	**εb**
Ground locomotion	321	-370	-490	414	-585	709	-97	386
Uphill locomotion	383	-273	-600	750	-925	922	-106	502
Downhill locomotion	312	-155	-477	623	-726	891	-69	405
Perching	55	-68	-1	283	-277	112	38	182
Jumping	207	-443	-656	1151	-1258	1071	-215	475
Aerial transition landing	-64	-486	-698	1068	-1473	931	-392	675

Supplemental Table 4: Averages of raw strain (με) and tensile strain orientation (°) outcome measures per group during steady activities.

		Longitudinal			Derived					
		Anterior	**Medial**	**Posterior**	ε_t	ε_c	θ_t	γ	ε_{ax}	ε_b
	Total	339	-266	-522	596	-745	49	840	-91	431
	B	300	-22	-583	527	-877	49	678	-130	457
	W	359	-509	-456	676	-621	47	1041	-49	409
	Conv	470	-257	-546	629	-862	42	852	-2	558
	Low	215	-255	-491	603	-592	49	813	-128	350
	High	329	-254	-546	564	-825	54	857	-125	425
B	***Conv***	464	-22	-593	576	-882	35	729	1	610
	Low	148	11	-490	511	-664	54	477	-150	315
	High	281	-49	-657	501	-1021	58	773	-197	466
W	***Conv***	478	-637	-486	727	-883	50	1069	-4	491
	Low	268	-466	-487	662	-536	45	1039	-105	384
	High	395	-479	-351	648	-567	47	976	22	356

Supplemental Table 5: Averages of raw strain (με) and tensile strain orientation (°) outcome measures per group during non-steady activities.

		Longitudinal			Derived					
		Anterior	**Medial**	**Posterior**	ε_t	ε_c	θ_t	γ	ε_{ax}	ε_b
	Total	66	-332	-452	834	-1003	52	705	-190	444
	B	15	-246	-464	532	-365	58	788	-208	381
	W	139	-418	-439	1232	-588	48	532	-160	514
	Conv	123	-440	-310	620	-344	49	676	-84	418
	Low	21	-236	-586	857	-429	44	442	-315	383
	High	104	-371	-365	1025	-622	61	935	-135	529
B	***Conv***	-84	-114	-307	426	-294	48	573	-169	347
	Low	-91	-250	-787	501	-290	50	661	-374	311
	High	224	-332	-293	650	-509	64	1048	-118	451
W	***Conv***	374	-712	-321	1002	-419	49	690	15	493
	Low	160	-242	-472	1211	-564	40	223	-277	425
	High	-159	-379	-496	1412	-707	55	660	-214	611

Supplemental Table 6: Averages of strain (με) and tensile strain orientation (°) outcome measures per group across all activities, considering normalized steady strains.

		Longitudinal			Derived					
		Anterior	**Medial**	**Posterior**	ε_t	ε_c	θ_t	γ	ε_{ax}	ε_b
	Total	202	-299	-487	715	-874	50	772	-140	438
	B	166	-139	-522	529	-617	51	733	-167	418
	W	251	-466	-446	953	-602	48	784	-104	461
	Conv	313	-254	-429	625	-601	46	764	-41	490
	Low	117	-253	-536	728	-507	47	625	-221	364
	High	217	-311	-451	793	-719	57	895	-129	474
B	***Conv***	216	-70	-450	500	-582	42	651	-81	481
	Low	25	-137	-638	504	-473	52	567	-262	311
	High	264	-187	-473	574	-762	61	912	-156	456
W	***Conv***	433	-682	-408	867	-654	50	878	5	496
	Low	217	-353	-475	935	-547	43	628	-191	403
	High	117	-429	-415	1027	-631	51	814	-95	480

Supplemental Table 7: Averages of strain (με) and tensile strain orientation (°) outcome measures per group across all activities, considering raw steady strains.

		Longitudinal			Derived					
		Anterior	**Medial**	**Posterior**	ε_t	ε_c	θ_t	γ	ε_{ax}	ε_b
	Total	202	-299	-487	715	-874	50	772	-140	438
	B	157	-134	-524	530	-621	51	733	-169	419
	W	249	-464	-447	954	-604	48	787	-105	461
	Conv	296	-349	-428	625	-603	46	764	-43	488
	Low	118	-246	-538	730	-510	47	627	-222	366
	High	216	-313	-455	795	-723	57	896	-130	477
B	***Conv***	190	-68	-450	501	-588	42	651	-84	479
	Low	29	-120	-639	506	-477	52	569	-262	313
	High	263	-190	-475	575	-765	61	911	-158	459
W	***Conv***	426	-675	-403	865	-651	50	879	5	492
	Low	214	-354	-479	936	-550	43	631	-191	405
	High	118	-429	-424	1030	-637	51	818	-96	483

References

Aamodt, A., Lund-Larsen, J., Eine, J., Andersen, E., Benum, P., & Husby, O. S. (1997). In vivo measurements show tensile axial strain in the proximal lateral aspect of the human femur. *Journal of Orthopaedic Research*, *15*(6), 927–931. https://doi.org/10.1002/jor.1100150620

Bassey, E. J., Rothwell, M. C., Littlewood, J. J., & Pye, D. W. (1998). Pre- and postmenopausal women have different bone mineral density responses to the same high-impact exercise. *Journal of Bone and Mineral Research*, *13*(12), 1805–1813. https://doi.org/10.1359/jbmr.1998.13.12.1805

Bertram, J. E. A., & Biewener, A. A. (1988). Bone curvature: Sacrificing strength for load predictability? *Journal of Theoretical Biology*, *131*(1), 75–92. https://doi.org/10.1016/S0022-5193(88)80122-X

Biewener, A. A. (1982). Bone strength in small mammals and bipedal birds: Do safety factors change with body size? *Journal of Experimental Biology*, *98*, 289–301. https://doi.org/10.1242/jeb.98.1.289

Biewener, A. A. (1992). In vivo measurement of bone strain and tendon force. In A. A. Biewener (Ed.), *Biomechanics: Structures and Systems: A Practical Approach* (pp. 123–147). Oxford University Press.

Biewener, A. A., & Bertram, J. E. (1993). Skeletal strain patterns in relation to exercise training during growth. *Journal of Experimental Biology*, *185*, 51–69. https://doi.org/10.1242/jeb.185.1.51

Biewener, A. A., & Bertram, J. E. (1994). Structural response of growing bone to exercise and disuse. *Journal of Applied Physiology*, *76*(2), 946–955. https://doi.org/10.1152/jappl.1994.76.2.946

Biewener, A. A., & Dial, K. P. (1995). In vivo strain in the humerus of pigeons (Columba livia) during flight. *Journal of Morphology*, *225*(1), 61–75. https://doi.org/10.1002/jmor.1052250106

Biewener, A. A., Fazzalari, N. L., Konieczynski, D. D., & Baudinette, R. V. (1996). Adaptive changes in trabecular architecture in relation to functional strain patterns and disuse. *Bone*, *19*(1), 1–8. https://doi.org/10.1016/8756-3282(96)00116-0

Biewener, A. A., Swartz, S. M., & Bertram, J. E. A. (1986). Bone modeling during growth: Dynamic strain equilibrium in the chick tibiotarsus. *Calcified Tissue International*, *39*(6), 390–395. https://doi.org/10.1007/BF02555177

Biewener, A. A., & Taylor, C. R. (1986). Bone strain: A determinant of gait and speed? *Journal of Experimental Biology*, *123*, 383–400. https://doi.org/10.1242/jeb.123.1.383

Biewener, A. A., Thomason, J., Goodship, A., & Lanyon, L. E. (1983). Bone stress in the horse forelimb during locomotion at different gaits: A comparison of two experimental methods. *Journal of Biomechanics*, *16*(8), 565–576. https://doi.org/10.1016/0021-9290(83)90107-0

Birkhold, A. I., Razi, H., Duda, G. N., Weinkamer, R., Checa, S., & Willie, B. M. (2014). The influence of age on adaptive bone formation and bone resorption. *Biomaterials*, *35*(34), 9290–9301. https://doi.org/10.1016/j.biomaterials.2014.07.051

Bishop, S. C., Fleming, R. H., McCormack, H. A., Flock, D. K., & Whitehead, C. C. (2000). Inheritance of bone characteristics affecting osteoporosis in laying hens. *British Poultry Science*, *41*(1), 33–40. https://doi.org/10.1080/00071660086376

Blob, R. W., & Biewener, A. A. (1999). In vivo locomotor strain in the hindlimb bones of alligator mississippiensis and iguana iguana: Implications for the evolution of limb bone safety factor and non-sprawling limb posture. *Journal of Experimental Biology*, *202 (Pt 9)*, 1023–1046. https://doi.org/10.1242/jeb.202.9.1023

Blob, R. W., Espinoza, N. R., Butcher, M. T., Lee, A. H., D'Amico, A. R., Baig, F., & Sheffield, K. M. (2014). Diversity of Limb-Bone Safety Factors for Locomotion in Terrestrial Vertebrates: Evolution and Mixed Chains. *Integrative and Comparative Biology*, *54*(6), 1058–1071. https://doi.org/10.1093/icb/icu032

Butcher, M. T., Espinoza, N. R., Cirilo, S. R., & Blob, R. W. (2008). In vivo strains in the femur of river cooter turtles (Pseudemys concinna) during terrestrial locomotion: Tests of force-platform models of loading mechanics. *Journal of Experimental Biology*, *211*(Pt 15), 2397–2407. https://doi.org/10.1242/jeb.018986

Butcher, M. T., White, B. J., Hudzik, N. B., Gosnell, W. C., Parrish, J. H. A., & Blob, R. W. (2011). In vivo strains in the femur of the Virginia opossum (Didelphis virginiana) during terrestrial locomotion: Testing hypotheses of evolutionary shifts in mammalian bone

loading and design. *Journal of Experimental Biology*, *214*(Pt 15), 2631–2640. https://doi.org/10.1242/jeb.049544

Carrano, M. T., & Biewener, A. A. (1999). Experimental alteration of limb posture in the chicken (Gallus gallus) and its bearing on the use of birds as analogs for dinosaur locomotion. *Journal of Morphology*, *240*(3), 237–249. https://doi.org/10.1002/(SICI)1097-4687(199906)240:3<237::AID-JMOR3>3.0.CO;2-N

Carter, D. R. (1978). Anisotropic analysis of strain rosette information from cortical bone. *Journal of Biomechanics*, *11*(4), 199–202. https://doi.org/10.1016/0021-9290(78)90013-1

Carter, D. R., Smith, D. J., Spengler, D. M., Daly, C. H., & Frankel, V. H. (1980). Measurement and analysis of in vivo bone strains on the canine radius and ulna. *Journal of Biomechanics*, *13*(1), 27–38. https://doi.org/10.1016/0021-9290(80)90005-6

Casey-Trott, T. M., Korver, D. R., Guerin, M. T., Sandilands, V., Torrey, S., & Widowski, T. M. (2017a). Opportunities for exercise during pullet rearing, Part I: Effect on the musculoskeletal characteristics of pullets. *Poultry Science*, *96*(8), 2509–2517. https://doi.org/10.3382/ps/pex059

Casey-Trott, T. M., Korver, D. R., Guerin, M. T., Sandilands, V., Torrey, S., & Widowski, T. M. (2017b). Opportunities for exercise during pullet rearing, Part II: Long-term effects on bone characteristics of adult laying hens at the end-of-lay. *Poultry Science*, *96*(8), 2518–2527. https://doi.org/10.3382/ps/pex060

Copploe, J. V., Blob, R. W., Parrish, J. H. A., & Butcher, M. T. (2015). In vivo strains in the femur of the nine-banded armadillo (Dasypus novemcinctus). *Journal of Morphology*, *276*(8), 889–899. https://doi.org/10.1002/jmor.20387

Currey, J. (2014). *Safety Factors and Scaling Effects in bones, The Mechanical Adaptation of Bones*. Princeton University Press.

Currey, J. D. (2003). The many adaptations of bone. *Journal of Biomechanics*, *36*(10), 1487–1495. https://doi.org/10.1016/s0021-9290(03)00124-6

de Margerie, E., Sanchez, S., Cubo, J., & Castanet, J. (2005). Torsional resistance as a principal component of the structural design of long bones: Comparative multivariate evidence in birds. *The Anatomical Record. Part A, Discoveries in Molecular, Cellular, and Evolutionary Biology*, *282*(1), 49–66. https://doi.org/10.1002/ar.a.20141

Demes, B., Qin, Y. X., Stern, J. T., Larson, S. G., & Rubin, C. T. (2001). Patterns of strain in the macaque tibia during functional activity. *American Journal of Physical Anthropology*, *116*(4), 257–265. https://doi.org/10.1002/ajpa.1122

Demes, B., Stern, J. T., Hausman, M. R., Larson, S. G., McLeod, K. J., & Rubin, C. T. (1998). Patterns of strain in the macaque ulna during functional activity. *American Journal of Physical Anthropology*, *106*(1), 87–100. https://doi.org/10.1002/(SICI)1096-8644(199805)106:1<87::AID-AJPA6>3.0.CO;2-A

Dunn, I. C., Fleming, R. H., McCormack, H. A., Morrice, D., Burt, D. W., Preisinger, R., & Whitehead, C. C. (2007). A QTL for osteoporosis detected in an F 2 population derived from White Leghorn chicken lines divergently selected for bone index. *Animal Genetics*, *38*(1), 45–49. https://doi.org/10.1111/j.1365-2052.2006.01547.x

Fleming, R. H., McCormack, H. A., McTeir, L., & Whitehead, C. C. (2006). Relationships between genetic, environmental and nutritional factors influencing osteoporosis in laying hens. *British Poultry Science*, *47*(6), 742–755. https://doi.org/10.1080/00071660601077949

Fritton, S. P., McLeod, K. J., & Rubin, C. T. (2000). Quantifying the strain history of bone: Spatial uniformity and self-similarity of low-magnitude strains. *Journal of Biomechanics*, *33*(3), 317–325. https://doi.org/10.1016/s0021-9290(99)00210-9

Frost, H. M. (2004). A 2003 update of bone physiology and Wolff's Law for clinicians. *The Angle Orthodontist*, *74*(1), 3–15. https://doi.org/10.1043/0003-3219(2004)074<0003:AUOBPA>2.0.CO;2

Gatesy, S. M., & Biewener, A. A. (1991). Bipedal locomotion: Effects of speed, size and limb posture in birds and humans. *Journal of Zoology*, *224*(1), 127–147. https://doi.org/10.1111/j.1469-7998.1991.tb04794.x

Goodship, A. E., Lanyon, L. E., & McFie, H. (1979). Functional adaptation of bone to increased stress. An experimental study. *The Journal of Bone and Joint Surgery*, *61*(4), 539–546.

Grant, P. G., Buschang, P. H., Drolet, D. W., & Pickerell, C. (1980). Invariance of the relative positions of structures attached to long bones during growth: Cross-sectional and longitudinal studies. *Acta Anatomica*, *107*(1), 26–34. https://doi.org/10.1159/000145225

Gross, T. S., McLeod, K. J., & Rubin, C. T. (1992). Characterizing bone strain distributions in vivo using three triple rosette strain gages. *Journal of Biomechanics*, *25*(9), 1081–1087. https://doi.org/10.1016/0021-9290(92)90044-2

Hester, P. Y., Enneking, S. A., Haley, B. K., Cheng, H. W., Einstein, M. E., & Rubin, D. A. (2013). The effect of perch availability during pullet rearing and egg laying on musculoskeletal health of caged White Leghorn hens. *Poultry Science*, *92*(8), 1972–1980. https://doi.org/10.3382/ps.2013-03008

Hsieh, Y. F., & Turner, C. H. (2001). Effects of loading frequency on mechanically induced bone formation. *Journal of Bone and Mineral Research*, *16*(5), 918–924. https://doi.org/10.1359/jbmr.2001.16.5.918

Hudson, H. A., Britton, W. M., Rowland, G. N., & Buhr, R. J. (1993). Histomorphometric Bone Properties of Sexually Immature and Mature White Leghorn Hens with Evaluation of Fluorochrome Injection on Egg Production Traits. *Poultry Science*, *72*(8), 1537–1547. https://doi.org/10.3382/ps.0721537

Javaheri, B., Razi, H., Gohin, S., Wylie, S., Chang, Y.-M., Salmon, P., Lee, P. D., & Pitsillides, A. A. (2020). Lasting organ-level bone mechanoadaptation is unrelated to local strain. *Science Advances*, *6*(10), eaax8301. https://dx.doi.org/10.1126/sciadv.aax8301

Judex, S., & Zernicke, R. F. (2000). High-impact exercise and growing bone: Relation between high strain rates and enhanced bone formation. *Journal of Applied Physiology*, *88*(6), 2183–2191. https://doi.org/10.1152/jappl.2000.88.6.2183

Keenan, K. E., Mears, C. S., & Skedros, J. G. (2017). Utility of osteon circularity for determining species and interpreting load history in primates and nonprimates. *American Journal of Physical Anthropology*, *162*(4), 657–681. https://doi.org/10.1002/ajpa.23154

Keller, T. S., & Spengler, D. M. (1982). In vivo strain gage implantation in rats. *Journal of Biomechanics*, *15*(12), 911–917. https://doi.org/10.1016/0021-9290(82)90009-4

Keller, T. S., & Spengler, D. M. (1989). Regulation of bone stress and strain in the immature and mature rat femur. *Journal of Biomechanics*, *22*(11–12), 1115–1127. https://doi.org/10.1016/0021-9290(89)90213-3

Klingensmith, P. M., Hester, P. Y., Elkin, R. G., & Ward, C. R. (1986). Relationship of high intensity step-up lighting to bone ash and growth plate closure of the tarso-metatarsus in

Turkeys. *British Poultry Science*, *27*(3), 487–492. https://doi.org/10.1080/00071668608416907

Lanyon, L. E. (1972). In vivo bone strain recorded from thoracic vertebrae of sheep. *Journal of Biomechanics*, *5*(3), 277–281. https://doi.org/10.1016/0021-9290(72)90044-9

Lanyon, L. E. (1973). Analysis of surface bone strain in the calcaneus of sheep during normal locomotion. Strain analysis of the calcaneus. *Journal of Biomechanics*, *6*(1), 41–49. https://doi.org/10.1016/0021-9290(73)90036-5

Lanyon, L. E. (1987). Functional strain in bone tissue as an objective, and controlling stimulus for adaptive bone remodelling. *Journal of Biomechanics*, *20*(11–12), 1083–1093. https://doi.org/10.1016/0021-9290(87)90026-1

Lanyon, L. E., & Bourn, S. (1979). The influence of mechanical function on the development and remodeling of the tibia. An experimental study in sheep. *The Journal of Bone and Joint Surgery*, *61*(2), 263–273.

Lanyon, L. E., Hampson, W. G. J., Goodship, A. E., & Shah, J. S. (1975). Bone Deformation Recorded in vivo from Strain Gauges Attached to the Human Tibial Shaft. *Acta Orthopaedica Scandinavica*, *46*(2), 256–268. https://doi.org/10.3109/17453677508989216

Lanyon, L. E., Paul, I. L., Rubin, C. T., Thrasher, E. L., DeLaura, R., Rose, R. M., & Radin, E. L. (1981). In vivo strain measurements from bone and prosthesis following total hip replacement. An experimental study in sheep. *The Journal of Bone and Joint Surgery*, *63*(6), 989–1001.

LeBlanc, C., Tobalske, B., Bowley, S., & Harlander-Matauschek, A. (2018). Development of locomotion over inclined surfaces in laying hens. *Animals*, *12*(3), 585–596. https://doi.org/10.1017/S1751731117001896

Lee, K. C. L., Maxwell, A., & Lanyon, L. E. (2002). Validation of a technique for studying functional adaptation of the mouse ulna in response to mechanical loading. *Bone*, *31*(3), 407–412. https://doi.org/10.1016/s8756-3282(02)00842-6

Levenston, M. E., Beaupré, G. S., & Carter, D. R. (1998). Loading Mode Interactions in Simulations of Long Bone Cross-Sectional Adaptation. *Computational Methods in*

Biomechanics and Biomedical Engineering, *1*(4), 303–319. https://doi.org/10.1080/01495739808936709

Lieberman, D. E., Polk, J. D., & Demes, B. (2004). Predicting long bone loading from cross-sectional geometry. *American Journal of Physical Anthropology*, *123*(2), 156–171. https://doi.org/10.1002/ajpa.10316

Loitz, B. J., & Zernicke, R. F. (1992). Strenuous exercise-induced remodelling of mature bone: Relationships between in vivo strains and bone mechanics. *Journal of Experimental Biology*, *170*, 1–18. https://doi.org/10.1242/jeb.170.1.1

Main, R. P. (2007). Ontogenetic relationships between in vivo strain environment, bone histomorphometry and growth in the goat radius. *Journal of Anatomy*, *210*(3), 272–293. https://doi.org/10.1111/j.1469-7580.2007.00696.x

Main, R. P. (2021). Basic Principles and Methodologies in Measuring Bone Biomechanics. In *Vertebrate Skeletal Histology and Paleohistology*. CRC Press.

Main, R. P., & Biewener, A. A. (2007). Skeletal strain patterns and growth in the emu hindlimb during ontogeny. *Journal of Experimental Biology*, *210*(15), 2676–2690. https://doi.org/10.1242/jeb.004580

Main, R. P., Lynch, M. E., & van der Meulen, M. C. H. (2014). Load-induced changes in bone stiffness and cancellous and cortical bone mass following tibial compression diminish with age in female mice. *Journal of Experimental Biology*, jeb.085522. https://doi.org/10.1242/jeb.085522

Manley, P. A., Schatzker, J., & Sumner-Smith, G. (1982). Evaluation of tension and compression forces in the canine femur in vivo. *Archives of Orthopaedic and Traumatic Surgery. Archiv Fur Orthopadische Und Unfall-Chirurgie*, *99*(3), 213–216. https://doi.org/10.1007/BF00379211

Meakin, L. B., Price, J. S., & Lanyon, L. E. (2014). The Contribution of Experimental in vivo Models to Understanding the Mechanisms of Adaptation to Mechanical Loading in Bone. *Frontiers in Endocrinology*, *5*, 154. https://doi.org/10.3389/fendo.2014.00154

Meakin, L. B., Sugiyama, T., Galea, G. L., Browne, W. J., Lanyon, L. E., & Price, J. S. (2013). Male mice housed in groups engage in frequent fighting and show a lower response to

additional bone loading than females or individually housed males that do not fight. *Bone*, *54*(1), 113–117. https://doi.org/10.1016/j.bone.2013.01.029

Milgrom, C., Burr, D. B., Finestone, A. S., & Voloshin, A. (2015). Understanding the etiology of the posteromedial tibial stress fracture. *Bone*, *78*, 11–14. https://doi.org/10.1016/j.bone.2015.04.033

Milgrom, C., Finestone, A., Simkin, A., Ekenman, I., Mendelson, S., Millgram, M., Nyska, M., Larsson, E., & Burr, D. (2000). In-vivo strain measurements to evaluate the strengthening potential of exercises on the tibial bone. *The Journal of Bone and Joint Surgery*, *82*(4), 591–594. https://doi.org/10.1302/0301-620x.82b4.9677

Milgrom, C., Voloshin, A., Novack, L., Milgrom, Y., Ekenman, I., & Finestone, A. S. (2022). In vivo strains at the middle and distal thirds of the tibia during exertional activities. *Bone Reports*, *16*, 101170. https://doi.org/10.1016/j.bonr.2022.101170

Moreno, C. A., Main, R. P., & Biewener, A. A. (2008). Variability in forelimb bone strains during non-steady locomotor activities in goats. *Journal of Experimental Biology*, *211*(Pt 7), 1148–1162. https://doi.org/10.1242/jeb.012419

Mosley, J. R., March, B. M., Lynch, J., & Lanyon, L. E. (1997). Strain magnitude related changes in whole bone architecture in growing rats. *Bone*, *20*(3), 191–198. https://doi.org/10.1016/s8756-3282(96)00385-7

Newman, S., & Leeson, S. (1998). Effect of housing birds in cages or an aviary system on bone characteristics. *Poultry Science*, *77*(10), 1492–1496. https://doi.org/10.1093/ps/77.10.1492

Nigg, B. M., & Wakeling, J. M. (2001). Impact Forces and Muscle Tuning: A New Paradigm: *Exercise and Sport Sciences Reviews*, *29*(1), 37–41. https://doi.org/10.1097/00003677-200101000-00008

Nunamaker, D. M., Butterweck, D. M., & Provost, M. T. (1990). Fatigue fractures in thoroughbred racehorses: Relationships with age, peak bone strain, and training. *Journal of Orthopaedic Research*, *8*(4), 604–611. https://doi.org/10.1002/jor.1100080417

Pauwels, F. (1980). *Biomechanics of the locomotor apparatus*. Springer-Verlag.

Pufall, A., Harlander-Matauschek, A., Hunniford, M., & Widowski, T. M. (2021). Effects of Rearing Aviary Style and Genetic Strain on the Locomotion and Musculoskeletal

Characteristics of Layer Pullets. *Animals*, *11*(3), 634. https://doi.org/10.3390/ani11030634

Rabkin, B. A., Szivek, J. A., Schonfeld, J. E., & Halloran, B. P. (2001). Long-term measurement of bone strain in vivo: The rat tibia. *Journal of Biomedical Materials Research*, *58*(3), 277–281. https://doi.org/10.1002/1097-4636(2001)58:3<277::aid-jbm1017>3.0.co;2-t

Raymond, B., Johansson, A. M., McCormack, H. A., Fleming, R. H., Schmutz, M., Dunn, I. C., & De Koning, D. J. (2018). Genome-wide association study for bone strength in laying hens1. *Journal of Animal Science*, *96*(7), 2525–2535. https://doi.org/10.1093/jas/sky157

Regmi, P., Deland, T. S., Steibel, J. P., Robison, C. I., Haut, R. C., Orth, M. W., & Karcher, D. M. (2015). Effect of rearing environment on bone growth of pullets. *Poultry Science*, *94*(3), 502–511. https://doi.org/10.3382/ps/peu041

Regmi, P., Smith, N., Nelson, N., Haut, R. C., Orth, M. W., & Karcher, D. M. (2016). Housing conditions alter properties of the tibia and humerus during the laying phase in Lohmann white Leghorn hens. *Poultry Science*, *95*(1), 198–206. https://doi.org/10.3382/ps/pev209

Reilly, G. C., & Currey, J. D. (1999). The development of microcracking and failure in bone depends on the loading mode to which it is adapted. *Journal of Experimental Biology*, *202*(Pt 5), 543–552. https://doi.org/10.1242/jeb.202.5.543

Rentsch, A. K., Harlander, A., Siegford, J., Vitienes, I., Willie, B., & Widowski, T. (2023). Rearing laying hens: The effect of aviary design and genetic strain on pullet exercise and perching behavior. *Frontiers*, *Under review*.

Riggs, C. M., Lanyon, L. E., & Boyde, A. (1993). Functional associations between collagen fibre orientation and locomotor strain direction in cortical bone of the equine radius. *Anatomy and Embryology*, *187*(3), 231–238. https://doi.org/10.1007/bf00195760

Ross, E. (n.d.). *The Effect of Early Rearing Environment on Musculoskeletal Traits and Proximate Composition in Laying Hen Pullets*. 148.

Ross, E. (2021). Thesis: The Effect of Early Rearing Environment on Musculoskeletal Traits and Proximate Composition in Laying Hen Pullets. In *Animal Biosciences: Vol. Master of Science*. University of Guelph.

Roux, W. (1881). *Der Kamf der Teile im Organismus*. Wilhelm Engelmann.

Rubin, C. T., Bain, S. D., & McLeod, K. J. (1992). Suppression of the osteogenic response in the aging skeleton. *Calcified Tissue International*, *50*(4), 306–313. https://doi.org/10.1007/BF00301627

Rubin, C. T., & Lanyon, L. E. (1982). Limb mechanics as a function of speed and gait: A study of functional strains in the radius and tibia of horse and dog. *Journal of Experimental Biology*, *101*, 187–211. https://doi.org/10.1242/jeb.101.1.187

Rubin, C. T., & Lanyon, L. E. (1984a). Dynamic strain similarity in vertebrates; an alternative to allometric limb bone scaling. *Journal of Theoretical Biology*, *107*(2), 321–327. https://doi.org/10.1016/S0022-5193(84)80031-4

Rubin, C. T., & Lanyon, L. E. (1984b). Regulation of bone formation by applied dynamic loads. *The Journal of Bone and Joint Surgery*, *66*(3), 397–402.

Rufener, C., & Makagon, M. M. (2020). Keel bone fractures in laying hens: A systematic review of prevalence across age, housing systems, and strains. *Journal of Animal Science*, *98*(Suppl 1), S36-s51. https://doi.org/10.1093/jas/skaa145

Sheffield, K. M., Butcher, M. T., Shugart, S. K., Gander, J. C., & Blob, R. W. (2011). Locomotor loading mechanics in the hindlimbs of tegu lizards (Tupinambis merianae): Comparative and evolutionary implications. *Journal of Experimental Biology*, *214*(15), 2616–2630. https://doi.org/10.1242/jeb.048801

Singer, A., Ben-Yehuda, O., Ben-Ezra, Z., & Zaltzman, S. (1990). Multiple Identical Stress Fractures in Monozygotic Twins. *The Journal of Bone and Joint Surgery*, *72*(3), 444–445.

Skedros, J. G., Mason, M. W., Nelson, M. C., & Bloebaum, R. D. (1996). Evidence of structural and material adaptation to specific strain features in cortical bone. *Anatomical Record*, *246*(1), 47–63. https://doi.org/10.1002/(sici)1097-0185(199609)246:1<47::Aid-ar6>3.0.Co;2-c

Skedros, J. G., Mendenhall, S. D., Kiser, C. J., & Winet, H. (2009). Interpreting cortical bone adaptation and load history by quantifying osteon morphotypes in circularly polarized light images. *Bone*, *44*(3), 392–403. https://doi.org/10.1016/j.bone.2008.10.053

Sugiyama, T., Meakin, L. B., Browne, W. J., Galea, G. L., Price, J. S., & Lanyon, L. E. (2012). Bones' adaptive response to mechanical loading is essentially linear between the low

strains associated with disuse and the high strains associated with the lamellar/woven bone transition. *Journal of Bone and Mineral Research*, *27*(8), 1784–1793. https://doi.org/10.1002/jbmr.1599

Sun, D., Brodt, M. D., Zannit, H. M., Holguin, N., & Silva, M. J. (2018). Evaluation of loading parameters for murine axial tibial loading: Stimulating cortical bone formation while reducing loading duration. *Journal of Orthopaedic Research*, *36*(2), 682–691. https://doi.org/10.1002/jor.23727

Swartz, S. M., Bennett, M. B., & Carrier, D. R. (1992). Wing bone stresses in free flying bats and the evolution of skeletal design for flight. *Nature*, *359*(6397), Article 6397. https://doi.org/10.1038/359726a0

Swartz, S. M., Bertram, J. E., & Biewener, A. A. (1989). Telemetered in vivo strain analysis of locomotor mechanics of brachiating gibbons. *Nature*, *342*(6247), 270–272. https://doi.org/10.1038/342270a0

Tanka Khanal, G. Y. B., Tina M. Widowski, Elijah G. Kiarie. (2020). Rearing cage type and dietary limestone particle size: II, effects on egg production, eggshell, and bone quality in Lohmann selected Leghorn-Lite hens. *Poultry Science*, *99*(11), 5763–5770.

Turner, C. H., Forwood, M. R., Rho, J. Y., & Yoshikawa, T. (1994). Mechanical loading thresholds for lamellar and woven bone formation. *Journal of Bone and Mineral Research*, *9*(1), 87–97. https://doi.org/10.1002/jbmr.5650090113

Umemura, Y., Ishiko, T., Yamauchi, T., Kurono, M., & Mashiko, S. (1997). Five jumps per day increase bone mass and breaking force in rats. *Journal of Bone and Mineral Research*, *12*(9), 1480–1485. https://doi.org/10.1359/jbmr.1997.12.9.1480

Warden, S. J., Mantila Roosa, S. M., Kersh, M. E., Hurd, A. L., Fleisig, G. S., Pandy, M. G., & Fuchs, R. K. (2014). Physical activity when young provides lifelong benefits to cortical bone size and strength in men. *Proceedings from the National Academy of Sciences of the United States of America*, *111*(14), 5337–5342. https://doi.org/10.1073/pnas.1321605111

Welten, D. C., Kemper, H. C., Post, G. B., Van Mechelen, W., Twisk, J., Lips, P., & Teule, G. J. (1994). Weight-bearing activity during youth is a more important factor for peak bone mass than calcium intake. *Journal of Bone and Mineral Research*, *9*(7), 1089–1096. https://doi.org/10.1002/jbmr.5650090717

Whitehead, C. C. (n.d.). Bone breakage and osteoporosis in laying hens: Causes and solutions. *Poultry Science*, *83*, 193–199.

Whitehead, C. C. (2004). Overview of bone biology in the egg-laying hen. *Poultry Science*, *83*(2), 193–199.

Widowski, T., Casey-Trott, T., Hunniford, M., & Morrissey, K. (2017). Welfare of laying hens: An overview. In *Achieving sustainable production of eggs* (Vol. 2, pp. 75–102). Burleigh Dodds Science Publishing.

Willie, B. M., Zimmermann, E. A., Vitienes, I., Main, R. P., & Komarova, S. V. (2020). Bone adaptation: Safety factors and load predictability in shaping skeletal form. *Bone*, *131*, 115114. https://doi.org/10.1016/j.bone.2019.115114

Yang, H., Embry, R. E., & Main, R. P. (2017). Effects of Loading Duration and Short Rest Insertion on Cancellous and Cortical Bone Adaptation in the Mouse Tibia. *PLoS One*, *12*(1), e0169519. https://doi.org/10.1371/journal.pone.0169519

Young, V. K. H., & Blob, R. W. (2015). Limb bone loading in swimming turtles: Changes in loading facilitate transitions from tubular to flipper-shaped limbs during aquatic invasions. *Biology Letters*, *11*(6), 20150110. https://doi.org/10.1098/rsbl.2015.0110

Young, V. K. H., Wienands, C. E., Wilburn, B. P., & Blob, R. W. (2017). Humeral loads during swimming and walking in turtles: Implications for morphological change during aquatic reinvasions. *Journal of Experimental Biology*, *220*(21), 3873–3877. https://doi.org/10.1242/jeb.156836

Chapter 4 – In vivo mechanical behaviour of the tibiotarsus of young chickens during controlled loading

In Chapter 3 I described a study wherein I measured the mechanical strain stimuli that the tibiotarsus is subjected to during different types of commonly performed activities, such as ground locomotion, ramp locomotion, jumping, and landing. Strain gauging is limited to measuring strains at discrete sites along the bone's surface. Oftentimes, surgical accessibility of the bone's surface and the bone size (dictating available surface area for gauge attachment) will limit the anatomical locations where strain can be measured. Finite element modelling overcomes this limitation, allowing the estimation of engendered strains and stresses throughout the entire bone volume, but requires the investigator to define the loading conditions, thus requiring prior knowledge of in vivo background loading boundary conditions which experimenters often do not have.

In the current chapter, I performed finite element modelling simulating the better-known loading conditions applied by our controlled loading device. I characterized the mechanical behaviour of the tibiotarsi by measuring estimated strains and stresses engendered by axial compressive loading at a load magnitude which engenders strains in the range of those measured during background activities. I then investigated how tissue mineral density and bone structural properties influence the bone's mechanical behaviour. Strains modelled at the sites of gauge attachment were similar to those measured during background in vivo loading, lending confidence to the generalizability of our findings beyond the context of controlled loading, to background loading conditions.

Manuscript status: In submission at *Bone Reports*

Tissue mineral density heterogeneity did not influence the in vivo mechanical behaviour of chicken tibiotarsi

Isabela Vitienes[a,b,c], Catherine Julien[b,c], Russell Main[d,e], Ana Rentsch[f], Tina Widowski[f], Sara Checa[g], Bettina M. Willie[a,b,c,†]

[a] *Department of Biomedical Engineering, McGill University, Montreal, Canada*

[b] *Research Centre, Shriners Hospital for Children-Canada, Montreal, Canada*

[c] *Faculty of Dental Medicine and Oral Health Science, McGill University, Montreal, Canada*

[d] *Weldon School of Biomedical Engineering, Purdue University, Indiana, U.S.A*

[e] *Department of Basic Medical Sciences, Purdue University, Indiana, U.S.A*

[f] *Department of Animal Bioscience, University of Guelph, Guelph, Canada*

[g] *Julius Wolff Institute, Charité-Universitätsmedizin Berlin, Berlin, Germany*

Abstract

Bone fragility in commercial egg-laying chickens is a major welfare concern. Efforts have successfully focused on stimulating increased bone volume and changes in bone structure by motivating increased physical activity through more spacious and complex housing systems. However, it remains unclear how these bone adaptations to different housing systems influence in vivo bone mechanical behaviour. We sampled female chickens of two genetic strains that were raised in housing environments that allowed for none, moderate, or high physical activity levels. We performed whole-bone microCT-imaging of the tibiotarsi for finite element modelling of in vivo tibiotarsal axial compression, with either homogeneous or heterogeneous material properties, to assess the effects of bone structure and material properties on engendered bone deformation and stress. We then quantified measures of bone structure along the bone-length and correlated these measures to the simulated mechanical behaviour. We found that variations in tissue mineral density (TMD) of up to 0.2 gHA/cm^3 had negligible effects on the stress magnitudes and patterns along the bone-length. Bone curvature was not an outstanding correlate to stress; instead, we found a set of structural parameters that all had significant, strong negative correlations to bone stress. We did see that stress and strain magnitudes, but not patterns, differed between bones from brown- and white-feathered genotypes, and between bones from chickens raised in the three housing styles. These results inform future interpretations of changes in TMD as to their physiological significance in their effect on bone stress, inform mechanical testing protocols that aim to replicate in vivo loading, and inform poultry housing and enrichment design that encourage physical activity levels which lead to bone stiffening adaptations.

Introduction

Commercial laying hens suffer from osteoporosis and high fracture incidence (Whitehead & Fleming, 2000), posing a significant welfare concern. Bone will fracture when the applied loads exceed the structural strength of bone. Osteoporosis occurs when there is low bone mineral density and deteriorated bone structure, which decrease both the bone's stiffness and strength. In humans with osteoporosis, bone mass is highly correlated to fracture risk, but bone mass overlaps significantly in people who fracture and those who don't indicating that bone mass alone is not adequate to predict fracture. The bone's ability to bear applied loads is a function of the whole bone volume, geometric distribution of the volume, and the material properties of the bone. Thus, other whole bone properties such as stiffness and curvature as well as material level properties are likely important determinants of fracture risk in humans as well as egg laying hens.

The stiffness of a bone is a function of 1) the properties of the bone material, and 2) the arrangement of the bone tissue in space (bone structure) (Burr, 2019; van der Meulen et al., 2001). The elastic modulus, a material property, describes how stiff the material itself is (which is not the same as the whole bone stiffness) and is assumed to be linearly related to the tissue mineral density (TMD) (J. D. Currey, 1988b, 2004b). Bone structure depends on how much bone there is (bone volume) and architectural properties such as whole bone curvature, bone length, cross-sectional thickness, cross-sectional area, among others. Many studies to date seeking to assess the severity of osteoporosis in commercial laying hens and test the effects of interventions have looked at bone mineral density and ash density as an indicator of bone stiffness and strength (Chen & Kim, 2020; Kim et al., 2012). Only recently have studies begun using high-resolution CT imaging to evaluate bone-type specific (cortical, trabecular) structural properties (Chen & Kim, 2020; Regmi et al., 2017). In rodents, much more research has been performed and it has been shown that tissue mineral density heterogeneity does not influence bone stiffness (Razi, Birkhold, Zaslansky, et al., 2015).

Recent work has shown that providing increased opportunities for physical activity by housing chickens in more spacious, complex environments, has positive effects on bone health related outcomes especially when these opportunities are provided from youth (T. M. Casey-Trott, Korver, et al., 2017a, 2017b; Enneking et al., 2012; Fleming et al., 2006; Heerkens et al., 2016; Hester et al., 2013). Chickens raised in aviaries had wider, longer bones with higher cortical bone

thickness, and higher bone mineral content (Vitienes et al., 2021). It remains unclear, however, how these adaptations relate to bone stiffness.

We aimed to address this gap in knowledge by performing finite element analyses modelling physiological axial compressive loading of the tibiotarsus to characterize the tibiotarsal mechanical behaviour and assess the relative effects of tissue mineral density heterogeneity (a material property) and structural properties on the mechanical behaviour. We sampled bones from two genetic strains of chickens that were raised in one of three styles of housing: a conventional cage that did not allow for any physical activity, and two types of aviary-style systems of low or high spatial complexity. We hypothesized that 1) bone mechanical behavior would be influenced by both mineral density heterogeneity and bone structure, 2) bone curvature would be the salient determinant of bone deformation due to loading, and 3) bone mechanical behavior and its relationship to bone structure would differ between genotype and housing groups.

Materials and Methods

1. Housing and management

All animal use and procedures were approved by the animal care committees at the University of Guelph (AUP #4127) and McGill University (AUP #8083). Housing and management are briefly described, whereas full details are reported elsewhere (Vitienes et al., 2023). Over a two-year period, three consecutive flocks of Lohmann Selected Leghorn Lite (white-feathered) and Lohmann Brown Lite (brown-feathered) female chicks (*Gallus gallus domesticus*) were obtained from a commercial hatchery at the age of one day old. The chickens were reared from 1 day of age to 14 weeks at the University of Guelph in either conventional rearing cages (Conv: Ford Dickinson, Mitchell, Ontario, Canada), or one of two styles of commercial aviaries. Conventional cages are spatially restrictive and do not allow for physical activity or movement - chickens are only able to stand and sit. Aviaries alternatively are more spacious and contain infrastructure that allows for more frequent and varied types of activity (e.g. jumping, ramp ascent and descent, perching, running) (Pufall et al., 2021; Rentsch et al., 2023a). The aviaries chosen for this study had either low or high spatial complexity (Low: Natura Primus, Big Dutchman, Holland, MI, U.S.A; High: NivoVaria, Jansen Poultry Equipment, Netherlands, and Farmer Automatic Portal Pullet, Clark Ag Systems, Caledonia, ON, Canada) and have been shown to motivate moderate or

high amounts of physical activity respectively (Pufall et al., 2021; Rentsch et al., 2023a). We have also previously shown that aviary-complexity has a genetic-strain dependent effect on dynamic load-bearing activity, where brown-feathered chickens in Low and High had similar activity levels, whereas white-feathered chickens in High were more active than those in Low (Rentsch et al., 2023a). Both brown- and white-feathered chickens were more active when housed in aviaries (either Low or High) compared to when housed in Conv.

Chickens of each genetic strain were housed separately. Conventional cages were populated with 30 chickens/cage (h: 40 cm, w: 76 cm, d: 66 cm) during weeks 0-6 (167 cm^2/chicken), and 15 chickens/cage during weeks 6-14 (344 cm^2/chicken). For each flock, a total of 300 chickens per genetic strain were reared in Low aviaries, whereas the High housing group had 600 chickens per genetic strain per flock. All other conditions (feed, vaccination, lighting, temperature) were held constant across housing groups.

A total of 48 fourteen-week-old white-feathered and brown-feathered chickens were randomly sampled (n=8 chickens/genetic strain [2]/rearing housing system [3]) and transported from the University of Guelph to McGill University (Donald McQueen Shaver Poultry Complex) on three separate occasions. Upon arrival at McGill, the white-feathered and brown-feathered chickens were housed in separate identical rooms consisting only of litter floor (total area of 13.2 m^2). Chickens were fed ad libitum standard age-appropriate crumble diet. A lighting schedule of 10h of light per day, at 10 lux, was maintained, and rooms were kept at 20°C. Chickens were allowed to acclimate for at least 72 h prior to the onset of the experiment. Time constraints allowed for experimentation on two chickens per day, and thus the experiment occurred over a 2-week period. Chickens were weighed the morning prior to undergoing surgery for strain gauge attachment.

2. *In vivo strain measurements at the tibiotarsal midshaft during axial compressive loading*

Chickens were instrumented with strain gauges at the right tibiotarsus midshaft. Following strain gauge attachment, chickens underwent in vivo background strain gauging, results of which are reported elsewhere (Vitienes et al., 2023). Strain gauge preparation and surgical procedures to attach strain gauges are also reported elsewhere. Briefly, chickens were sedated and instrumented with strain gauges at the tibiotarsus midshaft. Following a 2-3h period of recovery from surgery, chickens underwent in vivo background strain gauging (results reported elsewhere, (Vitienes et al., 2023)), after which time the chicken was anesthetized again for controlled loading. Chickens

were sedated with 0.5-1% of isoflurane at 1 L/min O_2 flow rate using a mask. Sufficient anesthetic depth was asserted via the loss of toe pinch reflex and palpebral reflex.

Chickens then underwent controlled in vivo loading wherein the tibiotarsus was subjected to bouts of controlled axial compressive load (120N) using a loading device (Testbench ElectroForce LM1, Bose, Framingham, USA), while engendered strains were recorded from a rosette strain gauge (FR-1-11, Tokyo Sokki Kenkyujo Co., Ltd, Tokyo, Japan) attached to the anterior surface of the tibiotarsus midshaft. We applied dynamic compressive loading at a frequency of 4 Hz by a triangular waveform with a 0.1s rest between each cycle (216 load cycles per trial). Applied peak loads, measured by a load cell, differed slightly from the target load level (125 ± 4 N average applied load). A pre-load of 10 N was maintained during the rest phase to hold the limb in place. The loading device was outfitted with custom 3D printed knee and ankle fixtures. Strain signals were measured by connecting the breakout plug at the flank region of the chicken to a 3m long shielded cable (326-BSV; Micro-Measurements, U.S.A) connected to a bridge amplifier (System 8000 Scanner; Micro-Measurements, U.S.A). Strains were recorded (StrainSmart, Micro-Measurements, U.S.A) using an excitation voltage of 3V and sampled at 1 kHz. A total of 4 channels were recorded, corresponding to the three elements of the rosette strain gauge at the anterior surface and input from the loading machine load cell, such that load and strain were recorded simultaneously. Following controlled loading, chickens were euthanized, and their carcasses frozen for later dissection, after which time the strain gauged tibiotarsi were dissected and stored in 70% ethanol.

3. *Microcomputed tomography of the tibiotarsus*

A total of 35 right-sided whole tibiotarsi (n=6-8/genetic strain [2]/housing [3]) were imaged to measure bone structure. A subset of these images (n=1/genetic strain [2]/housing [3]) were used for finite element analysis (FEA). Whole tibiotarsi were imaged at an isotropic voxel size of 40.5 μm (Skyscan 1276, Bruker, Massachusetts, U.S.A; 80 kV, 200 μA, 125 ms exposure time, 0.8° rotation step, Aluminum 0.5 mm filter, 180° scan, no frame averaging). Images were reconstructed with a dynamic range of 0-0.055 cm^{-1} and corrections for misalignment were applied when needed. microCT images were calibrated to units of gHA/cm^3 with calibration equations derived by imaging calibration phantoms (0.25 and 0.75 gHA/cm^3), measuring the average grey value of each

phantom ($GV_{0.25}$, $GV_{0.75}$), and solving the system of equations assuming a linear relationship between bone density and x-ray attenuation to derive calibration equation constants *a* and *b*:

$$\begin{cases} 0.25\dfrac{gHA}{cm^3} = a * GV_{0.25} + b \\ 0.75\dfrac{gHA}{cm^3} = a * GV_{0.75} + b \end{cases}$$

Bones were then binarized using a global threshold of 0.22 gHA/cm^3 to exclude background and soft tissue. The fibula was segmented and excluded from all analyses given a lack of bony connection to the tibiotarsus, implying it does not bear load applied in our in vivo controlled loading model.

4. *Finite element modeling of load-induced strain and stress across the entire tibiotarsus*

A total of 6 bones (n=1/strain [2]/housing [3]) were used in the FEA, randomly selected from the set of 35 bones included in this study.

Table 1: FEA parameters and validation. Max (abs) principal strain probed in FE models at the location of gauge attachment and compared to principal tensile strain measured experimentally at the anterior midshaft surface. Percent difference between experimental- and FE-derived strains quantified relative to the FE strains.

Genetic strain	Housing	Bone length [mm]	# FE elements [x 10^6]	Element characteristic length [mm]	Experimental strain [με]	Heterogeneous		Homogeneous		
						FE strain [με]	Δ(exp - FE)	FE strain [με]	Δ(exp - FE)	
B	Conv.	118	2.49	0.328	340	135	205	213	-37	
B	Low	117	3.62	0.306	390	311	79	393	1	
B	High	124	2.61	0.344	502	437	65	541	8	
W	Conv.	122	2.81	0.274	478	272	206	459	-4	
W	Low	120	2.90	0.288	236	152	84	245	4	
W	High	116	3.66	0.277	268	198	70	209	-22	
		120 ± 3	2.88 ± 0.51	0.303 ± 0.028	369 ± 108	251 ± 114	118 ± 68	343 ± 141	-8 ± 18	mean ± sd

4.1 Whole Bone Geometry

Whole bone microCT images selected for FEA were binarized with a global threshold of 0.22 gHA/cm^3 and segmented to separate cortical from trabecular bone at the proximal and distal metaphyses (10% bone length VOI size) and midshaft (5% bone length VOI size). It was not possible to distinguish trabecular from medullary bone in these images due to insufficient resolution relative to medullary bone size and consequent partial volume effects. Segmentation was automated using sequential morphological operations (XamFlow, Lucid Concepts AG, Zürich, Switzerland). The resulting multi-label mask of the whole bone with cortical and trabecular

sections at the proximal and distal metaphyses and midshaft was then converted to a tetrahedral mesh using Amira 3D software (Amira 3D 2022, Thermo Fisher Scientific, Massachusetts, U.S.A) (Table 1).

4.2 FEM Boundary Conditions

Boundary conditions replicated the controlled loading experiment (Fig. 1 A). Two reference points were placed at each end of the bone: at the medial and lateral condyle centers (distal) and at the centers of the contact points of the two femoral condyles (proximal). The midpoints of each pair of reference points were then used to define the bone's long axis (as the line joining these two midpoints). Contact surfaces were manually selected as the flexed tibiofemoral contact surfaces (proximal) and the contact surface between the distal tibiotarsus and the ankle fixture (distal) (Fig. 1 B). A load of 120 N was applied through the contact surface at the bone's distal end at an 10° angle from the bone's axis in the posterior direction (Fig. 1 A) while contact surface nodes at the proximal end were held fixed. This peak load value was selected as it engenders principal strains ranging from 236-502 με at the tibiotarsus anterior midshaft, which are similar in magnitude to what we previously measured during in vivo background activities (9).

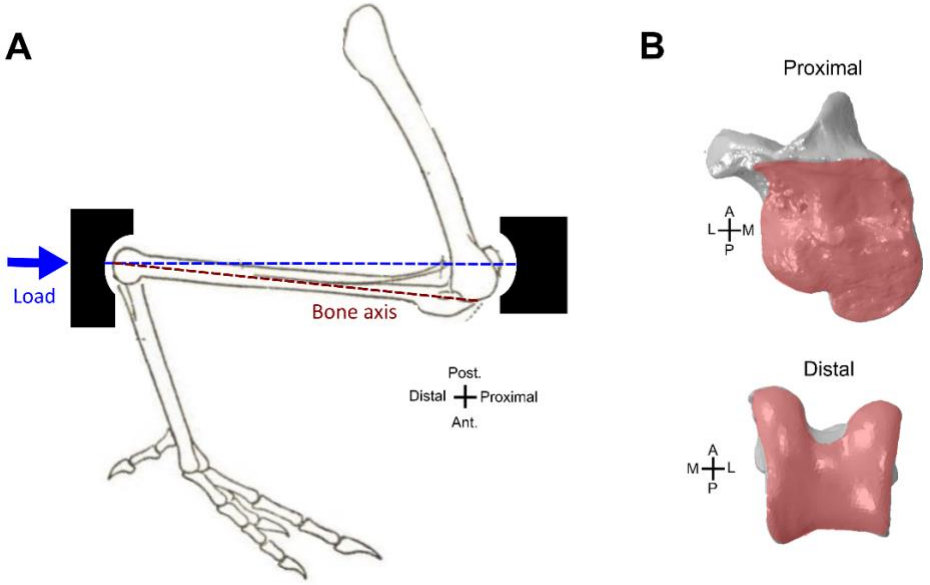

Figure 1: Finite element methods. A) In vivo experimental loading setup simulated by the finite element modelling. Load is applied to the ankle in the direction of the load axis (dashed blue line) while the knee is held fixed in a flexed position. The load axis was rotated by approximately 10° in the posterior direction relative to the bone's axis. B) FEM knee (proximal) and ankle (distal) contact surfaces mimicking the in vivo experimental conditions.

4.3 FEM Material Properties

To distinguish between the effects of material properties and bone structure on modelled strains and stress, two models were created for each bone:

(1) A heterogeneous model where each tetrahedral mesh element was assigned a specific elastic modulus as a function of the tissue mineral density measured at that location in the microCT image (Razi, Birkhold, Zaslansky, et al., 2015). Given the ash density-elastic modulus relationship

$$E = k\ \rho_{ash}{}^{1.5}$$

and assuming a linear relationship between ash density (ρ_{ash}) and linear attenuation coefficient (μ), an attenuation coefficient-modulus relationship can be derived as

$$E_{VOI_a} = \left(\frac{E_{VOI_b}}{\bar{\mu}_b{}^{1.5}}\right) \bar{\mu}_a{}^{1.5}$$

where E_{VOI_i} is the elastic modulus and $\bar{\mu}_i$ the average attenuation coefficient of a given volume of interest *i*. We used our measurements of the average tissue mineral density of the 6 FEA tibiotarsi (0.52 gHA/cm^3, Fig. 2 A) and reported mid-diaphyseal femoral tissue elastic moduli of age-matched female chickens (11 GPa) (S. Wang et al., 2019) as values for $\bar{\mu}_b$ and E_{VOI_b}, respectively, to derive an equation relating tissue mineral density to elastic modulus.

2) A homogenous model where all tetrahedral elements were assigned a fixed elastic modulus of 11 GPa, which we define as the modulus associated with the average tibiotarsal tissue mineral density (0.52 gHA/cm^3).

4.4 FEM outcomes

Bone meshes were divided into 20 sections along their long axis, each section consisting of 5% of the bone length. Average principal strains (tensile: $\bar{\varepsilon}_{\text{max}}$, compressive: $\bar{\varepsilon}_{\text{min}}$) and von Mises stress ($\bar{\sigma}_{\text{v}}$) were calculated within each region without distinguishing cortical from trabecular bone.

Average principal strains and von Mises stress were also calculated for cortical and trabecular bone separately at the midshaft and proximal and distal metaphyses. Results are reported for each tibiotarsus ($\bar{\varepsilon}$, $\bar{\sigma}_{\text{v}}$), as well as the mean across all tibiotarsi (mean $\bar{\varepsilon}$, mean $\bar{\sigma}_{\text{v}}$). Experimentally measured principal strains at the anterior midshaft surface were used to validate the models (Table 1).

5. Bone structure

Thresholded whole bone images were aligned such that the bone's longitudinal axis (defined as the chord joining the centroids at the proximal (5%) and distal (95%) ends of the bone) was in line with the global z-axis. At each slice, 2D measures of bone structure were computed and averaged across each 5% bone length section. We measured bone curvature (C_R, mm), bone area (B.Ar, mm^2), total area (T.Ar, mm^2), bone area fraction (B.Ar/T.Ar, mm^2/mm^2), bone thickness (B.Th, mm), bone thickness variation (B.Th.sd, mm), polar moment of inertia (pMOI = $I_{min} + I_{max}$, mm^4), eccentricity (I_{min}/I_{max}, mm^4/mm^4), normalized inner perimeter (I.Pm/T.Ar., mm/mm^2), normalized outer perimeter (O.Pm/T.Ar, mm/mm^2), normalized total perimeter (T.Pm/T.Ar, mm/mm^2), and inner-to-outer perimeter ratio (I.Pm/O.Pm, mm/mm) (XamFlow, Lucid Concepts AG, Zürich, Switzerland). Curvature measurements were normalized by each bone's midshaft anterior radius (distance between the midshaft slice centroid and the anterior periosteal surface), based on reported recommendations (Bertram & Biewener, 1992).

6. Statistics

The effect of bone length section, genetic strain, housing style, and their interactions on tibiotarsal bone structure was assessed by repeated measures ANOVA and unpaired t-tests with Tukey's post-hoc corrections (SAS 9.4, SAS Institute, North Carolina, U.S.A). The correlation between bone structural outcomes and FE-derived von Mises stress was quantified by Pearson correlation coefficients, a normalized measure of covariance. A Pearson correlation coefficient (PCC) and associated correlation p-value were computed for each structural outcome, for each bone or bone subregion. Differences between groups are reported as the difference in the given parameter in group A relative to group B ($\Delta\text{parameter}_{A-B} = \left({(|A| - |B|)}/{|B|}\right)$, where A, B, and parameter are specified in each case). Statistical significance was set at $p \leq 0.05$.

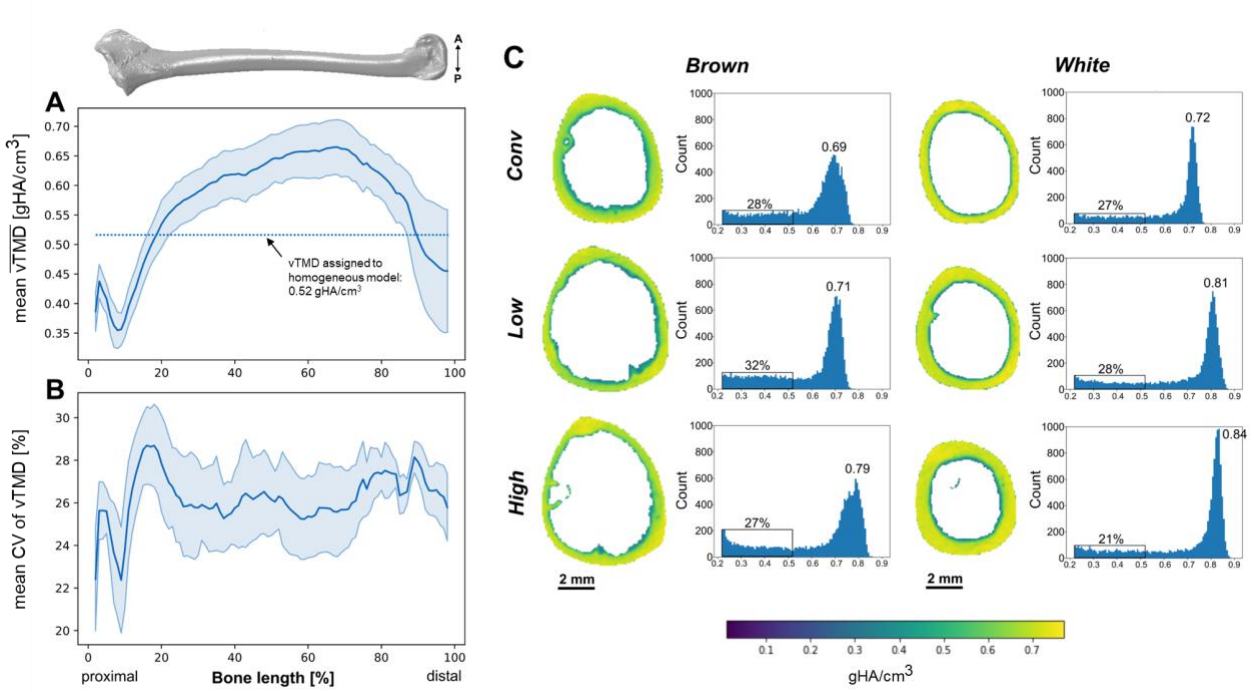

Figure 2: Tissue mineral density variation throughout the tibiotarsi (n=1/genetic strain [2]/housing [3])**.** A) Mean ± standard deviation of the average volumetric tissue mineral density (vTMD, gHA/cm^3) across the tibiotarsus length. For each bone, vTMD was averaged at 1% bone length intervals (denoted $\overline{vTMD}$), and the plotted mean ± sd is taken across the 6 bones. B) Mean ± standard deviation of the coefficient of variation (CV, %) of $\overline{vTMD}$ across the tibiotarsus length. For each bone, the CV was calculated at each 1% bone length interval, and then averaged across the 6 bones. C) Midshaft cross section of each bone showing variations in vTMD, and the respective slice histogram beside. Each histogram is annotated with the peak vTMD and the proportion (%) of pixels included in the box, which encompasses pixels below the average mean vTMD assigned to the homogeneous model (0.52 gHA/cm^3).

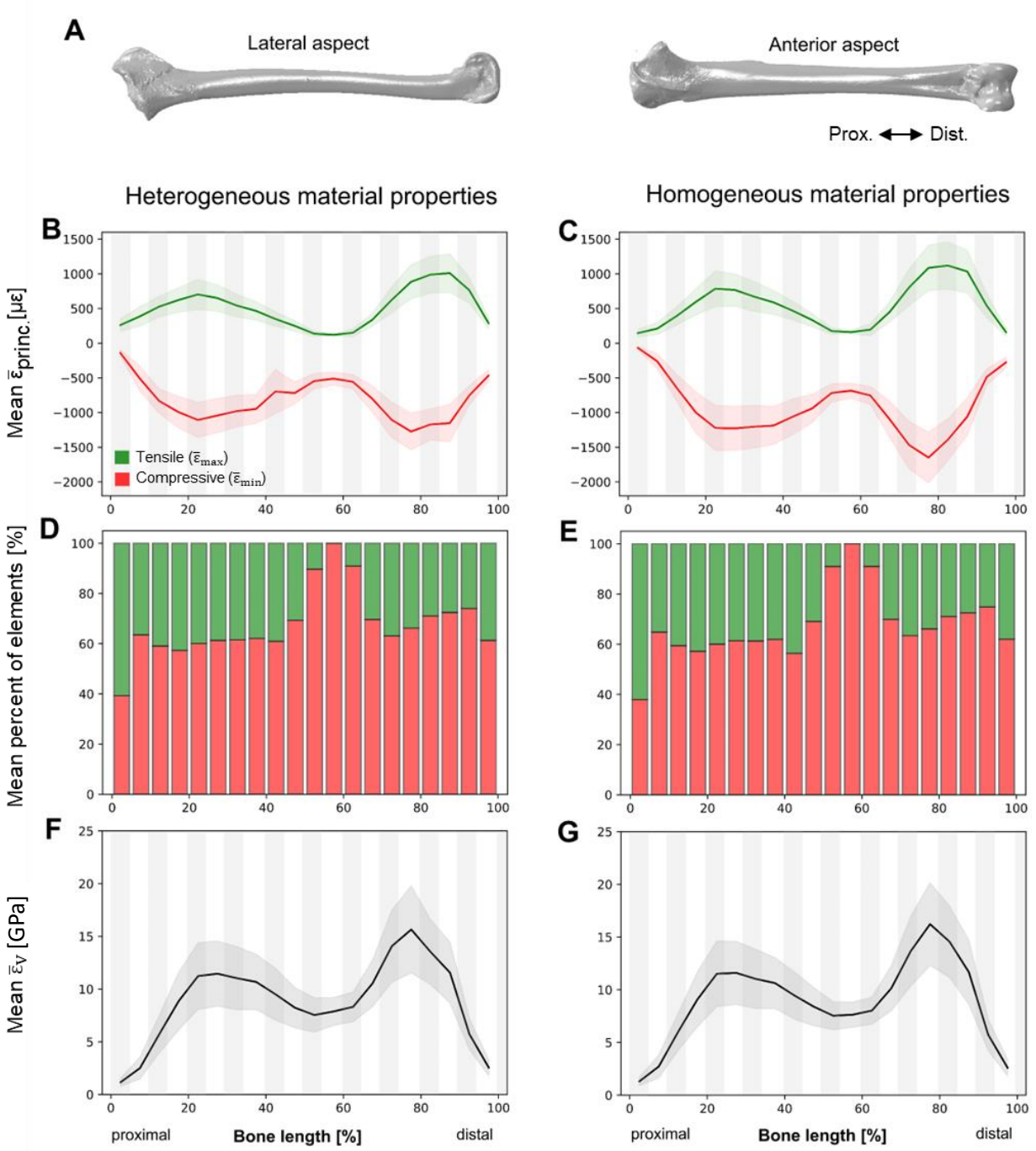

Figure 3: Average mechanical behaviour along the bone length (n=1 tibiotarsus/genetic strain [2]/housing [3])**.** Striped regions on the plot background indicate the 5% bone length sections across which data is averaged. A) Lateral and anterior aspect views of a tibiotarsus, scaled and aligned to the x axes of plots below. B-C) Mean (line) ± standard deviation (shaded) of the average principal strain (green: tensile, $\bar{\varepsilon}_{max}$; red: compressive, $\bar{\varepsilon}_{min}$) at 5% bone length sections for heterogeneous and homogeneous models, respectively. D-E) Mean of the percent of tensile and compressive elements within each 5% bone-length section for heterogeneous and homogeneous models, respectively. F-G) Mean ± sd of the average von Mises stress ($\overline{\sigma}_v$) at 5% bone length sections for heterogeneous and homogeneous models, respectively.

Results

Tissue mineral density heterogeneity had negligible effects on bone mechanical properties

Average volumetric tissue mineral density (vTMD, gHA/cm^3) measured at 5% bone length sections ranged from 0.32-0.7 gHA/cm^3. Bones were more highly mineralized along the diaphysis, compared to the less mineralized proximal and distal metaphyses (Fig. 2 A). There was also substantial cross-sectional variation in vTMD along the entire length of the bone, with a mean coefficient of variation in vTMD ranging between 20-31% (Fig. 2 B). We have observed the presence of medullary bone with a low level of mineralization at the midshaft endosteal surfaces of these 6 bones from higher resolution imaging, to which this cross-sectional variability in vTMD is attributed. The slice histograms provide evidence for what is seen visually in the cross-sectional images: there was lower peak mineralization in the brown-feathered (0.69-0.79 gHA/cm^3) compared to white-feathered (0.72-0.84 gHA/cm^3) chickens, and within the more highly mineralized area, vTMD was more homogeneous in the white-feathered compared to the brown-feathered chickens (narrower histogram peak) (Fig. 2 C). The homogeneous FEMs were defined such that the bones had a fixed mineral density of 0.52gHA/cm^3, with the implication that along 73% of the bone's length the homogeneous models had a mineral density up to 0.18 gHA/cm^3 lower than the heterogeneous model bones. At the proximal and distal regions, the homogeneous models had a mineral density up to 0.2 gHA/cm^3 higher than the heterogeneous models (Fig. 2 A). Cross-sectionally, in the homogeneous models there no longer was the consistent gradient in vTMD seen wherein the outer part of the cortex is more highly mineralized than the endosteal region (Fig. 2 C).

The inclusion of realistic, spatially heterogeneous vTMD in the heterogeneous models did not lead to striking differences in modelled mechanical properties. Section-wise differences in heterogeneous and homogeneous model strains ($\Delta\bar{\varepsilon}_{\max_{het-hom}}, \Delta\bar{\varepsilon}_{\min_{het-hom}}$) ranged from -222 to 201 με in tension and -376 to 267 με in compression. Peak mean average principal tensile (peak mean $\bar{\varepsilon}_{max}$) and compressive (peak mean $\bar{\varepsilon}_{min}$) strain magnitudes from the heterogeneous models were lower compared to the homogeneous models ($\Delta\bar{\varepsilon}_{\max_{het-hom}}$ = -126 με, $\Delta\bar{\varepsilon}_{\min_{het-hom}}$ = -397 με) (Fig. 3 B-C). Both models exhibited similar proportions of tensile and compressive elements within each bone section (Fig. 3 D-E). Peak mean average von Mises stress (peak mean $\bar{\sigma}_v$) was

also lower in the heterogeneous compared to homogeneous models ($\Delta\bar{\sigma}_{v_{het-hom}}$ = -1 GPa). Along the length of the bone, there was a consistent pattern in both heterogeneous and homogeneous models where strains and stress peaked at the proximal and distal regions. Given the minimal differences in strain and stress magnitude and patterns along the length of the bone, subsequent results will be presented only for homogeneous models to isolate the effects of bone geometry on bone mechanics.

Heterogeneity of stress distribution across the bone length and between bone compartments

Average principal tensile and compressive strain, and average von Mises stress, all had similar distributions along the bone length, with local peaks at the proximal and distal metaphyses, the latter being the global maximum (Fig. 3 B-C, 3 F-G). At the proximal metaphysis, strain and stress peaked at the 20-25% bone length region (mean $\bar{\varepsilon}_{max}$ = 916 με, mean $\bar{\varepsilon}_{min}$ = -1361 με, mean $\bar{\sigma}_v$ = 13 GPa). At the distal metaphysis, peak strains and stress occurred at 75-85% of the bone length (mean $\bar{\varepsilon}_{max}$ = 1248 με, mean $\bar{\varepsilon}_{min}$ = -1781 με, mean $\bar{\sigma}_v$ = 18 GPa). The local minima between these peaks occured at 50-60% bone length (mean $\bar{\varepsilon}_{max}$ = 160 με, mean $\bar{\varepsilon}_{min}$ = 708 με, mean $\bar{\sigma}_v$ = 8 GPa). At this location, the bone was completely under compression, whereas elsewhere there was a combination of tension and compression, with the proportion of tensile elements generally increasing with distance from this local minimum towards the proximal and distal ends of the bone (Fig. 3 E). Global minima also occurred at a consistent location, namely the 0-5% bone length region (mean $\bar{\varepsilon}_{max}$ = 163 με, mean $\bar{\varepsilon}_{min}$ = 69 με, mean $\bar{\sigma}_v$ = 1 GPa). Along the bone length, stress varied across a range nearly as large as the peak stress achieved (94%).

By observing strains plotted on the bone geometry, we saw that, from the anterior perspective, the bones exhibited convex bending (anterior tension, posterior compression) in the proximal region and concave bending (anterior compression, posterior tension) in the distal region (Fig. 4 A). The transition in bending direction (rotation of the neutral axis by nearly 180°) occurred at the distal midshaft (52-64% bone length) (Fig. 4 B), coinciding with the region of local strain and stress minima.

Bone stress was differentially distributed between cortical and trabecular bone at the proximal and distal metaphyses (Fig. 5 A), where the total cross-sectional stress (proximal: 10 GPa, distal: 16 GPa) was concentrated in the cortical bone tissue (proximal: 9 GPa, distal: 16 GPa).

At the midshaft, where total stress (8 GPa) was lower, it was similarly distributed between cortical (9 GPa) and trabecular (8 GPa) bone. Variation in stress along the bone length followed different patterns for cortical and trabecular bone: cortical bone stress peaked at the distal metaphysis and was lowest at the midshaft, whereas trabecular bone stress peaked at the midshaft, and was lowest at the proximal metaphysis.

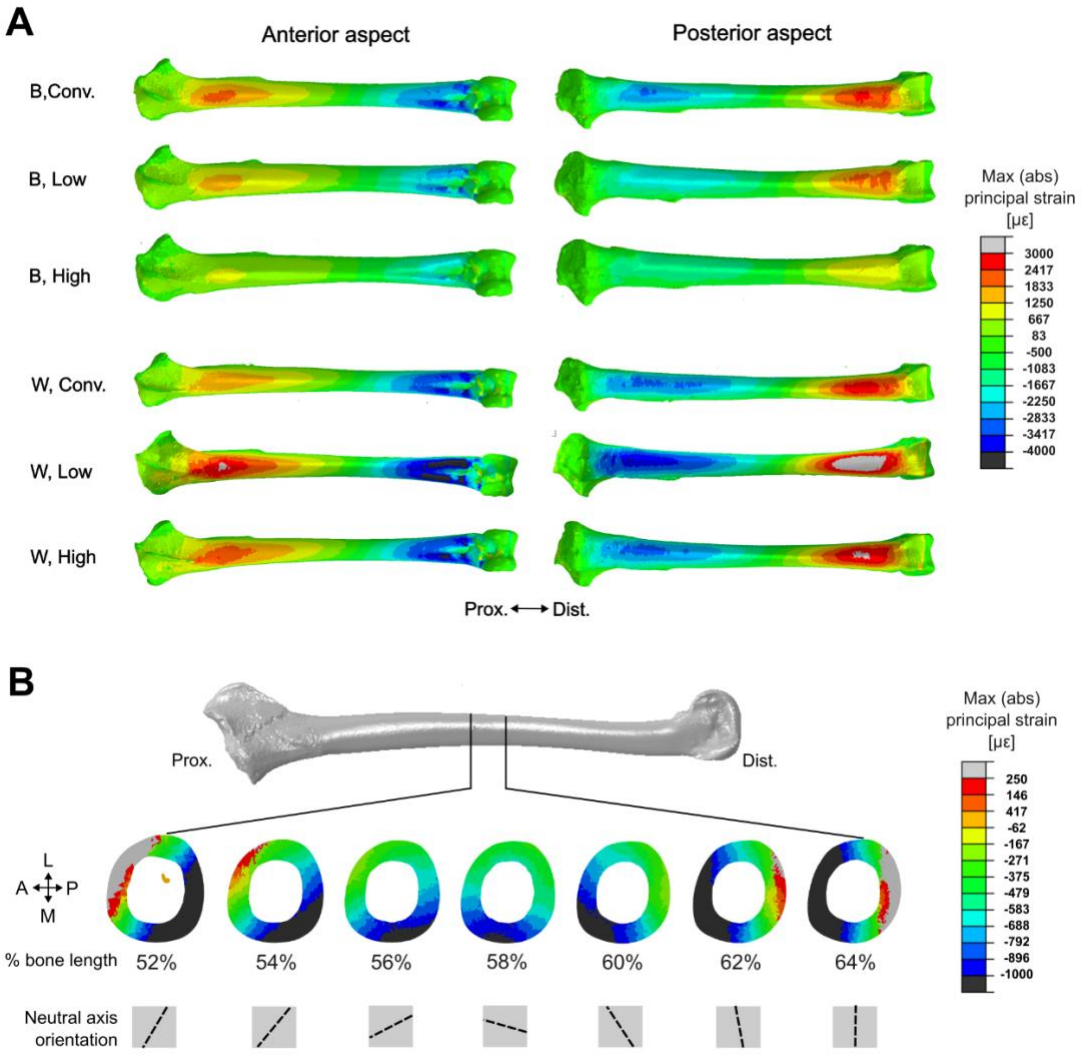

Figure 4: Principal strain distribution (n=1 tibiotarsus /genetic strain [2]/housing [3])**.** For each element, the principal strain with the highest magnitude (max (abs)) is shown. Positive strains are tensile, negative strains are compressive. A) Each bone seen from the anterior and posterior aspects. Bones are scaled to a common length. B) Cross sectional strain distributions of an exemplary bone at the 52-64% bone length region, where the transition from convex (proximal) to concave (distal) bending occurs (as visualized from the anterior aspect).

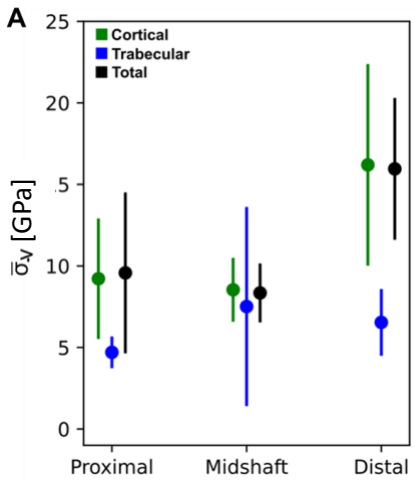

Figure 5: Regional variation in stress (n=1 tibiotarsus/genetic strain [2]/housing [3])**.** Mean ± standard deviation of the average von Mises stress $\overline{\sigma}_v$ in cortical (green), trabecular (blue), and total (cortical ∪ trabecular, black) elements at the proximal metaphysis, midshaft, and distal metaphysis.

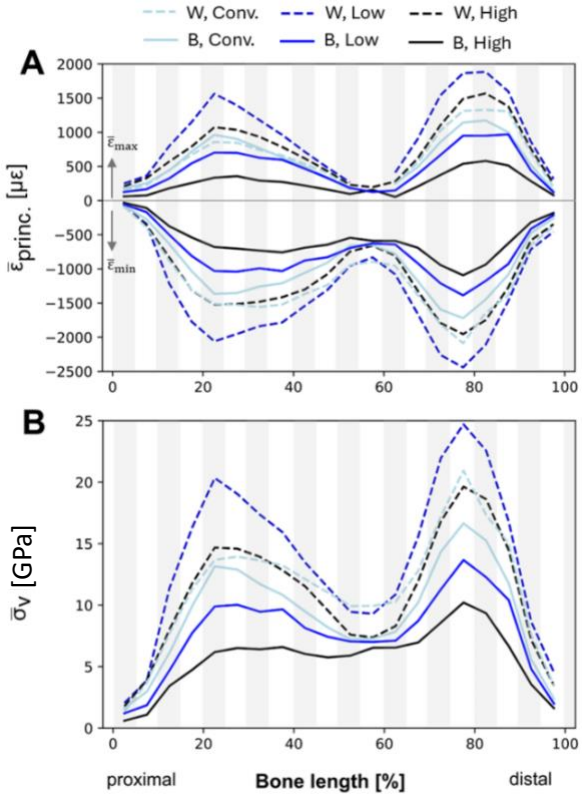

Figure 6: Homogeneous model strains and stresses in individual bones (n=1/genetic strain [2]/housing [3])**.** Shaded regions on the plot background indicate the 5% bone length sections across which data is averaged. A) Average principal strain (tensile: $\overline{\varepsilon}_{max}$, compressive: $\overline{\varepsilon}_{min}$) and B) von Mises stress ($\overline{\sigma}_v$) along the length of each bone. For each bone, strains or stress is averaged across elements within 5% bone length sections.

Strain and stress magnitudes, but not patterns, differed between brown- and white-feathered chickens

In all bones, the same pattern occurred in which strains and stress had local maxima at the proximal and distal regions. The white-feathered chicken bones exhibited higher strain and stress magnitudes compared to the brown-feathered chicken bones, particularly at these regions of local maxima (Fig. 6 A-B). Among brown-feathered chicken bones, there was a consistent pattern wherein Conv bones had the highest strains and stress, followed by Low and then High (Conv > Low > High). In the white-feathered group, Low bones consistently exhibited higher strains and stress compared to Conv and High which themselves exhibited similar strains and stress magnitudes (Low > High = Conv).

Structural determinants of stresses vary across the bone length

To investigate the relationship between bone structure the observed stress distribution along the bone length, we quantified bone structural parameters within 5% bone length regions for the full set of bones (n=6-8/genetic strain [2]/housing [3]). All structural parameters were influenced by bone-length section. We did not observe a clear bimodal curve in any of the measured structural parameters (Fig. 7) as consistently seen in our strain and stress results. In all groups, radius of curvature (C_R) peaked at the distal metaphysis (Fig. 7 A). Bone area (B.Ar), total area (T.Ar), polar moment of inertia (pMOI), normalized inner perimeter (I.Pm/T.Ar), normalized total perimeter (T.Pm/T.Ar), and inner-to-outer perimeter ratio (I.Pm/O.Pm) had similar patterns along the bone length, peaking at the proximal and distal ends, and remaining relatively constant along the bone shaft (Fig.7 B, C, G, I, K, L). Bone area ratio (B.Ar/T.Ar) and normalized outer perimeter (O.Pm/T.Ar) remained relatively constant throughout the bone length (Fig. 7 D, J). Bone thickness (B.Th), thickness variation (s(B.Th)), and eccentricity (I_{min}/I_{max}) exhibited a curved distribution along the bone length, peaking at the midshaft (Fig. 7 E, F, H).

Genetic strain influenced all parameters except C_R and B.Th, either independently or in a bone length section dependent fashion. Compared to W, B bones had higher B.Ar., T.Ar, s(B.Th), pMOI, I.Pm/T.Ar, and I.Pm/O.Pm, and lower B.Ar/T.Ar. Whereas for I_{min}/I_{max} and T.Pm/T.Ar, how one genetic strain compared to the other depended on the bone length section. Housing style influenced I.Pm/O.Pm independent of bone length section, and C_R and I.Pm/T.Ar in a genetic strain-dependent manner.

Whole-bone von Mises stress significantly correlated to B.Ar, T.Ar, B.Ar/T.Ar, B.Th, pMOI, I.Pm/T.Ar, T.Pm/T.Ar, and I.Pm/O.Pm. All these structural outcomes significantly negatively correlated to von Mises stress ($-0.75 < PCC < -0.46$) except for B.Th ($PCC = 0.49$) (Fig. 8). At the proximal 30% of the bone, B.Th had a significant positive correlation with stress ($PCC=0.72$) while s(B.Th), I.Pm/T.Ar, T.Pm/T.Ar, and I.Pm/O.Pm had significant negative correlations with stress ($-0.97 < PCC < -0.82$). Correlations at the distal 30% of the bone were similar to correlations of the whole bone: stress was negatively correlated to B.Ar, T.Ar, B.Ar/T.Ar, $I_{min}+I_{max}$, I.Pm/T.Ar, T.Pm/T.Ar, and I.Pm/O.Pm ($-0.97 < PCC < -0.78$) and positively correlated to O.Pm/T.Ar ($PCC = 0.57$) and B.Th ($PCC = 0.89$). In the middle section of the bone, there were no significant correlations between structural outcomes and stress.

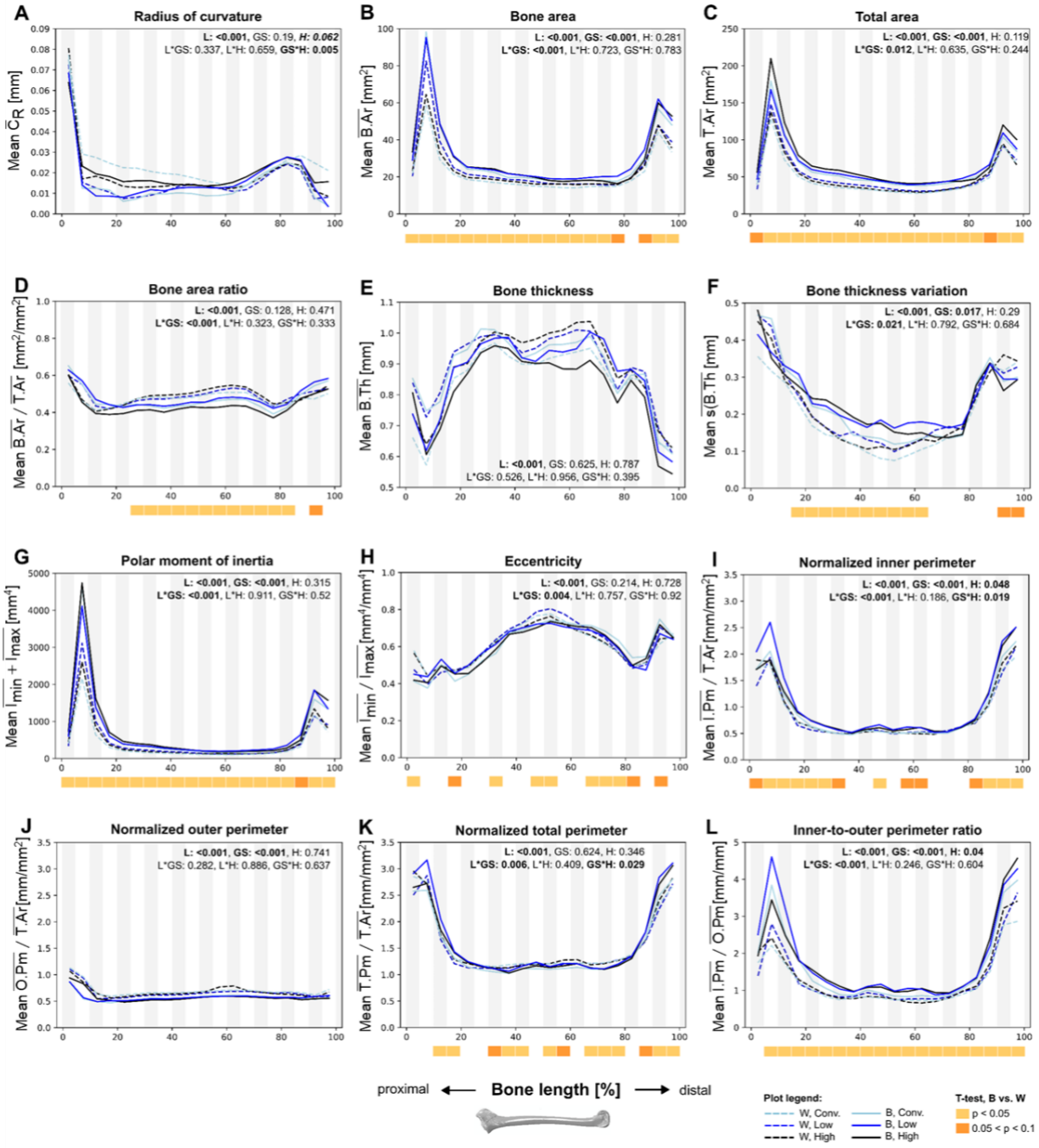

Figure 7: Bone morphology along the bone length (n=6-8 tibiotarsi/genetic strain [2]/housing [3]). For each bone, morphological outcomes were measured at each slice and averaged across 5% bone length sections (plot background stripes). Mean values per group (genetic strain x housing) are plotted. ANOVA p-values for the effects of bone length section (L), genetic strain (GS), housing (H), and all two-way interactions (L*GS, L*H, GS*H) are indicated within each plot. There were no section-dependent effects of housing (L*H); in the cases where there was a significant interaction between bone length section and genetic strain, significant (yellow) and trending (orange) pairwise comparisons between genetic strains are indicated below for each section.

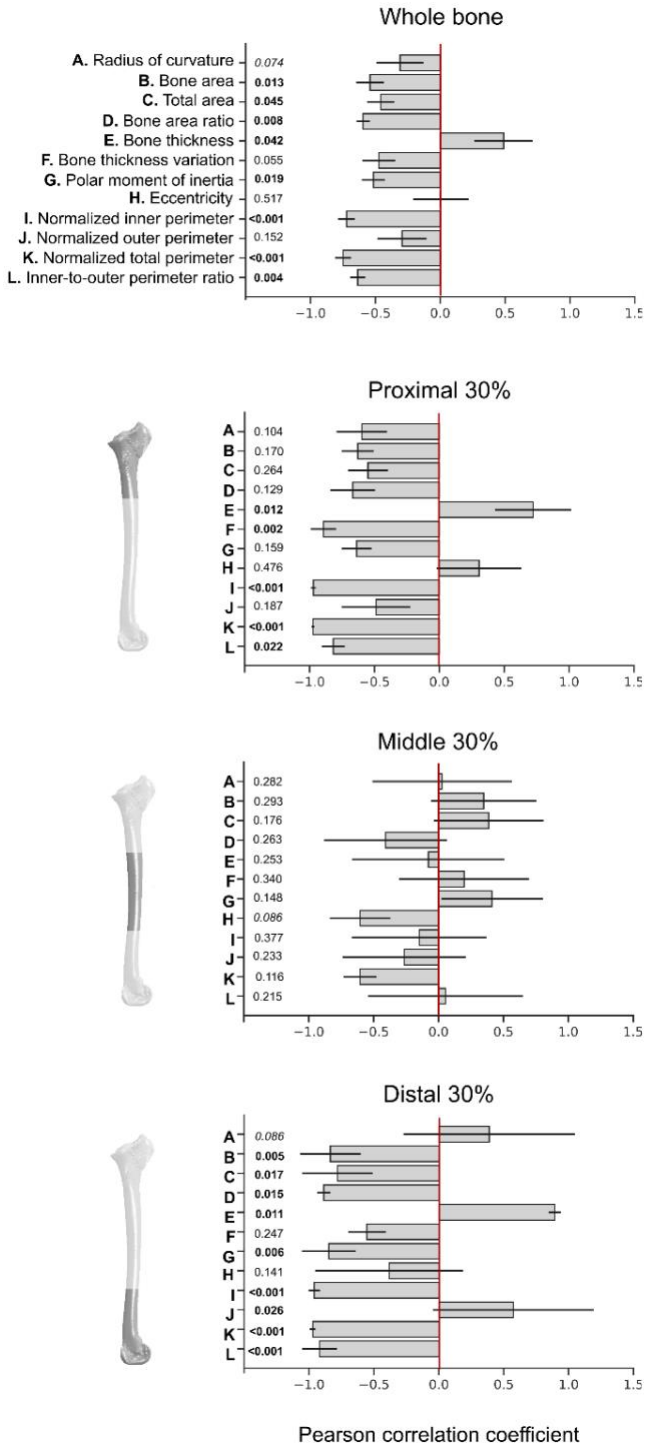

Figure 8: Correlation between bone morphology and mechanical properties (6 bones, n=1 tibiotarsus/genetic strain [2]/housing [3])**.** Mean ± standard deviation (across bones) of the Pearson correlation coefficients for the linear correlation between each morphological parameter and the von Mises stress along the bone length. Correlations were calculated for whole bone data, as well as separately for each third of the bone length (proximal, middle, and distal 33%). Listed on the left of each plot are the median correlation p-values.

Discussion

The focus of this study was to characterize the mechanical behaviour of the tibiotarsus under controlled in vivo loading and assess its relation to bone material and structural properties, while taking into consideration the effects of genotype and rearing housing (a determinant of loading history). We simulated our experimental in vivo tibiotarsal loading model to estimate engendered principal strains and von Mises stress throughout the whole bone and validated our simulation with in vivo principal strain measurements at the anterior midshaft. We then quantified the correlation between subject specific stress along the bone length and a variety of measures of bone structure along the bone length, to investigate whether certain structural features (and if so which) could explain the simulated spatial patterns of mechanical stress. We hypothesized that 1) bone mechanical behavior would be influenced by both mineral density heterogeneity and bone structure, 2) bone curvature would be the salient determinant of bone deformation due to in vivo tibiotarsus loading, and 3) bone mechanical behavior and its relationship to bone structure would differ between genotype and housing groups. We found that variations in tissue mineral density of up to 0.2 gHA/cm^3 had negligible effects on the stress magnitudes. Bone curvature was not an outstanding correlate to von Mises stress, but rather we found a set of structural parameters that all had significant, strong negative correlations to bone stress. We did see that stress and strain magnitudes, but not patterns, differed between brown- and white-feathered chicken bones, and between bones from chickens reared in the three housing styles.

To assess the influence of tissue mineral density heterogeneity, we modelled each bone twice with 1) heterogeneous elastic moduli and 2) homogeneous elastic moduli. The homogeneous models allowed us to isolate the effects of bone structure on the mechanical behaviour of the bone, and in comparing outcomes with the heterogeneous models we were able to assess whether the consideration of tissue mineral density heterogeneity and magnitude (from which the elastic moduli were derived), in addition to bone structure plays a determining role in the bone's mechanical behaviour.

We observed substantial tissue mineral density heterogeneity in the bones, both longitudinally and cross-sectionally. Along the bone diaphysis, the tissue mineral density was up to 0.3 gHA/cm^3 higher than at the metaphyseal regions. Throughout the bone cross-section, tissue mineral density was relatively homogeneous at the periosteal and intracortical regions, whereas

endosteally there was a sharp transition to lower-mineralized medullary bone. The elastic modulus assigned to the homogeneous models was derived as a function of the average tissue mineral density across the whole bone. Therefore, implementing a homogeneous material property approach not only removed the effect of mineral density heterogeneity, but also introduced a differential effect on the elastic modulus, dependent on the location in the bone. Thus, in some regions there was an increase in the elastic modulus of the homogenized model relative to the heterogeneous model (e.g. metaphyses, endosteal surface), and in other regions a decrease (e.g. diaphysis, intracortical region).

Our data indicated that mechanical strains and stress fluctuated along the bone length, with two peaks occurring at the proximal and distal regions. This spatial variation in strains and stress was not mediated by heterogeneity in tissue mineral density, as it was observed in both homogeneous and heterogeneous models. Furthermore, there was a negligible difference in engendered stress between the heterogeneous and homogeneous models. These results indicate that changes in tissue mineral density at or below 0.2 gHA/cm^3, which corresponds to approximately 25% of the average cortical diaphyseal vTMD of age- and genetic strain-matched chickens (Vitienes et al., 2021) were not influential on von Mises stress. These findings are relevant when it comes to assessing the physiological relevance of statistically significant increases in TMD and BMD, due to behavioural or pharmacological interventions in this population. These data highlight the importance of interventions that target structural adaptations rather than bone mineral density to stiffen bone.

We did however observe higher peak principal strain in the homogeneous compared to the heterogeneous models, with average peak strains differing by up to 397 με. This difference is likely physiologically relevant, since we have previously shown in chickens from the genotype and housing, that in vivo locomotor peak principal strains range from 525-1016 με in magnitude (Vitienes et al., 2023). Therefore, the magnitude of the discrepancy between homogeneous and heterogeneous models amounts to as much as 76% of the in vivo locomotor peak principal strains. Given that the von Mises stress is purely a function of shear stress, our results show that tissue mineral density heterogeneity did not contribute to the bones' ability to resist shear strain, but was relevant for resisting normal principal strain. Bones have generally been shown to be weakest in shear (Cowin, 2001; Keaveny et al., 2001). Together this suggests that efforts to prevent fractures

should not solely focus on improving tissue mineral density, but also consider other structural and ultrastructural determinants of bone stiffness and strength. These data also suggest that future studies involving FEA on avian tibiotarsi can directly implement a homogeneous material property model, without the need to create a much more complex FE model with heterogeneous, element-specific material properties calibrated to units of mineral density.

We observed a robust pattern in which both principal strains and von Mises stress have a bimodal distribution along the bone length, peaking at the proximal and distal metaphyses. The fact that both principal tensile and compressive strains peak simultaneously with the peak compressive strain being slightly higher than the peak tensile, indicates that there is a combination of compression and bending in these regions (Main, 2021b). The heat maps show anterior convex and concave bending in the proximal and distal ends, respectively. Bending occurs when the axis of applied load does not intersect with the centroid of the bone in the plane that is perpendicular to said load. This scenario occurs during off axis loading, or when there is a moment arm due to curvature of the bone. In the case of our FE models, load was applied along an axis rotated 10° posteriorly relative to the bone's axis, therefore producing a moment arm along all bone cross-sections. It has been theorized that, although bone is weaker in bending compared to pure compression, structural and tissue-level adaptations that enable bending of the bone are evolutionarily favourable, as they result in a predictable direction of deformation under variable load directions (Bertram & Biewener, 1988). Chickens are active and habitually perform a variety of activity types such as ground and ramp locomotion, wing-assisted locomotion, jumping, and perching (Pufall et al., 2021; Rentsch et al., 2023a), all of which likely produce variable magnitudes and directions of ground reaction forces acting on the tibiotarsi; this scenario would support the need to have structural features that result in consistent bone deformation directions under these variable conditions.

At the midshaft, both principal strains and von Mises stress decrease to a local minimum. Relative to their peaks there is a more substantial decrease in principal strains compared to von Mises stress, indicating a predominance of shear stress at the midshaft. This is corroborated by the fact that at the midshaft we saw a nearly 180° rotation of the neutral axis of bending across 12% of the bone length. These lower stress levels at the midshaft suggest that there is a higher safety factor in this region; a safety factor is the ratio of habitual stress to ultimate stress, quantifying how

overbuilt the bone is and serving as an indicator of how prepared the bone is to encounter unexpected loading conditions (Willie, Zimmermann, et al., 2020).

When we assessed the von Mises stress distribution between cortical and trabecular bone compartments, our results suggest that von Mises stress is shared relatively equally between cortical and trabecular bone at the midshaft when overall stresses are relatively low (proportional to the relative amounts of cortical and trabecular bone in this region), compared to the metaphyses where further increases in stress are disproportionately shared by cortical bone.

Overall our results agree with the single other study that has performed finite element modelling of in vivo controlled loading of an avian tibiotarsus, specifically the chukar partridge (Verner, 2017), which modelled the same in vivo loading conditions as we did. They showed that peak strains occur at the proximal and distal metaphyses, whereas at the midshaft strains were lower. Our von Mises stress data suggests that there is substantial shear occurring in addition to bending and compression. In the chukar partridge they similarly show that the tibiotarsus undergoes a combination of bending, compression, and torsion-induced shear. In the chukar partridge, however, the highest strains occur at the proximal metaphysis as opposed to the distal metaphysis, and minimum strains occur relatively more proximal that what we saw in the chicken tibiotarsus. The differences in modelled mechanical behavior between the two avian species may be due to the substantial difference in bone length and overall size of the birds (chukar: 0.4 kg, chicken: 1.3 kg).

These findings exemplify the complex relationship between bone structure and the mechanical strain and stress landscape that is produced upon loading, highlighting the importance of performing experimental studies to measure and model strains across a variety of species, genetic strains, ages, and disease states. They also show that different sites of the bone undergo different modes of loading (e.g. mainly axial compression and shear at the midshaft compared to substantial bending at the metaphyses) and therefore serve to inform mechanical testing protocols that aim to replicate physiological failure conditions.

In terms of differences in mechanical properties between genetic strains and between chickens with different loading histories (housing systems), we saw that the general patterns of strain and stress distribution across the bone length are present in all bones analyzed. Comparing genetic strains, most notably we saw that mechanical strains were higher in the white- compared

to brown-feathered chicken bones. In other words, brown-feathered chicken bones were better able at resisting deformation when subjected to our simulated in vivo controlled loading conditions. The brown-feathered Lohmann Brown genetic strain has a higher average body weight compared to the Lohmann Selected Leghorn Lite (Vitienes et al., 2023) and larger muscles (Pufall et al., 2021), therefore their bones are adapted to supporting these higher load levels habitually, which may explain this finding. We previously quantified bone microstructural properties at the tibiotarsus midshaft of chickens in these groups (Vitienes et al., 2021) and found that although white-feathered chicken bones had higher cortical thickness and cortical area fraction, they had lower polar moment of inertia and robusticity. Together these data suggest that the polar moment of inertia and robusticity adaptations are more successful in resisting bone deformation, at least at the midshaft when subjected to our controlled loading conditions. This is likely because a substantial source of the deformation we engender at the midshaft is shear , and increases to the polar moment of inertia and robusticity are particularly effective at resisting torsion-induced shear strain (Main, 2021b).

In looking at differences in mechanical strains and stress between bones from our three rearing housing groups, we hypothesized that chickens with more experience of physical activity will have acquired bone-stiffening adaptations such that, for a given applied force, their bones would deform less compared to chickens with a more sedentary history. We know that there is a genetic strain dependent effect of rearing housing on the amount of dynamic load bearing activity that these groups of chickens perform (Pufall et al., 2021; Rentsch et al., 2023a). Both genetic strains of chickens raised in conventional cages were less active than those raised in aviaries, but brown-feathered chickens performed similar levels of dynamic load bearing activity in Low and High housing environments (Rentsch et al., 2023a). In contrast, white-feathered chickens from High were more active than those in Low (B: Conv < Low = High; W: Conv < Low < High) (Rentsch et al., 2023a). We therefore expected to see similar genetic strain-specific patterns in the simulated strains and stress. We did see different patterns in the different genetic strains, but they did not mimic the patterns in activity levels. The discrepancy that we are observing – that chickens which presumably were more active did not necessarily have stiffer bones – could be due to an incomplete understanding of the force stimuli that these bones are receiving when the chickens are housed in the different rearing environments. Studies investigating bone's mechanoresponsiveness

in other species have shown that only a few cycles of dynamic load are sufficient to elicit a bone anabolic response, provided the strain engendered by these load cycles is sufficiently high (Main et al., 2020). Thus, it is possible that, for example, in the brown-feathered chickens there were indeed physiologically relevant differences in the amount of dynamic load bearing activity performed between Low and High groups, but we were unable to perceive them, statistically, in our previous study. Even if both brown-feathered and white-feathered chicken bones equally profited from opportunities for increased physical activity when housed in aviaries, there may be genetic-strain differences in osteocyte mechanosensitivity, mechanotransduction, and/or (re)modelling dynamics of mechanoresponse effector cells that could lead to different mechanoresponse outcomes to a given stimulus (Robling & Turner, 2002), all of which warrant further investigation.

We next sought to investigate how different bone structural features relate to its mechanical behaviour by measuring the correlation between structural parameters measured along the bone length and our modelled von Mises stress along the bone length. We looked at a variety of cross-sectional structural parameters known to influence bone deformation and chose to measure correlations from the whole bone as well as within one of three regions along the bone. The relationship between bone structure and stress along the whole bone was similar at the proximal and distal 1/3 of the bone, suggesting that the similar mechanical behaviour we observe in the proximal and distal metaphyses is mediated by similar bone structural features. At the midshaft, none of the parameters we measured significantly correlated to stress, possibly because there is little variation in stress in this region to begin with. This may suggest that the bone has a higher safety factor in this region, which is in line with the hypothesis that bone structural design prioritizes resisting shear deformation.

Our hypothesis that bone curvature would be a salient correlate to bone stress was not supported by our data. We found multiple measures that had significant correlations to bone stress, and curvature was not among them, although whole bone stress had a negative correlation with curvature that trended to significance. Bone area, total area, bone area ratio, and polar moment of inertia are all known bone stiffening adaptations, and this is confirmed by our findings that show they significantly negatively correlate to bone stress. Bone thickness is also a common parameter considered to be a determinant of stiffness, yet here we saw it to be positively correlated to bone

stress, along the whole bone and also in proximal and distal sections. This exemplifies how a bone's mechanical behaviour is a product of a complex interaction of structural features, each of which may not independently have the same effect on bone stress as they would in combination with other features.

Our study has limitations. It was not feasible to perform finite element analyses on a sample size higher than n=1, due to the extensive time required to create and run each model. We did however see similar strain and stress patterns in each bone, which lends confidence to the interpretations of our findings. In terms of experimental design, our ability to interpret our strain and stress findings in relation to the differences in activity levels between housing groups is limited by our ability to quantify their physical activity levels in ways which are relevant to the bone's mechanoresponse. The common practice in poultry research is to identify focal birds and observe them for a given amount of time (e.g. 5 min) and record the occurrence of different activity types (Pufall et al., 2021; Rentsch et al., 2023a). Future research is needed to investigate the effects of other microstructural features such as porosity and osteon density, and other material properties such as collagen fiber orientation, osteocyte lacuno-canalicular network topology and volume, among others which also influence the bone's mechanical properties.

In summary, our key findings were 1) variations in tissue mineral density of up to 0.2 gHA/cm^3 had negligible effects on the stress magnitudes 2) bone curvature was not an outstanding correlate to stress, and 3) stress and strain magnitudes, but not patterns, differed between brown- and white-feathered chicken bones, and between bones from chickens reared in the three housing styles. These data inform mechanical testing protocols that aim to replicate in vivo loading, as well as poultry housing and enrichment design to encourage certain levels and ranges of physical activities.

References

Bertram, J. E. A., & Biewener, A. A. (1988). Bone curvature: Sacrificing strength for load predictability? *Journal of Theoretical Biology*, *131*(1), 75–92. https://doi.org/10.1016/S0022-5193(88)80122-X

Bertram, J. E. A., & Biewener, A. A. (1992). Allometry and curvature in the long bones of quadrupedal mammals. *Journal of Zoology*, *226*(3), 455–467. https://doi.org/10.1111/j.1469-7998.1992.tb07492.x

Burr, D. B. (2019). *Basic and Applied Bone Biology* (2nd ed.).

Casey-Trott, T. M., Korver, D. R., Guerin, M. T., Sandilands, V., Torrey, S., & Widowski, T. M. (2017a). Opportunities for exercise during pullet rearing, Part I: Effect on the musculoskeletal characteristics of pullets. *Poultry Science*, *96*(8), 2509–2517. https://doi.org/10.3382/ps/pex059

Casey-Trott, T. M., Korver, D. R., Guerin, M. T., Sandilands, V., Torrey, S., & Widowski, T. M. (2017b). Opportunities for exercise during pullet rearing, Part II: Long-term effects on bone characteristics of adult laying hens at the end-of-lay. *Poultry Science*, *96*(8), 2518–2527. https://doi.org/10.3382/ps/pex060

Chen, C., & Kim, W. K. (2020). The application of micro-CT in egg-laying hen bone analysis: Introducing an automated bone separation algorithm. *Poultry Science*, *99*(11), 5175–5183. https://doi.org/10.1016/j.psj.2020.08.047

Cowin, S. C., 1934-. (2001). *Bone mechanics handbook* (2nd ed, 1–1 online resource (1 volume (various pagings)) : illustrations). CRC Press.

Currey, J. D. (1988). The effect of porosity and mineral content on the Young's modulus of elasticity of compact bone. *Journal of Biomechanics*, *21*(2), 131–139. https://doi.org/10.1016/0021-9290(88)90006-1

Currey, J. D. (2004). Tensile yield in compact bone is determined by strain, post-yield behaviour by mineral content. *Journal of Biomechanics*, *37*(4), 549–556. https://doi.org/10.1016/j.jbiomech.2003.08.008

Enneking, S. A., Cheng, H. W., Jefferson-Moore, K. Y., Einstein, M. E., Rubin, D. A., & Hester, P. Y. (2012). Early access to perches in caged White Leghorn pullets. *Poultry Science*, *91*(9), 2114–2120. https://doi.org/10.3382/ps.2012-02328

Fleming, R. H., McCormack, H. A., McTeir, L., & Whitehead, C. C. (2006). Relationships between genetic, environmental and nutritional factors influencing osteoporosis in laying hens. *British Poultry Science*, *47*(6), 742–755. https://doi.org/10.1080/00071660601077949

Heerkens, J. L. T., Delezie, E., Rodenburg, T. B., Kempen, I., Zoons, J., Ampe, B., & Tuyttens, F. a. M. (2016). Risk factors associated with keel bone and foot pad disorders in laying hens housed in aviary systems. *Poultry Science*, *95*(3), 482–488. https://doi.org/10.3382/ps/pev339

Hester, P. Y., Enneking, S. A., Haley, B. K., Cheng, H. W., Einstein, M. E., & Rubin, D. A. (2013). The effect of perch availability during pullet rearing and egg laying on musculoskeletal health of caged White Leghorn hens. *Poultry Science*, *92*(8), 1972–1980. https://doi.org/10.3382/ps.2013-03008

Keaveny, T. M., Morgan, E. F., Niebur, G. L., & Yeh, O. C. (2001). Biomechanics of trabecular bone. *Annual Review of Biomedical Engineering*, *3*, 307–333. https://doi.org/10.1146/annurev.bioeng.3.1.307

Kim, W. K., Bloomfield, S. A., Sugiyama, T., & Ricke, S. C. (2012). Concepts and methods for understanding bone metabolism in laying hens. *World's Poultry Science Journal*, *68*(1), 71–82. https://doi.org/10.1017/S0043933912000086

Main, R. P. (2021). Basic Principles and Methodoologies in Measuring Bone Biomechanics. In A. J. de R. Vivian de Buffrénil Louise Zylberberg, Kevin Padian (Ed.), *Vertebrate Skeletal Histology and Paleohistology*.

Main, R. P., Shefelbine, S. J., Meakin, L. B., Silva, M. J., Meulen, M. C. H., & Willie, B. M. (2020). Murine Axial Compression Tibial Loading Model to Study Bone Mechanobiology: Implementing the Model and Reporting Results. *Journal of Orthopaedic Research*, *38*(2), 233–252. https://doi.org/10.1002/jor.24466

Pufall, A., Harlander-Matauschek, A., Hunniford, M., & Widowski, T. M. (2021). Effects of Rearing Aviary Style and Genetic Strain on the Locomotion and Musculoskeletal Characteristics of Layer Pullets. *Animals*, *11*(3), 634. https://doi.org/10.3390/ani11030634

Razi, H., Birkhold, A. I., Zaslansky, P., Weinkamer, R., Duda, G. N., Willie, B. M., & Checa, S. (2015). Skeletal maturity leads to a reduction in the strain magnitudes induced within the bone: A murine tibia study. *Acta Biomaterialia*, *13*, 301–310. https://doi.org/10.1016/j.actbio.2014.11.021

Regmi, P., Cox, A. G., Robison, C. I., & Karcher, D. M. (2017). Correlation analysis of cortical geometry of tibia and humerus of white leghorns using clinical quantitative computed tomography and microcomputed tomography scans1. *Poultry Science*, *96*(8), 2950–2955. https://doi.org/10.3382/ps/pex064

Rentsch, A. K., Harlander, A., Siegford, J. M., Vitienes, I., Willie, B. M., & Widowski, T. M. (2023). Rearing laying hens: The effect of aviary design and genetic strain on pullet exercise and perching behavior. *Frontiers in Animal Science*, *4*. https://doi.org/10.3389/fanim.2023.1176702

Robling, A. G., & Turner, C. H. (2002). Mechanotransduction in bone: Genetic effects on mechanosensitivity in mice. *Bone*, *31*(5), 562–569. https://doi.org/10.1016/s8756-3282(02)00871-2

van der Meulen, M. C. H., Jepsen, K. J., & Mikić, B. (2001). Understanding bone strength: Size isn't everything. *Bone*, *29*(2), 101–104. https://doi.org/10.1016/S8756-3282(01)00491-4

Verner, K. A. (2017). *Skeletal Biomechanics and Response to Mechanical Load: A Comparative Approach in the Mouse and Chukar Partridge*. Purdue University.

Vitienes, I., Mikolajewicz, N., Hosseinitabatabaei, S., Bouchard, A., Julien, C., Graceffa, G., Rentsch, A., Widowski, T., Main, R. P., & Willie, B. M. (2023). Breed and loading history influence in vivo skeletal strain patterns in pre-pubertal female chickens. *Bone*, *173*, 116785. https://doi.org/10.1016/j.bone.2023.116785

Vitienes, I., Ross, E., Bouchard, A., Steyn, B., Widowski, T., & Willie, B. (2021, October). *Aviary rearing enhances bone microstructure in Lohmann LSL-Lite and bone mass in Lohmann Brown Lite egg-laying hen pullets compared to conventional cage-rearing*. American Society for Bone and Mineral Research, San Diego, California, U.S.A.

Wang, S., Hu, Y., Wu, Y., Liu, Y., Liu, G., Yan, Z., Li, Q., Zhou, Z., & Li, Z. (2019). Influences of bioapatite mineral and fibril structure on the mechanical properties of chicken bone

during the laying period. *Poultry Science*, *98*(12), 6393–6399. https://doi.org/10.3382/ps/pez474

Whitehead, C. C., & Fleming, R. H. (2000). Osteoporosis in cage layers. *Poultry Science*, *79*(7), 1033–1041. https://doi.org/10.1093/ps/79.7.1033

Willie, B. M., Zimmermann, E. A., Vitienes, I., Main, R. P., & Komarova, S. V. (2020). Bone adaptation: Safety factors and load predictability in shaping skeletal form. *Bone*, *131*, 115114. https://doi.org/10.1016/j.bone.2019.115114

Chapter 5 – Tibiotarsal mechanoresponse to in vivo controlled loading

In this chapter, I describe a study that aimed to examine the tibiotarsus' mechanoresponse. We performed an in vivo controlled loading experiment where chickens were subjected to a controlled load stimulus intended to elicit a bone mechanoresponse, which we then characterized in terms of its effect on bone structure and the resulting cellular level response. Based on the mechanostat theory, the common approach to eliciting a bone formation response to physiological loading is to load the bone to a level that engenders mechanical strain magnitudes which are above those habitually experienced by the bones. Thus, prior knowledge of these habitual strain magnitudes is needed, which is what was measured in Chapter 3. Based on these results, we selected a load level for out controlled loading experiment that engenders strains 4-9 times those which we measured to occur during a range of normal activities. In Chapter 4, I performed finite element modelling to simulate the strain and stress distributions throughout the bone using loading conditions that mimic our experimental in vivo controlled loading setup. The results from these finite element models thus provide us with an in depth understanding about the stimulus eliciting the bone mechanoresponse that we measure in the current study.

Manuscript status: In preparation for submission

Mechanical loading impaired tibiotarsal bone density and structure in prepubescent female chickens

Isabela Vitienes[a,b,c], Mayumi Umebayashi, Catherine Julien[a,c], Nabhaan Farooqi[a], Ana Rentsch[d], Tina Widowski[d], Russell Main[e], Bettina M. Willie[a,b,c,†]

[a]Research Centre, Shriners Hospital for Children-Canada, Montreal, Canada
[b]Department of Biomedical Engineering, McGill University, Montreal, Canada
[c]Faculty of Dental Medicine and Oral Health Science, McGill University, Montreal, Canada
[d]Department of Animal Bioscience, University of Guelph, Guelph, Canada
[e]Weldon School of Biomedical Engineering, Purdue University, Indiana, U.S.A

Abstract

Bone mechanoadaptation in avian species remains widely unexplored. It is a particular topic of interest in commercial egg-laying hens as it relates to interventions aiming to address widespread osteoporosis and high fracture incidence in this group by motivating increased bone anabolic physical activity. We have shown that housing chickens in non-cage systems leads to improvements to bone structure, both in white- and brown-feathered genetic strains. However, a recent study showed that the white-feathered strain is much more physically active than the brown-genetic strain when housed in non-caged systems, suggesting that there are genetic strain differences in mechanoresponsiveness. To investigate this, we sampled white- and brown-feathered chickens that were raised in either cages or two styles of aviary (non-cage) systems of low and high spatial complexity. We subjected the chickens' right tibiotarsi to two weeks of controlled in vivo loading, the left limb serving as an internal control, using a loading protocol that has been shown to be anabolic in murine models. We administered calcein to label surfaces of bone formation, and measured the mechanoresponse by comparing microCT-derived measures of bone density and structure, and calcein-labelled surfaces, between loaded and non-loaded limbs. We also measured circulating serum markers for bone formation (P1NP) and resorption (TRAP5b). We hypothesized that loading would induce a genetic-strain dependent effect, with white-feathered chickens exhibiting a less pronounced mechanoresponse. We found that indeed the response to loading was genetic strain dependent, where only white-feathered and not brown-feathered chickens exhibited a response. Surprisingly, loading impaired bone density and structure, and was associated to lower calcein labelling and lower circulating TRAP5b. These findings highlight how bone adaptation differs in chickens compared to murine models. Parametric studies aiming to elucidate the anabolic components of load stimuli are required.

Introduction

Osteoporosis and fragility-related bone fractures in commercial egg-laying hens are prevalent and have a negative impact on animal welfare (Whitehead & Fleming, 2000). These welfare concerns compounded with increasing consumer awareness and a shift towards a demand for more ethical practices in animal agriculture has motivated egg-farmers to seek out interventions to improve the bone health of their flocks. One intervention of interest makes use of bone's hallmark quality of being mechanoresponsive (Frost, 1987), providing chickens with increased opportunities for physical activity to stimulate bone formation and thereby strengthen their bones. The effect of mechanical stimuli on bone has been widely studied in mammalian (mainly murine) models. We know from controlled in vivo loading experiments that, when bones are dynamically loaded to an extent which produces mechanical strain magnitudes 2-3 times above those which occur habitually during everyday activity, a bone anabolic response ensues (Frost, 1987; Main et al., 2020). In addition to strain magnitude, other parameters describing the load induced strain stimulus also influence the osteogenic response, such as the frequency of cycles (which is related to the loading rate), and the number of cycles applied per day (Main et al., 2020).

Improvements to bone health-related outcomes have been reported in egg-laying hens housed in non-cage systems (T. M. Casey-Trott, Korver, et al., 2017c; Enneking et al., 2012; Fleming et al., 2006; Heerkens et al., 2016; Hester et al., 2013; Whitehead, 2004b), although they are also associated with increased fracture prevalence in the keel bone specifically (Harlander-Matauschek et al., 2015; Rufener & Makagon, 2020; M. Toscano et al., 2018; M. J. Toscano et al., 2020; Wilkins et al., 2011), likely attributed to, in part, increased collisions and injury. In light of this, researchers and farmers have observed that if chickens are housed in complex systems, they must be introduced to them from a young age such that they can develop the cognitive skills to safely navigate these environments and be able to find food and water. Providing these increased opportunities for physical activities early in life has also produce more pronounced benefits to bone health related outcomes which have long-lasting effects through adulthood, regardless of how much physical activity the chickens perform during adulthood (T. M. Casey-Trott, Korver, et al., 2017c). These findings mirror what has been shown in murine models and humans – that bones are most mechanoresponsive during youth (Birkhold et al., 2014) and that anabolic adaptations to loading during youth are long lasting (Warden et al., 2014).

The limitations of this intervention – providing increased *opportunities* for physical activity – is that compliance is uncontrollable. In both commercial (Pufall et al., 2021) and laboratory settings that replicate commercial barns (Rentsch et al., 2023a), the amount and types of physical activity that young chickens perform is dependent on both the style of housing system and the genetic strain of the chicken. Both studies looked at chickens that were raised in aviaries, which are open-concept types of non-cage housing systems equipped with platforms, perches, ramps, and floor space allowing birds to locomote. The relative amount and distribution of these different infrastructure components varies between manufacturers, and can generally be categorized as either low, moderate, or high complexity (Rentsch et al., 2023a).

Over the course of three visits spanning 3 months, the first study surveyed a total of 11 commercial farms with either a low, moderate, or high complexity aviary, housing either white-feathered or brown-feathered young chickens, and quantified the occurrence and duration of a set of activity types. Aviary style had an effect on the occurrence and duration of nearly all activity types measured, and this effect was often genetic-strain dependent, where white-feathered chickens were more active in more complex systems while brown-feathered chickens had similar activity levels in all three complexity level systems. The second study, which aimed to replicate the experimental model of the first study in a more controlled environment, arrived at similar findings: they found that white-feathered chickens were more active than brown-feathered chickens, and that aviary complexity level influenced behaviour levels almost exclusively in white- and not brown-feathered chickens (Rentsch et al., 2023a).

To assess the effect of these differing levels of physical activity on bone, we sampled tibiotarsi from these chickens, performed micro-computed tomographic imaging (microCT) of a mid-diaphyseal region of interest, and quantified bone density and cross-sectional microarchitectural parameters, which are associated to increased bone stiffness and strength (Vitienes et al., 2021). Based on what we know about bone adaptation (which has been almost exclusively informed by mammalian studies) we expected to observe improvements to bone in aviary-raised chickens, compared to cage-reared, with effects of aviary style and genetic strain that would mirror the effects that these factors had on activity levels – namely, chickens housed in more complex aviaries would have more substantial improvements to bone outcomes given the dose-dependent relationship between system complexity and activity levels, and that these

improvements would be almost exclusively observed in the white-feathered genetic strain. Instead, we saw that although aviary-reared chickens had better bone outcomes than cage-reared chickens, there were no significant differences across aviary-style groups, let alone any genetic strain dependent differences (Vitienes et al., 2021). Together, these findings suggest that there are differences in mechanoresponse between these genetic strains, and that the relationship between mechanical stimulus and anabolic response may not be dose-dependent in these groups. Genotypic variations in mechanoresponse have been shown in mice (Rummler et al., 2021).

Thus, although there is ample evidence that exercise results in bone anabolic effects in chickens, a deeper understanding of bone adaptation and osteogenic components of load stimuli is lacking. In vivo experimental model have been used to address these knowledge gaps (Main et al., 2020), wherein a controlled stimulus is applied to a limb of an animal while the contralateral serves as an internal control, and the mechanoresponse is quantified by comparing microCT-based microarchitectural outcomes (Bouxsein et al., 2010) and histomorphological measures of bone formation (Dempster et al., 2013) between loaded and non-loaded bones. To date, only three studies have performed in vivo controlled loading in avian species: on adult male chickens (Rubin & Lanyon, 1984b), adult turkeys (Rubin & Lanyon, 1987), and young male chukar partridges (Verner, 2017), the latter being the only one done non-invasively. The first two studies (among the first in vivo loading studies to be performed, in the 1980's) osteotomized and placed caps near the metaphyses of rooster and turkey ulnae with pins that allowed for the application of forces. The investigators aimed to assess how load-induced strain magnitude and dynamic versus compressive loading influenced the mechanoresponse, quantified by changes in bone area measured from radiographic images of bone cross-sections. They observed that only dynamic (not static) loading is osteogenic, and that the response to loading followed a dose-dependent relationship to engendered strain magnitude.

Only recently was there a new investigation into avian bone mechanoresponse, specifically of the chukar partridge (Verner, 2017). The authors employed a non-invasive axial compression dynamic loading protocol identical to one shown to consistently produce an anabolic response in mice (Willie et al., 2013), albeit with a peak applied load of 130N that engendered strains approximately 1.5-2.5 times those measured to occur during high speed locomotion birds. Interestingly, they showed that although loading led to increased endosteal mineral apposition rate

and mineralizing surface, there was a decrease in bone volume and a trending decrease in bone area, with no changes to mineral density.

In this current study, we aimed to address the gap in knowledge concerning chicken bone adaptation by conducting a non-invasive controlled in vivo loading experiment on the hindlimbs of young, pre-pubescent female chickens. In addition to characterizing the mechanoresponse in this group, we sought compare the mechanoresponse of white- and brown-feathered genetic strains raised in either conventional cages or two styles of aviaries (low and high complexity), to understand how genotype and loading history (rearing housing style) influence the bone mechanoresponse. We hypothesized that chickens raised in different aviaries would have similar responses to a controlled strain stimulus, and that there would be differences in mechanoresponse between genetic strains, with white-feathered chickens being less mechanoresponsive than brown-feathered chickens.

Materials and Methods

Pullet Housing and Management

All animal use and procedures were approved by the animal care committees at the University of Guelph (AUP #4127) and McGill University (AUP #8083). Housing and management are briefly described, whereas full details are reported elsewhere. A flock of Lohmann Selected Leghorn Lite (white-feathered) and Lohmann Brown Lite (brown-feathered) female chicks (*Gallus gallus domesticus*) were obtained from a commercial hatchery at the age of one day old. The chickens were reared from 1 day of age to 14 weeks at the University of Guelph in either conventional rearing cages (Conv: Ford Dickinson, Mitchell, Ontario, Canada), or one of two styles of commercial aviaries. Conventional cages are spatially restrictive, only allowing for standing and sitting, whereas aviaries are more spacious and contain infrastructure that allows for more frequent and varied types of activity (e.g. jumping, ramp ascent and descent, perching, running) (Pufall et al., 2021; Rentsch et al., 2023a). The aviaries chosen for this study had either low or high spatial complexity (Low: Natura Primus, Big Dutchman, Holland, MI, U.S.A; High: NivoVaria, Jansen Poultry Equipment, Netherlands, and Farmer Automatic Portal Pullet, Clark Ag Systems, Caledonia, ON, Canada) and have been shown to motivate moderate or high amounts of physical activity respectively (Pufall et al., 2021; Rentsch et al., 2023a). We have also previously

shown that aviary-complexity has a genetic-strain dependent effect on dynamic load-bearing activity, where brown-feathered chickens in Low and High had similar activity levels, whereas white-feathered chickens in High were more active than those in Low (Rentsch et al., 2023a). Both brown- and white-feathered chickens were more active when housed in aviaries (either Low or High) compared to when housed in Conv.

A total of 48 fourteen-week-old white-feathered and brown-feathered chickens were randomly sampled (n=8 chickens/genetic strain [2]/rearing housing system [3]) and transported from the University of Guelph to McGill University (Donald McQueen Shaver Poultry Complex) on three separate occasions. Upon arrival at McGill, the white-feathered and brown-feathered chickens were housed in separate identical rooms consisting only of litter floor (total area of 13.2 m^2). Chickens were allowed to acclimate for 72h prior to the onset of the loading experiment, which lasted two weeks. After these two weeks, all chickens were euthanized, and bones were dissected and stored in 70% ethanol.

Strain-load calibration

We sought to perform a strain-matched loading protocol, controlling for the amount of strain induced by in vivo loading across experimental groups. Differences in bone material and structural properties across groups may result in differences in whole bone stiffness, which in turn would require the application of group-specific load levels to engender a target fixed strain magnitude across groups. Therefore, prior to conducting the loading experiment, we measured whole bone stiffness on a separate set of chickens, to deduce group-specific equations relating load to strain (Main et al., 2010).

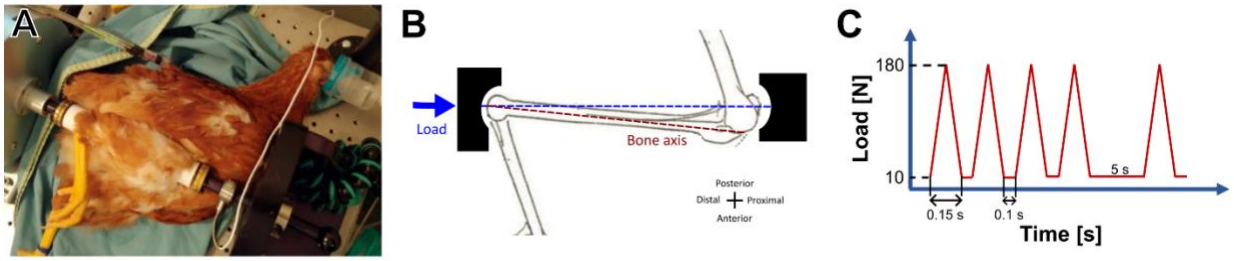

Figure 1: In vivo loading methodology. A. Image of a chicken undergoing axial compressive loading to the right hindlimb. The knee (right) is held fixed while load-controlled displacement is applied to the ankle (left). **B.** Illustration of the loading set up. Load is applied at an angle distal the bone's axis. **C.** Triangular waveform implemented in the controlled loading protocol. Oscillations between 10 (preload) and 180 (peak

load) N are applied, with a 0.1s rest period between each bout, and a 5s rest period every four bouts. Rest insertions have been shown to potentiate the response to loading (Srinivasan et al., 2002, 2003).

As part of a separate study assessing in vivo background strains engendered during habitual forms of physical activity, strain gauge sensors were surgically attached to a set of 48 chickens (n=8/genetic strain [2]/rearing housing [3]) at the tibiotarsal anterior, medial, and posterior surfaces. Data from habitual background activities have been reported elsewhere (Vitienes et al., 2023). After background strain gauging, chickens were anesthetized (1L/min O_2, 3% isoflurane). Chickens were then subjected to controlled in vivo cyclic axial compressive loading (Testbench ElectroForce LM1, Bose, Framingham, USA) of the tibiotarsus over a range of peak load magnitudes (30, 60, 90, 120, 150, 180, 200N), while the resulting mechanical strains at the sites of gauge attachment were simultaneously recorded (System 8000 Scanner; Micro-Measurements, U.S.A). The loads were applied to the right limb ankle, while the knee was held fixed (Fig. 1 A-B). The limb was secured at a preload of 10N. The loading waveform consisted of a triangular waveform where a total of 50 load cycles were applied, without any rest insertions, at a load rate of $(peak\ load - preload/0.075)\ N/s$. For each bone, two trials of loading were performed (i.e. bouts of load were applied for each load magnitude twice). For each trial, in vivo tibiotarsal axial stiffness was calculated as the ratio of the peak load to the peak strain:

$$S_{i,j} = {(peak\ load_{i,j})}\Big/{(peak\ strain_{i,j})}$$

for the *i'th* trial of the *j'th* load level. Stiffness data points were excluded if $\left|\Delta_{strain_{i,j}}\right| \leq 1$ or if $S_{i,j}$ fell further than 8 median absolute deviations away from the median stiffness. Two separate average axial stiffnesses were calculated across the 7 peak load levels, for trial 1 and trial 2, and the average with the lowest coefficient of variation was selected as the representative data point for a given chicken, denoted S. In vivo axial stiffness did not significantly differ across experimental groups (genetic strain, housing); therefore, a fixed load level was applied to all groups.

In vivo tibiotarsal loading

Chickens were subjected to two weeks (5 days/week) of in vivo controlled loading. Each day, chickens underwent a loading session wherein they were anesthetized, and a cyclical axial compressive load was applied to the right limb ankle while the knee was held fixed (Fig. 1 B). The

left limb served as a non-loaded internal control. Each session consisted of 216 cycles of load applied at a frequency of 4Hz (to mimic habitual step frequency (Vitienes et al., 2023)) (Fig. 1 C). We applied a target load level of 180N, which produces strain magnitudes of 270-2833 με, amounting to 4-9 times the amount of strain engendered during locomotion in these genetic strains of chickens (Table 1) (Vitienes et al., 2023). A preload of 10 N was maintained to secure the limb within the loading device. Load was applied with a triangular waveform, with a loading/unloading rate of 2266 N/s, a rest of 0.1s between each loading bout, and a 5s rest insertion after every 4 bouts (Fig. 1 C). Pullets recovered from anesthesia within 2-3 minutes and were observed for 10 minutes before returning them to their housing room. Pullets were monitored and no physical adverse effects of loading were observed (i.e. limping or bruising at ankle or knee). Loading sessions, including induction and recovery from anesthesia, lasted approximately 10 minutes. The loading of the 48 chickens included in the study took approximately 6 hours. Given that the response to loading has been shown to be influenced by circadian rhythm (Bouchard et al., 2022) we sampled birds randomly each day to account for this confounding variable.

Table 1: Average axial stiffness, walking strain, and deduced strain engendered by 180N of axial compressive loading, at the anterior, medial, and posterior surfaces of the tibiotarsus midshaft. Walking strains and axial stiffness were measured on a separate set of chickens (Vitienes et al., 2023).

	Anterior	Medial	Posterior
Axial stiffness [N/με]	0.632	-0.059	-0.107
Walking strain [με]	66	-322	-452
Strain at 180N [με]	270	-2833	-1454

After 3 and 10 days of loading, chickens were injected with calcein (5 mg/ml solution, dosage of 30 mg/kg, intraperitoneal administration) and alizarin (30mg/ml solution, dosage of 30 mg/kg, intraperitoneal administration), respectively, to label bone surfaces undergoing bone formation. At the end of the experiment (2 days after the last loading session), blood was collected from the brachial vein, chickens were euthanized, and both tibiotarsi dissected and stored in 70% ethanol. The alizarin staining was diffuse and non-specific, therefore we only report results for the calcein label.

Micro-computed tomography and static morphometry

To assess the effect of loading on bone length and curvature, whole tibiotarsi were imaged at an isotropic voxel size of 81 μm (Skyscan 1276, Bruker, Massachusetts, U.S.A; 80kV, 200uA, 45 ms integration time, 180° scan, no frame averaging). Images were then aligned such that the bone's long axis was parallel to the global z-axis, and the fibula was segmented and excluded from all analyses given a lack of bony connection to the tibiotarsus, implying it does not bear load. Whole bone images were binarized with a threshold of 0.24 gHA/cm^3. The longitudinal axis of whole bone binarized images was defined as the chord joining the centroids at the proximal (10% bone length) and distal (90% bone length) ends of the bone. Bones were then rotated such that the anterior surface of the bone faced the +x direction. Tibiotarsal curvature was measured at each slice, and then averaged across 1% bone length intervals (number of slices within each interval varied according to subject-specific bone length) (XamFlow, Lucid Concepts AG, Zürich, Switzerland). Radius of curvature (C_R) was computed as the distance between the slice centroid and the slice intercept of the bone's longitudinal axis. Subject specific measures of C_R were normalized by their respective midshaft anterior radii (distance between the midshaft slice centroid and the anterior periosteal surface), based on reported recommendations (Bertram & Biewener, 1992). Bone length was measured based on the number of slices containing bone.

To assess the effect of loading on bone structure and density, a region of interest comprised of 5% of the bone's length centered at the midshaft was also imaged at an isotropic voxel size of 9 μm (Skyscan 1276, Bruker, Massachusetts, U.S.A; 80 kV, 200 μA, 644 ms integration time, 360° scan, no frame averaging), which we then down-sampled by a factor of two (to 18 μm). Images were reconstructed with a dynamic range of 0-0.055 cm^{-1} and corrections for misalignment were applied when needed. Subsequent image calibration, alignment, segmentation, and microstructural analysis was performed using custom workflows (XamFlow, Lucid Concepts AG, Zürich, Switzerland). Images were calibrated to units of gHA/cm^3 with calibration equations derived by imaging calibration phantoms (0.25 and 0.75 gHA/cm^3), measuring the average grey value of each phantom ($GV_{0.25}$, $GV_{0.75}$), and solving the system of equations assuming a linear relationship between bone density and x-ray attenuation to derive calibration equation constants *a* and *b*:

$$\begin{cases} 0.25\dfrac{gHA}{cm^3} = a * GV_{0.25} + b \\ 0.75\dfrac{gHA}{cm^3} = a * GV_{0.75} + b \end{cases}$$

Midshaft images were segmented into cortical (containing cortical bone) and medullary (containing trabecular and medullary bone) compartments, and binarized to produce masks of cortical, trabecular, and medullary bone using density-based and morphometric thresholding. From the cortical compartment, cortical bone was defined as voxels with a density above 340 gHA/cm^2. From the medullary compartment, trabecular bone was defined as 1) voxels with a density between 480 gHA/cm^2 and 2) forming clusters above 100 μm^2 (below reported trabecular thickness of chickens of similar age (Chen & Kim, 2020)). Excluded clusters (density above 480 gHA/cm^2 but area below 100 μm^2) were considered as medullary bone, along with voxels of density between 225 and 480 gHA/cm^2. This dual criteria approach was based on findings showing the existence of regions of highly mineralized medullary bone, which the authors termed *calcium halos* (Kerschnitzki et al., 2014). Mineral density thresholds for cortical, trabecular, and medullary bone were determined by calculating the Otsu threshold (Otsu, 1979) for each compartment – in the case of the medullary compartment, using a multi-Otsu approach to distinguish between 3 (background, medullary bone, trabecular bone), instead of 2 (background, cortical bone) compartments – and then averaging the thresholds across all bones. We then tested out these average global thresholds (cortical, trabecular, and medullary) and percent variations of them (e.g. 85%, 95%, 105%) on a subset of images and selected the values which, upon visual inspection, produced the best binarization across this subset. Cortical, trabecular, and medullary bone volumes of interest were further sectioned into anatomical quadrants (anterior, medial, posterior, lateral), to assess whether the effect of loading is region-specific. All outcome measures listed below, except for polar moment of inertia and eccentricity, were measured for each quadrant.

Cortical bone outcomes were assessed at the midshaft; they consisted of cortical bone volumetric tissue mineral density (Ct.vTMD), cortical thickness (mean, Ct.Th; standard deviation, Ct.Th.sd), cortical area (Ct.Ar = cortical volume/length of region of interest), total area (area enclosed by periosteal perimeter, T.Ar = total volume/length of region of interest), cortical area fraction (Ct.Ar/T.Ar), polar moment of inertia (pMOI = I_{max} + I_{min}), cortical eccentricity (I_{min}/I_{max}), and cortical porosity (Ct.Po = cortical pore volume/cortical volume). Note that here we define

cortical volume to be the volume of thresholded cortical bone, that includes cortical bone and excludes cortical pores (as opposed to the volume of the cortical compartment mask which includes both bone and pores).

The trabecular bone outcomes were assessed at the midshaft; we measured trabecular volumetric tissue mineral density (Tb.vTMD), trabecular thickness (mean, Tb.Th; standard deviation, Tb.Th.sd), trabecular spacing (Tb.Sp), trabecular number (Tb.N), trabecular bone volume (Tb.BV), medullary canal volume (Tb.TV), and trabecular bone volume fraction (Tb.BV/Tb.TV). For the medullary bone, we measured medullary volumetric tissue mineral density (Md.vTMD), and medullary bone volume fraction (Md.BV/Tb.TV).

Histomorphometry

Following microCT imaging, bones were embedded in polymethyl-methacrylate and sectioned transversely at the midshaft. The exposed surface (of the proximal piece) was ground, polished, and imaged with a confocal microscope at 10x magnification to visualize the calcein and alizarin fluorochrome labels (Zeiss LSM-780-NLO). Images were then analyzed using a custom workflow (XamFlow, Lucid Concepts AG, Zürich, Switzerland) to measure periosteal and endosteal surfaces. Unfortunately, the alizarin labelling was diffuse and non-specific, and therefore could not be analyzed. Thus, the following parameters were assessed for the calcein label: (Ps.BS, Ec.BS, [mm]), and lengths along these surfaces containing a calcein label (Ps.sLS, Ec.sLS, [mm]). The amount of bone surface under formation was then quantified as the ratio of the labelled surface relative to the entire surface (Ps.sLS/Ps.BS, Ec.sLS/Ec.BS, [mm/mm]) (Dempster et al., 2013).

Statistics

The effect of genetic strain and rearing housing style on bone axial stiffness was assessed by ANOVA. For the microCT and histomorphometry analyses, the within subject effect of loading and/or region (cross-sectional quadrants for microCT outcomes, and surfaces – periosteal and endosteal – for histomorphometry), and their interactions with genetic strain, rearing housing, and each other, were assessed by repeated measures ANOVA. The effects of loading and its interaction with other fixed effects are reported in the manuscript. Differences between loaded and non-loaded limbs were assessed by paired t-tests and denoted by $\Delta = Loaded - Nonloaded$. When the difference is specific for a certain group, this will be specified as a subscript of Δ. The between

subject effect of genetic strain, housing, loading, and all two-way interactions on circulating serum markers was assessed by ANOVA, and differences between groups by t-test with Tukey's post-hoc correction. Significance was set at $p < 0.05$.

Results

Loading impaired cortical, trabecular, and medullary bone density and microarchitecture

Loading impaired cortical volumetric tissue mineral density (Fig. 2 A, $\Delta = -8$ mgHA/cm^3) independent of region, genetic strain, or housing. There was a region-specific effect of loading on cortical thickness (Fig. 2 B, $\Delta_{ant} = -0.022$ mm, $\Delta_{post} = -0.019$ mm, $\Delta_{lat} = -0.032$ mm), cortical area (Fig. 2 C, $\Delta_{post} = -0.082$ mm^2, $\Delta_{lat} = -0.098$ mm^2), total area (Fig. 2 D), cortical area fraction (Fig. 2 E, $\Delta_{lat} = -0.007$ mm^2/mm^2), trabecular bone volume fraction (Fig. 2 G, $\Delta_{lat} = -0.002$ mm^3/mm^3), and medullary bone volume fraction (Fig. 2 J, $\Delta_{ant} = -0.015$ mm^3/mm^3, $\Delta_{med} = -0.009$ mm^3/mm^3, $\Delta_{post} = -0.01$ mm^3/mm^3, $\Delta_{lat} = -0.011$ mm^3/mm^3), all of which were impaired by loading. Loading had a genetic-strain dependent effect on cortical thickness (Fig. 2 B, $\Delta_W = -0.029$ mm), medullary volumetric tissue mineral density (Fig. 2 I, $\Delta_W = -11$ mgHA/cm^3), and medullary volumetric bone volume fraction (Fig. 2 J, $\Delta_B = -0.005$ mgHA/cm^3, $\Delta_W = -0.017$ mgHA/cm^3). Loading impaired trabecular number in a housing-specific manner (Fig. 2 H, $\Delta_{conv} = -0.006$ mm^{-1}). Cortical porosity, trabecular separation, and trabecular thickness were unaffected by loading (Table 2).

Table 2: Average ± standard deviation of whole bone and cross-sectional structural parameters and circulating levels of P1NP (a byproduct of bone formation), which were all unaffected by loading or the interaction of loading with genetic strain, housing, or cross-sectional region. Mean and standard deviation of curvature is presented as the range measured along the bone length.

Parameter	Units	mean ± sd
Curvature	[mm/mm]	(0.004-0.079) ± (0.004-0.024)
Bone length	[mm]	118 ± 4.35
I_{min}/I_{max}	[mm^4/mm^4]	0.762 ± 0.045
pMOI	[mm^4]	122 ± 33.3
Ct.Po	[mm^3/mm^3]	0.002 ± 0.003
Tb.Sp	[mm]	0.009 ± 0.001
Tb.Th	[mm]	0.125 ± 0.046
P1NP	[pg/ml]	538 ± 192

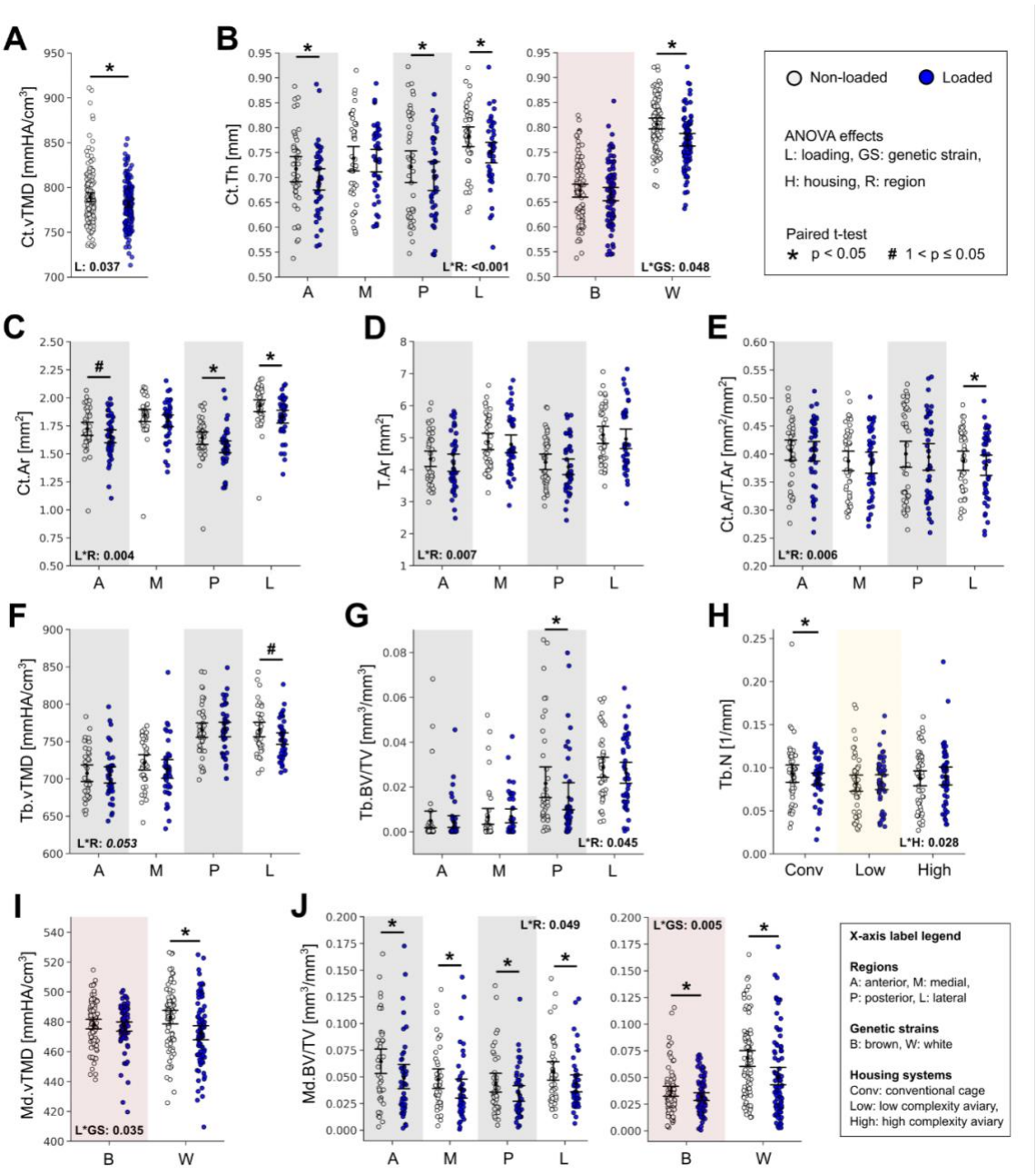

Figure 2: Effect of controlled loading on diaphyseal cortical, trabecular, and medullary bone. A) cortical volumetric tissue mineral density, B) cortical thickness, C) cortical area, D) total area, E) cortical area fraction, F) trabecular volumetric tissue mineral density, G) trabecular bone volume fraction, H) trabecular number, I) medullary volumetric tissue mineral density, J) medullary bone volume fraction. Outcomes were measured in a volume of interest centered at the tibiotarsal midshaft, comprising of 5% of the tibiotarsal length. The statistical model used included genetic strain (GS; white or brown), rearing housing (H; Conv, Low, or High), limb (L; non-loaded or loaded), anatomical region (R; A, M, P, L), and all 2-way interactions as predictors, and we present here only significant effects of limb (loading, L) and/or its interaction with the other 3 predictors. Significant pairwise comparison (paired t-test) between non-loaded and loaded limbs are indicated by *, while trending pairwise comparisons are indicated by #. Significance for all tests was set at $p < 0.05$, and trending as $1 < p \leq 0.05$.

Loading was associated to lower bone formation and resorption

The proportion of midshaft bone surface undergoing bone formation was affected by loading in a genetic strain-dependent manner (Fig. 3). Loading coincided with a significantly lower amount of proportion of labelled bone surface in white-feathered (Fig. 3 B, Δ_W = -0.062 mm/mm) but not brown-feathered chickens. Across all bones (pooling loaded and non-loaded), the average proportion of labelled surface was 0.93 mm/mm at the periosteum and 0.60 mm/mm at the endosteum.

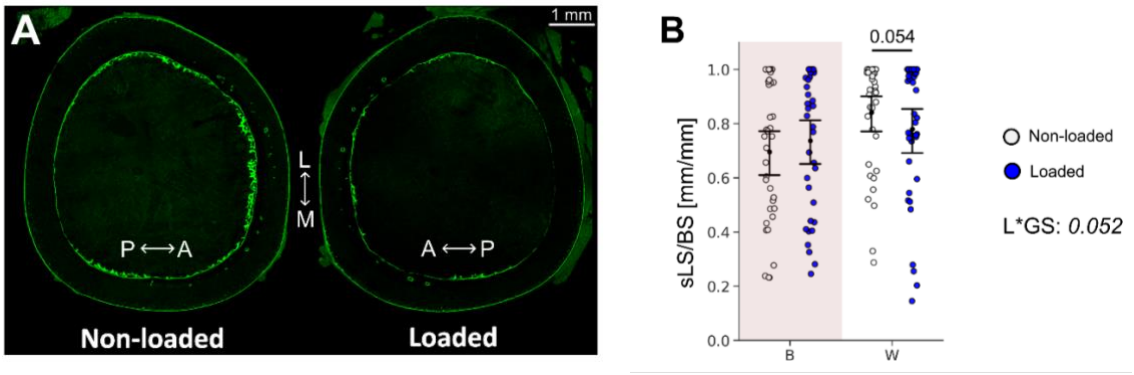

Figure 3: Histomorphometric measures of bone formation. A) Exemplary confocal images of a non-loaded and loaded midshaft surface. B) Single labelled surfaces normalized to bone surface were quantified for periosteal and endosteal surfaces of the tibiotarsus midshaft of non-loaded (white) and loaded (blue) limbs. The statistical model used included genetic strain (GS; white or brown), rearing housing (H; Conv, Low, or High), limb (L; non-loaded or loaded), surface (S; periosteal or endosteal) and all 2-way interactions as predictors, and we present here only significant ANOVA effects of limb (loading, L) and/or its interaction with the other 3 predictors. Significant (normal) and trending (italic) pairwise comparison p-values comparing non-loaded and loaded limbs are indicated. Significance for all tests was set at $p < 0.05$.

Circulating levels of the bone formation marker P1NP were unaffected by loading, whereas circulating levels of the bone resorption marker TRAP5b were affected by loading in a genetic strain-dependent manner, with significantly lower levels seen in loaded compared to non-loaded limbs of white-feathered but not brown-feathered chickens (Fig. 4, Δ_W = -0.943 mIU/ml).

Bone morphology was unaffected by loading

Bone length, curvature, midshaft polar moment of inertia, and midshaft eccentricity were all unaffected by loading. We measured an average (across all bones, loaded and nonloaded) bone length of 118 ± 4.35 mm. Bone curvature along the bone length, normalized to the midshaft anterior radius, ranged from 0.004 to 0.08 mm/mm. We quantified cross-sectional morphology by

polar moment of inertia (pMOI = $I_{min} + I_{max}$) and eccentricity (I_{min}/I_{max}), which we measured to be on average 122 ± 33.3 mm^4 and 0.762 ± 0.045 mm^4/mm^4 respectively.

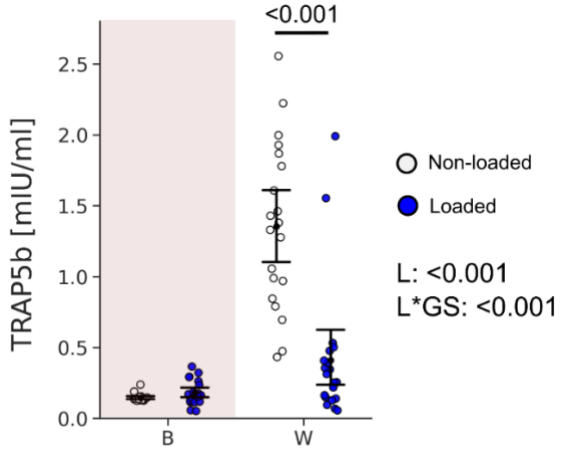

Figure 4: Serum markers for bone resorption measured in chickens that underwent loading (blue) and a separate non-loaded control group (white). The statistical model used included genetic strain (GS; white or brown), rearing housing (H; Conv, Low, or High), loading group (L; non-loaded or loaded), and all 2-way interactions as predictors, and we present here only significant ANOVA effects of loading group (L) and/or its interaction with the other 2 predictors. Significant Tukey's post hoc t-test between non-loaded and loaded chickens are indicated by *. Significance for all tests was set at $p < 0.05$.

Discussion

In the current study, we aimed to characterize the bone mechanoresponse in young, pre-pubescent female chickens and assess whether genotype and/or loading history influenced their mechanoresponse. Our study was both load and strain matched since the load level used (180N was the same for all chickens and our in vivo strain gauging data revealed a similar strain-load relationship (e.g. in vivo stiffness) across the two genetic strains of chickens. We employed once per day non-invasive controlled dynamic axial compressive load over 2 weeks to the right tibiotarsus, while the left limb remained a non-loaded internal control. We hypothesized that we would successfully induce a bone anabolic response. Furthermore, we hypothesized that the mechanoresponse to a strain-matched stimulus would not differ across groups of chickens with different loading histories, but would be less pronounced in the white-feathered genetic strain compared to the brown-feathered genetic strain. Such a result might explain why brown- and white-feathered genetic strains have similar bone structural adaptations to aviary-housing even though white-feathered chickens are significantly more active in these aviaries.

We employed a loading waveform previously shown to produce a bone anabolic response in mammalian species (Willie et al., 2013), with the only difference being the peak load level applied which we chose such that it engendered above habitual (4-9 times (Vitienes et al., 2023)) mechanical strains at the tibiotarsus midshaft; all other waveform parameters (number of cycles per session, cycle frequency, load rate, rest durations) were unchanged. Investigators arrived at this set of parameters used in murine loading studies by trying to mimic physiological loading – for example, the cycle frequency of 4 Hz approximates the locomotor step frequency of mice – and by parametric studies testing out different waveform parameter values. We have shown step frequency to be approximately 4 Hz in the current groups of chickens (Vitienes et al., 2023), and assumed that as in mice, rest insertions between loading cycles would be osteogenic, or at least neutral; therefore, we used these same parameters in our current loading waveform. Successful murine loading studies and the chukar partridge non-invasive loading study applied loads that engendered strains 2-3 times above those which occur habitually. In our current study, we increased this factor to 4-9, given the lack of response observed in chukar partridges.

Unexpectedly, we saw a negative effect of loading on bone density and structure. In line with our hypothesis, we saw that the mechanoresponse differed between genetic strains, but instead of the white-feathered genetic strain being less mechanoresponsive, we saw that they had a stronger negative response to loading, while brown-feathered chickens were generally unaffected by loading. Histomorphometry and serum measures, which shed light on the cellular level response also show a similar genetic-strain dependent effect of loading, where the effect is seen in white and not brown-feathered chickens. In the only other study that has performed controlled non-invasive loading on an avian specie (chukar partridge) also saw impairments to bone structure, namely cortical bone volume and bone area (trending). The authors conducted experiments on young (10-week-old) male chukars, applying dynamic axial compressive loading to the tibiotarsus, engendering strain patterns similar to those occurring during treadmill locomotion. They used a loading waveform identical to ours (216 cycles/day, 4 Hz cycle frequency), with the exception that they engendered lower strain levels (absolute values as well as a lower factor increase compared to background strains, 1.5-2.5 compared to 4-9 in our study) for 3 weeks.

The older invasive loading studies alternatively did elicit and measure a bone formation response. They performed osteotomies at the metaphyses of the ulnae of adult male chicken and

turkey and applied cyclical loading at 0.5 Hz cycle frequency for 6 weeks, applying 36-1800 cycles per day. In both studies, the peak strains engendered were similar in magnitude to what was measured to be engendered during vigorous wing flapping, but the cross-sectional strain pattern (strain mode) due to controlled loading was substantially different from in vivo strain patterns (~90° rotation of the neutral axis). They observed increases in bone mineral content arising after 14 days of loading, and the appearance of osteoid and periosteal and endosteal surfaces which began to mineralize at around day 28 of loading. The invasiveness of the loading model would at first instance raise concern that the observed bone formation is part of a healing response, however the control group that underwent the osteotomy but was not loaded exhibited bone resorption, as would be expected in the case of disuse.

Therefore, loading that engenders mildly (Verner, 2017) and moderately (this study) higher strains compared to background activity, in a physiological mode, resulted in impairments to bone structure, while loading that engendered strains similar in magnitude to those occurring physiologically but with differences in strain mode elicited an anabolic response. It is therefore possible that mammals and avian species differ in the relative sensitivity to different osteogenic components of strain, and that avian species are more sensitive to changes in strain mode as opposed to strain magnitude.

Bone impairment in response to in vivo controlled loading is not unprecedented in the mammalian literature – two studies from the same group report decreased trabecular bone volume fraction, trabecular thickness, and trabecular volumetric tissue mineral density in response to loading in young BALB/c mice (Brodt & Silva, 2010; Silva et al., 2012). They employed a triangular loading waveform with rest insertions after each load cycle, and loaded the animals for 60 cycles/day, for 3 weeks, engendering strain magnitudes ranging from 800 to 1300 με at the endosteal surface of the tibial midshaft. However, other studies loading BALB/c mice at similar or higher (Holguin et al., 2013; Rummler et al., 2021) target strain levels and employing similar waveforms report an anabolic response to loading, and therefore it remains unclear the cause of these drastically different responses.

The in vivo controlled loading methodology was originally developed to model fatigue loading and study the process of microdamage accumulation and repair in bone (Burr et al., 1985). In these early studies, investigators showed that microdamage could be produced in the bone not

only by engendering high strain magnitudes, but also by applying a high number of cycles of low strain-inducing loads (Burr et al., 1985). It is possible that our loading protocol induced microdamage, due to the engendered strain magnitudes either being too high, or the number of cycles per day applied being excessive. One study measured cycles-to-failure in chickens housed in either free-range or battery cage conditions and showed higher cycles-to-failure (i.e. superior fatigue resistance) in free-range chickens (Taylor et al., 2001). They measured cycles-to-failure ranging from 10,000 to 100,000. Our loading model applied 216 cycles of loading per day, for a total of 10 days, amounting to 2,160 cycles across the entirety of our experiment (15 day), applying strains at the medial tibiotarsus of -2,800 με. Overall peak strains engendered by our loading are likely higher, given that we show peak strains to occur at proximal and distal metaphyseal sights in the tibiotarsus when subjected to axial compressive loading (Vitienes et al., 2024). In humans, microdamage begins to appear at 2,500 με in tension and 4,000 με in compression (Pattin et al., 1996), and likely at lower shear strains given that bone is weakest in shear. Given that we have also showed the tibiotarsus to undergo substantial shear strain both in vivo (Vitienes et al., 2023) and during controlled loading (Vitienes et al., 2024), it is likely that our load levels induced microdamage, and this is contributing to the measured impairments to bone density and structure.

We measured impairments to cortical thickness, cortical area, but not total area, suggesting that it is at the endosteal and not periosteal surface that either bone formation is being inhibited, or increased bone resorption is occurring. At this age, the chickens are still growing, therefore the contralateral non-loaded limb should be undergoing both endosteal and periosteal expansion. Although the effect of surface (periosteal or endosteal) on the proportion of bone surface undergoing formation was not significant, we observed numerical differences in the effect of loading on the different surfaces, with the endosteal surface exhibiting numerically higher reduction to labelled surface in loaded compared to non-loaded limbs, which agrees with our microstructural findings. We also show that, systemically, there is a decrease in markers for bone resorption due to loading, suggesting that the mechanism by which loading is impairing bone structure is not by increased bone resorption but rather decreased bone formation.

We observed a robust genetic-strain dependent effect of loading, where loading affected white-feathered birds almost exclusively, which could explain why aviary rearing has similar effects on white- and brown-feathered chicken microarchitecture even though white-feathered

chickens were significantly more active than brown-feathered chickens (Pufall et al., 2021; Rentsch et al., 2023a). Further research into the molecular and cellular mechanisms responsible for this difference could shed light onto possible genetic-strain specific genetic-targets to enhance bone mechanoresponsiveness in these groups.

Our study naturally has multiple limitations. Unfortunately, the alizarin fluorochrome labelling was unsuccessful, which impaired us from being able to measure rates of mineral apposition. Furthermore, since the alizarin injection was second to the calcein, administered towards the end of the experiment as opposed to the beginning, we only have information about the immediate effect of loading on bone formation, and our measures of bone formation surfaces and microCT based bone density and structural outcomes are off by 10 days from each other. Other studies performing controlled loading have shown that background activity levels can mask the anabolic response to loading (Meakin et al., 2013) – if the animals become more active during the experiment, then the non-loaded limb will also undergo increased loading compared to at the onset of the experiment, and therefore the difference between the loaded and non-loaded limb is dampened. In the case of our study, chickens were raised at the University of Guelph in their respective housing systems and transported to McGill where they were housed together (each genetic strain in a separate room) in a free-range system for the 2-week duration of the experiment. We were not able to quantify their activity levels in this new environment to ascertain whether background activity was increased or not, and it is possible that it was. In rodents and small animals, this issue is mitigated thanks to the development of in vivo microCT imaging which allows investigators to image the loaded and non-loaded limbs at baseline. In this case, the outcome measure of interest is not a static measure taken at the end of the experiment, but rather the change in the measure from baseline to end.

Future studies are required to understand material level properties of these bones to study the process of microdamage formation and repair, how it may differ between genetic strains, and in light of the fact that, at this age, the bone (re)modelling machinery becomes concerned with the additional task of managing calcium homeostasis for egg-shell mineralization. Another avenue to further understand mechanoadaptation and mechanobiology in these groups is to perform parametric studies seeking a set of loading parameters that results in a bone anabolic response, and

then interpreting the significance of these parameter values in terms of what type of loading these bones have evolved to respond to.

In summary, our key findings were that 1) controlled in vivo axial compressive loading which engendered strains at the tibiotarsus midshaft ranging from 4-9 times what occurs during habitual background physical activity led to impairments in cortical, trabecular, and medullary bone density and cross-sectional microarchitecture, and 2) these impairments were genetic-strain dependent, occurring almost exclusively in the white-feathered and not brown-feathered genetic strain. These findings exemplify how bone adaptation differs in chickens to what we know to occur in mammals, highlighting the need for future research on chicken and avian bone mechanobiology. From a practical standpoint, our findings suggest that the efficacy of alternative housing systems that offer increased opportunities for physical activity should not be assessed by the amount of physical activity that the chickens perform in the systems, especially when seeking to compare between different genetic strains, but rather focus on direct outcomes that are determinants of bone strength, such as bone structure and mechanical behaviour/properties.

References

Bertram, J. E. A., & Biewener, A. A. (1992). Allometry and curvature in the long bones of quadrupedal mammals. *Journal of Zoology*, *226*(3), 455–467. https://doi.org/10.1111/j.1469-7998.1992.tb07492.x

Birkhold, A. I., Razi, H., Duda, G. N., Weinkamer, R., Checa, S., & Willie, B. M. (2014). The influence of age on adaptive bone formation and bone resorption. *Biomaterials*, *35*(34), 9290–9301. https://doi.org/10.1016/j.biomaterials.2014.07.051

Bouchard, A. L., Dsouza, C., Julien, C., Rummler, M., Gaumond, M.-H., Cermakian, N., & Willie, B. M. (2022). Bone adaptation to mechanical loading in mice is affected by circadian rhythms. *Bone*, *154*, 116218. https://doi.org/10.1016/j.bone.2021.116218

Bouxsein, M. L., Boyd, S. K., Christiansen, B. A., Guldberg, R. E., Jepsen, K. J., & Muller, R. (2010). Guidelines for Assessment of Bone Microstructure in Rodents Uding Micro-Computed Tomography. *Journal of Bone and Mineral Research*, *25*(7), 1468–1486. https://doi.org/10.1002/jbmr.141

Brodt, M. D., & Silva, M. J. (2010). Aged mice have enhanced endocortical response and normal periosteal response compared with young-adult mice following 1 week of axial tibial compression. *Journal of Bone and Mineral Research*, *25*(9), 2006–2015. https://doi.org/10.1002/jbmr.96

Burr, D. B., Martin, R. B., Schaffler, M. B., & Radin, E. L. (1985). Bone remodeling in response to in vivo fatigue microdamage. *Journal of Biomechanics*, *18*(3), 189–200. https://doi.org/10.1016/0021-9290(85)90204-0

Casey-Trott, T. M., Korver, D. R., Guerin, M. T., Sandilands, V., Torrey, S., & Widowski, T. M. (2017). Opportunities for exercise during pullet rearing, Part II: Long-term effects on bone characteristics of adult laying hens at the end-of-lay. *Poultry Science*, *96*(8), 2518–2527. https://doi.org/10.3382/ps/pex060

Chen, C., & Kim, W. K. (2020). The application of micro-CT in egg-laying hen bone analysis: Introducing an automated bone separation algorithm. *Poultry Science*, *99*(11), 5175–5183. https://doi.org/10.1016/j.psj.2020.08.047

Dempster, D. W., Compston, J. E., Drezner, M. K., Glorieux, F. H., Kanis, J. A., Malluche, H., Meunier, P. J., Ott, S. M., Recker, R. R., & Parfitt, A. M. (2013). Standardized

nomenclature, symbols, and units for bone histomorphometry: A 2012 update of the report of the ASBMR Histomorphometry Nomenclature Committee. *Journal of Bone and Mineral Research*, *28*(1), 2–17. https://doi.org/10.1002/jbmr.1805

Enneking, S. A., Cheng, H. W., Jefferson-Moore, K. Y., Einstein, M. E., Rubin, D. A., & Hester, P. Y. (2012). Early access to perches in caged White Leghorn pullets. *Poultry Science*, *91*(9), 2114–2120. https://doi.org/10.3382/ps.2012-02328

Fleming, R. H., McCormack, H. A., McTeir, L., & Whitehead, C. C. (2006). Relationships between genetic, environmental and nutritional factors influencing osteoporosis in laying hens. *British Poultry Science*, *47*(6), 742–755. https://doi.org/10.1080/00071660601077949

Frost, H. M. (1987). Bone "mass" and the "mechanostat": A proposal. *The Anatomical Record*, *219*(1), 1–9. https://doi.org/10.1002/ar.1092190104

Harlander-Matauschek, A., Rodenburg, T. B., Sandilands, V., Tobalske, B. W., & Toscano, M. J. (2015). Causes of keel bone damage and their solutions in laying hens. *World's Poultry Science Journal*, *71*(3), 461–472. https://doi.org/10.1017/S0043933915002135

Heerkens, J. L. T., Delezie, E., Rodenburg, T. B., Kempen, I., Zoons, J., Ampe, B., & Tuyttens, F. a. M. (2016). Risk factors associated with keel bone and foot pad disorders in laying hens housed in aviary systems. *Poultry Science*, *95*(3), 482–488. https://doi.org/10.3382/ps/pev339

Hester, P. Y., Enneking, S. A., Haley, B. K., Cheng, H. W., Einstein, M. E., & Rubin, D. A. (2013). The effect of perch availability during pullet rearing and egg laying on musculoskeletal health of caged White Leghorn hens. *Poultry Science*, *92*(8), 1972–1980. https://doi.org/10.3382/ps.2013-03008

Holguin, N., Brodt, M. D., Sanchez, M. E., Kotiya, A. A., & Silva, M. J. (2013). Adaptation of Tibial Structure and Strength to Axial Compression Depends on Loading History in Both C57BL/6 and BALB/c Mice. *Calcified Tissue International*, *93*(3), 211–221. https://doi.org/10.1007/s00223-013-9744-4

Kerschnitzki, M., Zander, T., Zaslansky, P., Fratzl, P., Shahar, R., & Wagermaier, W. (2014). Rapid alterations of avian medullary bone material during the daily egg-laying cycle. *Bone*, *69*, 109–117. https://doi.org/10.1016/j.bone.2014.08.019

Main, R. P., Lynch, M. E., & van der Meulen, M. C. H. (2010). In vivo tibial stiffness is maintained by whole bone morphology and cross-sectional geometry in growing female mice. *Journal of Biomechanics*, *43*(14), 2689–2694. https://doi.org/10.1016/j.jbiomech.2010.06.019

Main, R. P., Shefelbine, S. J., Meakin, L. B., Silva, M. J., Meulen, M. C. H., & Willie, B. M. (2020). Murine Axial Compression Tibial Loading Model to Study Bone Mechanobiology: Implementing the Model and Reporting Results. *Journal of Orthopaedic Research*, *38*(2), 233–252. https://doi.org/10.1002/jor.24466

Meakin, L. B., Sugiyama, T., Galea, G. L., Browne, W. J., Lanyon, L. E., & Price, J. S. (2013). Male mice housed in groups engage in frequent fighting and show a lower response to additional bone loading than females or individually housed males that do not fight. *Bone*, *54*(1), 113–117. https://doi.org/10.1016/j.bone.2013.01.029

Otsu, N. (1979). A Threshold Selection Method from Gray-Level Histograms. *IEEE Transactions on Systems, Man, and Cybernetics*, *9*(1), 62–66. IEEE Transactions on Systems, Man, and Cybernetics. https://doi.org/10.1109/TSMC.1979.4310076

Pattin, C. A., Caler, W. E., & Carter, D. R. (1996). Cyclic mechanical property degradation during fatigue loading of cortical bone. *Journal of Biomechanics*, *29*(1), 69–79. https://doi.org/10.1016/0021-9290(94)00156-1

Pufall, A., Harlander-Matauschek, A., Hunniford, M., & Widowski, T. M. (2021). Effects of Rearing Aviary Style and Genetic Strain on the Locomotion and Musculoskeletal Characteristics of Layer Pullets. *Animals*, *11*(3), 634. https://doi.org/10.3390/ani11030634

Rentsch, A. K., Harlander, A., Siegford, J. M., Vitienes, I., Willie, B. M., & Widowski, T. M. (2023). Rearing laying hens: The effect of aviary design and genetic strain on pullet exercise and perching behavior. *Frontiers in Animal Science*, *4*. https://doi.org/10.3389/fanim.2023.1176702

Rubin, C. T., & Lanyon, L. E. (1984). Regulation of bone formation by applied dynamic loads. *The Journal of Bone and Joint Surgery*, *66*(3), 397–402.

Rubin, C. T., & Lanyon, L. E. (1987). Kappa Delta Award paper. Osteoregulatory nature of mechanical stimuli: Function as a determinant for adaptive remodeling in bone. *Journal*

of Orthopaedic Research: Official Publication of the Orthopaedic Research Society, *5*(2), 300–310. https://doi.org/10.1002/jor.1100050217

Rufener, C., & Makagon, M. M. (2020). Keel bone fractures in laying hens: A systematic review of prevalence across age, housing systems, and strains. *Journal of Animal Science, 98*(Suppl 1), S36-s51. https://doi.org/10.1093/jas/skaa145

Rummler, M., Ziouti, F., Bouchard, A. L., Brandl, A., Duda, G. N., Bogen, B., Beilhack, A., Lynch, M. E., Jundt, F., & Willie, B. M. (2021). Mechanical loading prevents bone destruction and exerts anti-tumor effects in the MOPC315.BM.Luc model of myeloma bone disease. *Acta Biomaterialia*, *119*, 247–258. https://doi.org/10.1016/j.actbio.2020.10.041

Silva, M. J., Brodt, M. D., Lynch, M. A., Stephens, A. L., Wood, D. J., & Civitelli, R. (2012). Tibial Loading Increases Osteogenic Gene Expression and Cortical Bone Volume in Mature and Middle-Aged Mice. *PLoS ONE*, *7*(4), e34980. https://doi.org/10.1371/journal.pone.0034980

Srinivasan, S., Agans, S. C., King, K. A., Moy, N. Y., Poliachik, S. L., & Gross, T. S. (2003). Enabling bone formation in the aged skeleton via rest-inserted mechanical loading. *Bone, 33*(6), 946–955. https://doi.org/10.1016/j.bone.2003.07.009

Srinivasan, S., Weimer, D. A., Agans, S. C., Bain, S. D., & Gross, T. S. (2002). Low-magnitude mechanical loading becomes osteogenic when rest is inserted between each load cycle. *Journal of Bone and Mineral Research: The Official Journal of the American Society for Bone and Mineral Research*, *17*(9), 1613–1620. https://doi.org/10.1359/jbmr.2002.17.9.1613

Taylor, D., Falsetti, F., O'Brien, F., O'Reilly, P., Banville, E., & Clive Lee, T. (2001). A Fatigue-Based Model of Disuse Osteoporosis. *Computer Methods in Biomechanics and Biomedical Engineering*, *4*(5), 413–420. https://doi.org/10.1080/10255840108908017

Toscano, M., Booth, F., Richards, G., Brown, S., Karcher, D., & Tarlton, J. (2018). Modeling collisions in laying hens as a tool to identify causative factors for keel bone fractures and means to reduce their occurrence and severity. *PloS One, 13*(7), e0200025. https://doi.org/10.1371/journal.pone.0200025

Toscano, M. J., Dunn, I. C., Christensen, J.-P., Petow, S., Kittelsen, K., & Ulrich, R. (2020). Explanations for keel bone fractures in laying hens: Are there explanations in addition to elevated egg production? *Poultry Science*, *99*(9), 4183–4194. https://doi.org/10.1016/j.psj.2020.05.035

Verner, K. A. (2017). *Skeletal Biomechanics and Response to Mechanical Load: A Comparative Approach in the Mouse and Chukar Partridge*. Purdue University.

Vitienes, I., Mikolajewicz, N., Hosseinitabatabaei, S., Bouchard, A., Julien, C., Graceffa, G., Rentsch, A., Widowski, T., Main, R. P., & Willie, B. M. (2023). Breed and loading history influence in vivo skeletal strain patterns in pre-pubertal female chickens. *Bone*, *173*, 116785. https://doi.org/10.1016/j.bone.2023.116785

Vitienes, I., Rentsch, A., Widowski, T., Checa, S., & Willie, B. (2024, July). *Bone geometry and mineral density influence mechanical strain magnitude and patterns across the tibiotarsus*. Poultry Science Association Annual Meeting, Louisville, Kentucky, U.S.A.

Vitienes, I., Ross, E., Bouchard, A., Steyn, B., Widowski, T., & Willie, B. (2021, October). *Aviary rearing enhances bone microstructure in Lohmann LSL-Lite and bone mass in Lohmann Brown Lite egg-laying hen pullets compared to conventional cage-rearing*. American Society for Bone and Mineral Research, San Diego, California, U.S.A.

Warden, S. J., Mantila Roosa, S. M., Kersh, M. E., Hurd, A. L., Fleisig, G. S., Pandy, M. G., & Fuchs, R. K. (2014). Physical activity when young provides lifelong benefits to cortical bone size and strength in men. *Proceedings from the National Academy of Sciences of the United States of America*, *111*(14), 5337–5342. https://doi.org/10.1073/pnas.1321605111

Whitehead, C. C. (2004). Overview of bone biology in the egg-laying hen. *Poultry Science*, *83*(2), 193–199.

Whitehead, C. C., & Fleming, R. H. (2000). Osteoporosis in cage layers. *Poultry Science*, *79*(7), 1033–1041. https://doi.org/10.1093/ps/79.7.1033

Wilkins, L. J., McKinstry, J. L., Avery, N. C., Knowles, T. G., Brown, S. N., Tarlton, J., & Nicol, C. J. (2011). Influence of housing system and design on bone strength and keel bone fractures in laying hens. *The Veterinary Record*, *169*(16), 414. https://doi.org/10.1136/vr.d4831

Willie, B. M., Birkhold, A. I., Razi, H., Thiele, T., Aido, M., Kruck, B., Schill, A., Checa, S., Main, R. P., & Duda, G. N. (2013). Diminished response to in vivo mechanical loading in trabecular and not cortical bone in adulthood of female C57Bl/6 mice coincides with a reduction in deformation to load. *Bone*, *55*(2), 335–346. https://doi.org/10.1016/j.bone.2013.04.023

Chapter 6 – Validation of keel bone damage scoring

Chapters 3, 4, and 5 focus on characterizing the mechanical behaviour of the tibiotarsus bone and then using this information to inform a controlled loading experiment to study the bone's mechanoresponse. These results are valuable in that they are novel, and highlight differences between avian and mammalian bones which warrants further investigation. They also provide concrete information to egg farmers who are trying to address the widespread osteoporosis and bone fragility of their flocks, in terms of how physical activity may affect bone health, and how genetic strain plays a role in housing-derived interventions to motivate bone anabolic physical activity.

Chapter 6 also has direct applications to on-farm practices for the detection and monitoring of bone health in commercial flocks. Here we shift gears and focus on the keel bone (as opposed to the tibiotarsus), which is the most fractured bone in the commercial laying hen population. Detection and longitudinal monitoring of fractures within commercial flocks is difficult, due to the large population sizes and to the fact that chickens are experts at hiding pain and discomfort, making it nearly impossible to use behavioural cues as indicators of fracture presence. Two common methods to assess fracture status and severity in vivo are by palpation or by scoring of radiograph images. Both methods are known to lack precision but are currently the only feasible options for farmers. Palpation is particularly popular as it does not require any equipment. We sought to assess the accuracy of these two methods by comparing in vivo palpation and radiograph scores to ex vivo fracture and deviation scores and found that although palpation lacks precision, it significantly correlated to ex vivo fracture severity score. These results support the continued use of palpation to assess keel bone status in commercial hens.

Manuscript status: In preparation for submission

In vivo palpation based fracture detection correlates to ex vivo fracture severity score

Isabela Vitienes[a,b,c], Ana Rentsch[d], Hanna Gonzalez[a], Matthew Angoh[a], Tina Widowski[d], Bettina M. Willie[a,b,c,†]

[a]*Research Centre, Shriners Hospital for Children-Canada, Montreal, Canada*
[b]*Department of Biomedical Engineering, McGill University, Montreal, Canada*
[c]*Faculty of Dental Medicine and Oral Health Science, McGill University, Montreal, Canada*
[d]*Department of Animal Bioscience, University of Guelph, Guelph, Canada*

Abstract

Up to 95% of commercial egg-laying hens reach the end of their lives with at least one keel bone fracture. Many chickens also possess keel bone deviations, and a popular hypothesis is that the development of deviations prone keels to fracture. A barrier to elucidating the etiology of these fractures has been the ability to longitudinally track the status of individual chickens' keel bones, and reliably assess flock level fracture incidence and severity. To address this problem, we aimed to validate two common fracture assessment methods: in vivo palpation, and radiograph image scoring, and measure the correlation between fracture and deviation status. We sampled 101 adult female chickens and classified them as either having or lacking keel bone fractures by in vivo palpation. These chickens then underwent radiograph imaging, and images were scored for fracture severity. Chickens were then euthanized, and the true keel bone status was assessed by ex vivo fracture severity and deviation severity scoring. We then assessed the correlation of these different scores by Spearman's rho correlation. We found that ex vivo keel bone fracture and deviation severity scores were not correlated. Palpation scores correlated to both ex vivo fracture and deviation scores, while radiograph scores correlated to ex vivo deviation scores only. These results support the continued use of palpation, a cost- and time-efficient method to assess chicken fracture status. Furthermore, they suggest that deviations do not cause fractures.

Introduction

Commercial egg-laying hens produce billions of eggs each year, which substantially contributes to the global food source, but places a large burden on their bones and contributes to the observed osteoporosis and high fracture incidence (Whitehead & Fleming, 2000). In Canada, consumer interest and animal welfare advocates have pushed for a government-mandated transition away from conventional-style caged housing systems, replacing them with alternative systems that are more spacious and allow chickens to perform natural activities. In providing opportunities to be more active, these alternative housing systems have led to improvements in fore- and hind-limb bone density and strength (Abrahamsson & Tauson, 1995; Fleming et al., 2006, p. 2; Knowles & Broom, 1990; Leyendecker et al., 2005; Newman & Leeson, 1998; Shipov et al., 2010). Unfortunately, alternative housing systems are also correlated with increased keel bone fracture (KBF) incidence.

The keel bone exists in birds and evolved as an extension of the sternum, to provide a larger surface area of attachment for the large pectoral muscles required to power flight (Gill, 1995). Chickens use wing flapping to aid in locomotion (wing-assisted incline running, jumping up, landing, etc.) (Kozak et al., 2016). In the recent decade, an increasing number of studies have been published evaluating the prevalence of keel bone fracture across many countries, reporting a wide range of values (Rufener & Makagon, 2020). Some studies report as high as 97% KBF prevalence by the end of the laying period (Rodenburg et al., 2008; Wilkins et al., 2011), or as low as 11% (Riber & Hinrichsen, 2016). Furthermore, studies often are not precise about the prevalence reported, providing instead broad ranges (e.g. “52-73%” (Lay et al., 2011), “over 85%” (T. Casey-Trott et al., 2015), etc.). Therefore, the severity of this issue remains unclear. Convening on a precise and accurate approach to measure and report KBF prevalence is essential towards developing interventions to address this issue.

Two common methods used for detection of fractures are palpation and radiographic imaging. One main benefit of both of these methods is that they can be done in vivo, and therefore longitudinally, unlike the visual inspection of dissected bones which requires each chicken to be euthanized. Palpation is the most cost- and time-effective approach as it does not require any specialized equipment, although it must be conducted by trained personnel. The examiner palpates the ventral aspect of the keel, which is at the ventral surface of the abdomen. This method has been

shown to lack accuracy as it is biased against the detection of fresh fractures, which have yet to develop a fracture callus, hairline fractures, and fractures on the dorsal and caudal sides of the keel (Buijs et al., 2019; T. Casey-Trott et al., 2015; Richards et al., 2011). There also is variation across studies with respect to what is being taken into consideration when palpating – fractures, deviations, or both. Radiographic imaging overcomes some of the limitations of the palpation method, allowing the investigator to see many more features of the bone, with less regional bias. It also allows the visualization of fresh fractures that have yet to develop a callus. Radiographic images are taken of a lateral aspect of the keel bone, and then these images are scored (Rufener et al., 2018). When examiners completed freely available reliability training, excellent scoring agreement was observed between and within examiners, lending confidence to the precision of this method. The disadvantages of this method involve the purchase of costly radiography equipment and is more time-consuming (considering imaging and subsequent image scoring, both performed by trained personnel). Furthermore, the accuracy of radiograph scoring methods remains unclear.

In the current study, we aimed to characterize the fracture and deviation status of a set of keels from chickens sampled across different ages, genetic strains, and housing environments, by visually inspecting the keels, counting the number of fractures and deviations present, and assign each keel a fracture and deviation score calculated as a function of the number and types of fractures/deviations. Then, we sought to assess how well the commonly used in vivo detection methods – palpation and radiograph imaging/scoring – agreed with the dissected keel scores. We hypothesized that fracture and deviation presence would be highly correlated, and that radiographic scoring would be more highly correlated with dissected keel score than palpation, thus demonstrating it is a more accurate in vivo method to detect both fractures and deviations compared to palpation.

Materials and Methods

Animals

All animal use and procedures were approved by the animal care committee at the University of Guelph (AUP #4127). Housing and management during the pullet phase (0-16 weeks of age) are briefly described, whereas full details are reported elsewhere (Vitienes et al., 2023).

Lohmann Selected Leghorn Lite (white-feathered) and Lohmann Brown Lite (brown-feathered) female chicks (*Gallus gallus domesticus*) were obtained from a commercial hatchery at the age of one day old. The chickens were reared from 1 day of age to 16 weeks at the University of Guelph in either conventional rearing cages (Conv: Ford Dickinson, Mitchell, Ontario, Canada), or a low-complexity aviary (Natura Primus, Big Dutchman, Holland, MI, U.S.A). Conventional cages are spatially restrictive, only allowing for standing and sitting, whereas aviaries are more spacious and contain infrastructure that allows for more frequent and varied types of activity (e.g. jumping, ramp ascent and descent, perching, running) (Pufall et al., 2021; Rentsch et al., 2023a).

At 16 weeks of age, at the onset of sexual maturity when the chickens begin laying eggs, all chickens were transferred to enriched cages (Farmer Automatic Enrichable Furnished Cages, Clark Ag Systems, Caledonia, Ontario, Canada). Enriched cages are equipped with a nest box and perches and provide slightly more space compared to conventional cages (60 chickens per cage, 688 cm^2/chicken). Adult chickens were fed standard commercial layer crumble pellet diets. A total of 101 chickens were sampled at 30, 50, and 70 weeks of age. To decide which chickens were sampled, they underwent palpation, a non-invasive method to detect keel bone fracture presence in vivo (Buijs et al., 2019; Wilkins et al., 2004), and an equal number of chickens with and without palpation-identified keel bone fractures were selected. These chickens then underwent radiograph imaging for radiograph keel bone scoring (Rufener et al., 2018), and thereafter were euthanized. Keel bones were then dissected and stored in 70% ethanol, and were visually scored for keel bone fracture and deviation.

Scoring methods

i. In vivo palpation

This method involved trained examiners suspending the chickens by their feet and running two fingers across the ventral aspect of the keel bone, feeling for fracture calluses or malformations indicating a healing or recently healed fracture(s) (Wilkins et al., 2004). Suspending the chickens by their feet induces tonic immobility which aids in the palpation process. The outcome of this test is binary – either fractured or nonfractured keel.

ii. In vivo radiograph imaging and scoring

Chickens were suspended by their feet, inducing tonic immobility, and shackled within a wooden frame (Fig. 1 A). Chickens were oriented such that they were radiographed laterally

(Poskom VET-20BT portable X-ray unit, Promark Imaging, Toronto, ON, Canada). The imaging procedure lasted 10-20 seconds per chicken. Images were then scored by a trained examiner according to a published tagged visual analogue scale (Rufener et al., 2018). The scoring ranges from 0, no fracture, to 5, extremely severe fracture status. To score an image, the examiner chose a position within a tagged (0, 1, 2, 3, 4, 5) 10 cm line, and the exact score is then determined by measuring the position along the line with a ruler. The score is considered an ordinal variable (Fig. 1 B). This scoring system has been shown to have inter-observer and intra-observer reliability, so long as the observer completes a freely available online training module created by the authors, who developed this scoring rubric. In this current study, a single examiner performed all radiographic scoring.

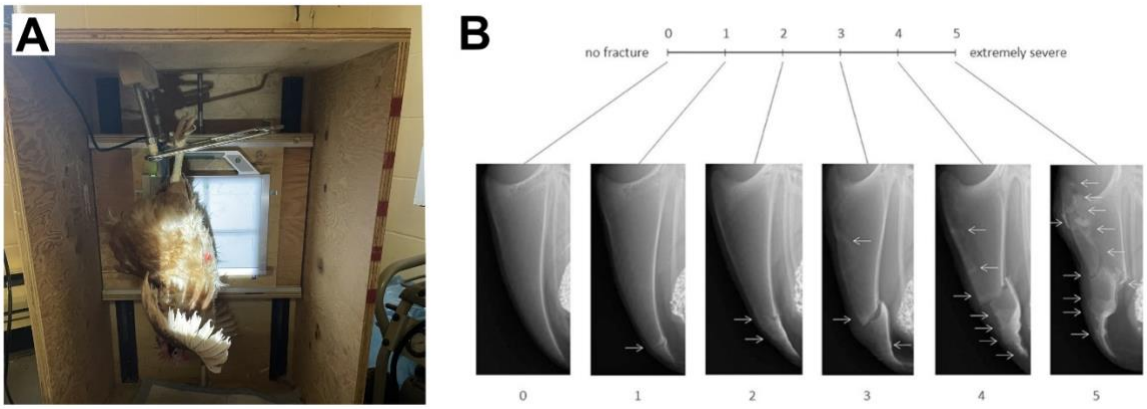

Figure 16: Keel bone radiography. A) Chickens are suspended by their feet for radiograph imaging. They are positioned with the lateral side of their body parallel to the detector. B) Tagged visual analogue scale used for radiograph image scoring of keel fracture severity. Reproduced from Rufener et al., 2018.

iii. Ex vivo bone fracture and deviation scoring

Dissected keels were scored for fracture and deviation severity by a single examiner, using a scoring rubric that we created based on previously published methods (Richards et al., 2011). Each fracture identified in a keel was categorized as either mild or moderate. A mild fracture was one where a callus or fracture line was visible but there was no substantial displacement (< 20°), and the two sides of the fracture were securely attached to each other. A moderate fracture was characterized by either a healed fracture with substantial displacement or a fracture where the bone was completely severed. The location of the fracture was also recorded (Fig. 2 A). Similarly, a deviation was categorized as either mild or moderate depending on whether the deviation was of

less or more than 20°, respectively. Deviation type was also recorded: mild deviations were classified as either washboard, boot, tip, ventral, or dorsal, whereas moderate deviations were of type tip, ventral, or dorsal (Fig. 2B). A washboard deviation is one where there is undulations in the dorsal surface of the keel bone (Fig. 2 B). A boot deviation is characterized by a small but acute curvature of the extreme tip of the keel (Fig. 2 B). Tip deviations were deviations about the keel's medial-lateral axis (Fig. 2 B). A ventral deviation is defined as lateral deviations of the ventral aspect of the keel about the keel's cranial-caudal axis, resulting in apparent "dents" of the ventral edge of the keel (Fig. 2 B). Dorsal deviations are lateral deviations of the keel about the keel's ventral-dorsal axis (Fig. 2B). Deviations directly associated (spatially) to a fracture were not counted as a deviation.

A fracture severity score of zero indicated no observable fractures (fresh, healing, or healed), a score of 1 was assigned to bones with a single mild fracture, a score of 2 where there were multiple mild or a single moderate fracture, and a score of 3 when there were multiple fractures where at least one of them was moderate. The deviation scoring followed the same rubric – zero for no deviations, 1 for one mild deviation, 2 for multiple mild or one moderate, and 3 for multiple deviations with at least one being moderate.

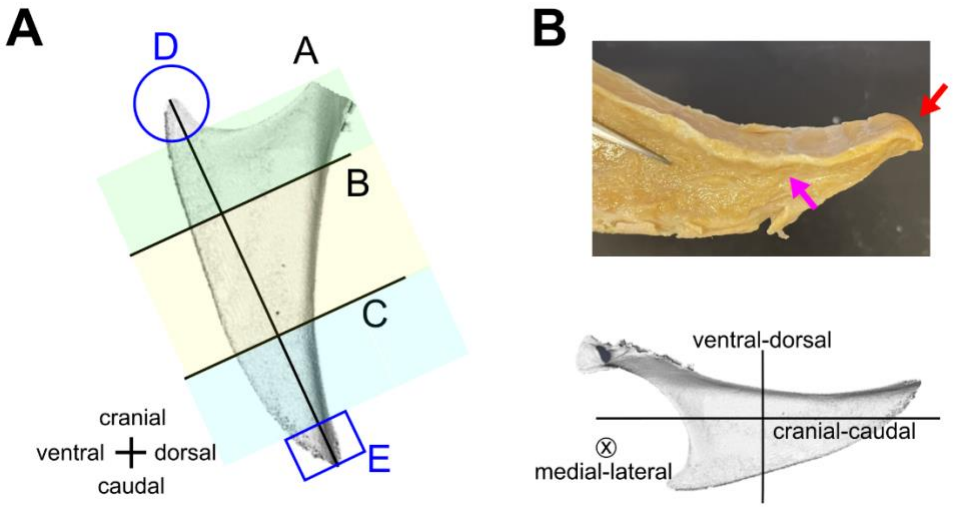

Figure 17: Ex vivo fracture and deviation scoring. A) Fractures were classified based on their location within illustrated regions A-E. B) Top image depicts a washboard deviation (pink arrow) and a boot deviation (red arrow). Below, axes about which tip (medial-lateral, axis perpendicular to page), ventral (cranial-caudal), and dorsal (ventral-dorsal) deviations occur.

Data analysis

All correlations were assessed by Spearman's rho correlation (ρ), which is a suitable method when assessing the association between ordinal variables. We present correlations that were statistically significant ($p < 0.05$) or trending ($1 < p \leq 0.05$).

Results

Ex vivo fracture and deviation severity score were not significantly correlated

Among the 101 sampled chickens, 64% had a non-zero fracture score (Fig. 3 A). We identified a total of 102 fractures. Among these chickens possessing fracture(s), 46% had a fracture severity score of 1, 37% had a score of 2, and the remaining 17% a score of 3. Most fractures, 77%, were mild as opposed to moderate (Fig. 3 B). Across all regions mild fractures predominated (Fig. 3 C). Most fractures occurred in the caudal third of the keel (region C and E). No fractures were found in regions A or D (Fig. 3 C).

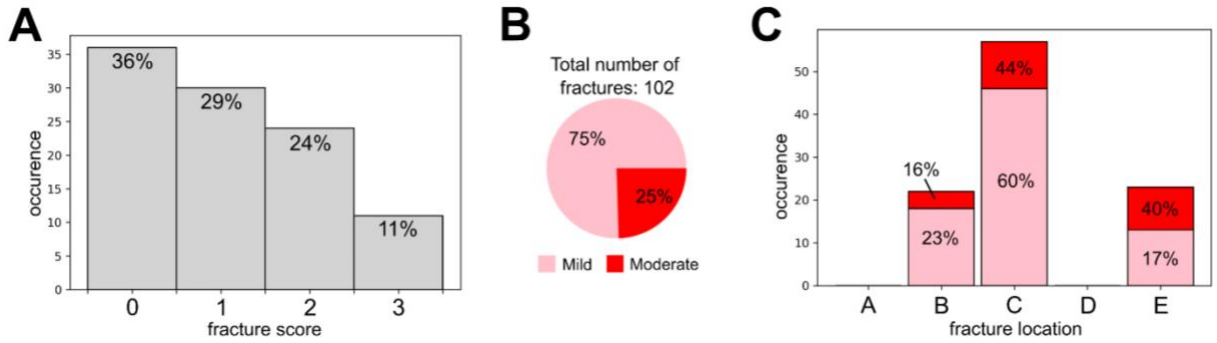

Figure 3: Fracture scoring. A) Histogram of fracture scores with annotated percentage of chickens assigned each score. B) Percentage of total fractures identified that were mild (pink) and moderate (red). C) Histogram of fractures by location, stratified by mild (pink) and moderate (red).

Chickens with deviation(s) accounted for 89% of all sampled chickens, with an average of 2.1 deviations per chicken. Among these chickens possessing deviation(s), 21% had a deviation severity score of 1, 39% a score of 2, and 40% a score of 3 (Fig. 4 A). Most deviations were mild (78%, Fig. 4 B). Among mild deviations, the majority (37%) where of the boot type, and moderate deviations were almost exclusively ventral (98%) (Fig. 4 C).

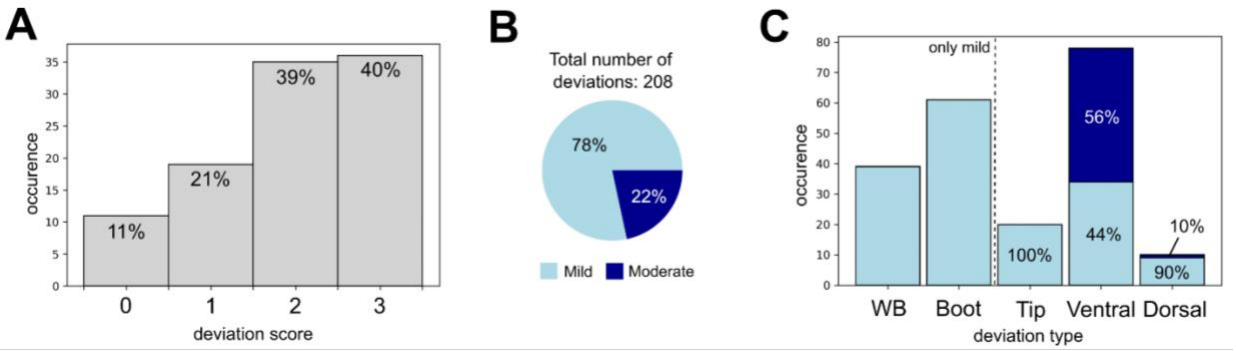

Figure 4: Deviation scoring. A. Histogram of deviation scores with annotated percentage of chickens assigned each score. B. Percentage of total deviations classified as either mild (light blue) and moderate (dark blue). C. Histogram of deviations according to type. *Washboard* (*WB*) and *Boot* are only of mild type, while *Tip*, *Ventral*, and *Dorsal* types are stratified into mild (light blue) and moderate (dark blue).

Among the 65 chickens that possessed at least one fracture, 58 (89%) also possessed at least one deviation, whereas a total of 32 (32%) chickens possessed deviation(s) without fracture. Therefore, only 10 (10%) chickens sampled did not possess a fracture or deviation. The correlation between fracture and deviation severity score was non-significant, albeit trending ($p = 0.097$), but weak ($\rho = 0.17$) (Fig. 5).

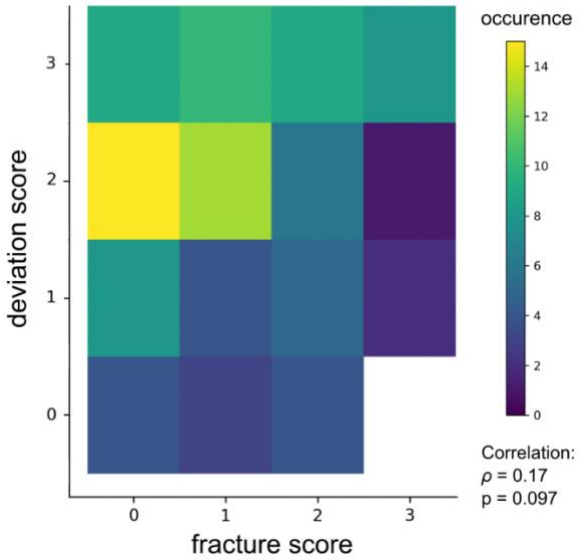

Figure 5: Correlation between fracture and deviation scores. 2D histogram of fracture and deviation scores, and the Spearman's rho correlation between them.

Palpation score was highly correlated to ex vivo fracture score and radiographic score

In vivo palpation, which categorizes chickens as either possessing or not possessing keel bone damage (without distinguishing between deviation or fracture), was highly correlated to ex

vivo fracture scores (ρ = 0.75, p < 0.001, Fig.6 C), and trended to a weak correlation with ex vivo deviation scores (ρ = 0.18, p = 0.079, Fig. 6 A). Radiographic score correlated moderately to both ex vivo fracture (ρ = 0.429, p < 0.001, Fig. 6 D) and deviation (ρ = 0.419, p < 0.01, Fig. 6 B) scores. Palpation and radiographic scores were highly correlated with one another (ρ = 0.750, p < 0.001).

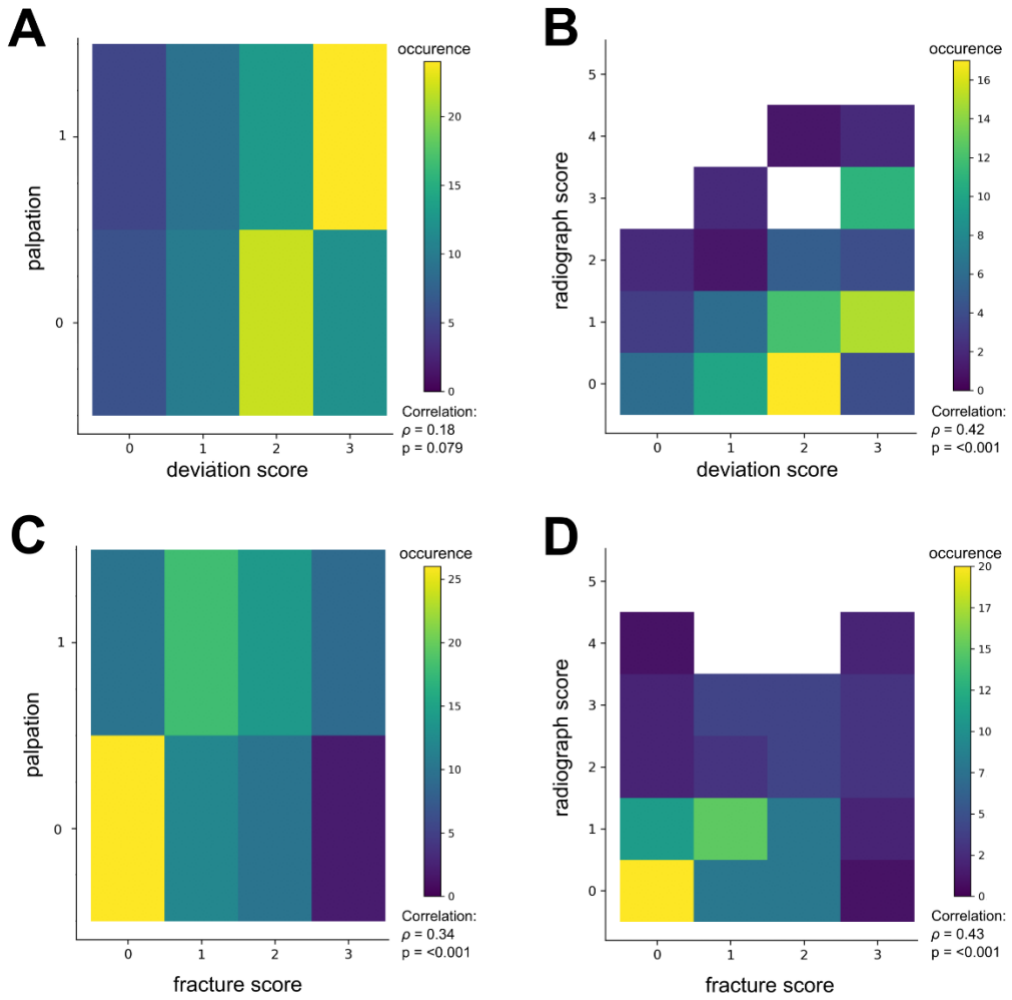

Figure 6: Correlations between palpation (A and C) or radiograph (B and D) scores and deviation (A and B) or fracture score (C and D). Spearman's correlation coefficient (ρ) and p value noted below each colour bar.

Discussion

In this study, we sought to characterize the keel bone fracture and deviation status of a group of adult commercial egg-laying hens (female chickens), measured by visual examination of

dissected bones, and assess the agreement with in vivo non-invasive fracture detection methods. We selected chickens based on identifying them via palpation as possessing or not possessing fractures. These chickens then underwent radiograph imaging, after which these images were scored to quantify fracture severity. Finally, the chickens were euthanized, their keels dissected and examined visually, and scored for fracture severity and deviation severity based on scoring rubrics that we developed, based upon previously published rubrics. We consider the ex vivo dissected bone scores to be the most accurate representation of the status of the bones, whereas palpation and radiograph-based scores serve as estimates of fracture severity.

We chose to score keels based on the number of mild and moderate fractures they possessed; a keel with multiple mild fractures would have the same score as one with a single moderate fracture. The classification of a fracture as being either mild or moderate was based in part by whether the fracture was healed or not. Therefore, our classification was biased towards categorizing fresh fractures as moderate, and well-healed fractures as mild. The rationale behind this approach was that the fracture score would be indicative not only of the number of fractures but would in essence weigh the fractures based on the extent to which it influences the chicken's welfare, under the assumption that a healed fracture would be less painful and bothersome compared to a fresh, unhealed fracture.

Most of the chickens we sampled possessed fractures, which were found exclusively in the caudal 60% of the keel bone (regions B, C, E). Among these, the majority were mild, indicating that they were already healed and healed in such a way that they did not deviate by more than 20° from the pre-fractured shape. It remains unclear whether there is a causal relationship between keel deviations and fractures. Some theorize that deviations arise when pressure is placed upon a mineralizing keel, such that the cartilage is deformed and then becomes stuck in this deformed state as the keel mineralizes (Jung et al., 2022). Given that bone morphology and structure is a critical determinant of its mechanical behaviours, it is plausible that deviations render the bone more susceptible to fracture. We found that most chickens possessed both fractures and deviations, but we are not able to know the relative timing of fracture and deviation development in our samples, nor has the process of keel bone mineralization been characterized in female chickens to date. Answering these questions requires longitudinal following of chickens to identify the

progression of deviations and fractures and keel bone mineralization, which itself requires effective and efficient in vivo assessment methods.

The chickens included in this study were sampled based on palpation to identify the presence of fracture. Among the 101 chickens sampled, 51 were identified as possessing fracture(s), and the remaining 50 as lacking any fracture. Fracture scoring on dissected keels indicated that 64% of these chickens actually possessed at least one fracture, thus the palpation method indeed underestimated the amount of fractures present. We identified a large number of fractures located at the tip of the keel, which is an area known to be difficult to examine by palpation, and likely contributed to this discrepancy.

Nevertheless, we found that palpation score was highly correlated to ex vivo fracture score. We also found palpation to be weakly correlated to ex vivo deviation score. Surprisingly, radiographic score correlated similarly to ex vivo fracture and deviation scores, even though radiographic scoring does not take into consideration deviations. This indicates that either what is visually seen as a deviation may have an associated fracture that is not perceivable visibly, but can be seen in the radiograph image, or that deviations are being confused for fractures in the radiographic image. Further investigation into deviated regions by high-resolution imaging such as micro-computed tomography would more accurately reveal the status of these bones.

Overall, we show that although palpation underestimates fracture severity, it is still a good method to assess the fracture severity status of chickens as it correlated with ex vivo fracture score. Thus, taking into consideration the cost and equipment required for radiographic imaging and scoring, palpation is a more efficient method to assess keel bone fracture status in vivo. However, improved methods of in vivo fracture detection at the individual fracture level are required to investigate the relationship between keel bone mineralization, deformation development, and fracture occurrence.

References

Abrahamsson, P., & Tauson, R. (1995). Aviary Systems and Conventional Cages for Laying Hens: Effects on Production, Egg Quality, Health and Bird Location in Three Hybrids. *Acta Agriculturae Scandinavica A - Animal Sciences*. https://doi.org/10.1080/09064709509415851

Buijs, S., Heerkens, J. L. T., Ampe, B., Delezie, E., Rodenburg, T. B., & Tuyttens, F. A. M. (2019). Assessing keel bone damage in laying hens by palpation: Effects of assessor experience on accuracy, inter-rater agreement and intra-rater consistency. *Poultry Science*, *98*(2), 514–521. https://doi.org/10.3382/ps/pey326

Casey-Trott, T., Heerkens, J. L. T., Petrik, M., Regmi, P., Schrader, L., Toscano, M. J., & Widowski, T. (2015). Methods for assessment of keel bone damage in poultry. *Poultry Science*, *94*(10), 2339–2350. https://doi.org/10.3382/ps/pev223

Fleming, R. H., McCormack, H. A., McTeir, L., & Whitehead, C. C. (2006). Relationships between genetic, environmental and nutritional factors influencing osteoporosis in laying hens. *British Poultry Science*, *47*(6), 742–755. https://doi.org/10.1080/00071660601077949

Gill, F. B. (1995). *Ornithology*. W. H. Freeman.

Jung, L., Rufener, C., & Petow, S. (2022). A tagged visual analog scale is a reliable method to assess keel bone deviations in laying hens from radiographs. *Frontiers in Veterinary Science*, *9*. https://doi.org/10.3389/fvets.2022.937119

Knowles, T. G., & Broom, D. M. (1990). Limb bone strength and movement in laying hens from different housing systems. *The Veterinary Record*, *126*(15), 354–356. https://doi.org/10.1136/vr.126.15.354

Kozak, M., Tobalske, B., Martins, C., Bowley, S., Wuerbel, H., & Harlander-Matauschek, A. (2016). Use of space by domestic chicks housed in complex aviaries. *Applied Animal Behaviour Science*, *181*, 115–121. https://doi.org/10.1016/j.applanim.2016.05.024

Lay, D. C., Fulton, R. M., Hester, P. Y., Karcher, D. M., Kjaer, J. B., Mench, J. A., Mullens, B. A., Newberry, R. C., Nicol, C. J., O'Sullivan, N. P., & Porter, R. E. (2011). Hen welfare in different housing systems1. *Poultry Science*, *90*(1), 278–294. https://doi.org/10.3382/ps.2010-00962

Leyendecker, M., Hamann, H., Hartung, J., Kamphues, J., Neumann, U., Sürie, C., & Distl, O. (2005). Keeping laying hens in furnished cages and an aviary housing system enhances their bone stability. *British Poultry Science*, *46*(5), 536–544. https://doi.org/10.1080/00071660500273094

Newman, S., & Leeson, S. (1998). Effect of housing birds in cages or an aviary system on bone characteristics. *Poultry Science*, *77*(10), 1492–1496. https://doi.org/10.1093/ps/77.10.1492

Pufall, A., Harlander-Matauschek, A., Hunniford, M., & Widowski, T. M. (2021). Effects of Rearing Aviary Style and Genetic Strain on the Locomotion and Musculoskeletal Characteristics of Layer Pullets. *Animals*, *11*(3), 634. https://doi.org/10.3390/ani11030634

Rentsch, A. K., Harlander, A., Siegford, J. M., Vitienes, I., Willie, B. M., & Widowski, T. M. (2023). Rearing laying hens: The effect of aviary design and genetic strain on pullet exercise and perching behavior. *Frontiers in Animal Science*, *4*. https://doi.org/10.3389/fanim.2023.1176702

Riber, A., & Hinrichsen, L. (2016). Keel-bone damage and foot injuries in commercial laying hens in Denmark. *Animal Welfare*, *25*(2), 179–184. https://doi.org/10.7120/09627286.25.2.179

Richards, G. J., Nasr, M. A., Brown, S. N., Szamocki, E. M. G., Murrell, J., Barr, F., & Wilkins, L. J. (2011). Use of radiography to identify keel bone fractures in laying hens and assess healing in live birds. *The Veterinary Record*, *169*(11), 279. https://doi.org/10.1136/vr.d4404

Rodenburg, B., Tuyttens, F., Reu, K., Herman, L., Zoons, J., & Sonck, B. (2008). Welfare assessment of laying hens in furnished cages and non-cage systems: An on-farm comparison. *Animal Welfare 17 (2008) 4*, *17*. https://doi.org/10.1017/S096272860002786X

Rufener, C., Baur, S., Stratmann, A., & Toscano, M. J. (2018). A Reliable Method to Assess Keel Bone Fractures in Laying Hens From Radiographs Using a Tagged Visual Analogue Scale. *Frontiers in Veterinary Science*, *5*. https://doi.org/10.3389/fvets.2018.00124

Rufener, C., & Makagon, M. M. (2020). Keel bone fractures in laying hens: A systematic review of prevalence across age, housing systems, and strains. *Journal of Animal Science*, *98*(Suppl 1), S36-s51. https://doi.org/10.1093/jas/skaa145

Shipov, A., Sharir, A., Zelzer, E., Milgram, J., Monsonego-Ornan, E., & Shahar, R. (2010). The influence of severe prolonged exercise restriction on the mechanical and structural properties of bone in an avian model. *Veterinary Journal (London, England: 1997)*, *183*(2), 153–160. https://doi.org/10.1016/j.tvjl.2008.11.015

Vitienes, I., Mikolajewicz, N., Hosseinitabatabaei, S., Bouchard, A., Julien, C., Graceffa, G., Rentsch, A., Widowski, T., Main, R. P., & Willie, B. M. (2023). Breed and loading history influence in vivo skeletal strain patterns in pre-pubertal female chickens. *Bone*, *173*, 116785. https://doi.org/10.1016/j.bone.2023.116785

Whitehead, C. C., & Fleming, R. H. (2000). Osteoporosis in cage layers. *Poultry Science*, *79*(7), 1033–1041. https://doi.org/10.1093/ps/79.7.1033

Wilkins, L. J., Brown, S. N., Zimmerman, P. H., Leeb, C., & Nicol, C. J. (2004). Investigation of palpation as a method for determining the prevalence of keel and furculum damage in laying hens. *The Veterinary Record*, *155*(18), 547–549. https://doi.org/10.1136/vr.155.18.547

Wilkins, L. J., McKinstry, J. L., Avery, N. C., Knowles, T. G., Brown, S. N., Tarlton, J., & Nicol, C. J. (2011). Influence of housing system and design on bone strength and keel bone fractures in laying hens. *The Veterinary Record*, *169*(16), 414. https://doi.org/10.1136/vr.d4831

Chapter 7 – Discussion and Future Directions

The general goal of this research was to provide data that would contribute to the prevention and treatment of bone fragility in commercial egg-laying hens. Firstly, I focused on investigating the determinants of bone health in this group and the etiology of bone fragility. I characterized the mechanical stimuli that tibiotarsal structure and material properties are tailored to withstand, and showed that among these two, bone structure is more influential on the bone's mechanical behaviour, shedding light on a set of bone stiffening structural parameters that can be targets for genetic selection. I further show that mechanical stimuli that is anabolic in murine models led to impairment of bone density and microarchitecture in young chickens, highlighting the need to expand our knowledge on bone adaptation to other species and broaden our general understanding of the osteogenic components of mechanical strain stimuli. Applying this knowledge towards the prevention and treatment of bone fragility, however, relies on the ability to detect and monitor fractures in commercial flocks, which is currently challenging. I found that, despite lacking precision and accuracy, in vivo palpation of adult hens to detect the presence of fracture(s) correlates significantly to fracture severity scores measured from dissected bones, thereby supporting the continued use of palpation as a time- and cost-effective method to assess fracture status in commercial laying hen flocks.

In the first study presented (chapter 3), I performed in vivo strain gauging at the tibiotarsus midshaft to measure mechanical strains engendered during a variety of activities. The focus specifically was to measure peak mechanical strain *magnitudes*, as is commonly done in the background strain gauging literature. This disproportionate focus on strain magnitude relative to other osteogenic components of strain (see section 2.3.1) is likely a reverberation of Frost's mechanostat theory, which frames bone adaptation solely as a function of mechanical stimulus magnitude. However, the downstream signal that osteocytes sense and respond to is thought to be primarily cell-membrane shear stress due to loading-induced fluid flow of the interstitial fluid surrounding the cells within the lacunocanalicular network (Schaffler & Kennedy, 2012). The magnitude and temporal dynamics of the fluid flow that shears the surfaces of the osteocytes is a function of the size of the lacunae and canaliculi through which it is moving, as well as the amplitude and frequency components of the loading conditions (Turner et al., 1995; van Tol,

Roschger, et al., 2020). Thus, the signal that the osteocytes are sensing is not only dependent on the strain magnitude, but also strain rate and cycle frequency. We initially knew, from parametric controlled loading studies, that that strain magnitude, rate, and frequency influence the mechanoresponse (see section 2.3.1 for references). The link however to this effect being mediated by effects on the signal itself which the osteocytes are sensing was highlighted in a study where fluid flow within the lacunocanalicular system was modelled as a function of strain rate, and the correlation between fluid flow velocity and the local mechanoresponse was measured (van Tol, Schemenz, et al., 2020). In this study, we also assessed the correlation between finite element-modelled strain magnitudes to the local mechanoresponse, and found that fluid flow velocity (modelled as a function of strain rate) was better at predicting the mechanoresponse than strain magnitude patterns (van Tol, Schemenz, et al., 2020). Although the main goal with this study was to show how the lacuno-canalicular network topology is an important consideration in understanding the downstream stimuli triggering the bone mechanoresponse, it also shows that strain rate in addition to magnitude is an important consideration. As opposed to (or in addition to) conducting parametric loading and in silico modelling studies to assess how strain magnitude, rate, and frequency together influence the mechanoresponse, future studies could characterize the frequency features of background strain stimuli. Well defined approaches exist to analyze the spectral components of signals, and data collected during background strain gauging which is often from continuous sampling is amenable to this type of analysis.

Strain rate in particular is also relevant to the accumulation of microdamage – when the load induced strain magnitude is held constant but the rate is increased, more microdamage accumulates in the bone (Schaffler et al., 1989). In the loading study presented in this thesis, peak strains engendered did not exceed 3,000 με, which is not high when situated among the bulk of measured background strains in the literature (Main, 2021c) and is well below reported levels of yield strain (Mirzaali et al., 2016; Morgan et al., 2018) (although these have not been measured in commercial laying hen chickens). However, it is possible that the strain rate required to engender the target strain magnitude in our loading study was high enough to cause substantial microdamage, particularly if the material properties of these bones are tailored to withstanding strain rates of lower magnitude; quantifying strain rates in background strain data would provide valuable insights. Whether or not rapid accumulation of microdamage could produce impairments to bone

structure such as those that we measured in the loaded bones also remains to be investigated. Microdamage has been shown to elicit bone remodelling to repair the damage (Bentolila et al., 1998; Burr et al., 1985; Mori & Burr, 1993), which could explain the decreased tissue mineral density observed in loaded limbs.

Background strain gauging is an error-prone experiment due to the potential for the introduction of noise at multiple steps of the signal acquisition process. Strain gauge sensors are sensitive to damage, which would alter the magnitude signal that they produce, and the measured strain magnitudes are highly dependent on the positioning and orientation of the strain gauge attached to the bone. As clearly seen in the finite element data presented in this thesis (chapter 4), strains are highly variable across the bone. This is another reason why it is valuable to measure strain frequency components – as they are independent of strain magnitude, they are impervious to noise and error associated to strain gauge positioning and circuit calibration and balancing. This not only would reduce the variability in the data (and increase statistical power) but also enhances comparability across studies conducted on different species or that chose different anatomical locations to attach gauges to.

A main limitation of strain gauging is that strains are measured at discrete sites of the bone surface, and interior regions of the bones are inaccessible. Finite element modelling is therefore useful because we can know (estimated) strains along and throughout the entire bone. Ideally, we would want to model whole bone mechanical behaviour during background activity loading conditions, but the boundary conditions are complex and difficult to replicate. Instead, in the study presented in this thesis, I modelled our in vivo controlled loading boundary conditions, which are 1) simpler and more feasible to simulate, and 2) can be (and were) validated by using strain gauges to measure strains engendered during controlled loading. This also has the benefit of providing insight about the stimulus that we are subjecting the bones to when conducting an in vivo loading experiment.

Our in vivo controlled loading boundary conditions are similar to the conditions the tibiotarsus encounters in vivo: in both cases, at the tibiotarsus midshaft the anterior surface is in tension and the posterior surface in compression. Although we do not know the exact boundary conditions occurring during in vivo activities, we know that generally load will be transmitted from one end of the bone (tibiotarsus-knee contact) to another (tibiotarsus-ankle contact). Given that these

contact surfaces are small relative to the length of the bone we can assume that our controlled axial compression approximates in vivo loading conditions. Furthermore, if we think about bone structure and shape as mechanisms that not only determine how the bone deforms, but that are capable of *canalizing* bone deformation under varied loading conditions (magnitude, direction, contact surfaces), which has been shown to be the case (e.g. curvature enabling load predictability (Bertram & Biewener, 1988)) then it becomes even more reasonable to assume that our in vivo loading produces physiological strain distributions. Boundary condition sensitivity analyses performed during the finite element analyses (not included in thesis) where contact surfaces, load application surfaces, and the direction of applied load were varied, indicated consistent strain patterns despite these changes, which further suggests that the bone is structured in a way such that strain distributions are robust against certain amounts of variation in boundary conditions, and by virtue of this, our controlled loading model likely induces a physiological strain distribution throughout the bone.

The results from the finite element modelling (chapter 4) indicate that at the proximal end of the tibiotarsus, the anterior surface is in compression while the posterior surface is in tension. Then, at the midshaft, the neutral axis rotates by 180° such that distally the anterior surface is in tension and the posterior in compression. The engendered strains and stresses simulated are highest at the proximal and distal regions where peak bending occurs, and the strain conditions in these regions are simpler (predominantly bending) that at the midshaft where there is a combination of axial compression, bending, and torsion, and a lot of variability in strain distributions within a relatively small volume due to the rotation of the neutral axis. We chose to quantify the effects of our controlled loading intervention (chapter 5) at the tibiotarsus midshaft, to replicate what is commonly done in other loading studies (with the intention of maximizing comparability across studies). Since engendered stresses were higher in these metaphyseal regions, if the impairment to bone structure seen due to loading at the midshaft is due to an accumulation of microdamage, we would expect these metaphyseal regions to have more microdamage and thus potentially more structural impairment. Subsequent analyses of these bones should assess the mechanoresponse at the proximal or distal metaphyses, and measure microdamage in metaphyseal and diaphyseal regions, to address these questions.

The loading protocol and waveform implemented in our controlled loading study (chapter 5) was identical to the one used in the single other non-invasive controlled loading study performed on an avian specie (Verner, 2017). The loading protocol waveform was also identical to what has been used by several groups, including ours, in murine controlled loading studies (Main et al., 2020). This waveform was selected for the current loading study 1) to allow for comparability across studies, and 2) because there was no good reason to use a different waveform – the arrival at this waveform and set of parameters came after many years of parametric studies seeking to find a stimulus that would reliably produce a robust anabolic response in rodents, and there was not a strong argument to use something completely different even if we were experimenting on a different animal model. Since Verner's study did not result in a bone anabolic response using this waveform, we decided to adjust the background-to-loading strain increase factor from 1.5-2.5 to 4-9. However, similar to Verner's findings, we showed impairments due to loading, thus indicating that it was not higher strain magnitudes that were lacking. We kept the same loading frequency of 4 Hz as rodent studies, which was originally chosen as it resembles background walking frequency in mice (Clarke & Still, 1999). Our background strain gauging data indicated that step frequency was lower in the chickens, approximately 2Hz; adjusting this parameter in subsequent loading studies may be a promising approach to yield an anabolic response and avoid microdamage based on what we know about the effect of strain rate on the accumulation of microdamage. By finding a waveform that can elicit a bone anabolic response in chickens (or birds generally) not only will we be able to study the mechanoresponse in this group (how strain distributions engendered relate to local bone formation, resorption, and their rates), but comparing the types of loading that birds compared to mice respond to would ultimately shed light onto the inter-species variability in bone adaptation.

In addition to characterizing the mechanical behaviour and mechanoresponse in young female chickens, I sought to assess how these outcomes are influenced by chicken genotype and by their loading history. Across these three studies, we consistently saw significant differences between genetic strains, but not nearly as often between chickens raised in different housing systems. The background strain gauging results indicated that, during locomotor activities, chickens raised in aviaries which increased history of physical activity exhibited lower strain levels, as we would expect given that the caged chickens are per se not habituated to these levels of mechanical loading.

But interestingly we did not see this pattern in other activity types measured. And although we were not able to perform statistical analyses on the effect of housing on the finite element modelled strains and stresses due to axial compressive loading, we did not see a consistent pattern in terms of differences between the housing groups. This points to a limitation in our experimental design which could have played a role in masking the effect of loading history on the outcomes measured: the chickens we studies were raised by collaborators at the University of Guelph, who have facilities with commercially sold housing systems. We sampled chickens from their flocks and transported them to McGill's poultry facility where we conducted our experiments. There, all chickens – caged and aviary-raised – were housed in floor-based open concept rooms for the duration of the experiment, which each time lasted no longer than 21 days. The opportunity for physical activity at the McGill facilities was therefore increased for the chickens previously raised in cages. In mice, it was shown that as little as one week of daily loading led to a measurable anabolic response; it is possible that housing all chickens in a common housing system abolished any previously present differences between them.

These three studies (chapters 3-5) focused on the tibiotarsus bone, however the bone that is fractured the most in the commercial egg-laying hen population is the keel. We chose to characterize bone mechanical and adaptive behaviour in the tibiotarsus because the experimental methodology developed to study these features has been developed for long bones and is not amenable currently to the keel bone. We do not have a detailed enough understanding of the way in which the keel is loaded to be able to create realistic, physiological finite element models of keel bone loading. And, since the pectoral muscles attach to the majority of the keel surface, attaching a strain gauge to the bone surface to obtain this information would require detaching muscle tissue, influencing the muscle-derived loading. Considering this, we proceeded with the tibiotarsus based on the assumption that genetic and environmental determinants of skeletal strength in this population would influence all skeletal sites, thus results derived from studying the tibiotarsus could be generalized to all bones. There are however many measures to investigate directly on the keel. Mineralization timelines and dynamics can be evaluated by fluorochrome tracking of bone formation, and high-resolution tomographic characterization of keel bone microarchitecture is lacking and could give some indications about the mechanical environment the keel is subjected to.

In this thesis, we approached the keel from an epidemiological angle as opposed to investigating the etiology of keel bone damage. I focused on the issue of fracture detection and severity assessment, which currently is a significant barrier to understanding the etiology of these fractures. Laying hen flocks are large, and especially when chickens are housed in non-cage systems tracking individual chickens longitudinally is very difficult. Inferring longitudinal data at the population-level by randomly sampling chickens is also challenging due to the high variability present within and between flocks. Time- and cost-effective methods to accurately and precisely track the fracture status of a sufficiently large sample size of chickens longitudinally, at the individual level, are needed. Currently, the two main methods used in commercial farms are palpation and fracture status scoring based on radiograph images. Palpation is the quickest and cheapest option, whereas radiography involves the purchase of radiograph equipment and more substantial training of personnel. It is therefore a positive result that we show that palpation correlates to our fracture severity score derived by visualizing dissected keels, as it supports the continued use of this method.

Chapter 8 – Conclusions

Throughout my doctoral research I studied the tibiotarsi and keel bones of young and adult commercial egg laying hens to gain a better understanding on the structural and material determinants of bone strength, bone mechanoadaptation, and assess the validity of fracture severity assessment methods. These aims were addressed throughout four studies, with the following specific findings:

Study 1 – In vivo mechanical behaviour of the tibiotarsus of young chickens during physical activity

- The tibiotarsus midshaft is subjected to a complex loading environment consisting of a combination of axial compression, bending, and, predominantly, torsion
- Among sampled activities, aerial transition landing produced the highest strain magnitudes, with unusual cross-sectional strain patterns
- Genetic strain and housing environment influenced in vivo strains
- Caged chickens exhibited higher in vivo strains during locomotor activity compared to aviary-raised chickens, but not during jumping, perching, or aerial transition landing.

Study 2 – In vivo mechanical behaviour of the tibiotarsus of young chickens during controlled loading

- Variations in tissue mineral density by up to 200 mgHA/cm3 had negligible effects on the mechanical behaviour of the tibiotarsus when subjected to axial compressive loading
- Engendered stress was negatively correlated to bone area, total area, bone area ratio, polar moment of inertia, endosteal perimeter, total perimeter, and endosteal-to-periosteal perimeter ratio
- Engendered stress was positively correlated to bone thickness
- Engendered stress patterns did not differ between genetic strains or housing environment groups
- Engendered stress magnitudes were higher in white-feathered than brown-feathered chickens.

Study 3 – Tibiotarsal mechanoresponse to in vivo controlled loading

- Controlled loading impaired tibiotarsal midshaft mineral density and structure
- Controlled loading coincided with lower bone formation surface and circulating resorption markers
- The effect of loading was genetic strain dependent, seen only in white-feathered chickens

Study 4 – Validation of keel bone damage scoring

- Palpation and radiograph scores both correlated to fracture severity
- Radiograph scores correlated to deviation severity
- Fracture and deviation severity were not correlated themselves
- Most fractures detected occurred at the caudal 30% of the keel bone
- Most sampled chickens possessed multiple deviations

References

Aamodt, A., Lund-Larsen, J., Eine, J., Andersen, E., Benum, P., & Husby, O. S. (1997). In vivo measurements show tensile axial strain in the proximal lateral aspect of the human femur. *Journal of Orthopaedic Research*, *15*(6), 927–931. https://doi.org/10.1002/jor.1100150620

Abrahamsson, P., & Tauson, R. (1995). Aviary Systems and Conventional Cages for Laying Hens: Effects on Production, Egg Quality, Health and Bird Location in Three Hybrids. *Acta Agriculturae Scandinavica A - Animal Sciences*. https://doi.org/10.1080/09064709509415851

Alexander, R. M. (1981). Factors of safety in the structure of animals. *Science Progress*, *67*(265), 109–130.

Ashman, R. B., Cowin, S. C., Van Buskirk, W. C., & Rice, J. C. (1984). A continuous wave technique for the measurement of the elastic properties of cortical bone. *Journal of Biomechanics*, *17*(5), 349–361. https://doi.org/10.1016/0021-9290(84)90029-0

Bain, S. D., Bailey, M. C., Celino, D. L., Lantry, M. M., & Edwards, M. W. (1993). High-dose estrogen inhibits bone resorption and stimulates bone formation in the ovariectomized mouse. *Journal of Bone and Mineral Research: The Official Journal of the American Society for Bone and Mineral Research*, *8*(4), 435–442. https://doi.org/10.1002/jbmr.5650080407

Baron, R., & Kneissel, M. (2013). WNT signaling in bone homeostasis and disease: From human mutations to treatments. *Nature Medicine*, *19*(2), 179–192. https://doi.org/10.1038/nm.3074

Bassey, E. J., Rothwell, M. C., Littlewood, J. J., & Pye, D. W. (1998). Pre- and postmenopausal women have different bone mineral density responses to the same high-impact exercise. *Journal of Bone and Mineral Research*, *13*(12), 1805–1813. https://doi.org/10.1359/jbmr.1998.13.12.1805

Beck, M. M., & Hansen, K. K. (2004). Role of estrogen in avian osteoporosis. *Poultry Science*, *83*(2), 200–206. https://doi.org/10.1093/ps/83.2.200

Bentolila, V., Boyce, T. M., Fyhrie, D. P., Drumb, R., Skerry, T. M., & Schaffler, M. B. (1998). Intracortical remodeling in adult rat long bones after fatigue loading. *Bone*, *23*(3), 275–281. https://doi.org/10.1016/S8756-3282(98)00104-5

Berendsen, A. D., & Olsen, B. R. (2015). Bone development. *Bone*, *80*, 14–18. https://doi.org/10.1016/j.bone.2015.04.035

Bertram, J. E. A., & Biewener, A. A. (1988). Bone curvature: Sacrificing strength for load predictability? *Journal of Theoretical Biology*, *131*(1), 75–92. https://doi.org/10.1016/S0022-5193(88)80122-X

Bertram, J. E. A., & Biewener, A. A. (1992). Allometry and curvature in the long bones of quadrupedal mammals. *Journal of Zoology*, *226*(3), 455–467. https://doi.org/10.1111/j.1469-7998.1992.tb07492.x

Biewener, A. A. (1982). Bone strength in small mammals and bipedal birds: Do safety factors change with body size? *Journal of Experimental Biology*, *98*, 289–301. https://doi.org/10.1242/jeb.98.1.289

Biewener, A. A. (1992). In vivo measurement of bone strain and tendon force. In A. A. Biewener (Ed.), *Biomechanics: Structures and Systems: A Practical Approach* (pp. 123–147). Oxford University Press.

Biewener, A. A. (1993). Safety factors in bone strength. *Calcified Tissue International*, *53 Suppl 1*, S68-74. https://doi.org/10.1007/BF01673406

Biewener, A. A., & Bertram, J. E. (1993). Skeletal strain patterns in relation to exercise training during growth. *Journal of Experimental Biology*, *185*, 51–69. https://doi.org/10.1242/jeb.185.1.51

Biewener, A. A., & Bertram, J. E. (1994). Structural response of growing bone to exercise and disuse. *Journal of Applied Physiology*, *76*(2), 946–955. https://doi.org/10.1152/jappl.1994.76.2.946

Biewener, A. A., & Dial, K. P. (1995). In vivo strain in the humerus of pigeons (Columba livia) during flight. *Journal of Morphology*, *225*(1), 61–75. https://doi.org/10.1002/jmor.1052250106

Biewener, A. A., Fazzalari, N. L., Konieczynski, D. D., & Baudinette, R. V. (1996). Adaptive changes in trabecular architecture in relation to functional strain patterns and disuse. *Bone*, *19*(1), 1–8. https://doi.org/10.1016/8756-3282(96)00116-0

Biewener, A. A., Swartz, S. M., & Bertram, J. E. A. (1986). Bone modeling during growth: Dynamic strain equilibrium in the chick tibiotarsus. *Calcified Tissue International*, *39*(6), 390–395. https://doi.org/10.1007/BF02555177

Biewener, A. A., & Taylor, C. R. (1986). Bone strain: A determinant of gait and speed? *Journal of Experimental Biology*, *123*, 383–400. https://doi.org/10.1242/jeb.123.1.383

Biewener, A. A., Thomason, J., Goodship, A., & Lanyon, L. E. (1983). Bone stress in the horse forelimb during locomotion at different gaits: A comparison of two experimental methods. *Journal of Biomechanics*, *16*(8), 565–576. https://doi.org/10.1016/0021-9290(83)90107-0

Birkhold, A. I., Razi, H., Duda, G. N., Weinkamer, R., Checa, S., & Willie, B. M. (2014). The influence of age on adaptive bone formation and bone resorption. *Biomaterials*, *35*(34), 9290–9301. https://doi.org/10.1016/j.biomaterials.2014.07.051

Birkhold, A. I., Razi, H., Duda, G. N., Weinkamer, R., Checa, S., & Willie, B. M. (2016). The Periosteal Bone Surface is Less Mechano-Responsive than the Endocortical. *Scientific Reports*, *6*, 23480. https://doi.org/10.1038/srep23480

Birkhold, A. I., Razi, H., Weinkamer, R., Duda, G. N., Checa, S., & Willie, B. M. (2015). Monitoring in vivo (re)modeling: A computational approach using 4D microCT data to quantify bone surface movements. *Bone*, *75*, 210–221. https://doi.org/10.1016/j.bone.2015.02.027

Bishop, S. C., Fleming, R. H., McCormack, H. A., Flock, D. K., & Whitehead, C. C. (2000). Inheritance of bone characteristics affecting osteoporosis in laying hens. *British Poultry Science*, *41*(1), 33–40. https://doi.org/10.1080/00071660086376

Blob, R. W., & Biewener, A. A. (1999). In vivo locomotor strain in the hindlimb bones of alligator mississippiensis and iguana iguana: Implications for the evolution of limb bone safety factor and non-sprawling limb posture. *Journal of Experimental Biology*, *202 (Pt 9)*, 1023–1046. https://doi.org/10.1242/jeb.202.9.1023

Blob, R. W., Espinoza, N. R., Butcher, M. T., Lee, A. H., D'Amico, A. R., Baig, F., & Sheffield, K. M. (2014). Diversity of Limb-Bone Safety Factors for Locomotion in Terrestrial Vertebrates: Evolution and Mixed Chains. *Integrative and Comparative Biology*, *54*(6), 1058–1071. https://doi.org/10.1093/icb/icu032

Bonewald, L. (2018). Osteocytes. In *Primer on the Metabolic Bone Diseases and Disorders of Mineral Metabolism* (pp. 38–45). https://doi.org/10.1002/9781119266594.ch5

Bonewald, L. F. (2011). The amazing osteocyte. *Journal of Bone and Mineral Research: The Official Journal of the American Society for Bone and Mineral Research*, *26*(2), 229–238. https://doi.org/10.1002/jbmr.320

Bonucci, E., & Gherardi, G. (1975). Histochemical and electron microscopy investigations on medullary bone. *Cell and Tissue Research*, *163*(1), 81–97. https://doi.org/10.1007/BF00218592

Boskey, A. L., & Coleman, R. (2010). Aging and Bone. *Journal of Dental Research*, *89*(12), 1333–1348. https://doi.org/10.1177/0022034510377791

Bouchard, A. L., Dsouza, C., Julien, C., Rummler, M., Gaumond, M.-H., Cermakian, N., & Willie, B. M. (2022). Bone adaptation to mechanical loading in mice is affected by circadian rhythms. *Bone*, *154*, 116218. https://doi.org/10.1016/j.bone.2021.116218

Bouxsein, M. L., Boyd, S. K., Christiansen, B. A., Guldberg, R. E., Jepsen, K. J., & Muller, R. (2010). Guidelines for Assessment of Bone Microstructure in Rodents Uding Micro-Computed Tomography. *Journal of Bone and Mineral Research*, *25*(7), 1468–1486. https://doi.org/10.1002/jbmr.141

Brodt, M. D., & Silva, M. J. (2010). Aged mice have enhanced endocortical response and normal periosteal response compared with young-adult mice following 1 week of axial tibial compression. *Journal of Bone and Mineral Research*, *25*(9), 2006–2015. https://doi.org/10.1002/jbmr.96

Buckner, G. D., Insko, W. M., Henry, A. H., & Wachs, E. F. (1948). Rate of Growth and Calcification of the Sternum of Male and Female New Hampshire Chickens1. *Poultry Science*, *27*(4), 430–433. https://doi.org/10.3382/ps.0270430

Buckner, G. D., Insko, W. M., Henry, A. H., & Wachs, E. F. (1949). Rate of Growth and Calcification of the Sternum of Male and Female New Hampshire Chickens Having Crooked Keels1. *Poultry Science*, *28*(2), 289–292. https://doi.org/10.3382/ps.0280289

Buijs, S., Heerkens, J. L. T., Ampe, B., Delezie, E., Rodenburg, T. B., & Tuyttens, F. A. M. (2019). Assessing keel bone damage in laying hens by palpation: Effects of assessor experience on accuracy, inter-rater agreement and intra-rater consistency. *Poultry Science*, *98*(2), 514–521. https://doi.org/10.3382/ps/pey326

Burr, D. B. (2019). *Basic and Applied Bone Biology* (2nd ed.).

Burr, D. B., Martin, R. B., Schaffler, M. B., & Radin, E. L. (1985). Bone remodeling in response to in vivo fatigue microdamage. *Journal of Biomechanics*, *18*(3), 189–200. https://doi.org/10.1016/0021-9290(85)90204-0

Butcher, M. T., Espinoza, N. R., Cirilo, S. R., & Blob, R. W. (2008). In vivo strains in the femur of river cooter turtles (Pseudemys concinna) during terrestrial locomotion: Tests of force-platform models of loading mechanics. *Journal of Experimental Biology*, *211*(Pt 15), 2397–2407. https://doi.org/10.1242/jeb.018986

Butcher, M. T., White, B. J., Hudzik, N. B., Gosnell, W. C., Parrish, J. H. A., & Blob, R. W. (2011). In vivo strains in the femur of the Virginia opossum (Didelphis virginiana) during terrestrial locomotion: Testing hypotheses of evolutionary shifts in mammalian bone loading and design. *Journal of Experimental Biology*, *214*(Pt 15), 2631–2640. https://doi.org/10.1242/jeb.049544

Carrano, M. T., & Biewener, A. A. (1999). Experimental alteration of limb posture in the chicken (Gallus gallus) and its bearing on the use of birds as analogs for dinosaur

locomotion. *Journal of Morphology*, *240*(3), 237–249. https://doi.org/10.1002/(SICI)1097-4687(199906)240:3<237::AID-JMOR3>3.0.CO;2-N

Carter, D. R. (1978). Anisotropic analysis of strain rosette information from cortical bone. *Journal of Biomechanics*, *11*(4), 199–202. https://doi.org/10.1016/0021-9290(78)90013-1

Carter, D. R., Smith, D. J., Spengler, D. M., Daly, C. H., & Frankel, V. H. (1980). Measurement and analysis of in vivo bone strains on the canine radius and ulna. *Journal of Biomechanics*, *13*(1), 27–38. https://doi.org/10.1016/0021-9290(80)90005-6

Casey-Trott, T., Heerkens, J. L. T., Petrik, M., Regmi, P., Schrader, L., Toscano, M. J., & Widowski, T. (2015). Methods for assessment of keel bone damage in poultry. *Poultry Science*, *94*(10), 2339–2350. https://doi.org/10.3382/ps/pev223

Casey-Trott, T. M., Guerin, M. T., Sandilands, V., Torrey, S., & Widowski, T. M. (2017). Rearing system affects prevalence of keel-bone damage in laying hens: A longitudinal study of four consecutive flocks. *Poultry Science*, *96*(7), 2029–2039. https://doi.org/10.3382/ps/pex026

Casey-Trott, T. M., Korver, D. R., Guerin, M. T., Sandilands, V., Torrey, S., & Widowski, T. M. (2017a). Opportunities for exercise during pullet rearing, Part I: Effect on the musculoskeletal characteristics of pullets. *Poultry Science*, *96*(8), 2509–2517. https://doi.org/10.3382/ps/pex059

Casey-Trott, T. M., Korver, D. R., Guerin, M. T., Sandilands, V., Torrey, S., & Widowski, T. M. (2017b). Opportunities for exercise during pullet rearing, Part II: Long-term effects on bone characteristics of adult laying hens at the end-of-lay. *Poultry Science*, *96*(8), 2518–2527. https://doi.org/10.3382/ps/pex060

Casey-Trott, T. M., & Widowski, T. M. (2016). Behavioral Differences of Laying Hens with Fractured Keel Bones within Furnished Cages. *Frontiers in Veterinary Science*, *3*, 42. https://doi.org/10.3389/fvets.2016.00042

Chen, C., & Kim, W. K. (2020). The application of micro-CT in egg-laying hen bone analysis: Introducing an automated bone separation algorithm. *Poultry Science*, *99*(11), 5175–5183. https://doi.org/10.1016/j.psj.2020.08.047

Chow, J., Tobias, J. H., Colston, K. W., & Chambers, T. J. (1992). Estrogen maintains trabecular bone volume in rats not only by suppression of bone resorption but also by stimulation of bone formation. *Journal of Clinical Investigation*, *89*(1), 74–78.

Christenson, R. H. (1997). Biochemical markers of bone metabolism: An overview. *Clinical Biochemistry*, *30*(8), 573–593. https://doi.org/10.1016/s0009-9120(97)00113-6

Clarke, K. A., & Still, J. (1999). Gait analysis in the mouse. *Physiology & Behavior*, *66*(5), 723–729. https://doi.org/10.1016/s0031-9384(98)00343-6

Copploe, J. V., Blob, R. W., Parrish, J. H. A., & Butcher, M. T. (2015). In vivo strains in the femur of the nine-banded armadillo (Dasypus novemcinctus). *Journal of Morphology*, *276*(8), 889–899. https://doi.org/10.1002/jmor.20387

Couch, J. R. (1955). Cage layer fatigue. *Feed Age*, *5*(88), 55–57.

Cowin, S. C. (2001). *Bone mechanics handbook* (2nd edition, volume 1). CRC Press.

Currey, J. (2014). *Safety Factors and Scaling Effects in bones, The Mechanical Adaptation of Bones*. Princeton University Press.

Currey, J. D. (1988a). The effect of porosity and mineral content on the Young's modulus of elasticity of compact bone. *Journal of Biomechanics*, *21*(2), 131–139. https://doi.org/10.1016/0021-9290(88)90006-1

Currey, J. D. (1988b). The effect of porosity and mineral content on the Young's modulus of elasticity of compact bone. *Journal of Biomechanics*, *21*(2), 131–139. https://doi.org/10.1016/0021-9290(88)90006-1

Currey, J. D. (2003). The many adaptations of bone. *Journal of Biomechanics*, *36*(10), 1487–1495. https://doi.org/10.1016/s0021-9290(03)00124-6

Currey, J. D. (2004a). Tensile yield in compact bone is determined by strain, post-yield behaviour by mineral content. *Journal of Biomechanics*, *37*(4), 549–556. https://doi.org/10.1016/j.jbiomech.2003.08.008

Dacke, C. (1979). *Calcium regulation in sub-mammalian vertebrates*.

Dacke, C. G., Arkle, S., Cook, D. J., Wormstone, I. M., Jones, S., Zaidi, M., & Bascal, Z. A. (1993). Medullary Bone and Avian Calcium Regulation. *Journal of Experimental Biology*, *184*(1), 63–88. https://doi.org/10.1242/jeb.184.1.63

de Margerie, E., Sanchez, S., Cubo, J., & Castanet, J. (2005). Torsional resistance as a principal component of the structural design of long bones: Comparative multivariate evidence in birds. *The Anatomical Record. Part A, Discoveries in Molecular, Cellular, and Evolutionary Biology*, *282*(1), 49–66. https://doi.org/10.1002/ar.a.20141

Demes, B., Qin, Y. X., Stern, J. T., Larson, S. G., & Rubin, C. T. (2001). Patterns of strain in the macaque tibia during functional activity. *American Journal of Physical Anthropology*, *116*(4), 257–265. https://doi.org/10.1002/ajpa.1122

Demes, B., Stern, J. T., Hausman, M. R., Larson, S. G., McLeod, K. J., & Rubin, C. T. (1998). Patterns of strain in the macaque ulna during functional activity. *American Journal of Physical Anthropology*, *106*(1), 87–100. https://doi.org/10.1002/(SICI)1096-8644(199805)106:1<87::AID-AJPA6>3.0.CO;2-A

Dempster, D. W., Compston, J. E., Drezner, M. K., Glorieux, F. H., Kanis, J. A., Malluche, H., Meunier, P. J., Ott, S. M., Recker, R. R., & Parfitt, A. M. (2013). Standardized nomenclature, symbols, and units for bone histomorphometry: A 2012 update of the report of the ASBMR Histomorphometry Nomenclature Committee. *Journal of Bone and Mineral Research*, *28*(1), 2–17. https://doi.org/10.1002/jbmr.1805

Dempster, D. W., & Lindsay, R. (1993). Pathogenesis of osteoporosis. *Lancet (London, England)*, *341*(8848), 797–801. https://doi.org/10.1016/0140-6736(93)90570-7

Dunn, I. C., Fleming, R. H., McCormack, H. A., Morrice, D., Burt, D. W., Preisinger, R., & Whitehead, C. C. (2007). A QTL for osteoporosis detected in an F $_2$ population derived from White Leghorn chicken lines divergently selected for bone index. *Animal Genetics*, *38*(1), 45–49. https://doi.org/10.1111/j.1365-2052.2006.01547.x

Eames, B. F., Amores, A., Yan, Y.-L., & Postlethwait, J. H. (2012). Evolution of the osteoblast: Skeletogenesis in gar and zebrafish. *BMC Evolutionary Biology*, *12*(1), 27–27. https://doi.org/10.1186/1471-2148-12-27

Enneking, S. A., Cheng, H. W., Jefferson-Moore, K. Y., Einstein, M. E., Rubin, D. A., & Hester, P. Y. (2012). Early access to perches in caged White Leghorn pullets. *Poultry Science*, *91*(9), 2114–2120. https://doi.org/10.3382/ps.2012-02328

Etches, R. J., & Cheng, K. W. (1981). Changes in the plasma concentrations of luteinizing hormone, progesterone, oestradiol and testosterone and in the binding of follicle-stimulating hormone to the theca of follicles during the ovulation cycle of the hen (Gallus domesticus). *The Journal of Endocrinology*, *91*(1), 11–22. https://doi.org/10.1677/joe.0.0910011

Fawcett, D. L., Casey-Trott, T. M., Jensen, L., Caston, L. J., & Widowski, T. M. (2020). Strain differences and effects of different stocking densities during rearing on the musculoskeletal development of pullets. *Poultry Science*, *99*(9), 4153–4161. https://doi.org/10.1016/j.psj.2020.05.046

Fleming, R. H., McCormack, H. A., McTeir, L., & Whitehead, C. C. (2006). Relationships between genetic, environmental and nutritional factors influencing osteoporosis in laying hens. *British Poultry Science*, *47*(6), 742–755. https://doi.org/10.1080/00071660601077949

Florencio-Silva, R., Sasso, G. R. S., Sasso-Cerri, E., Simões, M. J., & Cerri, P. S. (2018). Effects of estrogen status in osteocyte autophagy and its relation to osteocyte viability in alveolar process of ovariectomized rats. *Biomedicine & Pharmacotherapy = Biomedecine & Pharmacotherapie*, *98*, 406–415. https://doi.org/10.1016/j.biopha.2017.12.089

Fritton, S. P., McLeod, K. J., & Rubin, C. T. (2000). Quantifying the strain history of bone: Spatial uniformity and self-similarity of low-magnitude strains. *Journal of Biomechanics*, *33*(3), 317–325. https://doi.org/10.1016/s0021-9290(99)00210-9

Frost, H. M. (1969). Tetracycline-based histological analysis of bone remodeling. *Calcified Tissue Research*, *3*(1), 211–237. https://doi.org/10.1007/BF02058664

Frost, H. M. (1987). Bone "mass" and the "mechanostat": A proposal. *The Anatomical Record*, *219*(1), 1–9. https://doi.org/10.1002/ar.1092190104

Frost, H. M. (2004). A 2003 update of bone physiology and Wolff's Law for clinicians. *The Angle Orthodontist*, *74*(1), 3–15. https://doi.org/10.1043/0003-3219(2004)074<0003:AUOBPA>2.0.CO;2

Gatesy, S. M., & Biewener, A. A. (1991). Bipedal locomotion: Effects of speed, size and limb posture in birds and humans. *Journal of Zoology*, *224*(1), 127–147. https://doi.org/10.1111/j.1469-7998.1991.tb04794.x

Gill, F. B. (1995). *Ornithology*. W. H. Freeman.

Goodship, A. E., Lanyon, L. E., & McFie, H. (1979). Functional adaptation of bone to increased stress. An experimental study. *The Journal of Bone and Joint Surgery*, *61*(4), 539–546.

Grant, P. G., Buschang, P. H., Drolet, D. W., & Pickerell, C. (1980). Invariance of the relative positions of structures attached to long bones during growth: Cross-sectional and longitudinal studies. *Acta Anatomica*, *107*(1), 26–34. https://doi.org/10.1159/000145225

Gross, T. S., McLeod, K. J., & Rubin, C. T. (1992). Characterizing bone strain distributions in vivo using three triple rosette strain gages. *Journal of Biomechanics*, *25*(9), 1081–1087. https://doi.org/10.1016/0021-9290(92)90044-2

Hardin, E., Castro, F. L. S., & Kim, W. K. (2019). Keel bone injury in laying hens: The prevalence of injuries in relation to different housing systems, implications, and potential solutions. *World's Poultry Science Journal*, *75*(2), 285–292. https://doi.org/10.1017/S0043933919000011

Harlander-Matauschek, A., Rodenburg, T. B., Sandilands, V., Tobalske, B. W., & Toscano, M. J. (2015). Causes of keel bone damage and their solutions in laying hens. *World's Poultry Science Journal*, *71*(3), 461–472. https://doi.org/10.1017/S0043933915002135

Heerkens, J. L. T., Delezie, E., Rodenburg, T. B., Kempen, I., Zoons, J., Ampe, B., & Tuyttens, F. a. M. (2016). Risk factors associated with keel bone and foot pad disorders in laying hens housed in aviary systems. *Poultry Science*, *95*(3), 482–488. https://doi.org/10.3382/ps/pev339

Helgason, B., Taddei, F., Pálsson, H., Schileo, E., Cristofolini, L., Viceconti, M., & Brynjólfsson, S. (2008). A modified method for assigning material properties to FE models of bones. *Medical Engineering & Physics*, *30*(4), 444–453. https://doi.org/10.1016/j.medengphy.2007.05.006

Hester, P. Y., Enneking, S. A., Haley, B. K., Cheng, H. W., Einstein, M. E., & Rubin, D. A. (2013). The effect of perch availability during pullet rearing and egg laying on musculoskeletal health of caged White Leghorn hens. *Poultry Science*, *92*(8), 1972–1980. https://doi.org/10.3382/ps.2013-03008

Hogg, D. A. (1980). A re-investigation of the centres of ossification in the avian skeleton at and after hatching. *Journal of Anatomy*, *130*(Pt 4), 725–743.

Holguin, N., Brodt, M. D., Sanchez, M. E., Kotiya, A. A., & Silva, M. J. (2013). Adaptation of Tibial Structure and Strength to Axial Compression Depends on Loading History in Both C57BL/6 and BALB/c Mice. *Calcified Tissue International*, *93*(3), 211–221. https://doi.org/10.1007/s00223-013-9744-4

Hsieh, Y. F., & Turner, C. H. (2001). Effects of loading frequency on mechanically induced bone formation. *Journal of Bone and Mineral Research*, *16*(5), 918–924. https://doi.org/10.1359/jbmr.2001.16.5.918

Hudson, H. A., Britton, W. M., Rowland, G. N., & Buhr, R. J. (1993). Histomorphometric Bone Properties of Sexually Immature and Mature White Leghorn Hens with Evaluation of Fluorochrome Injection on Egg Production Traits. *Poultry Science*, *72*(8), 1537–1547. https://doi.org/10.3382/ps.0721537

Javaheri, B., Razi, H., Gohin, S., Wylie, S., Chang, Y.-M., Salmon, P., Lee, P. D., & Pitsillides, A. A. (2020). Lasting organ-level bone mechanoadaptation is unrelated to local strain. *Science Advances*, *6*(10), eaax8301. https://dx.doi.org/10.1126/sciadv.aax8301

Jendral, M. J., Korver, D. R., Church, J. S., & Feddes, J. J. R. (2008). Bone Mineral Density and Breaking Strength of White Leghorns Housed in Conventional, Modified, and Commercially Available Colony Battery Cages. *Poultry Science*, *87*(5), 828–837. https://doi.org/10.3382/ps.2007-00192

Jepsen, K. J., Silva, M. J., Vashishth, D., Guo, X. E., & van der Meulen, M. C. H. (2015). Establishing biomechanical mechanisms in mouse models: Practical guidelines for systematically evaluating phenotypic changes in the diaphyses of long bones. *Journal of Bone and Mineral Research: The Official Journal of the American Society for Bone and Mineral Research*, *30*(6), 951–966. https://doi.org/10.1002/jbmr.2539

Johnson, A. L., & van Tienhoven, A. (1980). Plasma concentrations of six steroids and LH during the ovulatory cycle of the hen, Gallus domesticus. *Biology of Reproduction*, *23*(2), 386–393. https://doi.org/10.1095/biolreprod23.2.386

Judex, S., & Zernicke, R. F. (2000). High-impact exercise and growing bone: Relation between high strain rates and enhanced bone formation. *Journal of Applied Physiology*, *88*(6), 2183–2191. https://doi.org/10.1152/jappl.2000.88.6.2183

Jung, L., Rufener, C., & Petow, S. (2022). A tagged visual analog scale is a reliable method to assess keel bone deviations in laying hens from radiographs. *Frontiers in Veterinary Science*, *9*. https://doi.org/10.3389/fvets.2022.937119

Kak, A. C., & Slaney, M. (2001). *Principles of computerized tomographic imaging* (1–1 online resource (xiv, 327 pages : illustrations). Society for Industrial and Applied Mathematics; WorldCat. http://www.books24x7.com/marc.asp?bookid=23044

Kameda, T., Mano, H., Yuasa, T., Mori, Y., Miyazawa, K., Shiokawa, M., Nakamaru, Y., Hiroi, E., Hiura, K., Kameda, A., Yang, N. N., Hakeda, Y., & Kumegawa, M. (1997). Estrogen Inhibits Bone Resorption by Directly Inducing Apoptosis of the Bone-resorbing Osteoclasts. *The Journal of Experimental Medicine*, *186*(4), 489–495.

Keaveny, T. M., Morgan, E. F., Niebur, G. L., & Yeh, O. C. (2001). Biomechanics of trabecular bone. *Annual Review of Biomedical Engineering*, *3*, 307–333. https://doi.org/10.1146/annurev.bioeng.3.1.307

Keenan, K. E., Mears, C. S., & Skedros, J. G. (2017). Utility of osteon circularity for determining species and interpreting load history in primates and nonprimates. *American Journal of Physical Anthropology*, *162*(4), 657–681. https://doi.org/10.1002/ajpa.23154

Keller, T. S., & Spengler, D. M. (1982). In vivo strain gage implantation in rats. *Journal of Biomechanics*, *15*(12), 911–917. https://doi.org/10.1016/0021-9290(82)90009-4

Keller, T. S., & Spengler, D. M. (1989). Regulation of bone stress and strain in the immature and mature rat femur. *Journal of Biomechanics*, *22*(11–12), 1115–1127. https://doi.org/10.1016/0021-9290(89)90213-3

Kerschnitzki, M., Zander, T., Zaslansky, P., Fratzl, P., Shahar, R., & Wagermaier, W. (2014). Rapid alterations of avian medullary bone material during the daily egg-laying cycle. *Bone*, *69*, 109–117. https://doi.org/10.1016/j.bone.2014.08.019

Khosla, S., Oursler, M. J., & Monroe, D. G. (2012). Estrogen and the Skeleton. *Trends in Endocrinology and Metabolism: TEM*, *23*(11), 576–581. https://doi.org/10.1016/j.tem.2012.03.008

Kim, W. K., Bloomfield, S. A., Sugiyama, T., & Ricke, S. C. (2012). Concepts and methods for understanding bone metabolism in laying hens. *World's Poultry Science Journal*, *68*(1), 71–82. https://doi.org/10.1017/S0043933912000086

Kittelsen, K. E., Toftaker, I., Tahamtani, F., Moe, R. O., Thøfner, I., & Vasdal, G. (2023). Keel bone fractures in broiler breeders: Is palpation a reliable diagnostic method? *Avian Pathology*, *52*(1), 78–83. https://doi.org/10.1080/03079457.2022.2147416

Klingensmith, P. M., Hester, P. Y., Elkin, R. G., & Ward, C. R. (1986). Relationship of high intensity step-up lighting to bone ash and growth plate closure of the tarso-metatarsus in Turkeys. *British Poultry Science*, *27*(3), 487–492. https://doi.org/10.1080/00071668608416907

Knowles, T. G., & Broom, D. M. (1990). Limb bone strength and movement in laying hens from different housing systems. *The Veterinary Record*, *126*(15), 354–356. https://doi.org/10.1136/vr.126.15.354

Kozak, M., Tobalske, B., Martins, C., Bowley, S., Wuerbel, H., & Harlander-Matauschek, A. (2016). Use of space by domestic chicks housed in complex aviaries. *Applied Animal Behaviour Science*, *181*, 115–121. https://doi.org/10.1016/j.applanim.2016.05.024

Krebs, J., Agellon, L. B., & Michalak, M. (2015). Ca(2+) homeostasis and endoplasmic reticulum (ER) stress: An integrated view of calcium signaling. *Biochemical and Biophysical Research Communications*, *460*(1), 114–121. https://doi.org/10.1016/j.bbrc.2015.02.004

Landauer, W., Pfeiffer, C. A., Gardner, W. U., & Shaw, J. C. (1941). Blood serum and skeletal changes in two breeds of ducks receiving estrogens. *Endocrinology*, *28*(3), 458–464. https://doi.org/10.1210/endo-28-3-458

Lanyon, L. E. (1972). In vivo bone strain recorded from thoracic vertebrae of sheep. *Journal of Biomechanics*, *5*(3), 277–281. https://doi.org/10.1016/0021-9290(72)90044-9

Lanyon, L. E. (1973). Analysis of surface bone strain in the calcaneus of sheep during normal locomotion. Strain analysis of the calcaneus. *Journal of Biomechanics*, *6*(1), 41–49. https://doi.org/10.1016/0021-9290(73)90036-5

Lanyon, L. E. (1987). Functional strain in bone tissue as an objective, and controlling stimulus for adaptive bone remodelling. *Journal of Biomechanics*, *20*(11–12), 1083–1093. https://doi.org/10.1016/0021-9290(87)90026-1

Lanyon, L. E., & Bourn, S. (1979). The influence of mechanical function on the development and remodeling of the tibia. An experimental study in sheep. *The Journal of Bone and Joint Surgery*, *61*(2), 263–273.

Lanyon, L. E., Hampson, W. G. J., Goodship, A. E., & Shah, J. S. (1975). Bone Deformation Recorded in vivo from Strain Gauges Attached to the Human Tibial Shaft. *Acta Orthopaedica Scandinavica*, *46*(2), 256–268. https://doi.org/10.3109/17453677508989216

Lanyon, L. E., Paul, I. L., Rubin, C. T., Thrasher, E. L., DeLaura, R., Rose, R. M., & Radin, E. L. (1981). In vivo strain measurements from bone and prosthesis following total hip replacement. An experimental study in sheep. *The Journal of Bone and Joint Surgery*, *63*(6), 989–1001.

Lanyon, L. E., & Rubin, C. T. (1984). Static vs dynamic loads as an influence on bone remodelling. *Journal of Biomechanics*, *17*(12), 897–905. https://doi.org/10.1016/0021-9290(84)90003-4

Lanyon, L. E., Rubin, C. T., & Baust, G. (1986). Modulation of bone loss during calcium insufficiency by controlled dynamic loading. *Calcified Tissue International*, *38*(4), 209–216. https://doi.org/10.1007/BF02556712

Lay, D. C., Fulton, R. M., Hester, P. Y., Karcher, D. M., Kjaer, J. B., Mench, J. A., Mullens, B. A., Newberry, R. C., Nicol, C. J., O'Sullivan, N. P., & Porter, R. E. (2011). Hen welfare in different housing systems1. *Poultry Science*, *90*(1), 278–294. https://doi.org/10.3382/ps.2010-00962

LeBlanc, C., Tobalske, B., Bowley, S., & Harlander-Matauschek, A. (2018). Development of locomotion over inclined surfaces in laying hens. *Animals*, *12*(3), 585–596. https://doi.org/10.1017/S1751731117001896

Lee, K. C. L., Maxwell, A., & Lanyon, L. E. (2002). Validation of a technique for studying functional adaptation of the mouse ulna in response to mechanical loading. *Bone*, *31*(3), 407–412. https://doi.org/10.1016/s8756-3282(02)00842-6

Levenston, M. E., Beaupré, G. S., & Carter, D. R. (1998). Loading Mode Interactions in Simulations of Long Bone Cross-Sectional Adaptation. *Computational Methods in Biomechanics and Biomedical Engineering*, *1*(4), 303–319. https://doi.org/10.1080/01495739808936709

Lewis, K. J., Frikha-Benayed, D., Louie, J., Stephen, S., Spray, D. C., Thi, M. M., Seref-Ferlengez, Z., Majeska, R. J., Weinbaum, S., & Schaffler, M. B. (2017). Osteocyte calcium signals encode strain magnitude and loading frequency in vivo. *Proceedings of*

the National Academy of Sciences of the United States of America, *114*(44), 11775–11780. https://doi.org/10.1073/pnas.1707863114

Leyendecker, M., Hamann, H., Hartung, J., Kamphues, J., Neumann, U., Sürie, C., & Distl, O. (2005). Keeping laying hens in furnished cages and an aviary housing system enhances their bone stability. *British Poultry Science*, *46*(5), 536–544. https://doi.org/10.1080/00071660500273094

Lieberman, D. E., Polk, J. D., & Demes, B. (2004). Predicting long bone loading from cross-sectional geometry. *American Journal of Physical Anthropology*, *123*(2), 156–171. https://doi.org/10.1002/ajpa.10316

Loitz, B. J., & Zernicke, R. F. (1992). Strenuous exercise-induced remodelling of mature bone: Relationships between in vivo strains and bone mechanics. *Journal of Experimental Biology*, *170*, 1–18. https://doi.org/10.1242/jeb.170.1.1

Main, R. P. (2007). Ontogenetic relationships between in vivo strain environment, bone histomorphometry and growth in the goat radius. *Journal of Anatomy*, *210*(3), 272–293. https://doi.org/10.1111/j.1469-7580.2007.00696.x

Main, R. P. (2021a). Basic Principles and Methodologies in Measuring Bone Biomechanics. In *Vertebrate Skeletal Histology and Paleohistology*. CRC Press.

Main, R. P. (2021b). Basic Principles and Methodoologies in Measuring Bone Biomechanics. In A. J. de R. Vivian de Buffrénil Louise Zylberberg, Kevin Padian (Ed.), *Vertebrate Skeletal Histology and Paleohistology*.

Main, R. P. (2021c). Basic Principles and Methodoologies in Measuring Bone Biomechanics. In A. J. de R. Vivian de Buffrénil Louise Zylberberg, Kevin Padian (Ed.), *Vertebrate Skeletal Histology and Paleohistology*.

Main, R. P., & Biewener, A. A. (2007). Skeletal strain patterns and growth in the emu hindlimb during ontogeny. *Journal of Experimental Biology*, *210*(15), 2676–2690. https://doi.org/10.1242/jeb.004580

Main, R. P., Lynch, M. E., & van der Meulen, M. C. H. (2010). In vivo tibial stiffness is maintained by whole bone morphology and cross-sectional geometry in growing female mice. *Journal of Biomechanics*, *43*(14), 2689–2694. https://doi.org/10.1016/j.jbiomech.2010.06.019

Main, R. P., Lynch, M. E., & van der Meulen, M. C. H. (2014). Load-induced changes in bone stiffness and cancellous and cortical bone mass following tibial compression diminish with age in female mice. *Journal of Experimental Biology*, jeb.085522. https://doi.org/10.1242/jeb.085522

Main, R. P., Shefelbine, S. J., Meakin, L. B., Silva, M. J., Meulen, M. C. H., & Willie, B. M. (2020). Murine Axial Compression Tibial Loading Model to Study Bone Mechanobiology: Implementing the Model and Reporting Results. *Journal of Orthopaedic Research*, *38*(2), 233–252. https://doi.org/10.1002/jor.24466

Malomane, D. K., Simianer, H., Weigend, A., Reimer, C., Schmitt, A. O., & Weigend, S. (2019). The SYNBREED chicken diversity panel: A global resource to assess chicken diversity at high genomic resolution. *BMC Genomics*, *20*(1), 345. https://doi.org/10.1186/s12864-019-5727-9

Manley, P. A., Schatzker, J., & Sumner-Smith, G. (1982). Evaluation of tension and compression forces in the canine femur in vivo. *Archives of Orthopaedic and Traumatic Surgery. Archiv Fur Orthopadische Und Unfall-Chirurgie*, *99*(3), 213–216. https://doi.org/10.1007/BF00379211

Meakin, L. B., Price, J. S., & Lanyon, L. E. (2014). The Contribution of Experimental in vivo Models to Understanding the Mechanisms of Adaptation to Mechanical Loading in Bone. *Frontiers in Endocrinology*, *5*, 154. https://doi.org/10.3389/fendo.2014.00154

Meakin, L. B., Sugiyama, T., Galea, G. L., Browne, W. J., Lanyon, L. E., & Price, J. S. (2013). Male mice housed in groups engage in frequent fighting and show a lower response to additional bone loading than females or individually housed males that do not fight. *Bone*, *54*(1), 113–117. https://doi.org/10.1016/j.bone.2013.01.029

Milgrom, C., Burr, D. B., Finestone, A. S., & Voloshin, A. (2015). Understanding the etiology of the posteromedial tibial stress fracture. *Bone*, *78*, 11–14. https://doi.org/10.1016/j.bone.2015.04.033

Milgrom, C., Finestone, A., Simkin, A., Ekenman, I., Mendelson, S., Millgram, M., Nyska, M., Larsson, E., & Burr, D. (2000). In-vivo strain measurements to evaluate the strengthening potential of exercises on the tibial bone. *The Journal of Bone and Joint Surgery*, *82*(4), 591–594. https://doi.org/10.1302/0301-620x.82b4.9677

Milgrom, C., Voloshin, A., Novack, L., Milgrom, Y., Ekenman, I., & Finestone, A. S. (2022). In vivo strains at the middle and distal thirds of the tibia during exertional activities. *Bone Reports*, *16*, 101170. https://doi.org/10.1016/j.bonr.2022.101170

Miller, S. C., & Bowman, B. M. (1981). Medullary bone osteogenesis following estrogen administration to mature male Japanese quail. *Developmental Biology*, *87*(1), 52–63. https://doi.org/10.1016/0012-1606(81)90060-9

Mirzaali, M. J., Schwiedrzik, J. J., Thaiwichai, S., Best, J. P., Michler, J., Zysset, P. K., & Wolfram, U. (2016). Mechanical properties of cortical bone and their relationships with

age, gender, composition and microindentation properties in the elderly. *Bone*, *93*, 196–211. https://doi.org/10.1016/j.bone.2015.11.018

Moreno, C. A., Main, R. P., & Biewener, A. A. (2008). Variability in forelimb bone strains during non-steady locomotor activities in goats. *Journal of Experimental Biology*, *211*(Pt 7), 1148–1162. https://doi.org/10.1242/jeb.012419

Morgan, E. F., Unnikrisnan, G. U., & Hussein, A. I. (2018). Bone Mechanical Properties in Healthy and Diseased States. *Annual Review of Biomedical Engineering*, *20*, 119–143. https://doi.org/10.1146/annurev-bioeng-062117-121139

Mori, S., & Burr, D. B. (1993). Increased intracortical remodeling following fatigue damage. *Bone*, *14*(2), 103–109. https://doi.org/10.1016/8756-3282(93)90235-3

Mosley, J. R., & Lanyon, L. E. (1998). Strain rate as a controlling influence on adaptive modeling in response to dynamic loading of the ulna in growing male rats. *Bone*, *23*(4), 313–318.

Mosley, J. R., March, B. M., Lynch, J., & Lanyon, L. E. (1997). Strain magnitude related changes in whole bone architecture in growing rats. *Bone*, *20*(3), 191–198. https://doi.org/10.1016/s8756-3282(96)00385-7

Nasr, M. A. F., Nicol, C. J., & Murrell, J. C. (2012). Do Laying Hens with Keel Bone Fractures Experience Pain? *PLOS ONE*, *7*(8), e42420. https://doi.org/10.1371/journal.pone.0042420

Nasr, M. A., Nicol, C. J., Wilkins, L., & Murrell, J. C. (2015). The effects of two non-steroidal anti-inflammatory drugs on the mobility of laying hens with keel bone fractures. *Veterinary Anaesthesia and Analgesia*, *42*(2), 197–204. https://doi.org/10.1111/vaa.12175

Newman, S., & Leeson, S. (1998). Effect of housing birds in cages or an aviary system on bone characteristics. *Poultry Science*, *77*(10), 1492–1496. https://doi.org/10.1093/ps/77.10.1492

Nigg, B. M., & Wakeling, J. M. (2001). Impact Forces and Muscle Tuning: A New Paradigm: *Exercise and Sport Sciences Reviews*, *29*(1), 37–41. https://doi.org/10.1097/00003677-200101000-00008

Nunamaker, D. M., Butterweck, D. M., & Provost, M. T. (1990). Fatigue fractures in thoroughbred racehorses: Relationships with age, peak bone strain, and training. *Journal of Orthopaedic Research*, *8*(4), 604–611. https://doi.org/10.1002/jor.1100080417

Nyman, J. S., Roy, A., Acuna, R. L., Gayle, H. J., Reyes, M. J., Tyler, J. H., Dean, D. D., & Wang, X. (2006). AGE-RELATED EFFECT ON THE CONCENTRATION OF COLLAGEN CROSSLINKS IN HUMAN OSTEONAL AND INTERSTITIAL BONE TISSUE. *Bone*, *39*(6), 1210–1217. https://doi.org/10.1016/j.bone.2006.06.026

Otsu, N. (1979). A Threshold Selection Method from Gray-Level Histograms. *IEEE Transactions on Systems, Man, and Cybernetics*, *9*(1), 62–66. IEEE Transactions on Systems, Man, and Cybernetics. https://doi.org/10.1109/TSMC.1979.4310076

Paschalis, E. P., Tatakis, D. N., Robins, S., Fratzl, P., Manjubala, I., Zoehrer, R., Gamsjaeger, S., Buchinger, B., Roschger, A., Phipps, R., Boskey, A. L., Dall'Ara, E., Varga, P., Zysset, P., Klaushofer, K., & Roschger, P. (2011). Lathyrism-induced alterations in collagen cross-links influence the mechanical properties of bone material without affecting the mineral. *Bone*, *49*(6), 1232–1241. https://doi.org/10.1016/j.bone.2011.08.027

Pattin, C. A., Caler, W. E., & Carter, D. R. (1996). Cyclic mechanical property degradation during fatigue loading of cortical bone. *Journal of Biomechanics*, *29*(1), 69–79. https://doi.org/10.1016/0021-9290(94)00156-1

Pauwels, F. (1980). *Biomechanics of the locomotor apparatus*. Springer-Verlag.

Peng, L., Bai, J., Zeng, X., & Zhou, Y. (2006). Comparison of isotropic and orthotropic material property assignments on femoral finite element models under two loading conditions. *Medical Engineering & Physics*, *28*(3), 227–233. https://doi.org/10.1016/j.medengphy.2005.06.003

Petrik, M. T., Guerin, M. T., & Widowski, T. M. (2013). Keel fracture assessment of laying hens by palpation: Inter-observer reliability and accuracy. *The Veterinary Record*, *173*(20), 500. https://doi.org/10.1136/vr.101934

Pezzotti, G., & Sakakura, S. (2003). Study of the toughening mechanisms in bone and biomimetic hydroxyapatite materials using Raman microprobe spectroscopy. *Journal of Biomedical Materials Research Part A*, *65A*(2), 229–236. https://doi.org/10.1002/jbm.a.10447

Pithioux, M., Lasaygues, P., & Chabrand, P. (2002). An alternative ultrasonic method for measuring the elastic properties of cortical bone. *Journal of Biomechanics*, *35*(7), 961–968. https://doi.org/10.1016/s0021-9290(02)00027-1

Prondvai, E., & Stein, K. H. W. (2014). Medullary bone-like tissue in the mandibular symphyses of a pterosaur suggests non-reproductive significance. *Scientific Reports*, *4*(1), 6253. https://doi.org/10.1038/srep06253

Pufall, A., Harlander-Matauschek, A., Hunniford, M., & Widowski, T. M. (2021). Effects of Rearing Aviary Style and Genetic Strain on the Locomotion and Musculoskeletal

Characteristics of Layer Pullets. *Animals*, *11*(3), 634. https://doi.org/10.3390/ani11030634

Rabkin, B. A., Szivek, J. A., Schonfeld, J. E., & Halloran, B. P. (2001). Long-term measurement of bone strain in vivo: The rat tibia. *Journal of Biomedical Materials Research*, *58*(3), 277–281. https://doi.org/10.1002/1097-4636(2001)58:3<277::aid-jbm1017>3.0.co;2-t

Raymond, B., Johansson, A. M., McCormack, H. A., Fleming, R. H., Schmutz, M., Dunn, I. C., & De Koning, D. J. (2018). Genome-wide association study for bone strength in laying hens1. *Journal of Animal Science*, *96*(7), 2525–2535. https://doi.org/10.1093/jas/sky157

Razi, H., Birkhold, A. I., Weinkamer, R., Duda, G. N., Willie, B. M., & Checa, S. (2015). Aging Leads to a Dysregulation in Mechanically Driven Bone Formation and Resorption. *Journal of Bone and Mineral Research: The Official Journal of the American Society for Bone and Mineral Research*, *30*(10), 1864–1873. https://doi.org/10.1002/jbmr.2528

Razi, H., Birkhold, A. I., Zaslansky, P., Weinkamer, R., Duda, G. N., Willie, B. M., & Checa, S. (2015). Skeletal maturity leads to a reduction in the strain magnitudes induced within the bone: A murine tibia study. *Acta Biomaterialia*, *13*, 301–310. https://doi.org/10.1016/j.actbio.2014.11.021

Regmi, P., Cox, A. G., Robison, C. I., & Karcher, D. M. (2017). Correlation analysis of cortical geometry of tibia and humerus of white leghorns using clinical quantitative computed tomography and microcomputed tomography scans1. *Poultry Science*, *96*(8), 2950–2955. https://doi.org/10.3382/ps/pex064

Regmi, P., Deland, T. S., Steibel, J. P., Robison, C. I., Haut, R. C., Orth, M. W., & Karcher, D. M. (2015). Effect of rearing environment on bone growth of pullets. *Poultry Science*, *94*(3), 502–511. https://doi.org/10.3382/ps/peu041

Regmi, P., Smith, N., Nelson, N., Haut, R. C., Orth, M. W., & Karcher, D. M. (2016). Housing conditions alter properties of the tibia and humerus during the laying phase in Lohmann white Leghorn hens. *Poultry Science*, *95*(1), 198–206. https://doi.org/10.3382/ps/pev209

Reilly, D. T., & Burstein, A. H. (1975). The elastic and ultimate properties of compact bone tissue. *Journal of Biomechanics*, *8*(6), 393–405. https://doi.org/10.1016/0021-9290(75)90075-5

Reilly, G. C., & Currey, J. D. (1999). The development of microcracking and failure in bone depends on the loading mode to which it is adapted. *Journal of Experimental Biology*, *202*(Pt 5), 543–552. https://doi.org/10.1242/jeb.202.5.543

Rentsch, A. K., Harlander, A., Siegford, J. M., Vitienes, I., Willie, B. M., & Widowski, T. M. (2023a). Rearing laying hens: The effect of aviary design and genetic strain on pullet exercise and perching behavior. *Frontiers in Animal Science*, *4*. https://doi.org/10.3389/fanim.2023.1176702

Rentsch, A. K., Harlander, A., Siegford, J., Vitienes, I., Willie, B., & Widowski, T. (2023b). Rearing laying hens: The effect of aviary design and genetic strain on pullet exercise and perching behavior. *Frontiers*, *Under review*.

Reznikov, N., Bilton, M., Lari, L., Stevens, M. M., & Kröger, R. (2018). Fractal-like hierarchical organization of bone begins at the nanoscale. *Science*, *360*(6388), eaao2189. https://doi.org/10.1126/science.aao2189

Reznikov, N., Shahar, R., & Weiner, S. (2014). Bone hierarchical structure in three dimensions. *Acta Biomaterialia*, *10*(9), 3815–3826. https://doi.org/10.1016/j.actbio.2014.05.024

Riber, A., & Hinrichsen, L. (2016). Keel-bone damage and foot injuries in commercial laying hens in Denmark. *Animal Welfare*, *25*(2), 179–184. https://doi.org/10.7120/09627286.25.2.179

Richards, G. J., Nasr, M. A., Brown, S. N., Szamocki, E. M. G., Murrell, J., Barr, F., & Wilkins, L. J. (2011). Use of radiography to identify keel bone fractures in laying hens and assess healing in live birds. *The Veterinary Record*, *169*(11), 279. https://doi.org/10.1136/vr.d4404

Riggs, C. M., Lanyon, L. E., & Boyde, A. (1993). Functional associations between collagen fibre orientation and locomotor strain direction in cortical bone of the equine radius. *Anatomy and Embryology*, *187*(3), 231–238. https://doi.org/10.1007/bf00195760

Riggs, C. M., Vaughan, L. C., Evans, G. P., Lanyon, L. E., & Boyde, A. (1993). Mechanical implications of collagen fibre orientation in cortical bone of the equine radius. *Anatomy and Embryology*, *187*(3), 239–248. https://doi.org/10.1007/BF00195761

Robling, A. G., Burr, D. B., & Turner, C. H. (2000). Partitioning a daily mechanical stimulus into discrete loading bouts improves the osteogenic response to loading. *Journal of Bone and Mineral Research: The Official Journal of the American Society for Bone and Mineral Research*, *15*(8), 1596–1602. https://doi.org/10.1359/jbmr.2000.15.8.1596

Robling, A. G., & Turner, C. H. (2002). Mechanotransduction in bone: Genetic effects on mechanosensitivity in mice. *Bone*, *31*(5), 562–569. https://doi.org/10.1016/s8756-3282(02)00871-2

Roche, R., Abel, R., Johnson, K., & Perry, C. (2010). Quantification of porosity in Acropora pulchra (Brook 1891) using X-ray micro-computed tomography techniques. *Journal of*

Experimental Marine Biology and Ecology, *396*. https://doi.org/10.1016/j.jembe.2010.10.006

Rodenburg, B., Tuyttens, F., Reu, K., Herman, L., Zoons, J., & Sonck, B. (2008). Welfare assessment of laying hens in furnished cages and non-cage systems: An on-farm comparison. *Animal Welfare 17 (2008) 4*, *17*. https://doi.org/10.1017/S096272860002786X

Romanoff, A. L. (1960). *The Avian Embryo*. Macmillan.

Ross, E. (2021). Thesis: The Effect of Early Rearing Environment on Musculoskeletal Traits and Proximate Composition in Laying Hen Pullets. In *Animal Biosciences: Vol. Master of Science*. University of Guelph.

Roux, W. (1881). *Der Kamf der Teile im Organismus*. Wilhelm Engelmann.

Rubin, C. T., Bain, S. D., & McLeod, K. J. (1992). Suppression of the osteogenic response in the aging skeleton. *Calcified Tissue International*, *50*(4), 306–313. https://doi.org/10.1007/BF00301627

Rubin, C. T., & Lanyon, L. E. (1982). Limb mechanics as a function of speed and gait: A study of functional strains in the radius and tibia of horse and dog. *Journal of Experimental Biology*, *101*, 187–211. https://doi.org/10.1242/jeb.101.1.187

Rubin, C. T., & Lanyon, L. E. (1984a). Dynamic strain similarity in vertebrates; an alternative to allometric limb bone scaling. *Journal of Theoretical Biology*, *107*(2), 321–327. https://doi.org/10.1016/S0022-5193(84)80031-4

Rubin, C. T., & Lanyon, L. E. (1984b). Regulation of bone formation by applied dynamic loads. *The Journal of Bone and Joint Surgery*, *66*(3), 397–402.

Rubin, C. T., & Lanyon, L. E. (1985). Regulation of bone mass by mechanical strain magnitude. *Calcified Tissue International*, *37*(4), 411–417. https://doi.org/10.1007/BF02553711

Rubin, C. T., & Lanyon, L. E. (1987). Osteoregulatory nature of mechanical stimuli: Function as a determinant for adaptive remodeling in bone. *Journal of Orthopaedic Research: Official Publication of the Orthopaedic Research Society*, *5*(2), 300–310. https://doi.org/10.1002/jor.1100050217

Rufener, C., Baur, S., Stratmann, A., & Toscano, M. J. (2018). A Reliable Method to Assess Keel Bone Fractures in Laying Hens From Radiographs Using a Tagged Visual Analogue Scale. *Frontiers in Veterinary Science*, *5*. https://doi.org/10.3389/fvets.2018.00124

Rufener, C., & Makagon, M. M. (2020). Keel bone fractures in laying hens: A systematic review of prevalence across age, housing systems, and strains. *Journal of Animal Science*, *98*(Suppl 1), S36-s51. https://doi.org/10.1093/jas/skaa145

Rummler, M., Ziouti, F., Bouchard, A. L., Brandl, A., Duda, G. N., Bogen, B., Beilhack, A., Lynch, M. E., Jundt, F., & Willie, B. M. (2021). Mechanical loading prevents bone destruction and exerts anti-tumor effects in the MOPC315.BM.Luc model of myeloma bone disease. *Acta Biomaterialia*, *119*, 247–258. https://doi.org/10.1016/j.actbio.2020.10.041

Samuels, A., Perry, M. J., & Tobias, J. H. (1999). High-Dose Estrogen Induces De Novo Medullary Bone Formation in Female Mice. *Journal of Bone and Mineral Research*, *14*(2), 178–186. https://doi.org/10.1359/jbmr.1999.14.2.178

Schaffler, M. B., & Kennedy, O. D. (2012). Osteocyte Signaling in Bone. *Current Osteoporosis Reports*, *10*(2), 118–125. https://doi.org/10.1007/s11914-012-0105-4

Schaffler, M. B., Radin, E. L., & Burr, D. B. (1989). Mechanical and morphological effects of strain rate on fatigue of compact bone. *Bone, 10*(3), 207–214. https://doi.org/10.1016/8756-3282(89)90055-0

Shahar, R., Zaslansky, P., Barak, M., Friesem, A. A., Currey, J. D., & Weiner, S. (2007). Anisotropic Poisson's ratio and compression modulus of cortical bone determined by speckle interferometry. *Journal of Biomechanics, 40*(2), 252–264. https://doi.org/10.1016/j.jbiomech.2006.01.021

Shapiro, F., & Wu, J. Y. (2019). Woven bone overview: Structural classification based on its integral role in developmental, repair and pathological bone formation throughout vertebrate groups. *European Cells & Materials, 38*, 137–167. https://doi.org/10.22203/eCM.v038a11

Sheffield, K. M., Butcher, M. T., Shugart, S. K., Gander, J. C., & Blob, R. W. (2011). Locomotor loading mechanics in the hindlimbs of tegu lizards (Tupinambis merianae): Comparative and evolutionary implications. *Journal of Experimental Biology, 214*(15), 2616–2630. https://doi.org/10.1242/jeb.048801

Shipov, A., Sharir, A., Zelzer, E., Milgram, J., Monsonego-Ornan, E., & Shahar, R. (2010). The influence of severe prolonged exercise restriction on the mechanical and structural properties of bone in an avian model. *Veterinary Journal (London, England: 1997), 183*(2), 153–160. https://doi.org/10.1016/j.tvjl.2008.11.015

Silva, M. J., Brodt, M. D., Lynch, M. A., Stephens, A. L., Wood, D. J., & Civitelli, R. (2012). Tibial Loading Increases Osteogenic Gene Expression and Cortical Bone Volume in Mature and Middle-Aged Mice. *PLoS ONE, 7*(4), e34980. https://doi.org/10.1371/journal.pone.0034980

Singer, A., Ben-Yehuda, O., Ben-Ezra, Z., & Zaltzman, S. (1990). Miltiple Identical Stress Fractures in Monozygotic Twins. *The Journal of Bone and Joint Surgery*, *72*(3), 444–445.

Skedros, J. G., Dayton, M. R., Sybrowsky, C. L., Bloebaum, R. D., & Bachus, K. N. (2006). The influence of collagen fiber orientation and other histocompositional characteristics on the mechanical properties of equine cortical bone. *The Journal of Experimental Biology*, *209*(Pt 15), 3025–3042. https://doi.org/10.1242/jeb.02304

Skedros, J. G., Hunt, K. J., & Bloebaum, R. D. (2004). Relationships of loading history and structural and material characteristics of bone: Development of the mule deer calcaneus. *Journal of Morphology*, *259*(3), 281–307. https://doi.org/10.1002/jmor.10167

Skedros, J. G., Mason, M. W., Nelson, M. C., & Bloebaum, R. D. (1996). Evidence of structural and material adaptation to specific strain features in cortical bone. *Anatomical Record*, *246*(1), 47–63. https://doi.org/10.1002/(sici)1097-0185(199609)246:1<47::Aid-ar6>3.0.Co;2-c

Skedros, J. G., Mendenhall, S. D., Kiser, C. J., & Winet, H. (2009). Interpreting cortical bone adaptation and load history by quantifying osteon morphotypes in circularly polarized light images. *Bone*, *44*(3), 392–403. https://doi.org/10.1016/j.bone.2008.10.053

Skedros, J. G., Sorenson, S. M., Hunt, K. J., & Holyoak, J. D. (2007). Ontogenetic structural and material variations in ovine calcanei: A model for interpreting bone adaptation. *Anatomical Record (Hoboken, N.J.: 2007)*, *290*(3), 284–300. https://doi.org/10.1002/ar.20423

Sperrin, M., & Winder, J. (2014). Computed tomography. In *Scientific Basis of the Royal College of Radiologists Fellowship: Illustrated questions and answers*. IOP Publishing. https://doi.org/10.1088/978-0-7503-1058-1ch5

Srinivasan, S., Agans, S. C., King, K. A., Moy, N. Y., Poliachik, S. L., & Gross, T. S. (2003). Enabling bone formation in the aged skeleton via rest-inserted mechanical loading. *Bone*, *33*(6), 946–955. https://doi.org/10.1016/j.bone.2003.07.009

Srinivasan, S., Weimer, D. A., Agans, S. C., Bain, S. D., & Gross, T. S. (2002). Low-magnitude mechanical loading becomes osteogenic when rest is inserted between each load cycle. *Journal of Bone and Mineral Research: The Official Journal of the American Society for Bone and Mineral Research*, *17*(9), 1613–1620. https://doi.org/10.1359/jbmr.2002.17.9.1613

Stratmann, A., Fröhlich, E. K., Gebhardt-Henrich, S. G., Harlander-Matauschek, A., Würbel, H., & Toscano, M. J. (2016). Genetic selection to increase bone strength affects prevalence of keel bone damage and egg parameters in commercially housed laying hens. *Poultry Science*, *95*(5), 975–984. https://doi.org/10.3382/ps/pew026

Sugiyama, T., Meakin, L. B., Browne, W. J., Galea, G. L., Price, J. S., & Lanyon, L. E. (2012). Bones' adaptive response to mechanical loading is essentially linear between the low strains associated with disuse and the high strains associated with the lamellar/woven bone transition. *Journal of Bone and Mineral Research*, *27*(8), 1784–1793. https://doi.org/10.1002/jbmr.1599

Sun, D., Brodt, M. D., Zannit, H. M., Holguin, N., & Silva, M. J. (2018). Evaluation of loading parameters for murine axial tibial loading: Stimulating cortical bone formation while

reducing loading duration. *Journal of Orthopaedic Research*, *36*(2), 682–691. https://doi.org/10.1002/jor.23727

Swartz, S. M., Bennett, M. B., & Carrier, D. R. (1992). Wing bone stresses in free flying bats and the evolution of skeletal design for flight. *Nature*, *359*(6397), Article 6397. https://doi.org/10.1038/359726a0

Swartz, S. M., Bertram, J. E., & Biewener, A. A. (1989). Telemetered in vivo strain analysis of locomotor mechanics of brachiating gibbons. *Nature*, *342*(6247), 270–272. https://doi.org/10.1038/342270a0

Tanka Khanal, G. Y. B., Tina M. Widowski, Elijah G. Kiarie. (2020). Rearing cage type and dietary limestone particle size: II, effects on egg production, eggshell, and bone quality in Lohmann selected Leghorn-Lite hens. *Poultry Science*, *99*(11), 5763–5770.

Taylor, D., Falsetti, F., O'Brien, F., O'Reilly, P., Banville, E., & Clive Lee, T. (2001). A Fatigue-Based Model of Disuse Osteoporosis. *Computer Methods in Biomechanics and Biomedical Engineering*, *4*(5), 413–420. https://doi.org/10.1080/10255840108908017

Thøfner, I., Hougen, H. P., Villa, C., Lynnerup, N., & Christensen, J. P. (2020). Pathological characterization of keel bone fractures in laying hens does not support external trauma as the underlying cause. *PloS One*, *15*(3), e0229735. https://doi.org/10.1371/journal.pone.0229735

Toscano, M., Booth, F., Richards, G., Brown, S., Karcher, D., & Tarlton, J. (2018). Modeling collisions in laying hens as a tool to identify causative factors for keel bone fractures and means to reduce their occurrence and severity. *PloS One*, *13*(7), e0200025. https://doi.org/10.1371/journal.pone.0200025

Toscano, M. J., Dunn, I. C., Christensen, J.-P., Petow, S., Kittelsen, K., & Ulrich, R. (2020). Explanations for keel bone fractures in laying hens: Are there explanations in addition to elevated egg production? *Poultry Science*, *99*(9), 4183–4194. https://doi.org/10.1016/j.psj.2020.05.035

Turner, C. H., Forwood, M. R., Rho, J. Y., & Yoshikawa, T. (1994). Mechanical loading thresholds for lamellar and woven bone formation. *Journal of Bone and Mineral Research*, *9*(1), 87–97. https://doi.org/10.1002/jbmr.5650090113

Turner, C. H., Owan, I., & Takano, Y. (1995). Mechanotransduction in bone: Role of strain rate. *The American Journal of Physiology*, *269*(3 Pt 1), E438-442. https://doi.org/10.1152/ajpendo.1995.269.3.E438

Umemura, Y., Ishiko, T., Yamauchi, T., Kurono, M., & Mashiko, S. (1997). Five jumps per day increase bone mass and breaking force in rats. *Journal of Bone and Mineral Research*, *12*(9), 1480–1485. https://doi.org/10.1359/jbmr.1997.12.9.1480

van der Meulen, M. C. H., Jepsen, K. J., & Mikić, B. (2001). Understanding bone strength: Size isn't everything. *Bone*, *29*(2), 101–104. https://doi.org/10.1016/S8756-3282(01)00491-4

van der Meulen, M. C. H., Morgan, T. G., Yang, X., Baldini, T. H., Myers, E. R., Wright, T. M., & Bostrom, M. P. G. (2006). Cancellous bone adaptation to in vivo loading in a rabbit model. *Bone*, *38*(6), 871–877. https://doi.org/10.1016/j.bone.2005.11.026

van Tol, A. F., Roschger, A., Repp, F., Chen, J., Roschger, P., Berzlanovich, A., Gruber, G. M., Fratzl, P., & Weinkamer, R. (2020). Network architecture strongly influences the fluid flow pattern through the lacunocanalicular network in human osteons. *Biomechanics and Modeling in Mechanobiology*, *19*(3), 823–840. https://doi.org/10.1007/s10237-019-01250-1

van Tol, A. F., Schemenz, V., Wagermaier, W., Roschger, A., Razi, H., Vitienes, I., Fratzl, P., Willie, B. M., & Weinkamer, R. (2020). The mechanoresponse of bone is closely related to the osteocyte lacunocanalicular network architecture. *Proceedings of the National Academy of Sciences of the United States of America*, *117*(51), 32251–32259. https://doi.org/10.1073/pnas.2011504117

Verner, K. A. (2017). *Skeletal Biomechanics and Response to Mechanical Load: A Comparative Approach in the Mouse and Chuckar Partridge*. Purdue University.

Vitienes, I., Mikolajewicz, N., Hosseinitabatabaei, S., Bouchard, A., Julien, C., Graceffa, G., Rentsch, A., Widowski, T., Main, R. P., & Willie, B. M. (2023). Breed and loading history influence in vivo skeletal strain patterns in pre-pubertal female chickens. *Bone*, *173*, 116785. https://doi.org/10.1016/j.bone.2023.116785

Vitienes, I., Rentsch, A., Widowski, T., Checa, S., & Willie, B. (2024, July). *Bone geometry and mineral density influence mechanical strain magnitude and patterns across the tibiotarsus*. Poultry Science Association Annual Meeting, Louisville, Kentucky, U.S.A.

Vitienes, I., Ross, E., Bouchard, A., Steyn, B., Widowski, T., & Willie, B. (2021, October). *Aviary rearing enhances bone microstructure in Lohmann LSL-Lite and bone mass in Lohmann Brown Lite egg-laying hen pullets compared to conventional cage-rearing*. American Society for Bone and Mineral Research, San Diego, California, U.S.A.

Wagner, D. O., & Aspenberg, P. (2011). Where did bone come from? *Acta Orthopaedica*, *82*(4), 393–398. https://doi.org/10.3109/17453674.2011.588861

Wang, M.-S., Thakur, M., Peng, M.-S., Jiang, Y., Frantz, L. A. F., Li, M., Zhang, J.-J., Wang, S., Peters, J., Otecko, N. O., Suwannapoom, C., Guo, X., Zheng, Z.-Q., Esmailizadeh, A., Hirimuthugoda, N. Y., Ashari, H., Suladari, S., Zein, M. S. A., Kusza, S., … Zhang, Y.-

P. (2020). 863 genomes reveal the origin and domestication of chicken. *Cell Research*, *30*(8), 693–701. https://doi.org/10.1038/s41422-020-0349-y

Wang, S., Hu, Y., Wu, Y., Liu, Y., Liu, G., Yan, Z., Li, Q., Zhou, Z., & Li, Z. (2019). Influences of bioapatite mineral and fibril structure on the mechanical properties of chicken bone during the laying period. *Poultry Science*, *98*(12), 6393–6399. https://doi.org/10.3382/ps/pez474

Warden, S. J., Mantila Roosa, S. M., Kersh, M. E., Hurd, A. L., Fleisig, G. S., Pandy, M. G., & Fuchs, R. K. (2014). Physical activity when young provides lifelong benefits to cortical bone size and strength in men. *Proceedings from the National Academy of Sciences of the United States of America*, *111*(14), 5337–5342. https://doi.org/10.1073/pnas.1321605111

Warden, S. J., & Turner, C. H. (2004). Mechanotransduction in the cortical bone is most efficient at loading frequencies of 5-10 Hz. *Bone*, *34*(2), 261–270. https://doi.org/10.1016/j.bone.2003.11.011

Welten, D. C., Kemper, H. C., Post, G. B., Van Mechelen, W., Twisk, J., Lips, P., & Teule, G. J. (1994). Weight-bearing activity during youth is a more important factor for peak bone mass than calcium intake. *Journal of Bone and Mineral Research*, *9*(7), 1089–1096. https://doi.org/10.1002/jbmr.5650090717

Whitehead, C. C. (n.d.). Bone breakage and osteoporosis in laying hens: Causes and solutions. *Poultry Science*, *83*, 193–199.

Whitehead, C. C. (2004a). Overview of bone biology in the egg-laying hen. *Poultry Science*, *83*(2), 193–199.

Whitehead, C. C. (2004b). Overview of bone biology in the egg-laying hen. *Poultry Science*, *83*(2), 193–199.

Whitehead, C. C., & Fleming, R. H. (2000). Osteoporosis in cage layers. *Poultry Science*, *79*(7), 1033–1041. https://doi.org/10.1093/ps/79.7.1033

Widowski, T., Casey-Trott, T., Hunniford, M., & Morrissey, K. (2017). Welfare of laying hens: An overview. In *Achieving sustainable production of eggs* (Vol. 2, pp. 75–102). Burleigh Dodds Science Publishing.

Wilkins, L. J., Brown, S. N., Zimmerman, P. H., Leeb, C., & Nicol, C. J. (2004). Investigation of palpation as a method for determining the prevalence of keel and furculum damage in laying hens. *The Veterinary Record*, *155*(18), 547–549. https://doi.org/10.1136/vr.155.18.547

Wilkins, L. J., McKinstry, J. L., Avery, N. C., Knowles, T. G., Brown, S. N., Tarlton, J., & Nicol, C. J. (2011). Influence of housing system and design on bone strength and keel bone fractures in laying hens. *The Veterinary Record*, *169*(16), 414. https://doi.org/10.1136/vr.d4831

Willie, B. M., Birkhold, A. I., Razi, H., Thiele, T., Aido, M., Kruck, B., Schill, A., Checa, S., Main, R. P., & Duda, G. N. (2013). Diminished response to in vivo mechanical loading in trabecular and not cortical bone in adulthood of female C57Bl/6 mice coincides with a reduction in deformation to load. *Bone*, *55*(2), 335–346. https://doi.org/10.1016/j.bone.2013.04.023

Willie, B. M., Zimmerman, E. A., Vitienes, I., Main, R. P., & Komarova, S. V. (2020). Bone adaptation: Safety factors and load predictability in shaping skeletal form. *Bone*, *131*, 12.

Willie, B. M., Zimmermann, E. A., Vitienes, I., Main, R. P., & Komarova, S. V. (2020). Bone adaptation: Safety factors and load predictability in shaping skeletal form. *Bone*, *131*, 115114. https://doi.org/10.1016/j.bone.2019.115114

Wolff, J., 1836-1902. (1892). *Das Gesetz der Transformation der Knochen*. Hirschwald; WorldCat.

Yamada, M., Chen, C., Sugiyama, T., & Kim, W. K. (2021). Effect of Age on Bone Structure Parameters in Laying Hens. *Animals : An Open Access Journal from MDPI*, *11*(2), 570. https://doi.org/10.3390/ani11020570

Yang, H., Embry, R. E., & Main, R. P. (2017). Effects of Loading Duration and Short Rest Insertion on Cancellous and Cortical Bone Adaptation in the Mouse Tibia. *PLoS One*, *12*(1), e0169519. https://doi.org/10.1371/journal.pone.0169519

Young, V. K. H., & Blob, R. W. (2015). Limb bone loading in swimming turtles: Changes in loading facilitate transitions from tubular to flipper-shaped limbs during aquatic invasions. *Biology Letters*, *11*(6), 20150110. https://doi.org/10.1098/rsbl.2015.0110

Young, V. K. H., Wienands, C. E., Wilburn, B. P., & Blob, R. W. (2017). Humeral loads during swimming and walking in turtles: Implications for morphological change during aquatic reinvasions. *Journal of Experimental Biology*, *220*(21), 3873–3877. https://doi.org/10.1242/jeb.156836